NASA Conference Publication 2321

ACEE Composite Structures Technology

Review of Selected NASA Research on Composite Materials and Structures

Papers presented at a
NASA conference held at
Seattle, Washington
August 13–16, 1984

NASA
National Aeronautics
and Space Administration

Scientific and Technical
Information Branch

1984

Page intentionally left blank

Page intentionally left blank

Page intentionally left blank

CONTENTS

Page intentionally left blank

ACEE COMPOSITE STRUCTURES TECHNOLOGY CONFERENCE

A G E N D A

MONDAY, AUGUST 13, 1984

[1]SESSION 1: OUTLOOK FOR COMPOSITES IN FUTURE AIRCRAFT

SESSION CHAIRMAN: Robert L. James, Jr., Manager, ACEE Project Office, NASA Langley Research Center

AIR TRANSPORTATION SYSTEMS AT THE END OF THE MILLENNIUM - Howard T. Wright, Director for Projects, NASA Langley Research Center

FUTURE COMMERCIAL VIABILITY OF COMPOSITES - Kenneth F. Holtby, Corporate Senior Vice President, The Boeing Company

"THE WAY AHEAD" - Russell H. Hopps, Vice President and General Manager, Engineering and Development, Lockheed-California Company

"COMPOSITE AIRCRAFT MATERIALS - THE FUTURE" - John B. DeVault, Vice President, Composite Materials and Structures, Hercules Aerospace

TUESDAY MORNING, AUGUST 14, 1984

SESSION 2: ACEE SECONDARY AND MEDIUM PRIMARY COMPOSITE STRUCTURES - STATUS REPORT

SESSION CHAIRMAN: Andrew J. Chapman, Technical Manager, Composites, ACEE Project Office, NASA Langley Research Center

[2]737, 757 and 767 COMPONENTS - John T. Quinlivan, Boeing Commercial Airplane Company

[3]DAMAGE TOLERANCE AND FAILSAFE TESTING OF THE DC-10 COMPOSITE VERTICAL STABILIZER - John M. Palmer, Jr., Clive O. Stephens, and Jason O. Sutton, Douglas Aircraft Company

[4]INITIAL STRENGTH AND HYGROTHERMAL RESPONSE OF L-1011 VERTICAL FIN COMPONENTS - Anthony C. Jackson, Lockheed-California Company

[5]RESIDUAL-STRENGTH TESTS OF L-1011 VERTICAL FIN COMPONENTS AFTER 10 AND 20 YEARS OF SIMULATED FLIGHT SERVICE - Osvaldo F. Lopez, NASA Langley Research Center

[5]WORLDWIDE FLIGHT AND GROUND BASED EXPOSURE OF COMPOSITE MATERIALS - H. Benson Dexter, NASA Langley Research Center, and Donald J. Baker, U. S. Army Structures Laboratory, NASA Langley Research Center

---

Footnotes on page x.

TUESDAY MORNING, AUGUST 14, 1984

[5]COMPARISON OF TOUGHENED COMPOSITE LAMINATES USING NASA STANDARD DAMAGE TOLERANCE TESTS - Jerry G. Williams, NASA Langley Research Center, T. Kevin O'Brien, U.S. Army Structures Laboratory, NASA Langley Research Center, and Andrew J. Chapman, NASA Langley Research Center

TUESDAY AFTERNOON, AUGUST 14, 1984

SESSION 3: REVIEW OF SELECTED NASA RESEARCH IN COMPOSITE MATERIALS AND STRUCTURES

SESSION CHAIRMAN: James H. Starnes, Jr., Head, Structural Mechanics Branch, NASA Langley Research Center

[5]SYNTHESIS AND TOUGHNESS PROPERTIES OF RESINS AND COMPOSITES - Norman J. Johnston, NASA Langley Research Center

[5]TENSILE STRENGTH OF COMPOSITE SHEETS WITH UNIDIRECTIONAL STRINGERS AND CRACK-LIKE DAMAGE - Clarence C. Poe, Jr., NASA Langley Research Center

[5]IMPACT DYNAMICS RESEARCH ON COMPOSITE TRANSPORT STRUCTURES - Huey D. Carden, NASA Langley Research Center

[5]POSTBUCKLING BEHAVIOR OF GRAPHITE/EPOXY PANELS - James H. Starnes, Jr., NASA Langley Research Center; John N. Dixon, Lockheed-Georgia Company; Marshall Rouse, NASA Langley Research Center

[1]DAMAGE TOLERANCE RESEARCH ON COMPOSITE COMPRESSION PANELS - Jerry G. Williams, NASA Langley Research Center

[5]STUDIES OF NOISE TRANSMISSION IN ADVANCED COMPOSITE MATERIAL STRUCTURES - Louis A. Roussos, Michael C. McGary, and Clemans A. Powell, NASA Langley Research Center

WEDNESDAY MORNING, AUGUST 15, 1984

SESSION 4: ACEE WING KEY TECHNOLOGIES

SESSION CHAIRMAN: Marvin B. Dow, Technical Manager, Composites, ACEE Project Office, NASA Langley Research Center

[2]COMPOSITE WING PANEL DURABILITY AND DAMAGE TOLERANCE TECHNOLOGY DEVELOPMENT - Robert D. Wilson, Boeing Commercial Airplane Company

[2]DESIGN DEVELOPMENT OF HEAVILY LOADED WING PANELS - Peter J. Smith, Boeing Commercial Airplane Company

---

Footnotes on page x.

WEDNESDAY MORNING, AUGUST 15, 1984

[3]THEORY AND ANALYSIS FOR OPTIMIZATION OF COMPOSITE MULTI-ROW BOLTED JOINTS - L. John Hart-Smith, Douglas Aircraft Company

[3]DESIGN AND TEST OF LARGE WING JOINT DEMONSTRATION COMPONENTS - Bruce L. Bunin, Douglas Aircraft Company

[4]COMPOSITE WING FUEL CONTAINMENT AND DAMAGE TOLERANCE TECHNOLOGY DEVELOPMENT - Charles F. Griffin, Lockheed-California Company

[4]COMPOSITE WING FUEL CONTAINMENT AND DAMAGE TOLERANCE TECHNOLOGY DEMONSTRATION - Tom W. Anderson, Lockheed-California Company

WEDNESDAY AFTERNOON, AUGUST 15, 1984

SESSION 5: REVIEW OF SELECTED DOD PROGRAMS

SESSION CHAIRMAN: H. Benson Dexter, NASA Langley Research Center

[6]MANUFACTURING TECHNOLOGY FOR LARGE AIRCRAFT COMPOSITE PRIMARY STRUCTURE (FUSELAGE) - DESIGN SELECTION - Hank R. Fenbert, Boeing Commercial Airplane Company; Harry S. Reinert, U.S. Air Force, MLTN, Wright-Patterson AFB, Vere S. Thompson, Boeing Commercial Airplane Company

[6]MANUFACTURING TECHNOLOGY FOR LARGE AIRCRAFT COMPOSITE WING STRUCTURE - Melvin A. Price, North American Aircraft Operations, Rockwell International Corporation, and D. R. Beeler, U.S. Air Force, AFWAL/MLTN, Wright-Patterson AFB

[6]MANUFACTURING TECHNOLOGY FOR LARGE COMPOSITE FUSELAGE STRUCTURE - Richard L. Circle and R. Dennis O'Brien, Lockheed-Georgia Company

[6]DAMAGE TOLERANCE OF COMPOSITES - John E. McCarty, Boeing Military Airplane Company.

[1]ADVANCED COMPOSITE AIRFRAME PROGRAM (ACAP) - Tom Mazza, U.S. Army Applied Technology Laboratory, Fort Eustis

[6]COMPOSITE STRUCTURES - IMPROVED DESIGNS FOR MILITARY AIRCRAFT - Anthony Manno, Mark S. Libeskind, Ramon Garcia, and Edward F. Kautz, U.S. Navy, Naval Air Development Center

[1]COMPOSITE STRUCTURES IN THE JVX AIRCRAFT - Keith Stevenson, Bell Helicopter Corporation

---

Footnotes on page x.

THURSDAY MORNING, AUGUST 16, 1984

SESSION 6: ACEE ADVANCED COMPOSITE STRUCTURES TECHNOLOGY

SESSION CHAIRMAN: Jon S. Pyle, Technical Manager, Composites, ACEE Project Office, NASA Langley Research Center

[2]BOEING - PRESSURE CONTAINMENT AND DAMAGE TOLERANCE IN FUSELAGE STRUCTURE - Ronald W. Johnson, Boeing Commercial Airplane Company

[3]DOUGLAS - JOINTS AND CUTOUTS IN FUSELAGE STRUCTURE - D. Joseph Watts, Douglas Aircraft Company

[4]LOCKHEED - IMPACT DYNAMICS AND ACOUSTIC TRANSMISSION IN FUSELAGE STRUCTURE - Anthony C. Jackson, Lockheed-California Company

[4]LOCKHEED COMPOSITE TRANSPORT WING TECHNOLOGY DEVELOPMENT

COVER/RIB CONCEPTS - Arthur M. James, Lockheed-California Company

SPAR/ASSEMBLY CONCEPTS - William E. Harvill, Jr., Lockheed-Georgia Company

---

[1]Oral presentations only.
[2]Papers contained in NASA CR-172358.
[3]Papers contained in NASA CR-172359.
[4]Papers contained in NASA CR-172360.
[5]Papers contained in NASA CP-2321.
[6]Papers contained in NASA CP-2322.

RESIDUAL-STRENGTH TESTS OF L-1011 VERTICAL FIN COMPONENTS AFTER 10 AND 20 YEARS OF SIMULATED FLIGHT SERVICE

Osvaldo F. Lopez
NASA Langley Research Center
Hampton, VA 23665

ACEE Composite Structures Technology Conference
Seattle, Washington

August 13-15, 1984

INTRODUCTION

A major issue facing the Aerospace Industry today is the effect of flight service exposure on the performance of large graphite-epoxy aircraft structural components. It is essential that these composite structures survive extensive cyclic loading and environmental conditioning of sufficient severity to develop the necessary confidence for flight service durability.

Part of the NASA/ACEE sponsored Production Readiness Verification Test (PRVT) plan (refs. 1, 2) for the Lockheed Advanced Composite Vertical Fin (ACVF) program was to determine the effect of long-term durability testing on the residual strength of graphite-epoxy cover panel and spar components of the Lockheed L-1011 aircraft vertical stabilizer.

Lockheed designed and fabricated 22 cover panels and 22 spar components. Ten of each of the components were statically tested to failure to determine their static strength. The results of these tests established the strength variability and production quality of the original components. The remaining 12 cover panels and 12 spar specimens were subjected to long-term durability testing which simulated 10 and 20 years of flight service exposure.

To determine the effect of simulated flight testing exposure on the residual strength of the cover panel and spar specimens, NASA Langley Research Center performed eleven static tests to failure on these specimens. This paper presents the results of these residual-strength tests. The structural behavior and failure mode of both cover panel and spar specimens are addressed, and the test results obtained are compared with the static test results obtained by Lockheed. In addition, the effect of damage on one of the spar specimens is described.

PRVT DURABILITY TESTING

The long-term durability testing of 12 cover and 12 spar specimens was conducted by the Lockheed-California Company (CALAC). These structural components were placed in environmental chambers and subjected to several test spectra. A spectrum of temperature and humidity and a cyclic load spectrum were applied. A brief description of the durability test program is shown below. Several spar and cover specimens were subjected to half a life cycle, or the equivalent of 10 years of simulated flight service. The other specimens were subjected to a full 20-year life cycle spectrum. (See fig. 1.)

- Environment
  - Temperatures: -30°F to 140°F
  - Humidity: 0 to 100%
- Cyclic Loading
  - Spectrum Fatigue
  - 20 Year Life (36000 Flights)
  - 6.2 Flight/Thermal Cycle

Figure 1

STIFFENED COVER PANEL SPECIMENS

A typical stiffened cover panel (refs. 1, 3) constructed from T300/5208 graphite-epoxy tape is shown in figure 2. The cover panel specimen measures five feet in length and two feet in width. The upper half, or top bay, of the cover panel specimen is shown in this figure. The cover panel specimen consists of three hat stiffeners which are co-cured with the skin. The panel skin is composed of 0^{o} and $\pm 45^{o}$ layers and tapers in thickness from 34 plies at the top bay to 16 plies at the bottom bay.

CALAC designed and constructed 22 of these cover panel specimens. The design of these cover panel specimens was based on a stiffness criterion which required the graphite-epoxy panel to match its metal counterpart. Twelve of these specimens were subjected to durability tests (conditioned) and ten were statically tested to failure. Six of the conditioned cover panel specimens were tested at NASA Langley to assess the effects of long-term durability testing on residual strength. Two 20 year conditioned specimens were loaded, during one cycle, to design ultimate load (54600 lb) and held at this load for a few seconds.

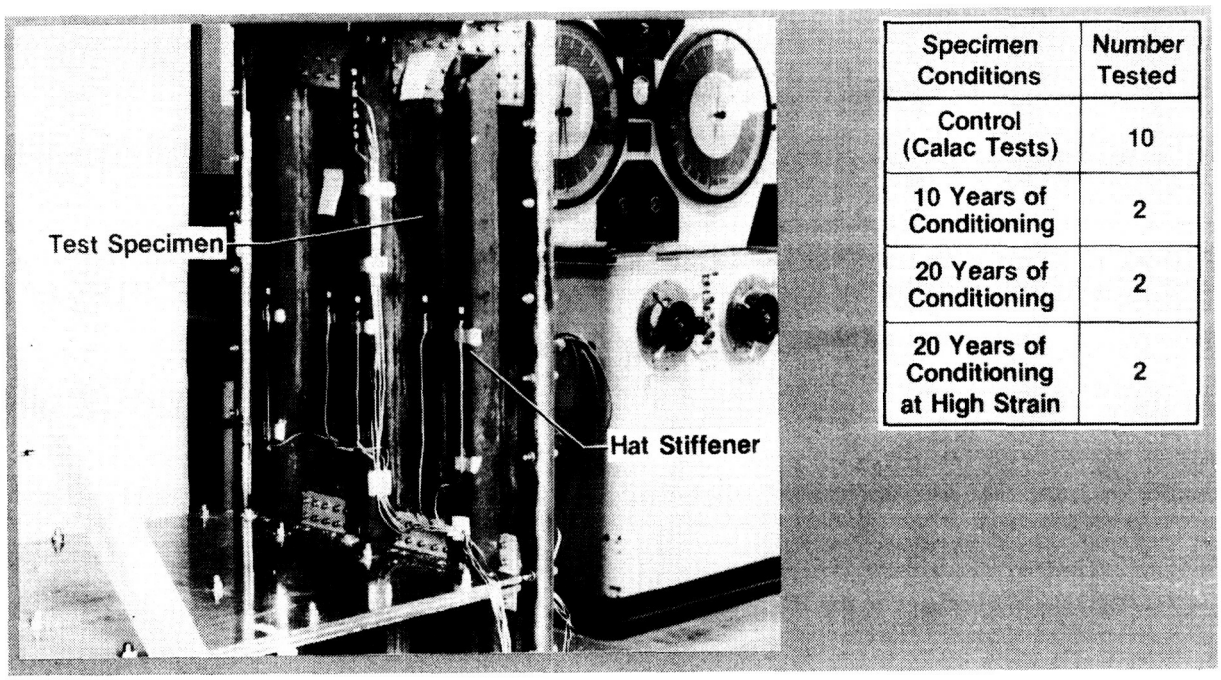

Specimen Conditions	Number Tested
Control (Calac Tests)	10
10 Years of Conditioning	2
20 Years of Conditioning	2
20 Years of Conditioning at High Strain	2

Figure 2

TEST SET-UP FOR STIFFENED COVER PANEL SPECIMENS

The test set-up for the stiffened cover panel specimens is shown in figure 3. The test set-up consists of two steel I-beams which form the reaction frame, supporting three aluminum alloy plates which simulate rib structures. The frame also provides stability while the cover panel specimen is loaded in compression. There are four steel link bars and two aluminum angle bars which connect the cover panel specimen to the frame and carry the reaction loads from the specimen. The cover panel is fixed at both ends by the two end fixtures and subjected to compression loading in the NASA Langley one million pound testing machine.

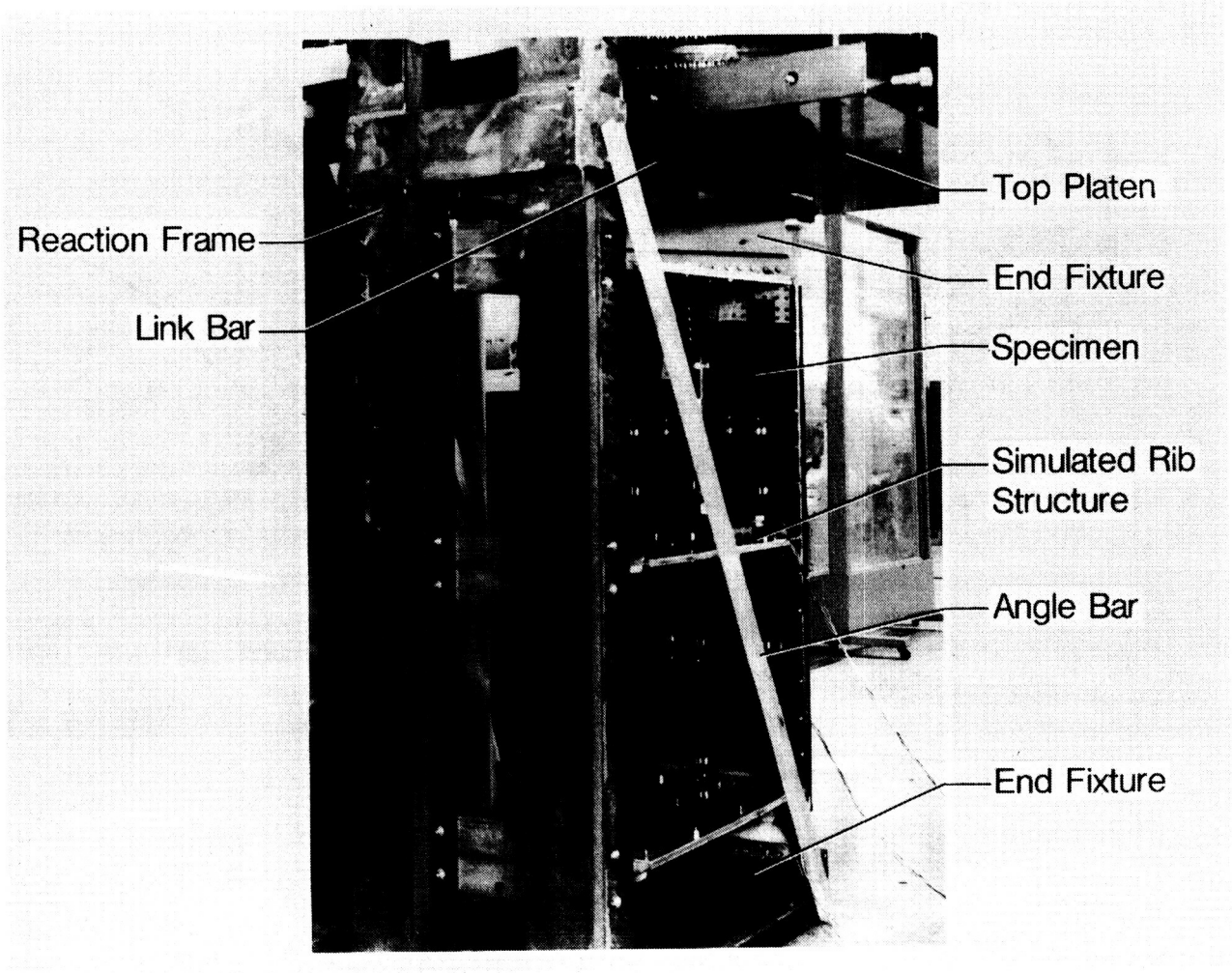

Figure 3

TYPICAL RESULTS FOR COVER PANEL SPECIMENS

Some typical results for the cover panels are shown in figure 4. On the left is a photograph of a typical moire fringe pattern showing the buckling mode of the lower 16-ply-thick bay of the cover panel specimen. Large amounts of deformation occur in the skin between stiffeners as indicated by the closely space fringes.

Plotted on the right are some typical back-to-back strain gage results. The plots for gages A and B (located on the skin between stiffeners) indicate strain gage reversal at 55000 lb, which is the onset of buckling. Buckling occurred above the design limit load of 30000 lb. The specimen is loaded well into the post-buckling range and fails at 92000 lb. Gages C and D, located respectively on the cap and skin sides of the stiffener, show that some bending occurs in the stiffener, but is not as pronounced as in the skin.

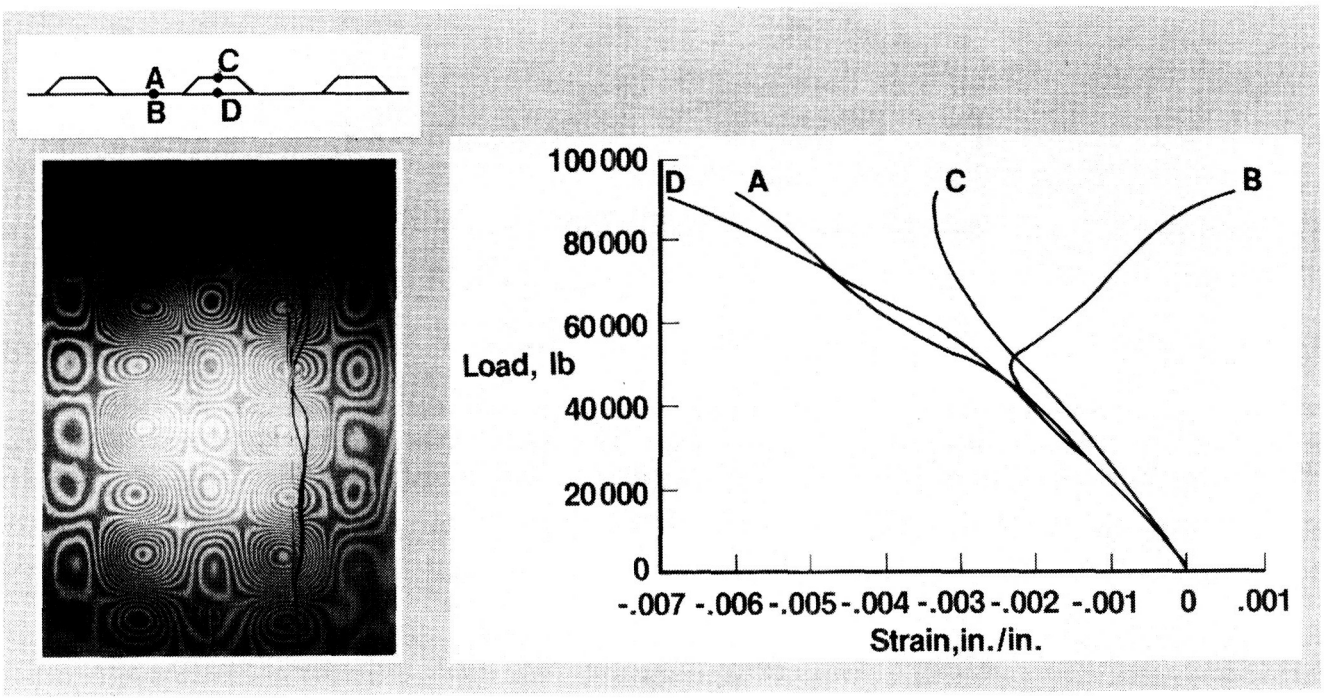

Figure 4

TYPICAL COVER PANEL FAILURE MODE

The typical failure mode for the cover panel specimens is shown in figure 5. On the left and center are front and rear views of the failed cover panel. The failure propagated across the bottom bay of the cover panel from one edge of the specimen to the other. The front of the specimen is painted white to provide a reflective surface for the moire fringe technique. The close-up photograph on the right shows the failure around the center stiffener. The hat stiffener has separated from the skin as indicated by the darker gap region slightly to the right of the scale. The center stiffener separated from the skin due to large post-buckling deformations, and the resulting damage propagated to fail the specimen.

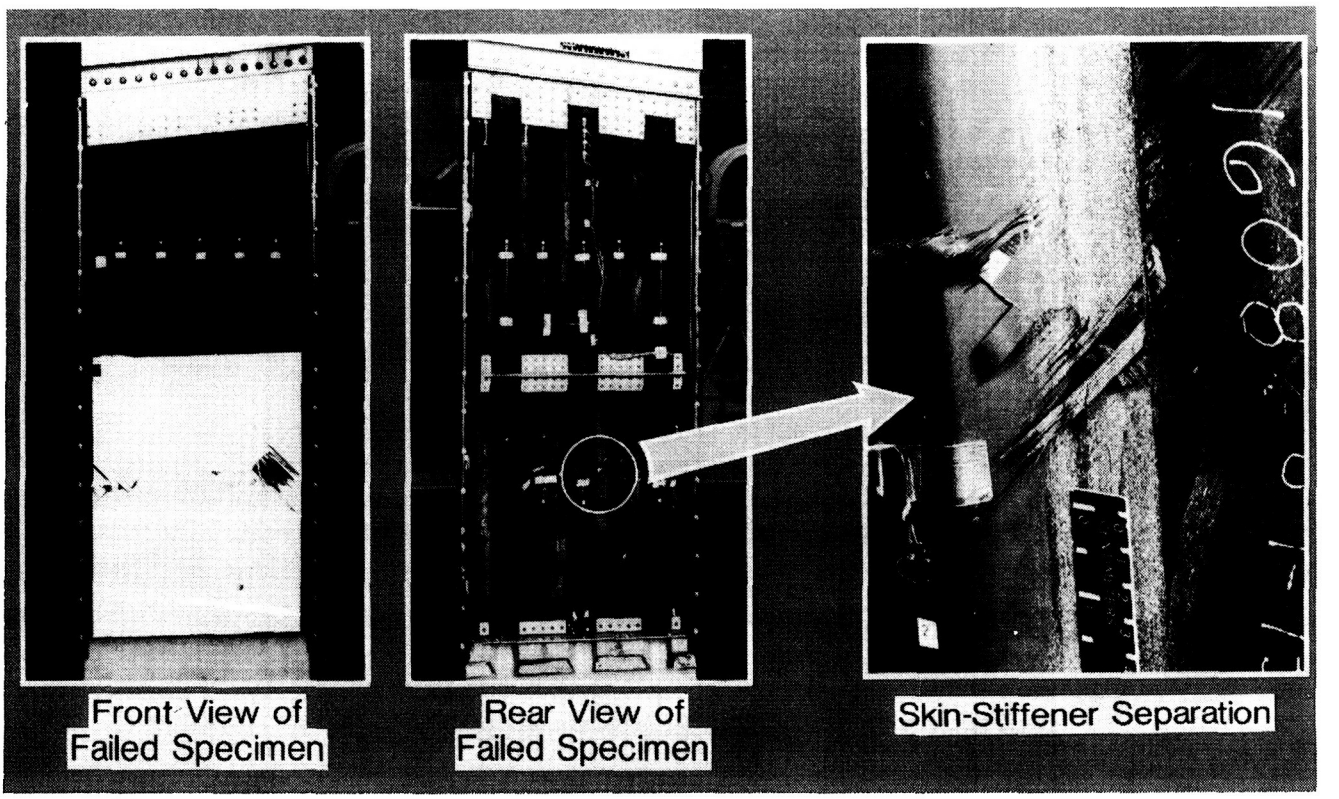

Figure 5

COMPARISON OF FAILURE LOADS FOR COVER PANEL SPECIMENS

Below is a comparison of the failure loads for the statically tested covers (control specimens) and the cover panels subjected to durability testing (conditioned specimens). The first bar represents the failure loads of the ten control tests. The range of failure loads is from 88000 lb to 96000 lb with an average failure load of 93000 lb. The remaining bars show the failure loads for the conditioned cover panel specimens. (See fig. 6.) The results indicate that the six conditioned cover panel specimens failed within, or slightly above, the failure range of the control specimens. The high-strain cover panels, which were loaded to design ultimate load during one cycle of the durability testing, showed no strength reduction. These results indicate that environmental conditioning and cyclic loading did not affect the performance of these cover panel specimens.

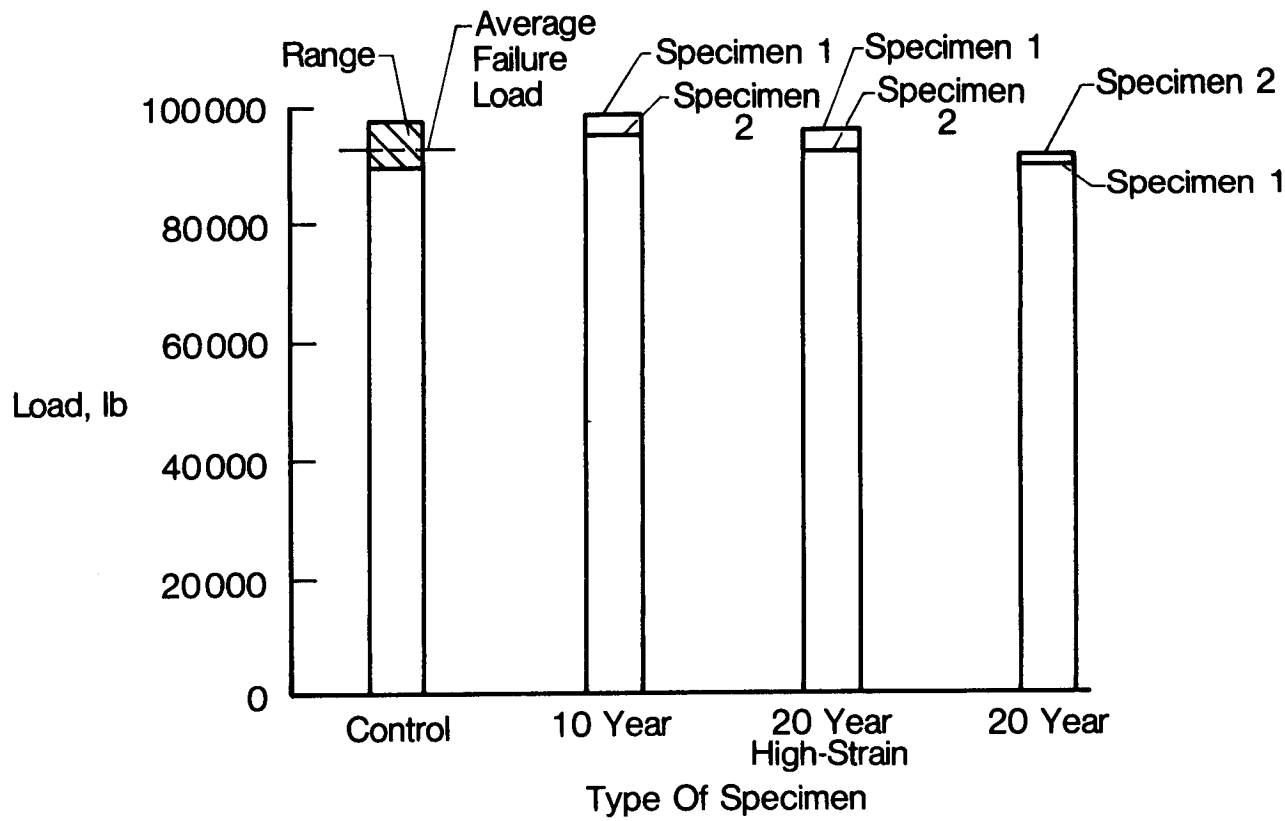

Figure 6

SPAR SPECIMENS

Two views of a typical leading-edge spar specimen (refs. 1, 3) are shown in figure 7. The spar specimen is 84 inches long, 28 inches wide at root and 21 inches wide at the tip. It is constructed from T300/5208 graphite-epoxy tape. The aft view of the spar shows several rib supports and stiffeners on the spar web. The spar specimens had two aluminum spar caps and three access holes. Some specimens had a fourth hole toward the tip. The forward view shows the smooth front surface of the specimen.

Lockheed constructed 22 of these spar specimens, ten of which were statically tested (control). The remaining 12 were subjected to long-term durability testing (conditioned). Five of the conditioned specimens were statically tested at NASA Langley Research Center to assess their residual strength. Two 10-year conditioned specimens and three 20-year specimens were tested at Langley. One of the 20-year conditioned specimens had sustained some damage around the edge of the bottom access hole prior to residual strength testing.

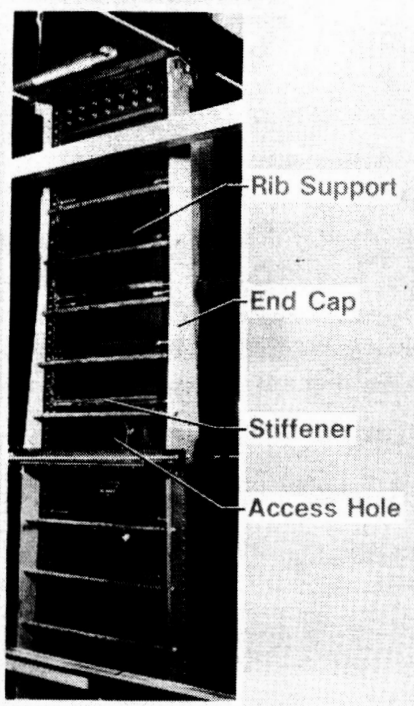

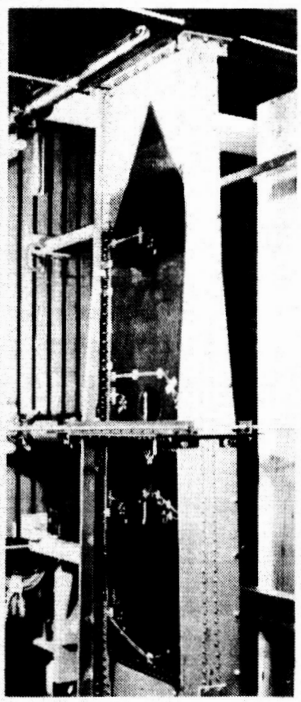

Specimen Conditions	Number Tested
Control (Calac)	10
10 Years of Conditioning	2
20 Years of Conditioning	3

Figure 7

TEST SET-UP FOR THE SPAR SPECIMENS

The test set-up for the front spar specimens is shown below. The test set-up consists of the specimen and four aluminum support frames which are attached to the laboratory floor. Eight threaded steel tie rods, attached to the frames, prevent lateral buckling at the spar specimen. The specimen is secured to the laboratory floor by use of a steel attachment base plate, and is loaded by two hydraulic jacks which bend the spar toward a steel back-stop. (See fig. 8.)

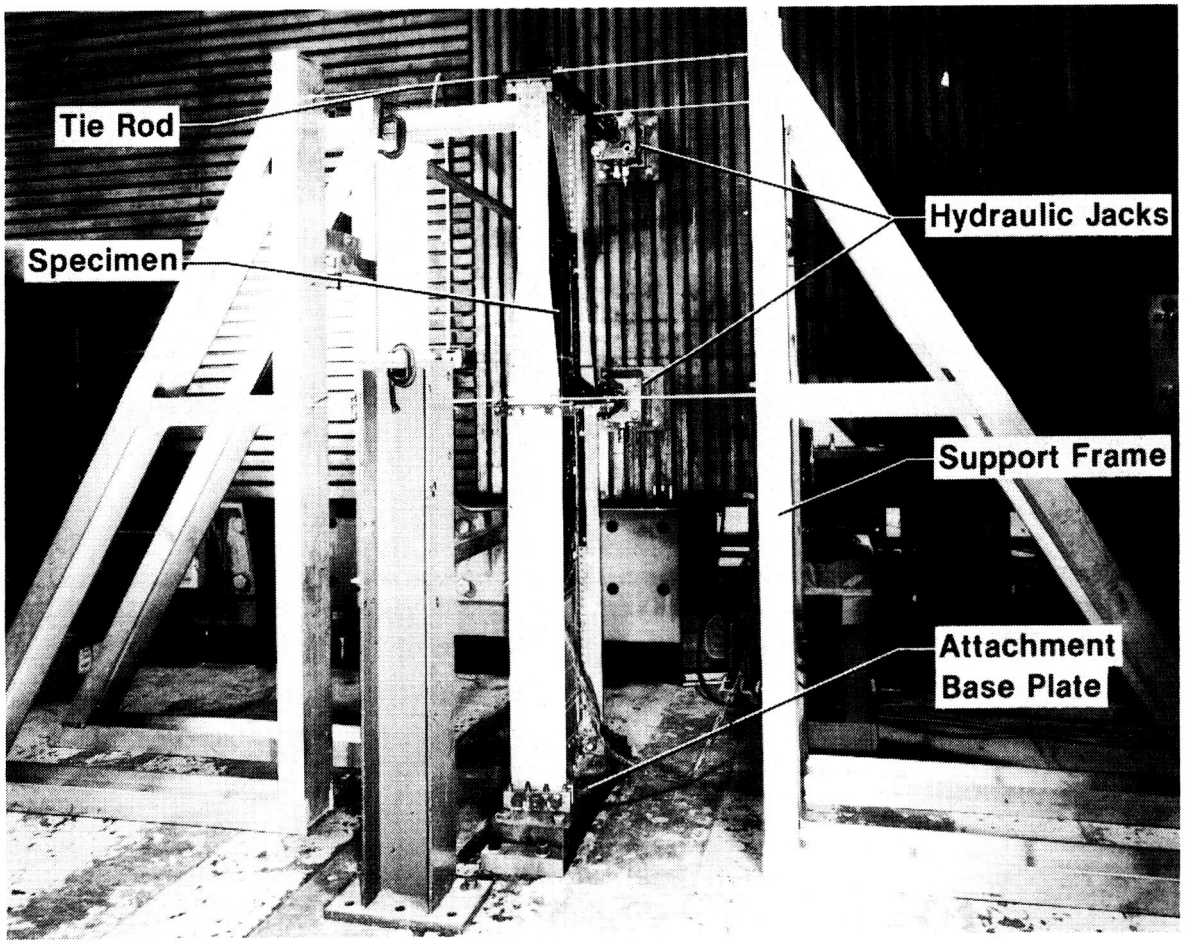

Figure 8

TYPICAL RESULTS FOR THE SPAR SPECIMENS

A photograph of a typical moire fringe pattern representing the buckling mode of the middle and lower access holes is shown in figure 9. A large amount of deformation around the upper edge of both access holes is indicated by the closely space fringes. The accompanying plots shows some typical strain gage results from a set of back-to-back strain gages located at the edge of the middle access hole.

Strain reversal occurs at an applied load of 25000 lb, indicating the onset of buckling. Buckling occurred well above the design limit load of 14000 lb. The specimen was loaded into the post-buckling range and failed at 32000 lb.

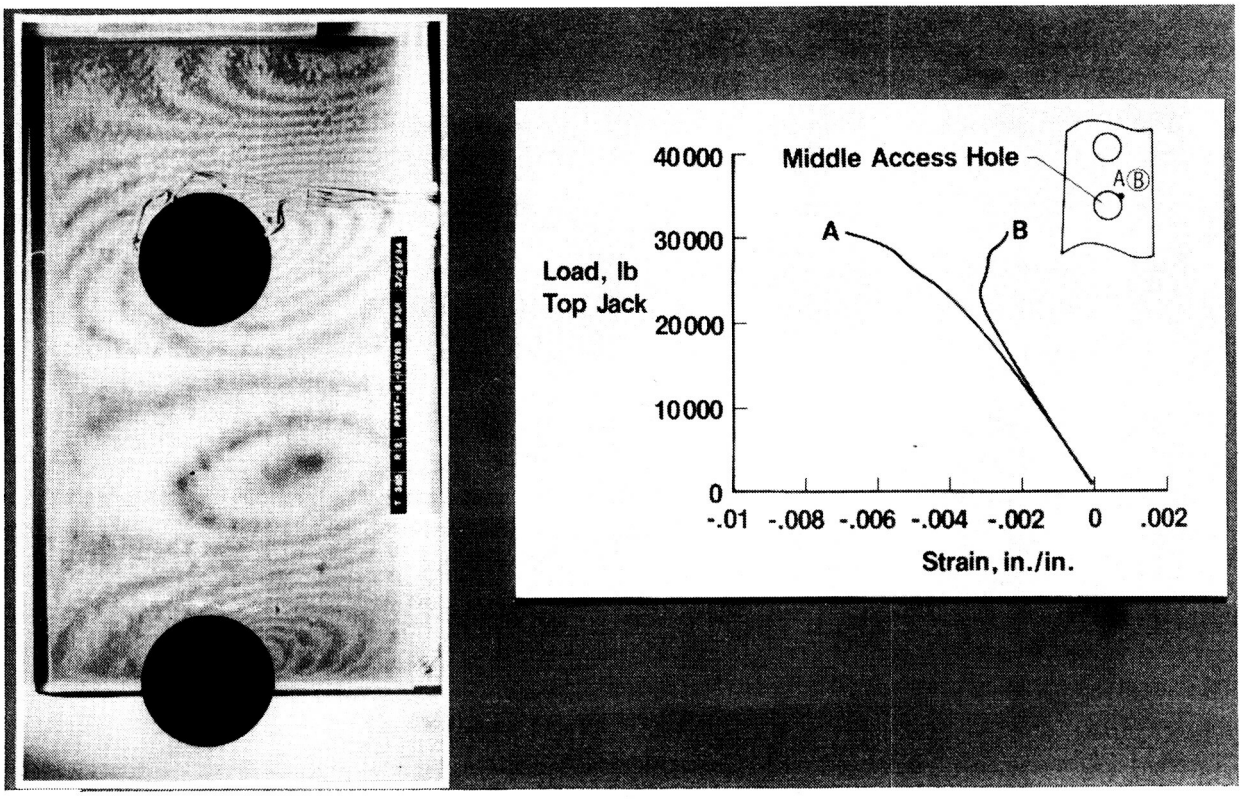

Figure 9

TYPICAL FAILURE MODE OF SPAR SPECIMENS

The typical failure mode of the spar specimens is shown in figure 10. The photograph on the left shows a shearing type failure which occurred around the middle access hole and propagated to both of the spar caps. As a secondary failure effect, the shear failure propagated along the spar caps causing fasteners to pull through the spar.

The photograph on the right is a close-up view of the failure and shows a large amount of delamination around the middle access hole. These local delaminations initiated at the edge of the middle access hole and propagated to fail the specimen. As the shear failure propagated across the spar web, two stiffeners located near the middle access hole separated from the spar web.

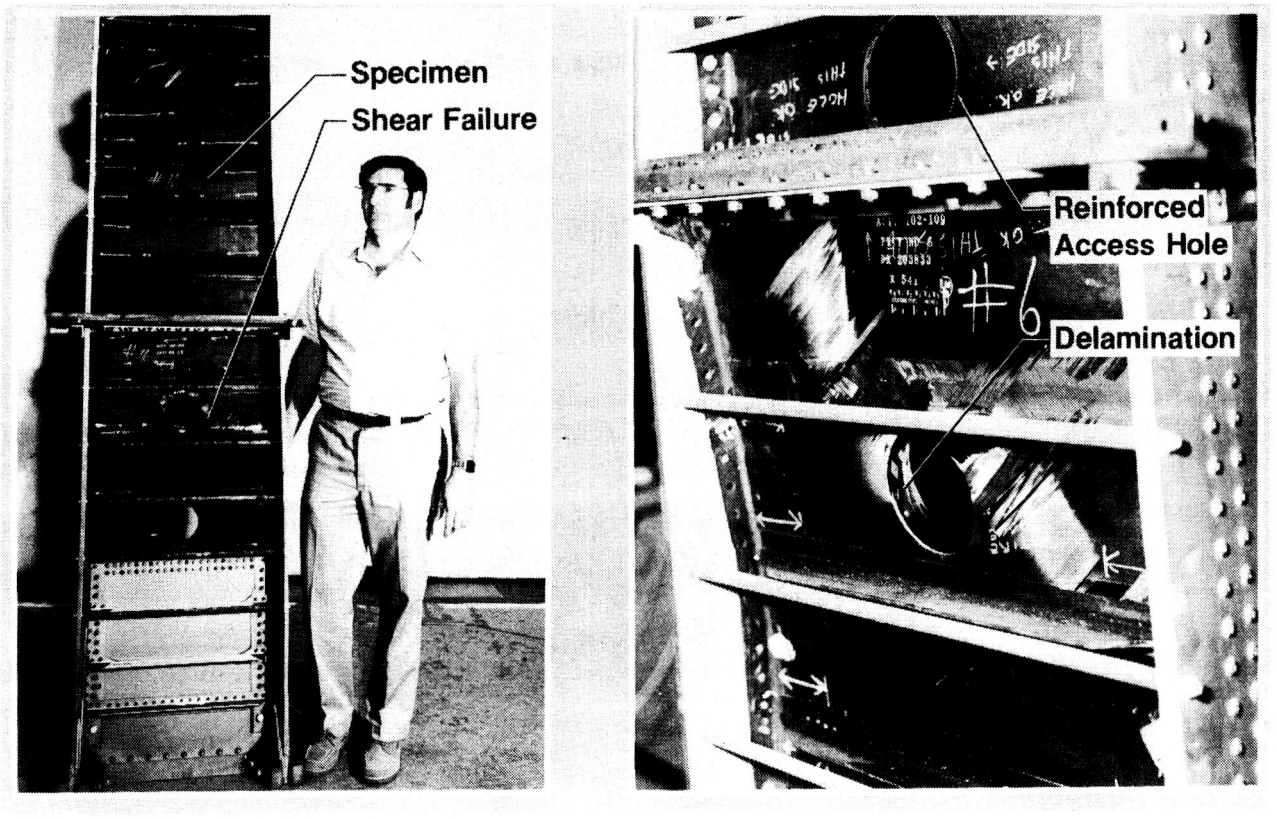

Figure 10

FAILURE MODE OF DAMAGED SPAR SPECIMEN

The failure mode of a 20-year conditioned spar specimen containing damage is shown in figure 11. Visual inspection of the spar specimen revealed, prior to residual-strength testing, a significant amount of delamination near the edge of the lower access hole. An ultrasonic inspection of the spar specimen identified an area of extensive damage around the lower access hole as indicated by the shaded region in the sketch on the left. A photograph of the failed specimen is shown on the right. The damaged spar failed differently from the other specimens, failing along the bottom access hole. However, the damaged spar failed within the failure load range of the other spar specimens. It appears that the damage affected the failure mode, but did not greatly affect the failure load of the damaged specimen.

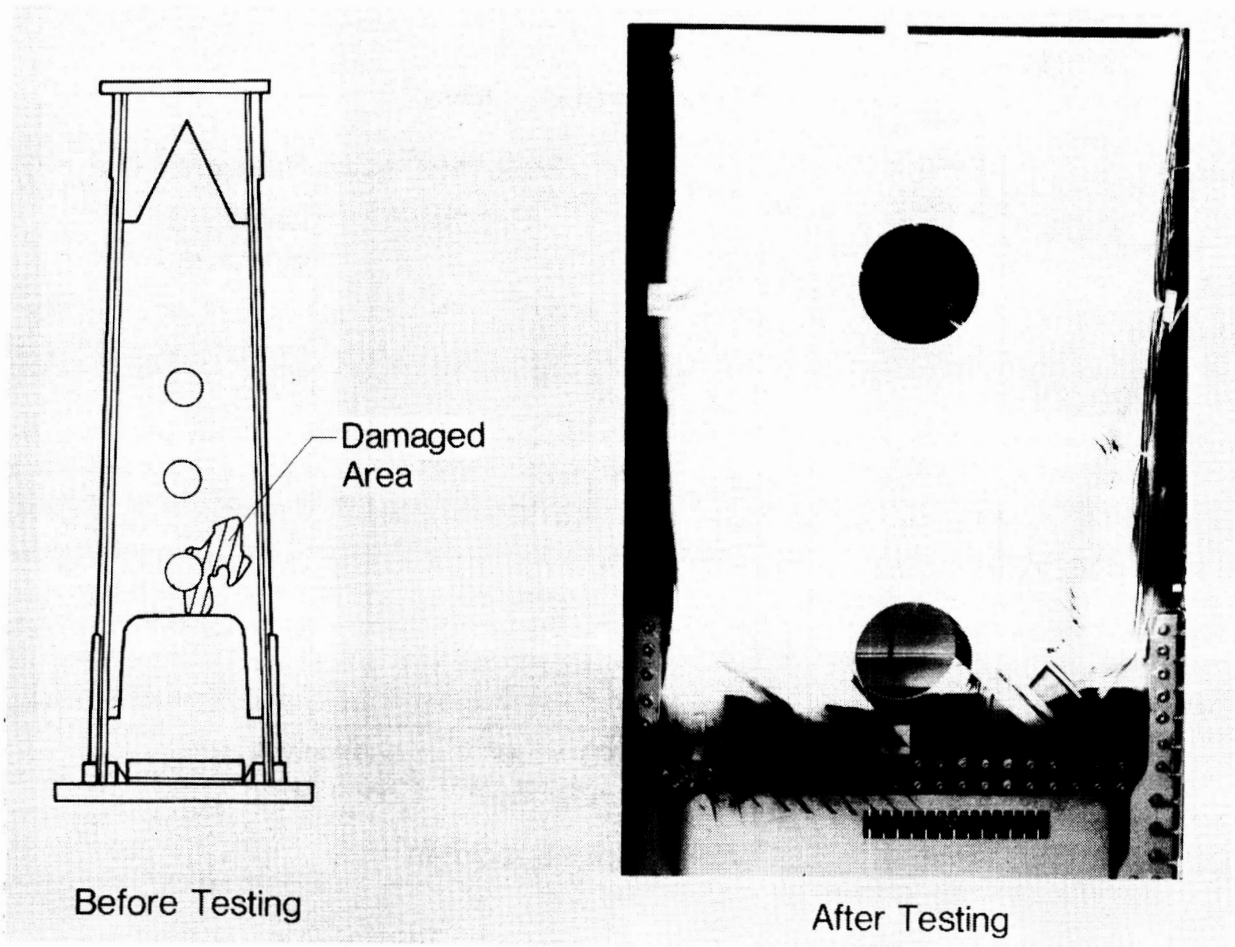

Figure 11

COMPARISON OF FAILURE LOADS FOR SPAR SPECIMENS

Plotted below are the failure loads for the statically tested spar (control) specimens and the spar specimens (conditioned) subjected to durability testing. The first graph represents the failure loads of ten control specimens. The failure loads range from 26000 lb to 31000 lb and the average failure load is 28000 lb. The remaining graphs show the failure loads of the conditioned spar specimens (fig. 12). The results indicate that all five conditioned specimens failed within the failure range of the control specimens or slightly above the average failure load for the control specimens. The spar containing damage failed at 31000 lb, which is above the average failure load for the control specimens. The results indicate that environmental conditioning and cyclic loading did not affect the failure loads of the conditioned spar specimens.

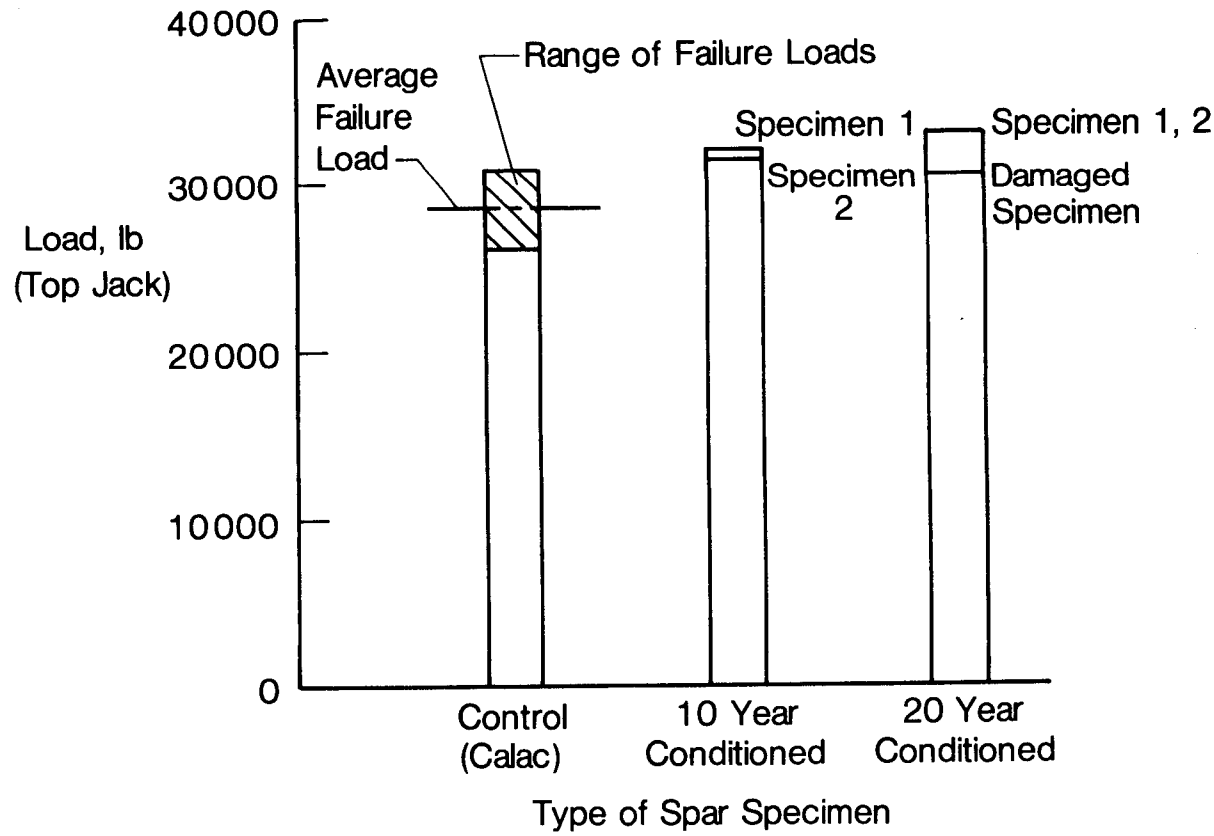

Figure 12

CONCLUDING REMARKS

- The failure loads of the specimens tested in this study were unaffected by simulated flight service conditioning.
- The cover panel specimens failed following large postbuckling deformations.
- The high-strain cover panel specimens did not experience additional strength reduction.
- The undamaged spar specimens failed around the middle access hole in the post-buckling range.
- The damaged spar specimen failed within the failure load range of the control specimens.

REFERENCES

1. Ary, A.; Axtell, C.; Fogg, L.; Jackson, A.; James, A.; Mosesian B.; Vanderwier, J.; Van Hamerveld, J.: Flight Service Evaluation of an Advanced Composite Empennage Component on Commercial Transport Aircraft: Phase I - Final Report Engineering Development. NASA CR-144986, 1976.

2. Dorward, F.; Ketola, R. N.: Static and Damage Tolerance Tests of an Advanced Composite Vertical Fin for L-1011 Aircraft. AIAA Paper No. 83-0970, Presented at AIAA/ASME/ASCE/AHS 24th Structures, Structural Dynamics and Materials Conference, May 2-4, 1984.

3. Jackson, A. C.; Crocker, J. F.; Ekvall, J. C.; Eudialy, R. R.; Mosesian, B.; Van Cleave, R. R.; Van Hamersveld, J.: Advanced Manufacturing Development of a Composite Empennage Component for L-1011 Aircraft: Phase II - Final Report Design and Analysis. NASA CR-165634, 1981.

WORLDWIDE FLIGHT AND GROUND-BASED EXPOSURE OF COMPOSITE MATERIALS

H. Benson Dexter and Donald J. Baker
NASA Langley Research Center
Hampton, Virginia

ACEE Composite Structures Technology Conference
Seattle, Washington
August 13-16, 1984

INTRODUCTION

The NASA Langley Research Center has had programs underway for the past 12 years to establish a data base on the long-term durability of advanced composite materials for application to aircraft structures. A series of flight service programs are obtaining worldwide service experience with secondary and primary composite components installed on commercial and military transport aircraft and helicopters. Included are spoilers, rudders, elevators, ailerons, fairings, wing boxes, and horizontal stabilizers on transport aircraft, and doors, fairings, tail rotors, vertical fins, and horizontal stabilizers on helicopters. A wide variety of materials, including boron/epoxy, Kevlar/epoxy, graphite/epoxy, and boron/aluminum, are being evaluated. Results of inspection, in-service damage incidents, repair procedures, and residual strength of components removed from service are reported. The effects of environmental exposure of composite materials are reported for up to 10 years of outdoor ground-based exposure. Included are the effects of moisture absorption, ultraviolet radiation, and aircraft fuels and fluids. Residual strength as a function of exposure time is compared with baseline properties. Figure 1 outlines the scope of the flight service and ground-based exposure program reported herein.

Flight service of composite components

- Inspection, damage, and repair
- Residual strength

Environmental effects on composite materials

- Worldwide ground-based outdoor exposure
- Moisture, fuels, fluids, and UV radiation
- Residual strength

Figure 1

FLIGHT SERVICE COMPOSITE COMPONENTS ON TRANSPORT AIRCRAFT

Confidence in the long-term durability of advanced composites is being developed through flight service of numerous composite components on transport aircraft. Emphasis has been on commercial aircraft because of their high utilization rates, exposure to worldwide environmental conditions, and systematic maintenance procedures. The composite components currently being evaluated on transport aircraft are shown in figure 2. Eighteen Kevlar/epoxy fairings have been in service on Lockheed L-1011 aircraft since 1973. In April 1982 eight graphite/epoxy ailerons developed under the NASA Aircraft Energy Efficiency (ACEE) program were installed on four L-1011 aircraft for service evaluation. One hundred and eight B-737 graphite/epoxy spoilers have been in service on six different commercial airlines in worldwide service since 1973. Four B-737 graphite/epoxy horizontal stabilizers were installed on two aircraft in March 1984 for commercial service. Thirteen graphite/epoxy DC-10 upper aft rudders are in service on five commerical airlines and three boron/aluminum aft pylon skins have been in service on DC-10 aircraft since 1975. Ten graphite/epoxy elevators have been in service on B-727 aircraft since 1980. In addition to the commercial aircraft components shown in figure 2, two boron/epoxy reinforced aluminum center-wing boxes have been in service on U.S. Air Force C-130 transport aircraft since 1974. Additional details on the design, development, test, and flight service evaluation of the composite components discussed above are given in references 1 through 7.

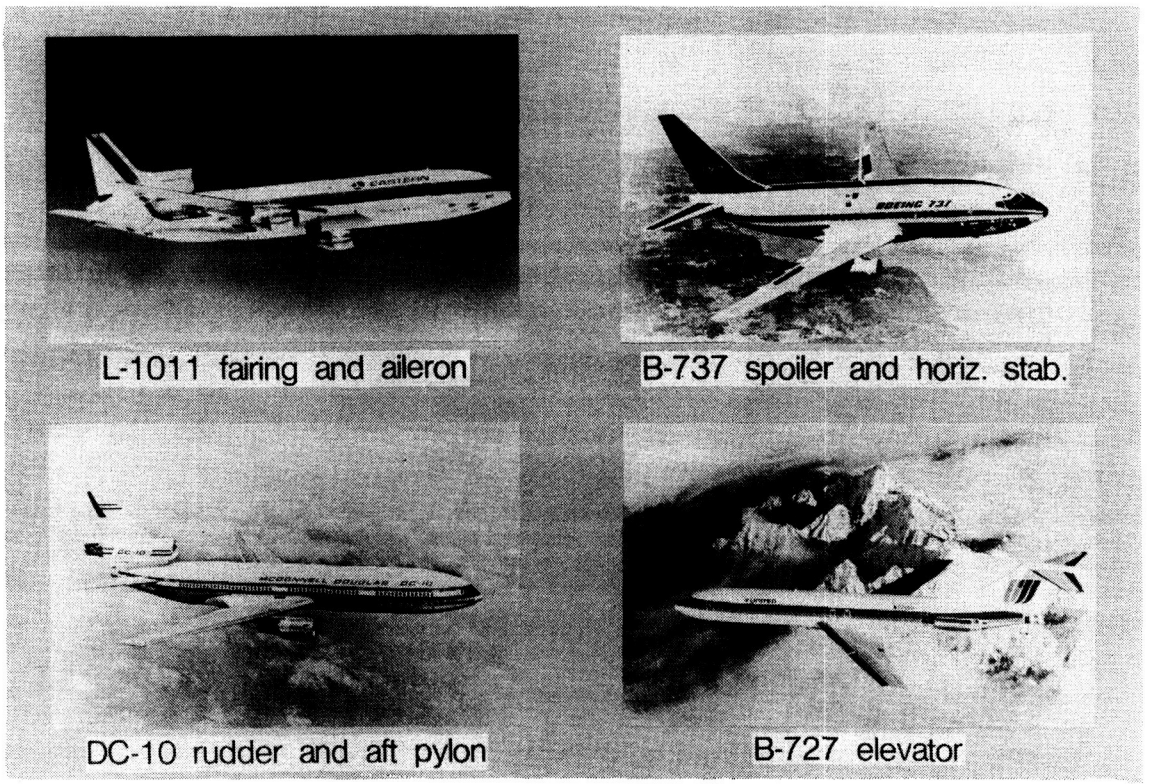

Figure 2

ACEE COMPOSITE COMPONENTS IN FLIGHT SERVICE

As part of the NASA Aircraft Energy Efficiency (ACEE) Program, Boeing, Douglas, and Lockheed have been under NASA contract to design, fabricate, and test large composite structural components. Each of the graphite/epoxy components shown in figure 3 has been certified by the FAA, and flight service evaluation is underway. The four components utilize different design concepts. The B-737 horizontal stabilizers have stringer-reinforced skins, laminated spars, and Nomex honeycomb reinforced ribs. The B-727 elevators are constructed with Nomex honeycomb reinforced laminated skins, the DC-10 rudders are multi-rib stiffened, and the L-1011 aileron skin design features a syntactic-core sandwich with laminated facesheets. An overall mass saving of 24 percent was achieved for the four components when compared to the production aluminum designs. In addition to the components shown in figure 3, Douglas is currently fabricating a graphite/epoxy DC-10 vertical stabilizer for service evaluation.

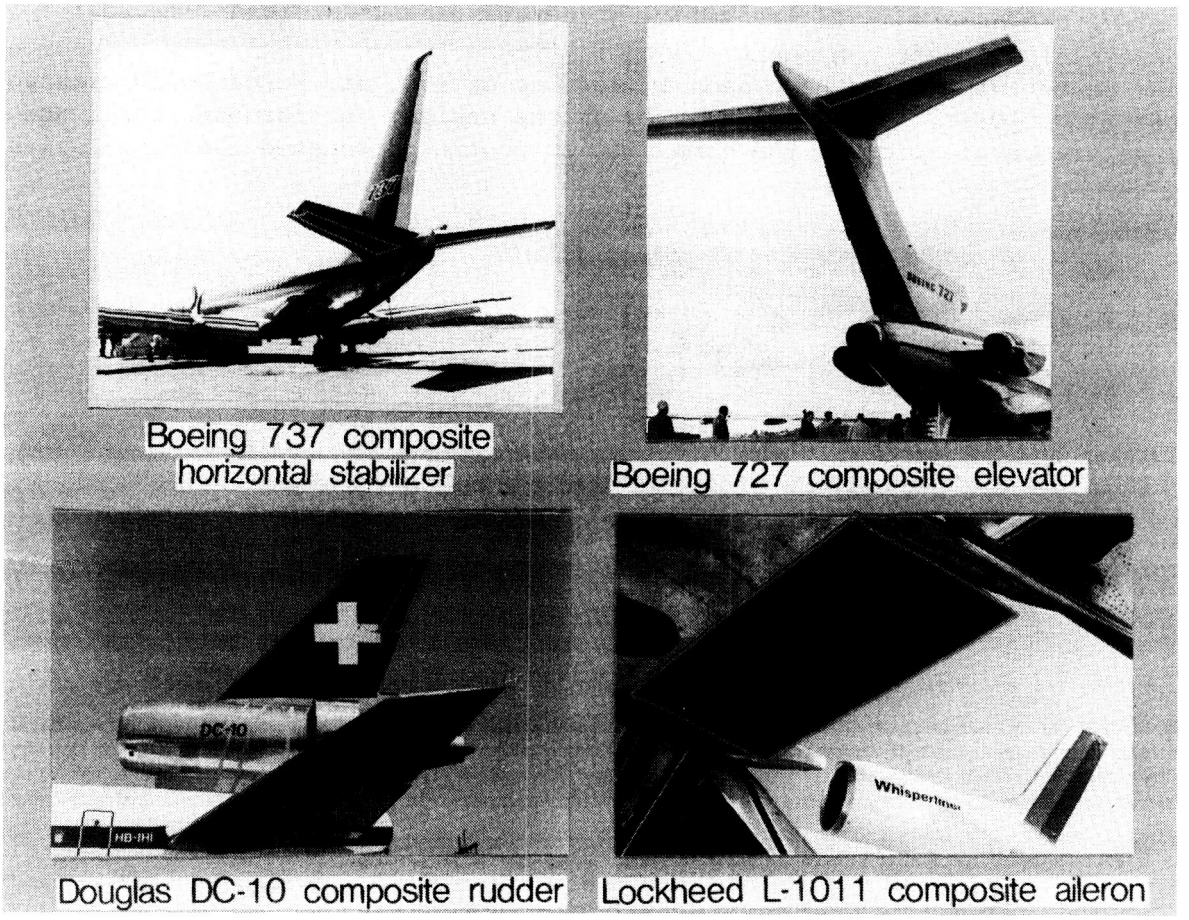

Figure 3

FLIGHT SERVICE COMPOSITE COMPONENTS ON HELICOPTERS

Composite components are being evaluated in service on commercial and military helicopters, as shown in figure 4. Forty shipsets of Kevlar/epoxy doors and fairings and graphite/epoxy vertical fins are being installed on Bell 206L commercial helicopters for 5 to 10 years of service evaluation. The helicopters are operating in diverse environments in Alaska, Canada, U.S. Gulf Coast, and Southwest U.S. Selected components will be removed from service for residual strength testing. Additional details on the Bell 206L program can be found in references 8 and 9. Ten tail rotors and four horizontal stabilizers will be removed from Sikorsky S-76 production helicopters to determine the effects of realistic operational service environments on composite primary helicopter components (ref. 10). Static and fatigue tests will be conducted on the components removed from service and the results will be compared with baseline certification test results. In addition, several hundred composite coupons exposed to the outdoor environment will be tested for comparison with the component test results. A Kevlar/epoxy cargo ramp is being evaluated on a U.S. Marine Corps CH-53D helicopter. The laminated fabric skin may encounter severe handling such as rough runway abrasion and impact. Maintenance characteristics of the Kevlar skin will be compared to those of production aluminum skins.

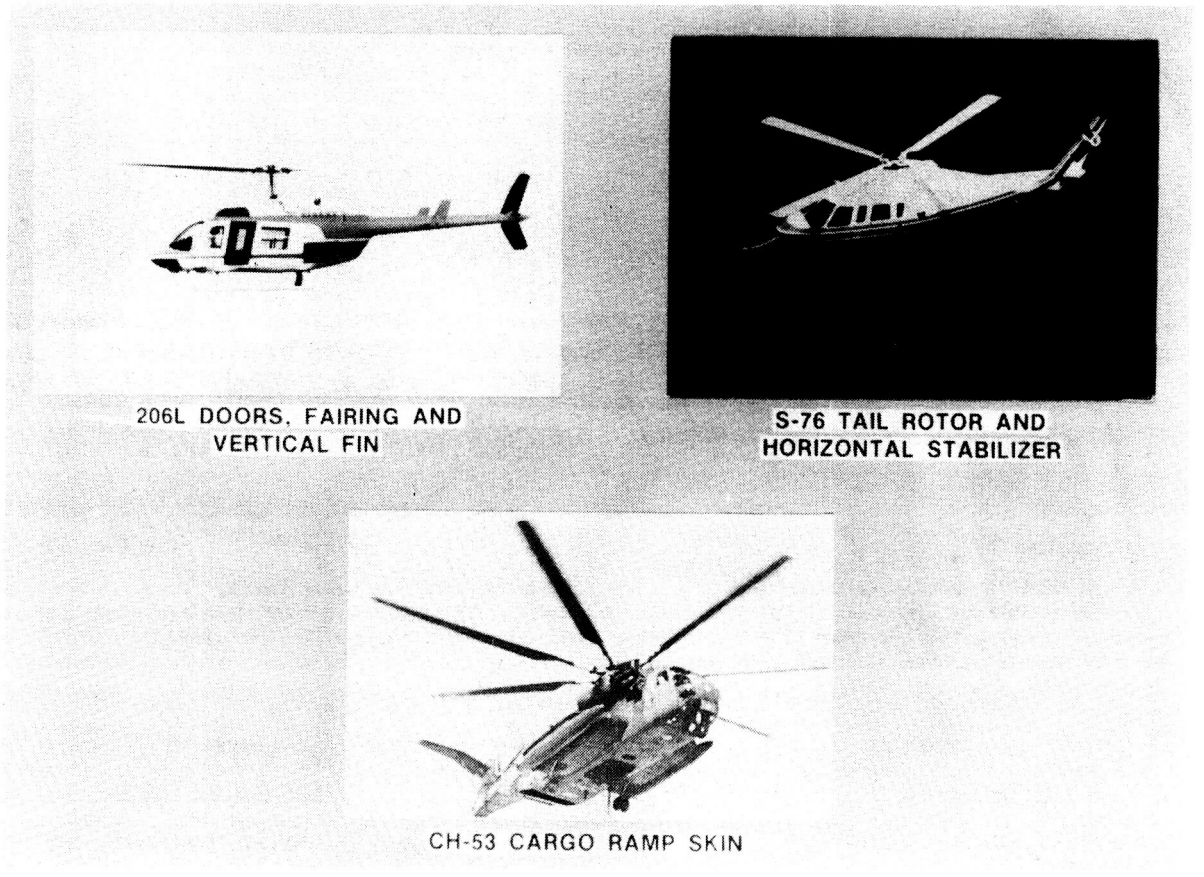

Figure 4

BELL 206L HELICOPTER COMPOSITE COMPONENTS

The four composite components that are being evaluated on the Bell 206L are the forward fairing, litter door, baggage door, and vertical fin, as shown in figure 5. Four different structural design concepts were used in the composite components. The forward fairing is a sandwich structure with a single ply of Kevlar/epoxy fabric co-cured on a polyvinylchloride foam core. The litter door is a hollow section design with Kevlar/epoxy inner and outer skins. Unidirectional Kevlar/epoxy tape is used for local reinforcement at hinges, latches, and in the hat-section stiffeners. The baggage door is constructed with Kevlar/epoxy fabric facesheets and Nomex honeycomb core. Additional reinforcements are added in the latch area and along the edges. The vertical fin is constructed with graphite/epoxy facesheets bonded to a FIBERTRUSS honeycomb core. Composite material coupons are being exposed to outdoor environments at the locations where the flight components are being flown. Tension, compression, and short-beam shear tests are being conducted to establish material degradation as a function of exposure time and location. Strength retention of the materials is being compared with strength retention of components removed from service.

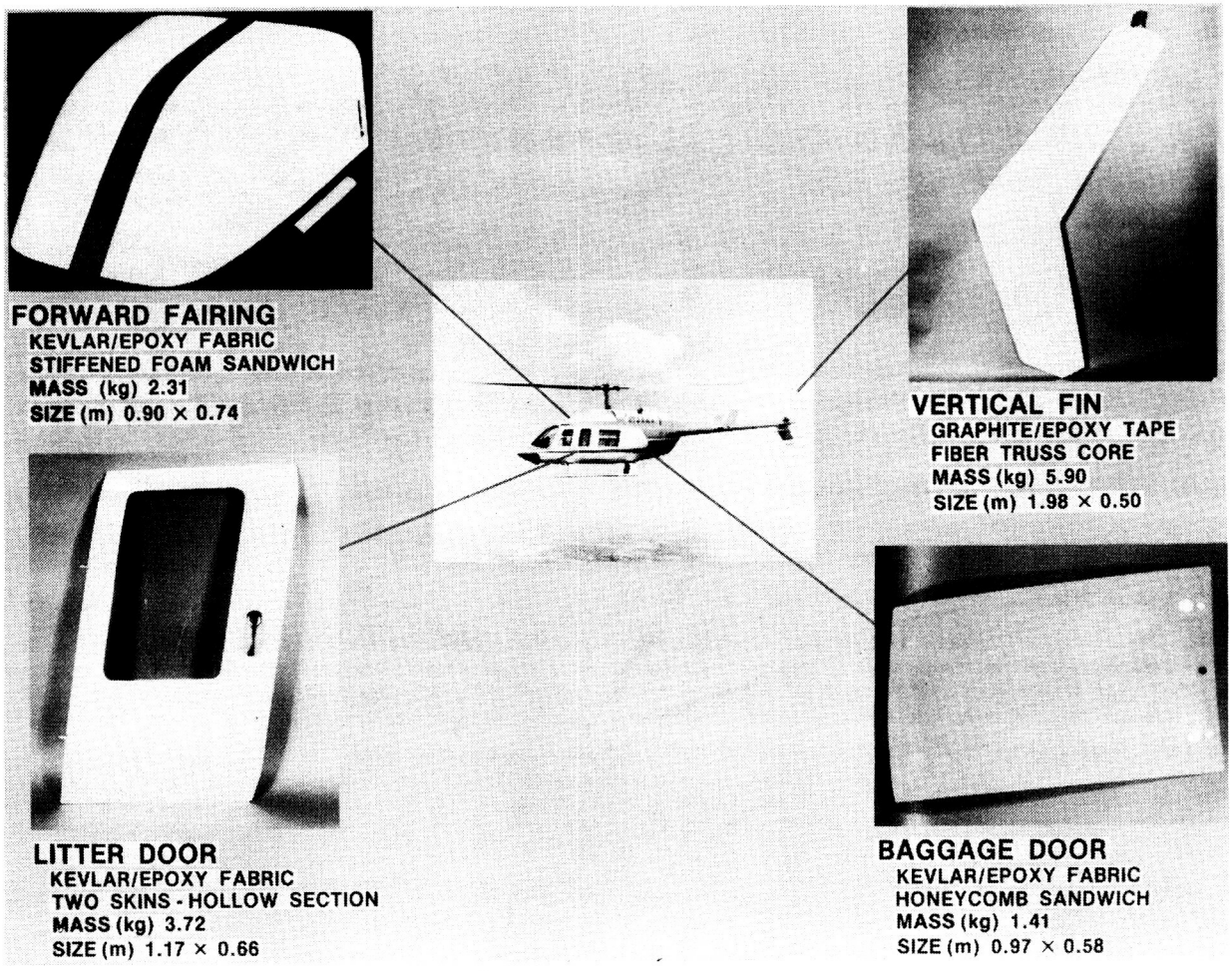

Figure 5

SIKORSKY S-76 HELICOPTER COMPOSITE COMPONENTS

The two composite components that are being evaluated on the Sikorsky S-76 are shown in figure 6. The composite components are baseline designs for the S-76 and are currently in commercial production. The tail rotor has a laminated graphite/epoxy spar with a glass/epoxy skin. The horizontal stabilizer has a Kevlar/epoxy torque tube reinforced with full-depth aluminum honeycomb and graphite/epoxy spar caps, full-depth Nomex honeycomb sandwich core, and Kevlar/epoxy skins. Eight tail rotor spars and two horizontal stabilizers have been removed from helicopters and tested after four years of service. Six of the tail rotor spars were fatigue tested to the same requirements as for FAA certification. Test coupons were cut from the other two spars and tested for residual strength and moisture content. The two horizontal stabilizers were static and fatigue tested, respectively. No significant strength reduction was noted for the spars or stabilizers. Painted composite panels are being exposed to the outdoor environment at Stratford, CT and West Palm Beach, FL. These panels are machined into test coupons to establish materials degradation as a function of exposure time and location. Strength retention results are discussed in a subsequent figure.

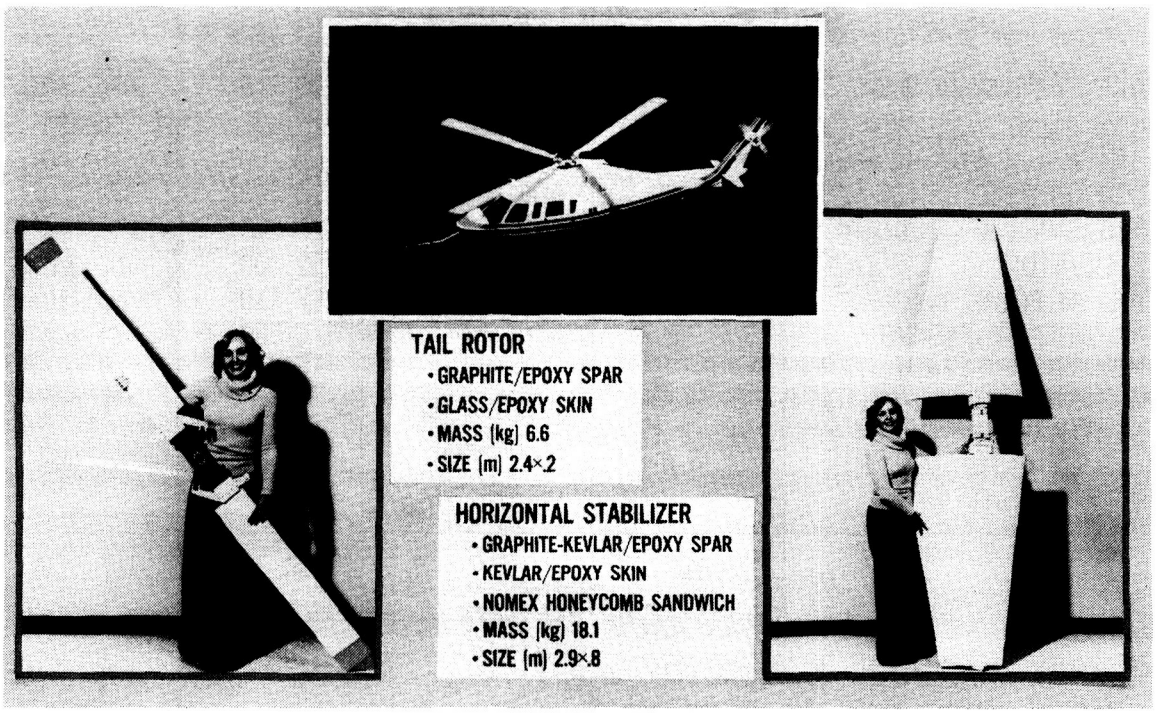

Figure 6

NASA COMPOSITE STRUCTURES FLIGHT SERVICE SUMMARY

Over 300 composite components have been in service with numerous operators, including foreign and domestic airlines, the U.S. Army, the U.S. Marines, and the U.S. Air Force. The NASA Flight Service Program was initiated in 1973 for the components indicated in figure 7. Over 3 million component flight hours have been accumulated with the high-time aircraft having more than 29,000 hours. The 108 graphite/epoxy spoilers installed on B-737 aircraft have accumulated the highest total component flight hours, nearly 2.0 million, during 10 years of service. Over 200,000 total component flight hours have been accumulated on the 206L and S-76 composite helicopter components.

Formal tracking of the L-1011 Kevlar/epoxy fairings under NASA contract was completed in May 1984. The results of the final component inspection conducted by Lockheed-California personnel are presented in reference 1.

AIRCRAFT COMPONENT	TOTAL COMPONENTS	START OF FLIGHT SERVICE	CUMULATIVE FLIGHT HOURS	
			HIGH-TIME AIRCRAFT	TOTAL COMPONENT
L-1011 FAIRING PANELS	18	JANUARY 1973	29,310	480,840
737 SPOILER	108	JULY 1973	29,430	1,996,880
C-130 CENTER WING BOX	2	OCTOBER 1974	6,700	13,300
DC-10 AFT PYLON SKIN	3	AUGUST 1975	24,700	66,700
DC-10 UPPER AFT RUDDER	14*	APRIL 1976	27,600	243,100
727 ELEVATOR	10	MARCH 1980	12,600	108,000
L-1011 AILERON	8	MARCH 1982	7,110	53,110
S-76 TAIL ROTORS AND HORIZONTAL STABILIZERS	14	FEBRUARY 1979	4,200	41,300
206L FAIRING, DOORS, AND VERTICAL FIN	144**	MARCH 1981	3,050	176,000
CH-53 CARGO RAMP SKIN	1	MAY 1981	600	600
737 HORIZONTAL STAB.	4***	MARCH 1984	------	------
GRAND TOTAL	326			3,179,830

* 6 MORE RUDDERS TO BE INSTALLED

** 16 MORE COMPONENTS TO BE INSTALLED

*** 6 MORE STABILIZERS TO BE INSTALLED

APRIL 1984

Figure 7

TYPICAL IN-SERVICE CONDITION OF L-1011 KEVLAR/EPOXY FAIRINGS

During the past 11 years, the Kevlar/epoxy fairings on L-1011 aircraft have been inspected annually to document their condition. The photographs shown in figure 8 indicate various types of damage incurred in service. Minor impact damage from equipment and foreign objects has been noted on several fairings, primarily the honeycomb sandwich wing-to-body fairings. Surface cracks and indentations have been repaired with filler epoxy patches and, in general, the cracks have not propagated with continued service. Paint adherence has been a minor problem, in particular with parts that have been in contact with hydraulic fluid. Frayed fastener holes have been noted in several fairings. This condition is related to nonoptimum drilling and countersinking techniques used during assembly of the fairings in 1972. Several elongated fastener holes have been noted during the annual inspections. This condition is probably related to improper fit and nonuniform fastener load distribution for the fairings. None of the conditions noted above is considered to be major and, in general, the Kevlar/epoxy fairings performed similar to production fiberglass/epoxy fairings.

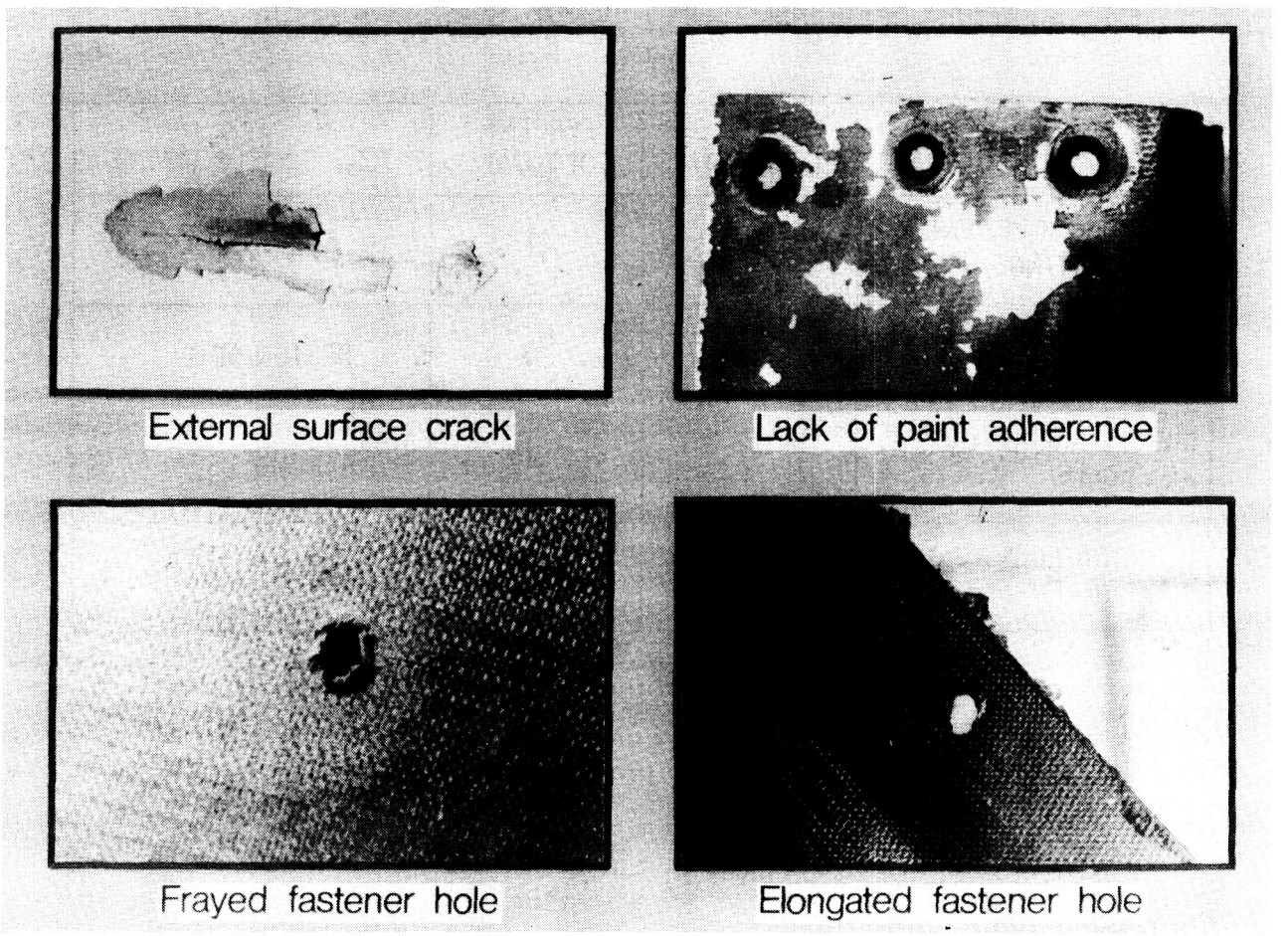

Figure 8

B-737 SPOILER IN-SERVICE DAMAGE AND REPAIR DURING 10 YEARS OF SERVICE

During the first 10 years of flight service, there have been 78 instances in which graphite/epoxy spoilers have received damage in service sufficient to require repair. Typical damage includes skin blisters, corrosion of the aluminum spar and doublers, miscellaneous cuts and dents, and trailing-edge delamination, as shown in figure 9. Over 40 percent of the damage incidents were caused by a design problem wherein actuator rod-end interference caused upper surface skin blisters. The actuator rods have been modified to prevent future damage. One-third of the repairs have been required as a result of corrosion damage to the aluminum spar and doublers. The corrosion initiated at a spar splice and is probably caused by moisture intrusion through a crack in the sealant material coupled with manufacturing defects in the aluminum surface preparation and corrosion protection scheme. There have been 12 incidents of cuts and dents caused by airline use and six trailing-edge delaminations that were apparently caused by normal aircraft maintenance and moisture intrusion. Minor repairs are currently being conducted by the airlines after proper instruction by Boeing. Because of the expense involved, spoilers with major damage are removed from service and retired from the program. Additional details on the spoiler inspection results are reported in reference 3.

PROBLEM	NUMBER OF INCIDENTS	PERCENT OF TOTAL	CAUSE
BLISTER ABOVE CENTER HINGE FITTING	34	44	DESIGN
SPAR AND DOUBLER CORROSION	26	33	DESIGN/MFG.
MISCELLANEOUS CUTS AND DENTS	12	15	AIRLINE USE
TRAILING-EDGE DELAMINATION	6	8	ENVIRONMENT

Figure 9

CORROSION OF B-737 GRAPHITE/EPOXY SPOILERS

Corrosion damage to the B-737 graphite/epoxy spoilers can be characterized by three phases of development (fig. 10). Phase 1 involves corrosion initiation at an aluminum fitting or at the aluminum spar splice. The corrosion is probably initiated by moisture intrusion through cracked paint and sealant material. If the corrosion is not repaired, the damage progresses to phase 2 where moisture is allowed to penetrate under the graphite/epoxy skin along the aluminum C-channel front spar. Normal service loads combined with the moisture contribute to crack initiation and subsequent corrosion between the graphite/epoxy skin and aluminum spar. If the phase 2 corrosion is not repaired, the damage progresses to phase 3 where extensive skin-to-spar separation takes place. The various phases of corrosion damage can result in significant spoiler strength reductions as will be shown in figure 11. There have been no incidents of galvanic corrosion between the graphite/epoxy skins and the aluminum honeycomb substructure. In addition, post-test teardown and core plug samples have not indicated any moisture intrusion into the aluminum honeycomb.

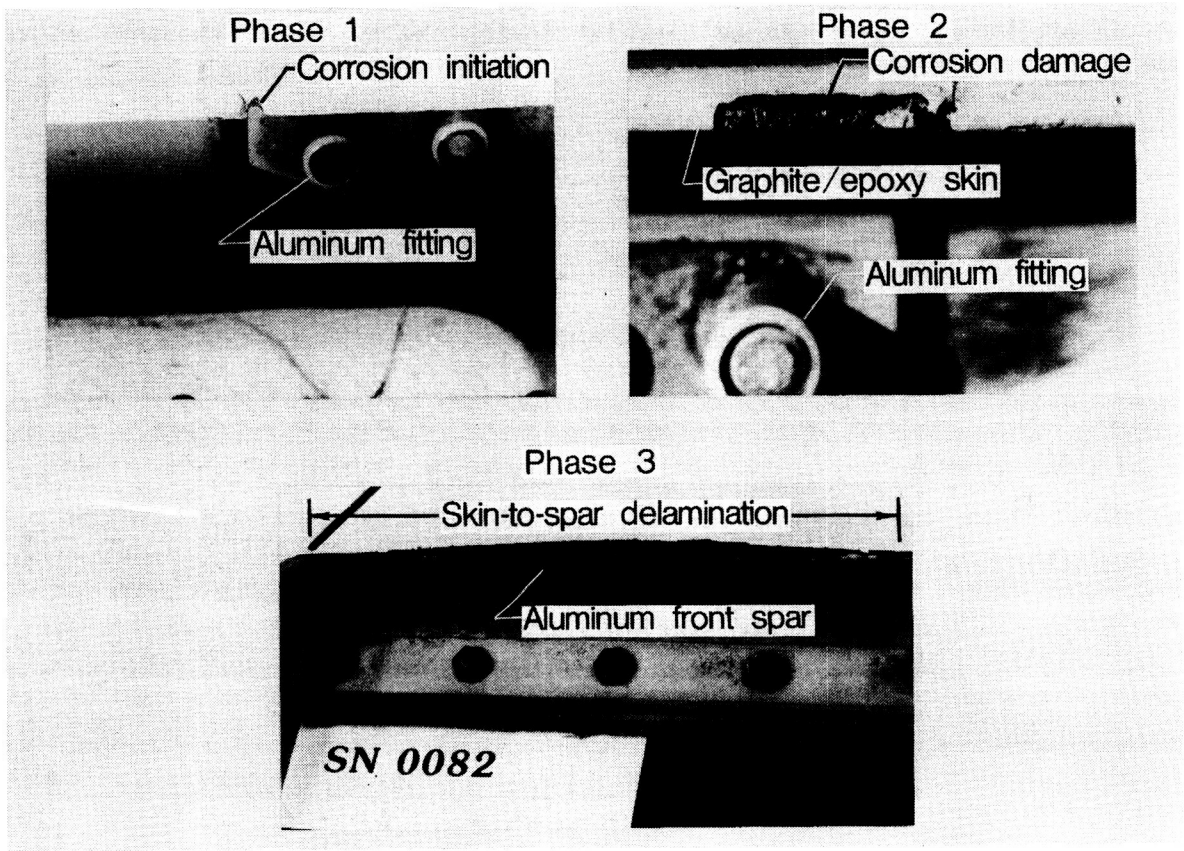

Figure 10

RESIDUAL STRENGTH OF GRAPHITE/EPOXY SPOILERS

Three graphite/epoxy spoilers, one of each material system used in fabricating the spoilers, have been removed from service annually for the past nine years to establish residual strengths. The test results are compared with the strength of 16 new spoilers in figure 11. The strength for each spoiler through six years of service generally falls within the same scatter band as was defined by the strengths of the new spoilers. However, spoilers with significant corrosion damage which were tested after seven and eight years of service, respectively, indicated a 35-percent strength reduction. An additional T300/2544 spoiler with essentially no corrosion damage was tested after seven and one-half years of service to verify that the seven-year strength reduction was in fact related to corrosion damage. Also, three spoilers tested after nine years of service with little or no corrosion damage exhibited strengths equal to the strength of new spoilers with no service hours. In general, spoilers that have been tested after being repaired have not shown any significant strength reduction due to the repairs. The NASA flight-service contract with Boeing has been extended to 15 years. Additional spoiler tests are planned to be conducted after 10, 12, and 15 years of service. Strength retention of the spoilers will be correlated with the size of disbonds that are caused by corrosion damage.

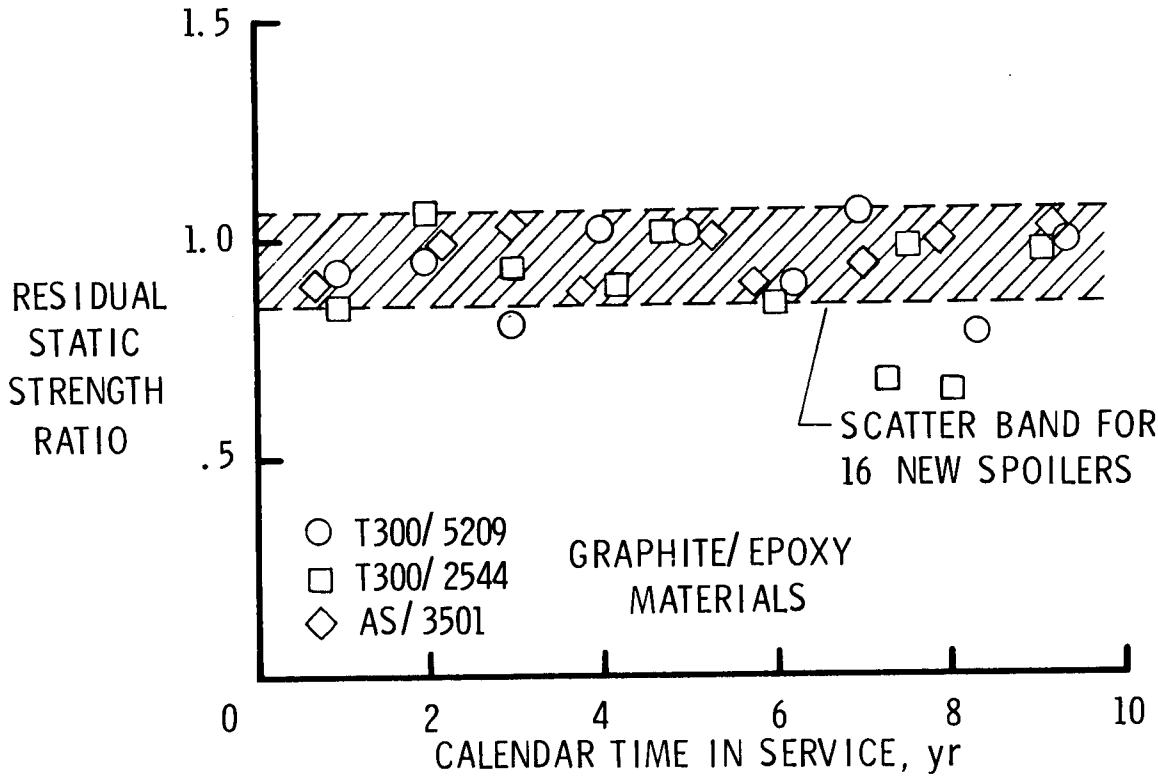

Figure 11

LOAD DEFLECTION RESPONSE OF T300/2544 GRAPHITE/EPOXY SPOILERS FOR B-737 AIRCRAFT

The load deflection respsonse of two T300/2544 graphite/epoxy spoilers tested after eight and nine years, respectively, is compared with a baseline (no service) spoiler in figure 12. The eight-year spoiler with 20,364 flight hours on Piedmont failed at 160 percent of limit load compared to 246 percent limit load for the baseline spoiler. The eight-year spoiler had doubler corrosion and some exfoliation corrosion of the aluminum spar. Note that the eight-year spoiler strength is still above the design ultimate load requirement as indicated in figure 12. The nine-year spoiler with 23,433 flight hours on Piedmont failed at 236 percent of limit load. The nine-year spoiler had some minor corrosion products near the center hinge fitting; however, the corrosion damage was not as severe as for the eight-year spoiler. The stiffness variation between the eight- and nine-year spoilers is typical of other spoilers tested throughout the program. In general, more extensive corrosion causes more skin-to-spar separation and a subsequent reduction in overall spoiler stiffness.

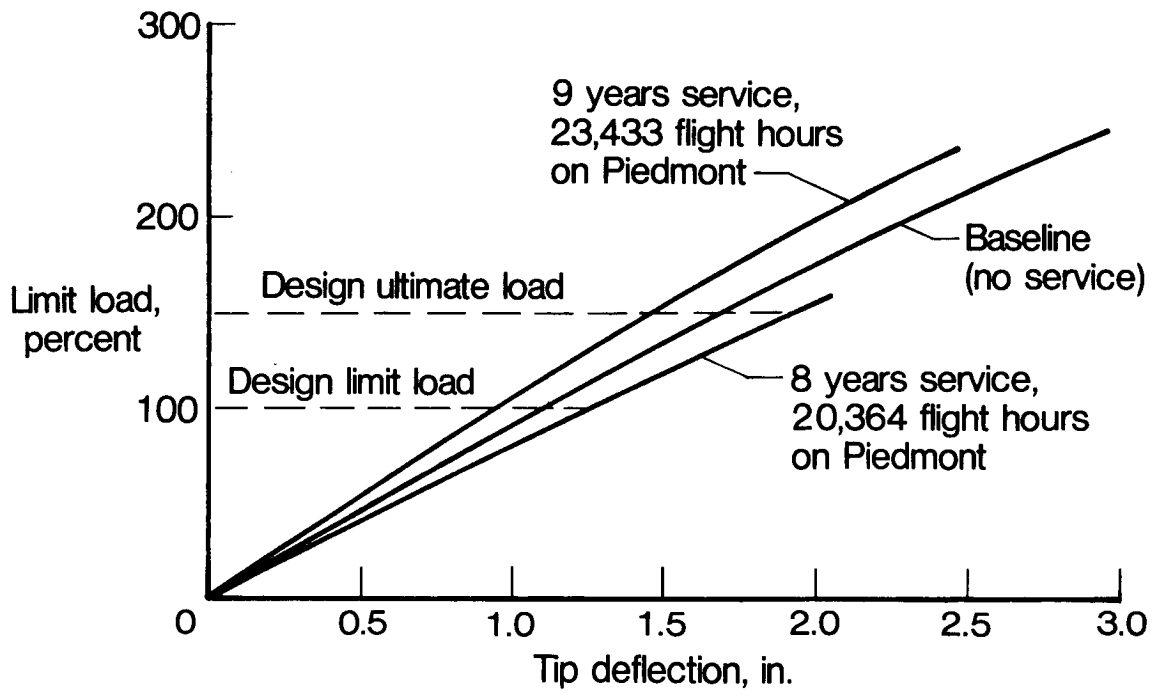

Figure 12

SPOILER MOISTURE LEVELS DETERMINED FROM PLUGS

In addition to structural tests of the spoilers, tests have been conducted to determine absorbed moisture content of the graphite/epoxy skins. The moisture content is determined from plugs cut near the trailing edge as shown in figure 13. The plugs consist of aluminum honeycomb core, two graphite/epoxy facesheets, two layers of epoxy film adhesive, and two exterior coats of polyurethane paint. About 90 percent of the plug mass is in the composite faces, including the paint and adhesive. The moisture content is determined by drying the plugs and recording the mass change. The data shown in figure 13 for plugs removed from three spoilers after nine years of service indicate moisture levels in the graphite/epoxy skins ranging from 0.59 to 0.90 percent for T300/5209, T300/2544, and AS/3501 material systems. The moisture levels for the T300/5209 and AS/3501 systems are similar to moisture levels determined for unpainted material coupons exposed to worldwide outdoor environments. However, the moisture content of 0.90 percent for the T300/2544 plugs is only about one-half the moisture content of the unpainted material coupons. Severe ultraviolet radiation degradation to the T300/2544 unpainted material coupons may explain part of the difference in moisture absorption. Additional results for the material coupons are presented in a subsequent figure.

9 YEARS SERVICE

GRAPHITE/EPOXY	MOISTURE CONTENT PERCENT	AIRLINE
T300/5209	0.59	LUFTHANSA
T300/2544	0.90	PIEDMONT
AS/3501	0.86	PIEDMONT

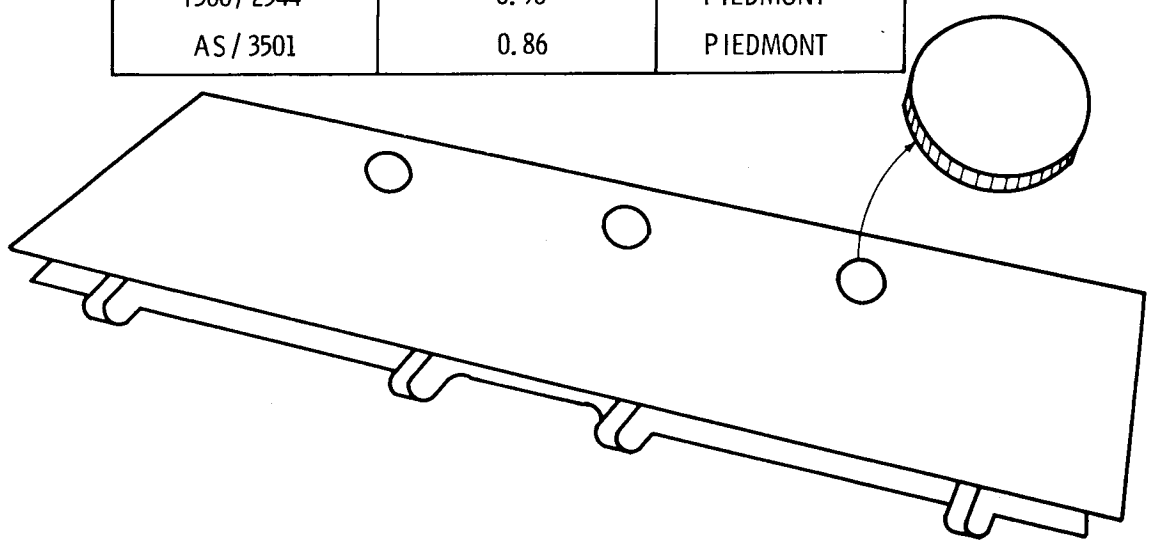

Figure 13

DC-10 GRAPHITE/EPOXY RUDDER DAMAGE

Six DC-10 graphite/epoxy rudders have sustained minor damage since entering into commercial service in 1976. There have been two rudders with minor rib-to-skin disbonds, three rudders with minor lightning strikes, and one rudder sustained rib damage during ground handling while the rudder was off the aircraft. Figure 14 shows photographs of the most severe lightning strike and the rib damage. The lightning damage was localized in an area measuring approximately 0.5 inch by 1.5 inches near the trailing edge of the structural box. Damage was limited to the outer four layers of graphite/epoxy and a room temperature repair was performed in accordance with procedures established at the time the rudders were certified by the FAA. The rib damage was more extensive and a portion of a rib had to be removed and rebuilt. A detailed discussion of the repair procedure is given in reference 11. After completion of the repair, the rudder was returned to the airline for continuation of service.

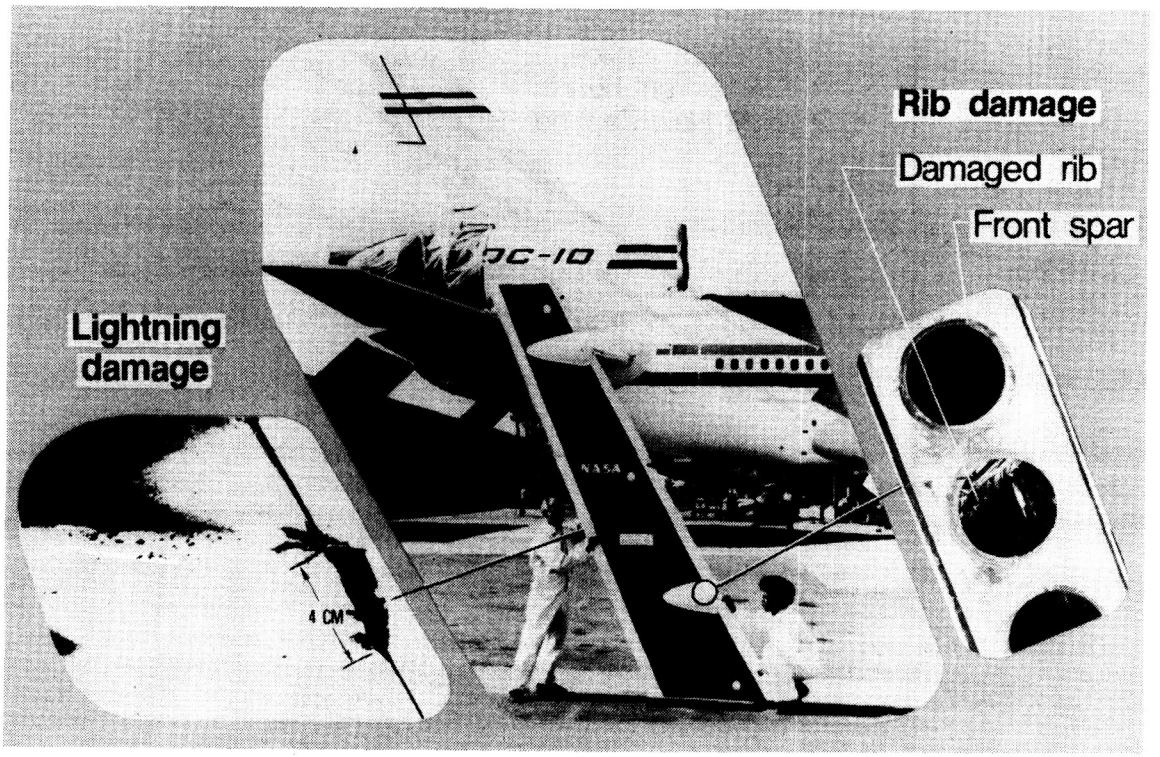

Figure 14

LOAD DEFLECTION RESPONSE OF T300/5208 GRAPHITE/EPOXY RUDDERS
FOR DC-10 AIRCRAFT

A DC-10 graphite/epoxy rudder was removed from service for residual strength testing after 5.7 years and 22,265 flight hours on Air New Zealand. The load deflection response shown in figure 15 indicates that the 5.7-year rudder had an initial stiffness higher than the baseline rudder but the overall response is similar for the two rudders. The baseline and the 5.7-year tests were stopped at approximately 400-percent limit load because of instability of the loading apparatus. Although the rudders are designed by stiffness considerations and only one residual strength test has been conducted, the overall response of the rudder indicates that no degradation has occurred as a result of 22,265 flight hours.

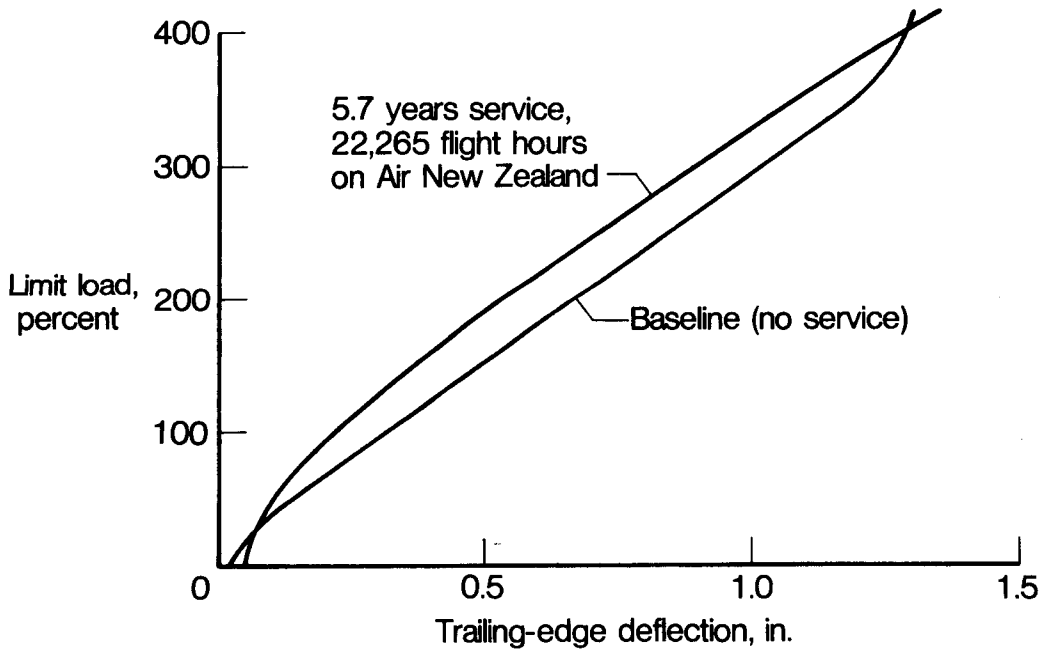

Figure 15

B-727 GRAPHITE/EPOXY ELEVATOR DAMAGE

Since initiation of flight service in 1980, there have been two B-727 graphite/epoxy elevators damaged by minor lightning strikes and two elevators damaged during ground handling. Figure 16 shows typical lightning damage to the trailing edge of an elevator and trailing-edge fracture of another elevator caused by impact from a deicing apparatus while the aircraft was being serviced. Damage from lightning strikes ranged in severity from scorched paint to a minor skin delamination. The most severe damage to an elevator occurred during a ground collision at Portland, Oregon, in 1982. Skin panels were punctured, four holes in the lower surface and one hole in the upper surface, and the lower horizontal flange at the front spar was cut inboard of the outboard hinge. All the elevator repairs were performed by United Airlines maintenance personnel in San Francisco, California. The lightning damage was repaired with epoxy filler and milled glass fibers. The skin punctures were repaired with T300/5208 prepreg fabric and Nomex honeycomb core plugs. The front spar was repaired with a machined titanium doubler, which was mechanically fastened to the lower skin flange of the spar chord.

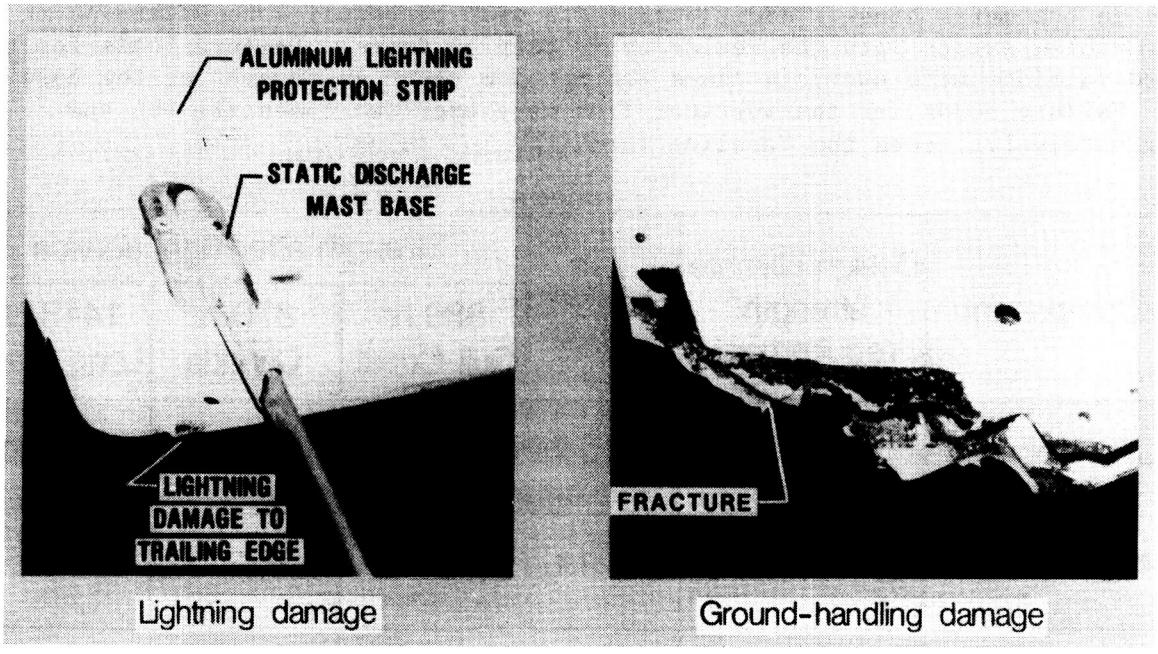

Figure 16

EFFECT OF ONE-YEAR FLIGHT SERVICE ON STRENGTH OF BELL 206L COMPOSITE COMPONENTS

Three sets of Bell 206L composite components have been statically tested after one year of flight service. The components were removed from helicopters flying in the following areas: U.S. Gulf Coast, Canada, and Long Island, NY, and had 880, 870, and 1413 flight hours, respectively, at the time of removal (figure 17). Average failure load for the litter doors was approximately 1.6 times the design ultimate load (DUL) and 85 percent of the baseline average strength. All litter doors failed by the latch pins slipping from the test fixture. The baggage door from the Gulf Coast failed at 1.8 times the DUL and 1.3 times the baseline average strength. The baggage door from Canada failed at 1.08 times the DUL and at 77 percent of the baseline average. The baggage door from Long Island failed at 63 percent of the DUL and 45 percent of the baseline strength. This baggage door failed by a large disbond between the outer skin and the honeycomb core. The lack of an adhesive layer between the outer skin and the honeycomb core could possibly explain the poor bond strength. The other baggage doors (U.S. Gulf Coast and Canada) failed in the metal hinge. Additional tests will be required to determine if a major problem exists with the Kevlar/epoxy baggage doors. Failure loads for the forward fairings were over six times the DUL and about 70 percent of the baseline load. Failure loads for the vertical fins were over two times the DUL and approximately 1.1 times the baseline load.

Component	Design ultimate strength requirement	Baseline strength	Strength after flight service		
			880 hr Gulf Coast	870 hr Canada	1413 hr Long Island
Litter door	634 lb	1215 lb	1009 lb	980 lb	1115 lb
Baggage door	440 lb	613 lb	795 lb	473 lb	275 lb
Forward fairing	0.30 psi	3.13 psi	1.80 psi	2.50 psi	1.80 psi
Vertical fin	1040 lb	2097 lb	2497 lb	2219 lb	2100 lb

Figure 17

EFFECT OF GROUND-BASED EXPOSURE ON STRENGTH OF COMPOSITE MATERIALS USED TO FABRICATE BELL 206L COMPONENTS

The average strength retention ratios for two material systems used in the 206L flight service components are shown in figure 18 after one and three years of outdoor exposure. Three different tests, short-beam shear (SBS), IITRI (Illinois Institute of Technology Research Institute) compression, and tension, were conducted to establish strength as a function of exposure time. The Kevlar/epoxy used in the baggage doors exhibited the lowest strength retention of the three Kevlar/epoxy material systems used in the components. The lowest strength retention, 0.85, was for compression specimens exposed at Ft. Greely, AK, and Toronto, Canada, after one and three years of exposure, repsectively. The specimens exposed for three years in Ft. Greely, AK, will be tested in the summer of 1984. The graphite/epoxy materials used in the vertical fin did not indicate any significant changes in strength after one or three years of exposure at any of the exposure locations indicated in figure 18. Additional tests will be conducted after 5, 7, and 10 years of exposure.

Material-component	Exposure location	Strength retention ratio*					
		1 yr exposure			3 yr exposure		
		SBS	COMP	TEN	SBS	COMP	TEN
Kevlar/ LRF-277 baggage door style 120 fab. (0/90/±45)	Cameron, LA	0.93	0.94	1.03	0.87	0.87	1.04
	Oil platform**	0.90	0.93	0.99	0.90	0.86	1.02
	Hampton, VA	0.97	0.89	1.00	0.90	0.90	1.03
	Toronto, Canada	0.95	0.89	1.04	0.90	0.85	1.05
	Ft. Greely, AK	0.88	0.85	1.02	—	—	—
T-300/E-788 vertical fin (0/±45/0)	Cameron, LA	1.01	1.03	0.97	1.01	0.91	1.01
	Oil platform**	1.02	1.00	0.97	1.04	0.93	1.01
	Hampton, VA	1.02	1.01	1.01	1.04	1.00	1.01
	Toronto, Canada	1.00	1.01	1.08	1.07	0.98	1.02
	Ft. Greely, AK	0.97	1.02	1.00	—	—	—

*Strength retention ratio = $\frac{\text{strength (exposed)}}{\text{strength (baseline)}}$

**Gulf of Mexico

Figure 18

EFFECT OF SERVICE ENVIRONMENT ON S-76 COMPOSITE TAIL ROTOR SPARS

Full-scale fatigue tests have been conducted on six graphite/epoxy S-76 tail rotor spars removed from commercial service and the results are shown in figure 19. Two spars had 25 months and 150 hours of service on a Sikorsky flight test helicopter in West Palm Beach, FL, and four of the spars were removed from helicopters operating in the Lake Charles, LA, area with up to 49 months and 3358 hours of service. The test results are compared to the baseline room temperature dry strength of 10 spars tested for FAA certification. The results indicate that the minimum strength retention is 93 percent of the FAA certification curve shown in figure 19. These results compare well with strength retention factors projected from laboratory-conditioned specimens (ref. 10). Additional tests will be conducted on tail rotor spars with up to eight years of service.

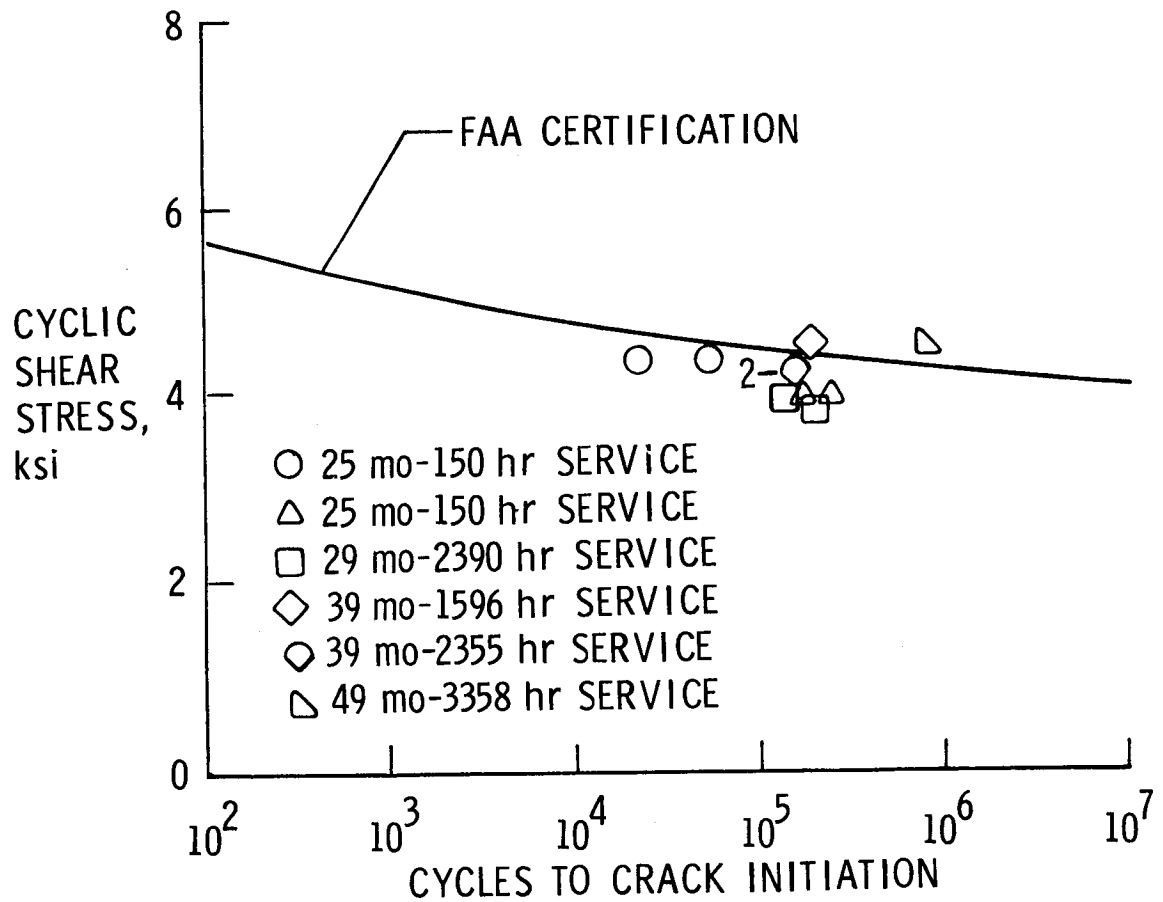

Figure 19

EFFECT OF THREE YEARS GROUND-BASED EXPOSURE ON STRENGTH OF SIKORSKY S-76 COMPOSITE MATERIALS

Results of tests conducted on specimens machined from panels exposed for three years at Stratford, CT, and West Palm Beach, FL, are shown in figure 20. Short-beam shear (SBS), flexure, and tension tests were conducted to establish strength retention factors. The lowest strength retention, 0.78, occurred for the 6-ply graphite/epoxy SBS specimens exposed at West Palm Beach, FL. In addition to strength tests, moisture contents were measured for all the panels after outdoor exposure and the results are shown in figure 20. Laboratory-conditioned specimens were tested during the design phase of the S-76 production program and strength as a function of moisture content was established (ref. 10). The SBS strength for the outdoor exposed specimens closely follows the trend for the laboratory-conditioned specimens. The three-year flexure strength for the outdoor-exposed specimens is slightly higher than the flexure strength for the laboratory conditioned specimens. The moisture content of coupons machined from two spars that had 37 months of service ranged from 0.46 to 0.55 percent. The coupons were removed from the 14-ply thick area of the spars and the results compare well with the 14-ply moisture data presented in figure 20 for three-years exposure at Stratford, CT.

Material	Number of plies	Exposure location	Measured moisture (percent weight)	Strength retention ratio*		
				SBS	Flexure	Tension
Graphite/epoxy	6	Stratford, CT	1.00	0.83	0.79	—
Graphite/epoxy	14		0.48	0.81	1.02	—
Graphite/epoxy	33		0.23	0.87	1.02	—
Kevlar/epoxy	5		1.72	—	—	1.06
Graphite/epoxy	6	W. Palm Beach, FL	1.22	0.78	0.80	—
Graphite/epoxy	33		0.37	0.89	0.98	—
Kevlar/epoxy	5		2.08	—	—	1.07

$$*\text{Strength retention ratio} = \frac{\text{strength (exposed)}}{\text{strength (baseline)}}$$

Figure 20

MOISTURE ABSORPTION OF 6-PLY GRAPHITE/EPOXY PANELS
EXPOSED AT WEST PALM BEACH, FL

A moisture absorption analysis was made for 6-ply graphite/epoxy panels exposed at West Palm Beach, FL (WPB). Average weather bureau data for WPB were used to generate the predicted moisture absorption curve shown in figure 21. The test points shown in figure 21 after two and three years of exposure are the average of four specimens machined from two panels. The test results are in good agreement with the predicted results.

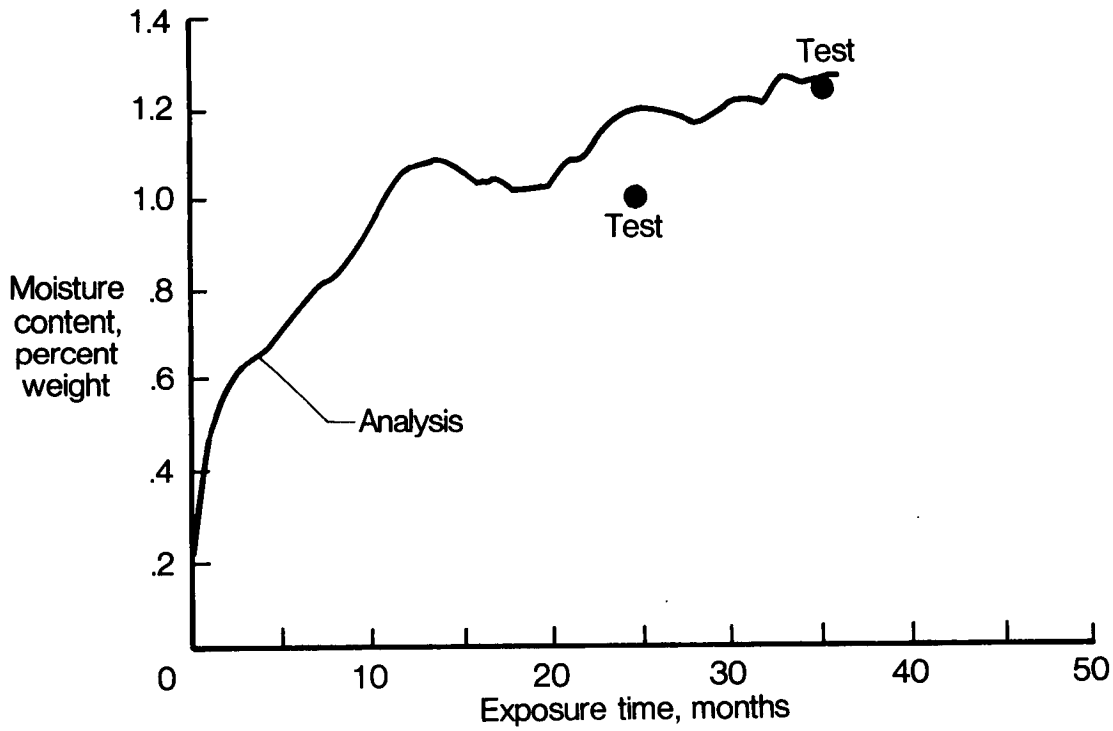

Figure 21

WORLDWIDE ENVIRONMENTAL EXPOSURE OF COMPOSITE MATERIALS
USED IN FLIGHT SERVICE PROGRAMS

Concurrent with the flight service evaluation of composite structural components, NASA Langley initiated a program to determine the outdoor environmental effects on composite materials used in fabrication of the flight components (fig. 22). Unstressed short-beam shear, compression, and flexure specimens have been exposed in racks outdoors for 10 years at NASA Langley in Hampton, VA; San Diego, CA; Honolulu, HA; Wellington, New Zealand; São Paulo, Brazil; and Frankfurt, W. Germany. Tension specimens under a sustained load of 25 percent ultimate have been exposed for 10 years at NASA Langley and San Francisco, CA. Residual strength tests have been conducted after 1, 3, 5, 7, and 10 years of exposure and the results are compared with baseline (no exposure) test results. In addition to strength tests, moisture absorption measurements have been made for six different composite material systems.

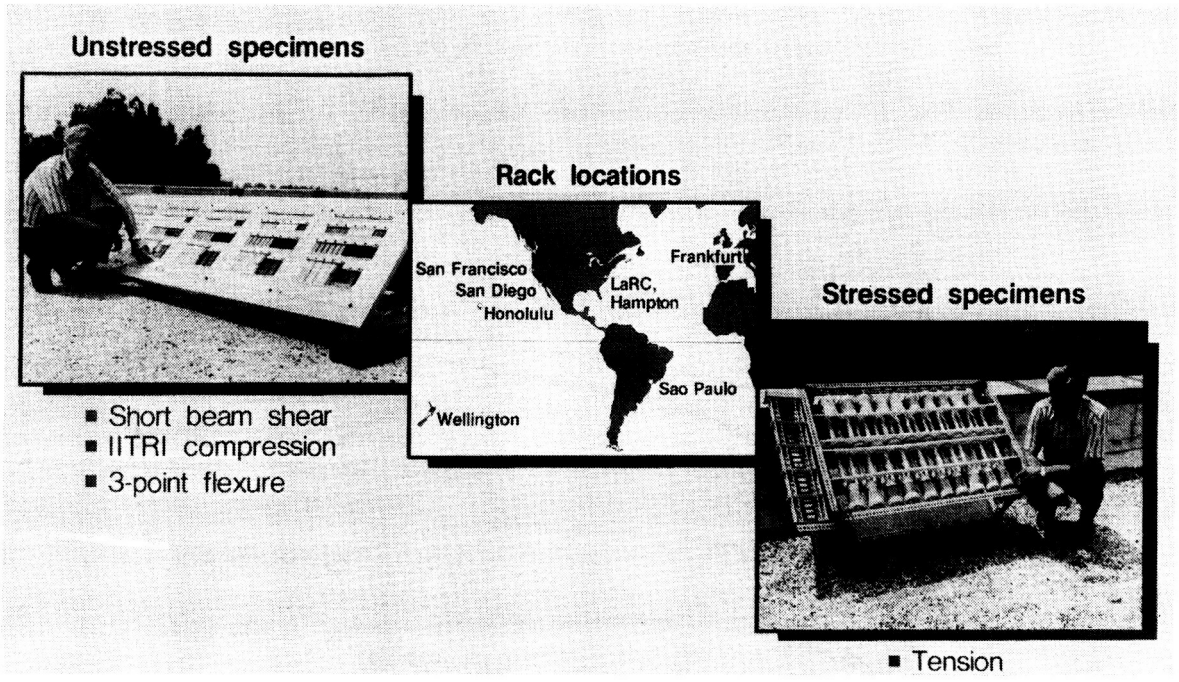

Figure 22

MOISTURE ABSORPTION OF COMPOSITE MATERIALS AFTER WORLDWIDE OUTDOOR EXPOSURE

The moisture contents of four graphite/epoxy and two Kevlar/epoxy material systems after seven years of exposure at six exposure sites are shown in figure 23. The data shown were obtained from flexure coupons that were exposed on outdoor racks located at NASA Langley in Hampton, VA; San Diego, CA; Honolulu, HA; Wellington, New Zealand; São Paulo, Brazil; and Frankfurt, W. Germany. Each data point represents an average value for 18 specimens, three at each of the six exposure locations. The Kevlar/epoxy materials indicate moisture levels above 2.0 percent after seven years of exposure. The T300/2544 graphite/epoxy material indicated a decrease in moisture content from 2.0 percent after five years of exposure to 1.8 percent after seven years of exposure. The reduction may possibly be related to severe ultraviolet degradation of the 2544 epoxy matrix. The AS/3501 graphite/epoxy material appears to have stabilized at about 1.0 percent moisture, although a slight downward trend is noted after seven years of exposure. The T300/5209 and T300/5208 graphite/epoxy materials appear to have stabilized at approximately 0.6 percent moisture. In general, the specimens exposed at São Paulo, Brazil, had the highest moisture content. This result is somewhat expected since the average annual relative humidity is about 80 percent at São Paulo. The specimens exposed for 10 years are currently being dried in an oven to establish moisture content.

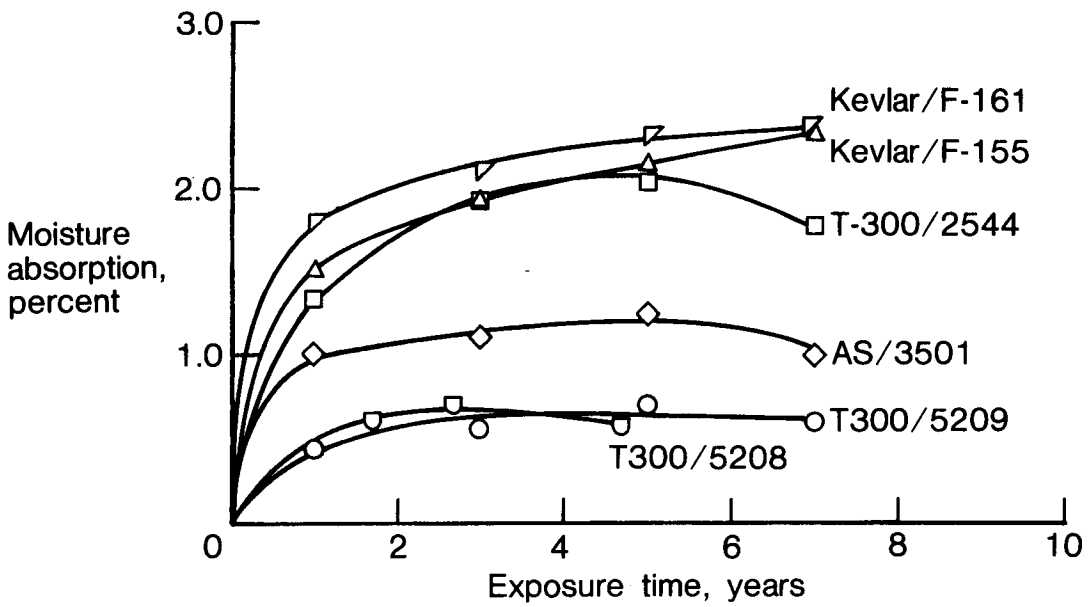

Figure 23

RESIDUAL STRENGTH OF COMPOSITE MATERIALS AFTER WORLDWIDE EXPOSURE

Residual strength data for unpainted graphite/epoxy and Kevlar/epoxy specimens exposed for 10 years at six exposure sites are shown in figure 24. The data points represent a comparison of the average strength value at six exposure sites with the average baseline strength value for that material system. The shaded area represents a plus-or-minus 10-percent scatter in the baseline strength values. Three-point flexure, IITRI compression, and short-beam shear tests were conducted on three replicate specimens after 1, 3, 5, 7, and 10 years of outdoor exposure. Since the T300/5208 material entered the exposure program at a later date, the exposure times are different than for the other five material systems. Also, the 10-year specimens from the Brazil exposure rack were not to be tested until the summer of 1984 because of a later deployment date. Results of the flexure tests indicate that the two Kevlar/epoxy materials and the T300/2544 graphite/epoxy material incurred the largest strength loss after 10 years of exposures. These three materials also had the highest moisture content, approximately 2.0 percent, and the T300/2544 material incurred the most severe surface degradation from ultraviolet radiation. The compression and shear tests indicate a similar trend in that the same three materials show the largest strength reduction after 10 years of exposure. Over the 10-year period the shear and compression specimens show a consistently slightly higher strength reduction than the flexure specimens. This trend indicates that the shear and compression specimens are more sensitive to matrix degradation and moisture than the flexure specimens.

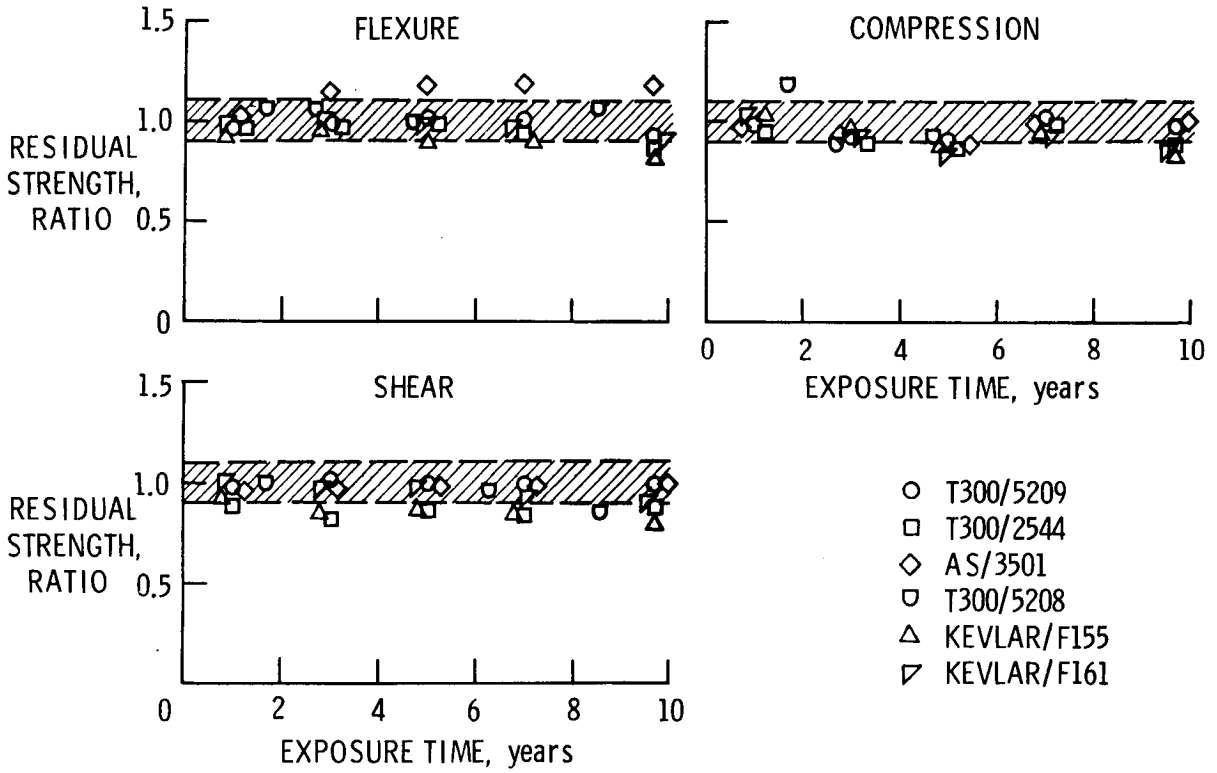

Figure 24

EFFECT OF EXPOSURE LOCATION AND TIME ON COMPRESSION STRENGTH OF COMPOSITE MATERIALS

Compression strength data for three material systems, T300/5209 (250°F cure), Kevlar-49/F-155 (250°F cure), and AS/3501 (350°F cure), are shown in figure 25 to indicate the effect of exposure location. Note that the 10-year Brazil data are not yet available. Each data point is the average of three tests for a particular exposure time and exposure location. Average annual temperature and relative humidity data obtained from the U. S. Air Force indicate that Frankfurt, W. Germany, has the lowest average annual temperature of 49°F and Honolulu, Hawaii, has the highest temperature of 77°F of the six exposure locations. The relative humidity is similar for most of the exposure locations with a range from about 70 percent in Hawaii to about 80 percent in Brazil. The data shown in figure 25 do not indicate any definite trend for the most severe environment. The Kevlar-49/F-155 material shows a consistent compression strength reduction during the 10-year period. A maximum reduction of 27 percent is shown for the specimens exposed in Hawaii. The data for the T300/5209 and AS/3501 materials are somewhat more erratic with the maximum strength reduction occurring after five years of exposure at New Zealand.

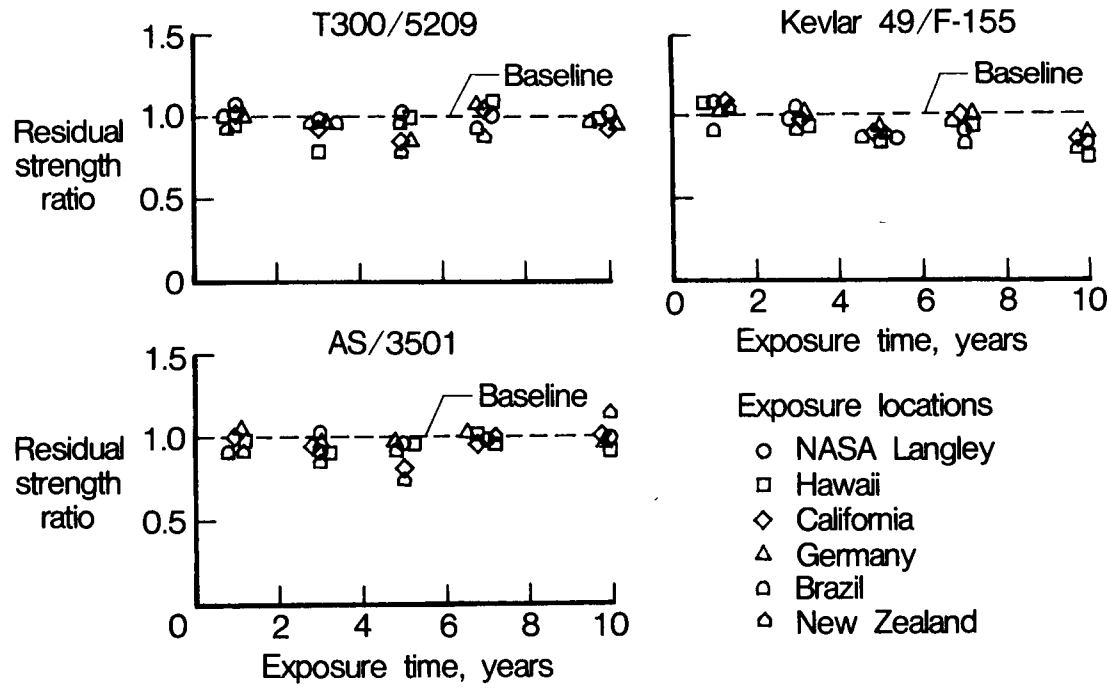

Figure 25

SURFACE DEGRADATION OF UNPAINTED COMPOSITE MATERIALS

Scanning electron micrographs were taken of AS/3501 graphite/epoxy and Kevlar-49/F-155 flexure specimens with no outdoor exposure and seven years of outdoor exposure. The micrographs shown on the left of figure 26 indicate that the surface fibers are coated with resin for the specimens with no outdoor exposure. The micrographs on the right of figure 26 indicate that the surface fibers are exposed due to ultraviolet degradation of the surface layer of epoxy. These micrographs substantiate the need to keep composite aircraft structure painted to prevent utlraviolet radiation damage to composite matrix materials. Controlled laboratory weatherometer test results reported in reference 12 indicated that polyurethane aircraft paint offered substantial protection against ultraviolet degradation.

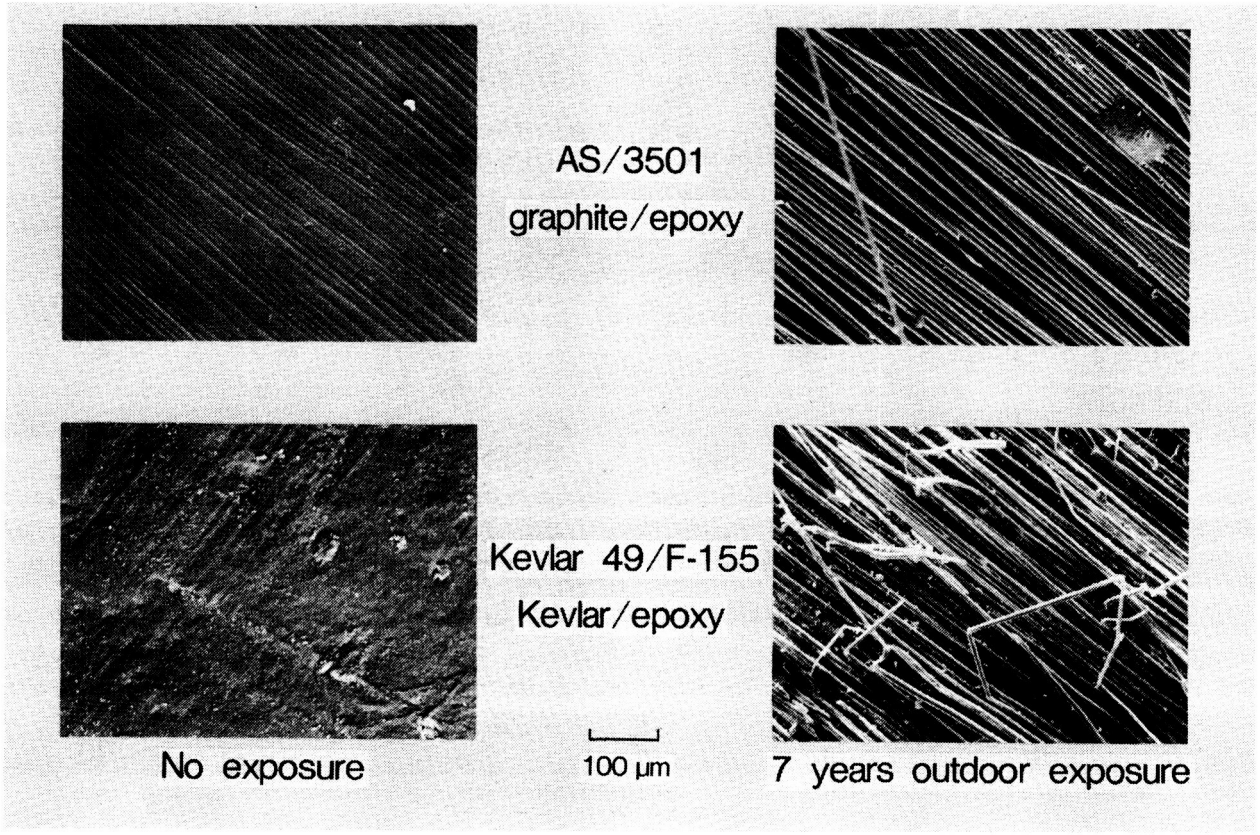

Figure 26

RESIDUAL TENSILE STRENGTH AFTER SUSTAINED-STRESS OUTDOOR EXPOSURES

Effects of sustained-stress during outdoor environmental exposure are being evaluated by exposing tension specimens to 40 percent of ultimate baseline strength. Residual tensile strengths of T300/5208 quasi-isotropic laminated specimens after seven years of outdoor exposure at the Langley Research Center in Hampton, VA, and San Francisco, CA, are shown in figure 27. The residual tensile strength is within the scatter band for the strength of unexposed specimens. Results indicate that the T300/5208 quasi-isotropic tensile specimens were unaffected by either outdoor environment or sustained tensile stress at the two exposure sites indicated. Additional data will be obtained after 10 years of outdoor exposure.

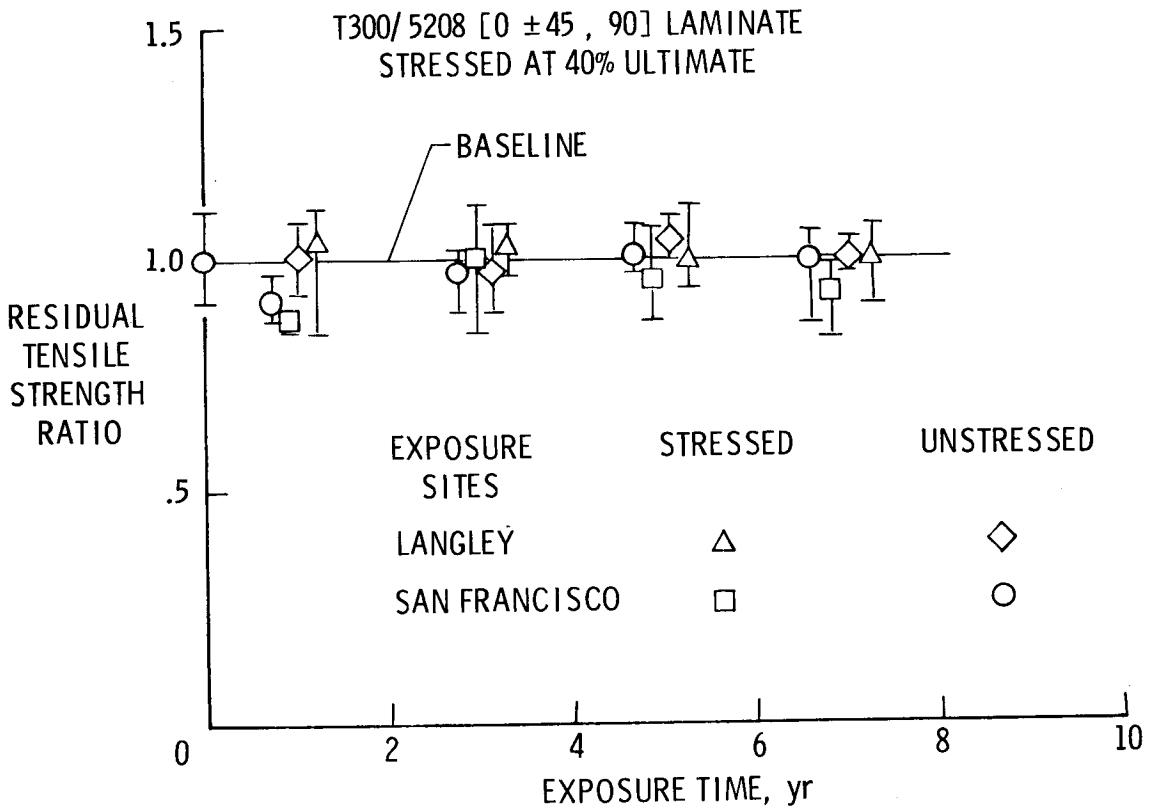

Figure 27

EFFECT OF AIRCRAFT FLUIDS ON COMPOSITE MATERIALS AFTER FIVE YEARS OF EXPOSURE

Although aircraft composite structures are exposed almost continuously to various levels of moisture in the atmosphere, they are frequently exposed to various other fluids used in aircraft such as fuel and hydraulic fluid. The effects of various combinations of these fluids on composite materials have been evaluated after five years of exposure. Specimens were exposed to six different environmental conditions as follows: ambient air, water, JP-4 fuel, Skydrol hydraulic fluid, fuel/water mixture, and fuel/air cycling. The water, JP-4 fuel, and Skydrol were replaced monthly to maintain fresh exposure conditions. Specimens exposed in the fuel/water mixture were positioned with the fuel/water interface at the center of the test specimens. The fuel/air cycling environment consisted of 24 hours of fuel immersion followed by 24 hours of exposure to air. Residual tensile strengths of T300/5208 graphite/epoxy, T300/5209 graphite/epoxy, and Kevlar-49/5209 specimens after strength exposure to the six environments are shown in figure 28. The residual tensile strength of T300/5208 was not degraded by any of the six environments indicated in figure 28. The most degrading environment on the T300/5209 and Kevlar-49/5209 materials was the fuel/water combination. The T300/5209 specimens lost about 11 percent in tensile strength, whereas the Kevlar-49/5209 specimen lost about 25 percent in tensile strength. The ambient air results are consistent with other data obtained from the NASA Langley sponsored ground and flight environmental studies. The tests reported in figure 28 were more severe than actual aircraft flight exposures and the results should represent an upper bound on material property degradation. Additional details on the five-year exposure program, including interlaminar shear test results, can be found in reference 13.

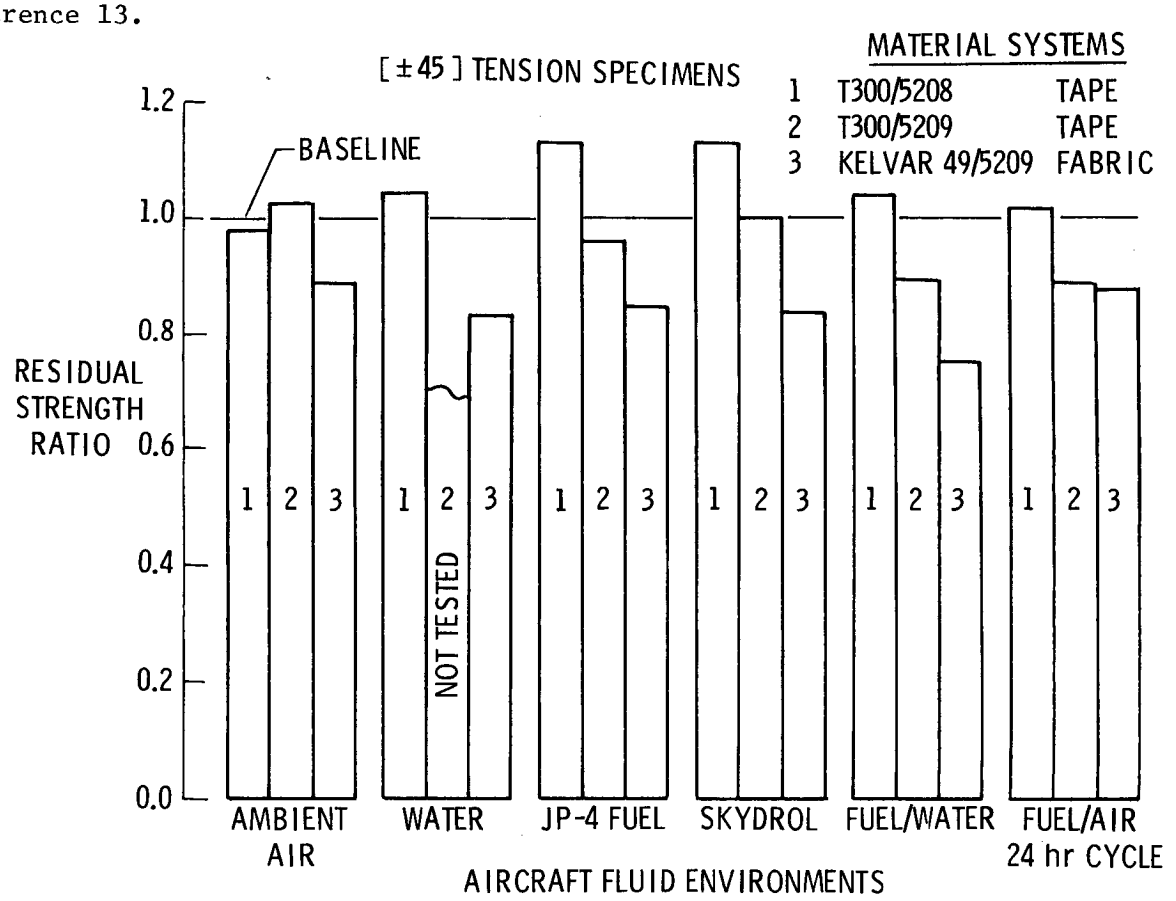

Figure 28

OUTDOOR SUSTAINED-LOAD ENVIRONMENTAL TESTS ON GRAPHITE/EPOXY BOLTED WING SPLICES

Graphite/epoxy panels with bolted joints representative of commercial transport wing splices are being exposed outdoors under a sustained load of 25 percent of the static ultimate to establish the effect of environment on residual strength. The test specimens are installed in loading frames as shown in figure 29. The laminates are approximately 0.50-inch thick and were designed to support a static load of 15,000 pounds/inch. The two configurations that are being tested are 7.5-inch wide T300/5209 graphite/epoxy panels with a double row of fasteners and 8.0-inch wide T300/5208 panels with a single row of fasteners. In addition to sustained-load outdoor exposure for 1, 3, 5, 7, and 10 years, 0.4 lifetimes of spectrum fatigue loads are being applied to the test panels at the end of each year of exposure. Therefore, the 10-year test panel will have 10 years of sustained-load exposure plus an accumulation of four lifetimes of fatigue loading. Test results after 1, 3, and 5 years of exposure are shown in figure 30.

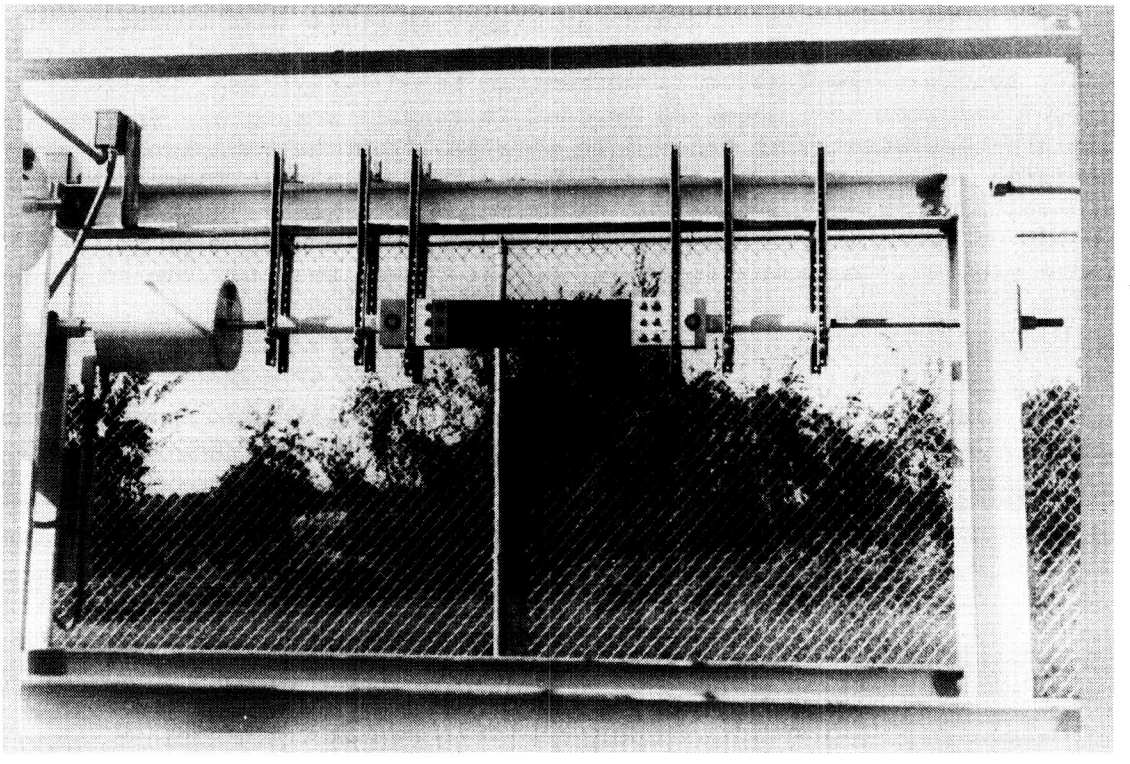

Figure 29

EFFECT OF OUTDOOR EXPOSURE AND LOAD HISTORY ON STRENGTH OF GRAPHITE/EPOXY BOLTED WING SPLICES

Test results for outdoor-exposed graphite/epoxy panels representative of commercial transport bolted wing splices are shown in figure 30. Baseline panels with no outdoor exposure were tested with no fatigue loading and 4.0 lifetimes of fatigue loading. The results shown in figure 30 indicate that the 4.0 lifetimes of fatigue loading did not degrade the strength of the panels. The T300/5209 panel tested after five years of sustained load at 25 percent of static ultimate and an accumulation of 2.0 lifetimes of fatigue loading did not show any significant strength reduction. The five-year T300/5208 panel incurred a 7.5 percent strength reduction. The scatter band for these tests is not known since only one panel is being tested at each test condition, including the baseline. Additional tests are planned after 7 and 10 years of outdoor exposure and additional fatigue loading.

Static strength	Constant load exposure (years) (25% ultimate)	Fatigue loading (lifetimes)	Failure load (kips)	
			Material and joint configuration	
			T300/5209 double row	T300/5208 single row
Baseline	0 0	0 4.0	120.0 119.0	117.8 119.0
Residual	1 3 5 7 10	0.4 1.2 2.0 2.8 4.0	117.2 117.2 116.5 2/85 2/88	113.0 110.7 109.0 N/A 3/89

Figure 30

CONCLUDING REMARKS

The NASA Langley Research Center has sponsored design, development, and flight service evaluation of over 300 composite components for transport aircraft and helicopters. Key findings of these programs are summarized in figure 31. Good in-service performance and maintenance experience have been achieved during 10 years and over three million total component flight hours. Boeing 737 graphite/epoxy reinforced aluminum spoilers have incurred design-related corrosion damage and strength reduction up to 35 percent after seven years and approximately 20,000 flight hours of service. Disbonds have been noted between Kevlar/epoxy facesheets and Nomex honeycomb core on a Bell 206L baggage door, and a strength reduction of about 50 percent resulted. Additional tests are required to establish if a problem exists with other baggage doors.

No significant room temperature strength reductions have been noted for several unpainted composite material systems after 10 years of worldwide outdoor exposure. Test results indicate that Kevlar/epoxy composites absorb more moisture than most widely used graphite/epoxy composites. Composite materials must be kept painted with standard aircraft paint to protect the matrix from ultraviolet degradation. Test results for graphite/epoxy panels with bolted joints representative of transport aircraft wing splices did not indicate any significant strength reduction after five years of sustained-load outdoor exposure and accumulated fatigue cycles of 2.0 lifetimes.

Confidence developed through NASA-sponsored programs for service evaluation of transport aircraft and helicopter components, long-term environmental test results, and advanced composite components developed under the ACEE Program has led transport and helicopter manufacturers to make production commitments to selected composite components.

- Good service performance with over 300 composite components during 10 years and three million flight hours
- Corrosion damage to B-737 graphite/epoxy spoilers resulted in 35 percent strength reduction after 7 years service
- No significant strength reduction for composite materials after 10 years outdoor exposure
- Strength of bolted wing splices not affected by fatigue, sustained load, or 5 years outdoor exposure

Figure 31

REFERENCES

1. Stone, R. H.: Flight Service Evaluation of Kevlar-49/Epoxy Composite Panels in Wide-Bodied Commercial Transport Aircraft - Tenth and Final Annual Flight Service Report. NASA CR-172344, June 1984.

2. Stone, R. H.: Flight Service Evaluation of Advanced Composite Ailerons on the L-1011 Transport Aircraft - First Annual Flight Service Report. NASA CR-172246, September 1983.

3. Coggeshall, Randy L.: 737 Graphite Composite Flight Spoiler Flight Service Evaluation - Seventh Annual Report. NASA CR-165826, February 1982.

4. McCarty, John E. and Wilson, David R.: Advanced Composite Stabilizer for Boeing 737 Aircraft. Proceedings of the Sixth Conference on Fibrous Composites in Structural Design. Army Materials & Mechanics Research Center, AMMRC MS 83-2, November, 1983.

5. Lehman, G. M.: Flight-Service Program for Advanced Composite Rudders on Transport Aircraft - First Annual Summary Report. NASA CR-145385, July 1977.

6. Elliott, S. Y.: Boron/Aluminum Skins for the DC-10 Aft Pylon. NASA CR-132645, May 1975.

7. McCarty, John E., et al: Advanced Composite Elevator for Boeing 727 Aircraft. Volume I - Technical Summary. NASA CR-3290, March 1981.

8. Zinberg, Herbert: Flight Service Evaluation of Composite Components on the Bell Model 206L: Design, Fabrication, and Testing. NASA CR-166002, November 1982.

9. Zinberg, Herbert: Flight Service Evaluation of Composite Components on the Bell Model 206L - First Annual Flight Service Report. NASA CR-172296, March 1984.

10. Rich, Melvin J. and Lowry, David W.: Flight Service Evaluation of Composite Helicopter Components - First Annual Report. NASA CR-165952, June 1982.

11. Kam, C. Y. and Gaidulis, Juris: Flight Service of Composite Structures on McDonnell Douglas Commercial Airplanes. Published in the proceedings of the 15th National SAMPE Technical Conference, pp. 251-262, October 1983.

12. Dexter, H. Benson and Chapman, Andrew J.: NASA Service Experience with Composite Components. Published in the proceedings of the 12th National SAMPE Technical Conference, pp. 77-99, October 1980.

13. Tanimoto, E. Y.: Effects of Long-Term Exposure to Fuels and Fluids on Behavior of Advanced Composite Materials. NASA CR-165763, August 1981.

Page intentionally left blank

COMPARISON OF TOUGHENED COMPOSITE LAMINATES USING NASA STANDARD DAMAGE TOLERANCE TESTS

Jerry G. Williams
NASA Langley Research Center
Hampton, Virginia

T. Kevin O'Brien
Army Structures Laboratory, USARTL (AVSCOM)
Hampton, Virginia

A. J. Chapman III
NASA Langley Research Center
Hampton, Virginia

ACEE COMPOSITE STRUCTURES TECHNOLOGY CONFERENCE

Seattle, Washington

August 13-15, 1984

INTRODUCTION

Composite structures technology for large transport aircraft has been successfully developed through contracts sponsored by the NASA Aircraft Energy Efficiency (ACEE) Project Office. Secondary and empennage composite components developed to replace metal structures on existing transport aircraft have demonstrated weight reductions of twenty to twenty-eight percent. The success of the NASA sponsored programs has encouraged manufacturers to employ composite structures in numerous components of their new generation transport aircraft. To translate the weight saving potential of composites into significant increases in operating efficiency, NASA is currently sponsoring contract programs with the commercial transport manufacturers to develop the technology required to design and build composite wing and fuselage structures.

An important consideration in attaining the potential structural efficiency improvements with resin matrix composite structures is the need to improve their resistance to impact damage which may occur in normal service, and to improve resistance to delamination which could result from unforseen out-of-plane loads. Such improvements would enable the use of higher design strains and avoid penalizing factors to account for reduced structural properties resulting from damage or unforseen loads. To meet the need for improved damage tolerance, the manufacturers of composite materials are developing materials having tougher resin matrices, where toughness is defined as the ability to deform elastically under interlaminar shear and peel stresses without the brittle fracture characteristic of the first generation resin matrices which are currently in use.

To promote systematic evaluation of the new materials, NASA and industry representatives have selected and standardized a set of five common tests for characterizing the toughness of resin matrix/graphite fiber composites. Procedures and specifications for these tests are described in Reference 1. Notch sensitivity is evaluated through open hole tension and open hole compression tests. Impact damage tolerance is evaluated through compression test following impact at selected energy levels. Resistance to delamination is evaluated through tension edge-delamination tests and double cantilever beam tests.

Several new resin/graphite fiber materials have been subjected to standard damage tolerance tests and results are compared to ascertain which materials may have superior toughness. In addition, test results from the various company and NASA laboratories are compared to indicate repeatability of test results and feasibility for developing a common data base. The materials tested represent the aircraft manufacturers' initial selection of newer toughened resin composites, and do not represent an endorsement of or commitment to use any particular material.

NASA/INDUSTRY STANDARD DAMAGE TOLERANCE TEST HISTORY

Proposed application of composites to transport wing and fuselage structures has prompted the search for tougher materials having improved resistance to impact damage and delamination. To evaluate the toughness of new materials against the more demanding requirements, NASA and the ACEE Contractors have identified and selected a set of "standard tests" which are now used by all of the ACEE Contractors as well as researchers at the Langley Research Center (figure 1). The tests were selected through workshops involving both NASA and Contractor representatives.

The need for standard evaluation of newly available toughened composites was agreed upon during the initial Peer Review for the Composite Wing Key Technology programs, held at Lockheed (Burbank, CA) during November 1981. Following this initial agreement, a workshop was held at Boeing (Seattle, WA) in December 1981, during which five tests were selected and specifications and procedures were worked out and mutually agreed upon. Each test was sponsored by one representative having wide experience with its application and results.

The five selected tests evaluate interlaminar fracture toughness (edge delamination tension and double cantilever beam tests), notch sensitivity (open-hole tension and compression tests), and the effect of impact damage on compression strength. Specifications and procedures for the standard tests are published in NASA Reference Publication 1092 (ref. 1) which is available for general distribution.

- NASA and ACEE contractors identified mutual need for standard test methods to evaluate merit of new toughened resin and fiber materials
- Test methods selected through NASA/Industry workshops
  - Key technology peer review - Lockheed - November 1981
  - Standard tests workshop - Boeing - December 1981
- Proposed tests
  - Interlaminar fracture toughness
    - Edge delamination
    - Double cantilever beam
  - Damage tolerance
    - Open-Hole tension and compression
    - Compression after impact
- NASA Reference Publication 1092: "Standard Tests for Toughened Resin Composites"
  - Published May 1982
  - Revised 1983

Figure 1

Specimens used in the five standard damage tolerance tests designated ST1 through ST5 are shown drawn to the same scale in figure 2. Details of the specimens and test methods are described in reference 1. A quasi-isotropic laminate approximately 0.25 in. thick is specified for compression after impact (ST1), open hole tension (ST3), and open hole compression (ST4) tests. Two different orthotropic laminates designed to yield high transverse normal tension stresses are used in the edge delamination test (ST2) and a unidirectional laminate is used for the double cantilever beam test (ST5). An impact energy of 20 ft-lb obtained by dropping a 10-lb weight with a 0.5-in diameter hemispherical tip a distance of 2 feet is the specified impact test condition.

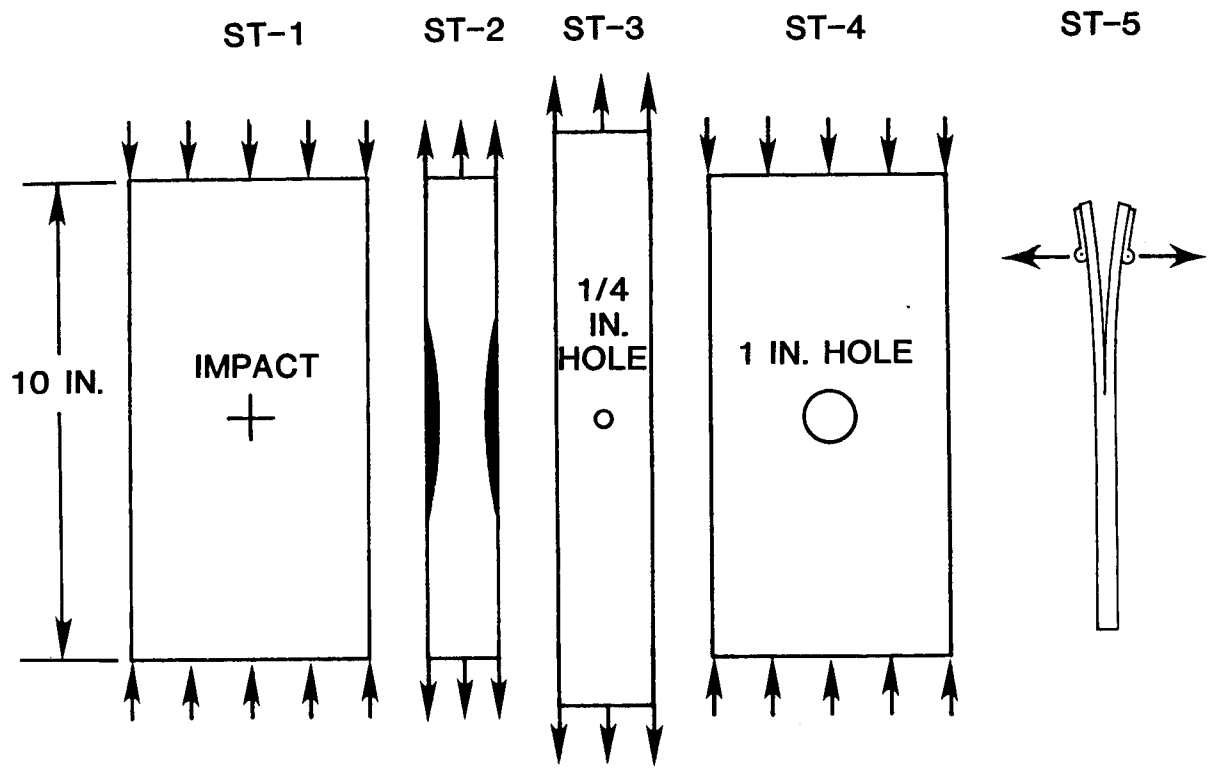

Figure 2

MATERIALS SYSTEMS

The eighteen materials systems studied in the current investigation along with the corresponding fiber and resin suppliers are presented in figure 3. The materials systems include combinations of seven fibers and thirteen resins provided by eight individual suppliers. Data for materials systems 1 and 2 are provided as a baseline for comparison purposes. T300/5208 is representative of the deficiency characteristic of most currently popular materials relative to reduced compression strength following impact damage (refs. 2, 3). Improved performance following impact damage has been demonstrated for several materials systems including T300/BP907 (ref. 4). Most of these toughened materials, however, have reduced strength properties at elevated temperatures or other deficiencies. Materials systems 3, 6-8, and 10-15 were selected by either Boeing, Douglas, or Lockheed for evaluation as toughened material candidates for evaluation under the NASA ACEE program. Data for materials systems 9, 16, and 17 were made available by Lockheed from independent study. Data for materials system 18 is taken from reference 5.

No.	Fiber	Resin	Fiber Supplier	Resin Supplier	Laminate Fabricator
1	● T300	5208	Union Carbide	Narmco	NASA
2	■ T300	BP907	Union Carbide	Amer. Cyanamid	NASA
3	T300	914	Union Carbide	Ciba Geigy	Douglas
4	T700	BP907	Union Carbide	Amer. Cyanamid	NASA
5	AS4	3502	Hercules	Hercules	NASA
6	AS4	2220-1	Hercules	Hercules	Lockheed
7	AS4	2220-3	Hercules	Hercules	Boeing
8	AS4	5245C	Hercules	Narmco	Boeing
9	AS6	2220-1	Hercules	Hercules	Lockheed[a]
10	AS6	2220-3	Hercules	Hercules	Boeing
11	AS6	5245C	Hercules	Narmco	Boeing
12	Celion	982	Celanese	Amer. Cyanamid	Lockheed
13	Celion HS	2566	Celanese	Ciba Geigy	Douglas
14	Celion HS	1504	Celanese	Hexcel	Lockheed
15	Celion HS	5245	Celanese	Narmco	Lockheed
16	Celion HS	806-2	Celanese	Amer. Cyanamid	Lockheed[a]
17	Celion HS	HST-7	Celanese	Amer. Cyanamid	Lockheed[a]
18	Courtaulds	Peek APC-1	ICI	ICI	ICI[b]

a Data from independent study
b Reference 5

Figure 3

EDGE DELAMINATION TENSION TEST MEASURES INTERLAMINAR FRACTURE TOUGHNESS (ST-2)

A simple tension test has been developed for measuring the interlaminar fracture toughness of composites made with toughened matrix resins (refs. 6-10). The test involves measuring the modulus, E_{LAM}, and the nominal strain at onset of edge delamination, ε_c, during a tension test of an 11-ply $[\pm 30/\pm 30/90/\overline{90}]_s$ or an 8-ply $[\pm 35/0/90]_s$ laminate (fig. 4). These quantities, along with the measured thickness, t, are substituted into a closed form equation for the strain energy release rate, G, for edge delamination growth in an unnotched laminate (ref. 6). The E* term in the equation is the modulus of the laminate if the 0/90 interface is completely delaminated. The delamination modulus, E*, may be calculated from the simple rule of mixtures equations shown in the figure by using laminated plate theory to calculate the sublaminate moduli. The critical value of G_c at delamination onset is a measure of the interlaminar fracture toughness of the composite. Furthermore, finite element analysis of the two edge delamination test (EDT) layups indicates that the $[\pm 30/\pm 30/90/\overline{90}]_s$ layup consisted of 57 percent G_I due to interlaminar tension, whereas the $[\pm 35/0/90]_s$ layup consisted of nearly 90 percent G_I. In both cases, the remainder of G was due to G_{II}, resulting from interlaminar shear. Both of these layups were used to measure the interlaminar fracture toughness of toughened resin composites (ref. 1).

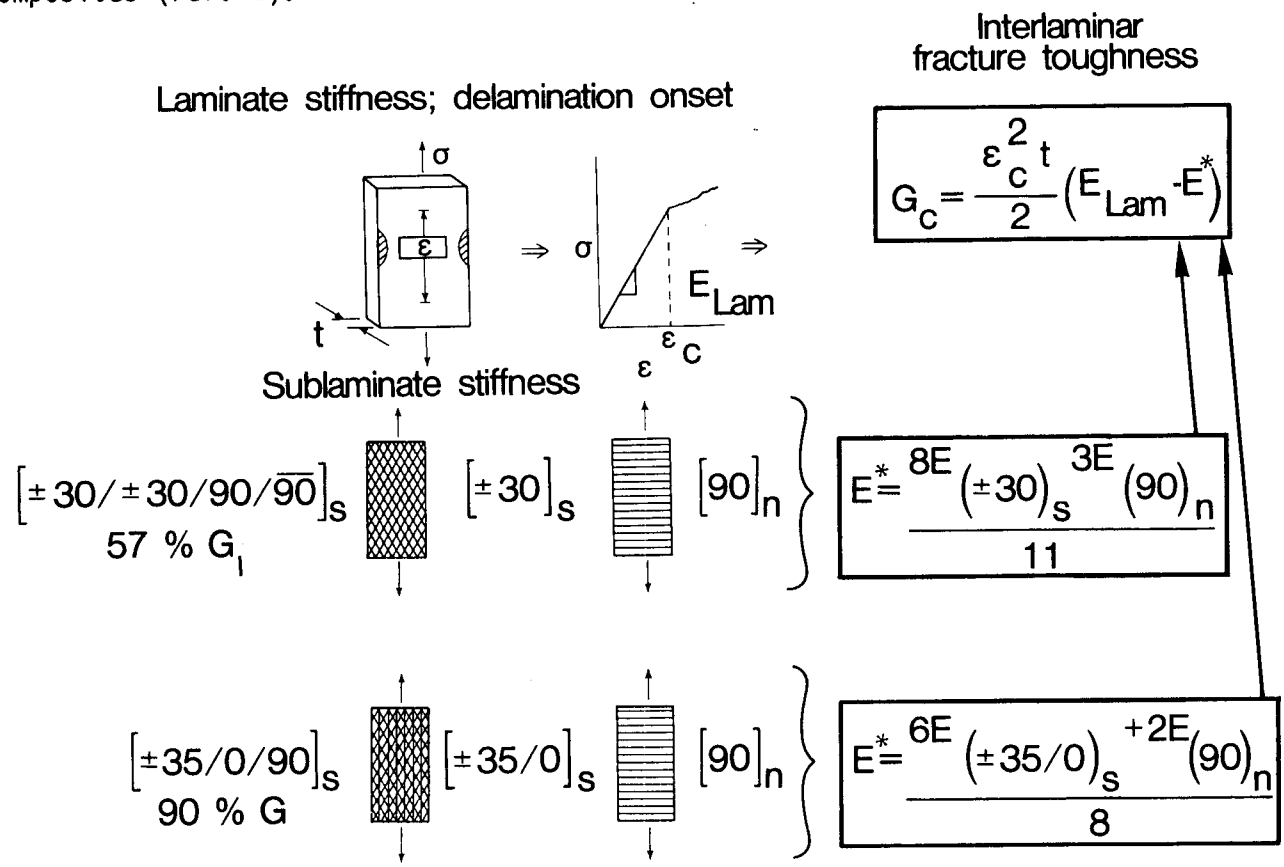

Figure 4

EDGE DELAMINATION TEST REPEATABILITY

Figures 5 and 6 show G_c values for five different graphite reinforced composite materials measured using the $[\pm 30/+30/90/\overline{90}]_s$ and $[\pm 35/0/90]_s$ edge delamination tests, respectively. Each material was tested by NASA Langley and by one of the key technologies contractors (Lockheed, Boeing, or Douglas). As the figures indicate, good repeatability of G_c measurements was achieved from tests conducted at the different laboratories.

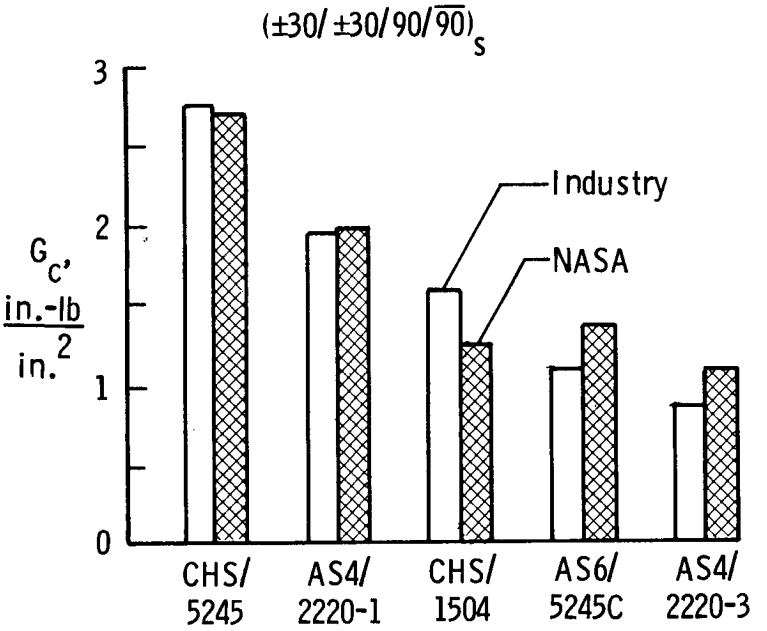

Figure 5

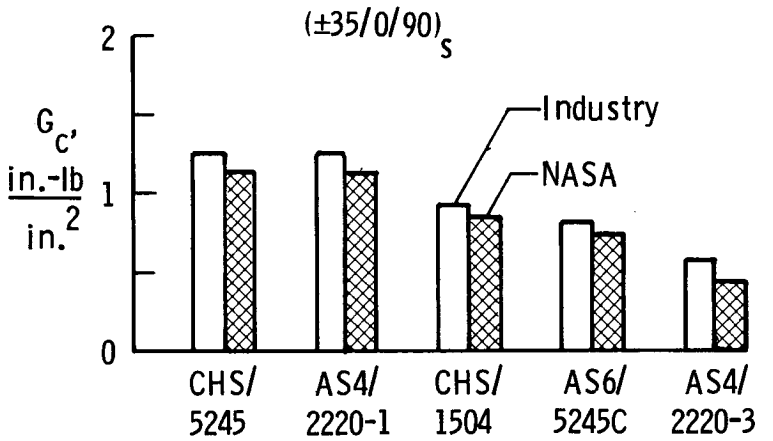

Figure 6

COMPARISON OF G_I COMPONENT OF G_c FOR TWO EDT LAYUPS

Figure 7 shows a comparison of the mode one component of G_c measured using the two Edge Delamination Test (EDT) layups for the five materials tested. With the possible exception of CHS/5245 material, which had the highest G_c values, the G_I component at delamination onset is nearly identical for both EDT layups. These results imply that delamination is governed in these materials by the critical value of G_{Ic} and is nearly independent of the G_{II} shear component.

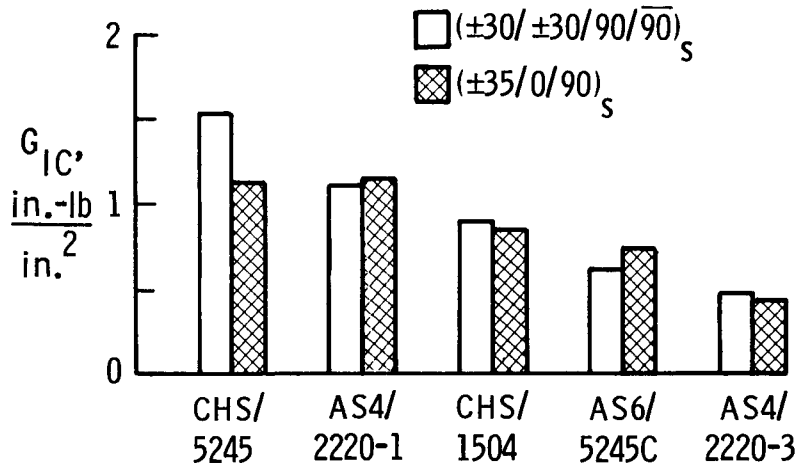

Figure 7

COMPARISON OF DCB AND EDT G_{Ic} MEASUREMENT

Figure 8 shows a comparison of G_{Ic} for five different materials systems as measured by a double cantilever beam (DCB) test, along with the average of the mode I components of G_c measured by the two EDT layups.

The G_{Ic} values agree fairly well for the brittle T300/5208 material and the tougher CHS/5245 material. However, DCB values are consistently higher than EDT values for the intermediate toughness materials. The higher DCB values may result from fiber bridging that occurs when the delamination grows between similar zero degree plies. This mechanism may result in greater delamination resistance as the delamination grows. Such a change may be characterized by plotting G_{Ic} as a function of delamination length. These "R-curve" plots, as shown in the figure, have been generated by several authors (refs. 11-12) to demonstrate that G_{Ic} values taken at large delamination lengths, or average values over the entire length, may be higher than delamination onset values. Because the onset values are lowest and more realistically represent matrix behavior in multiplied laminates, they should be used for comparing materials. The edge delamination test data are reduced based on the initiation of delamination.

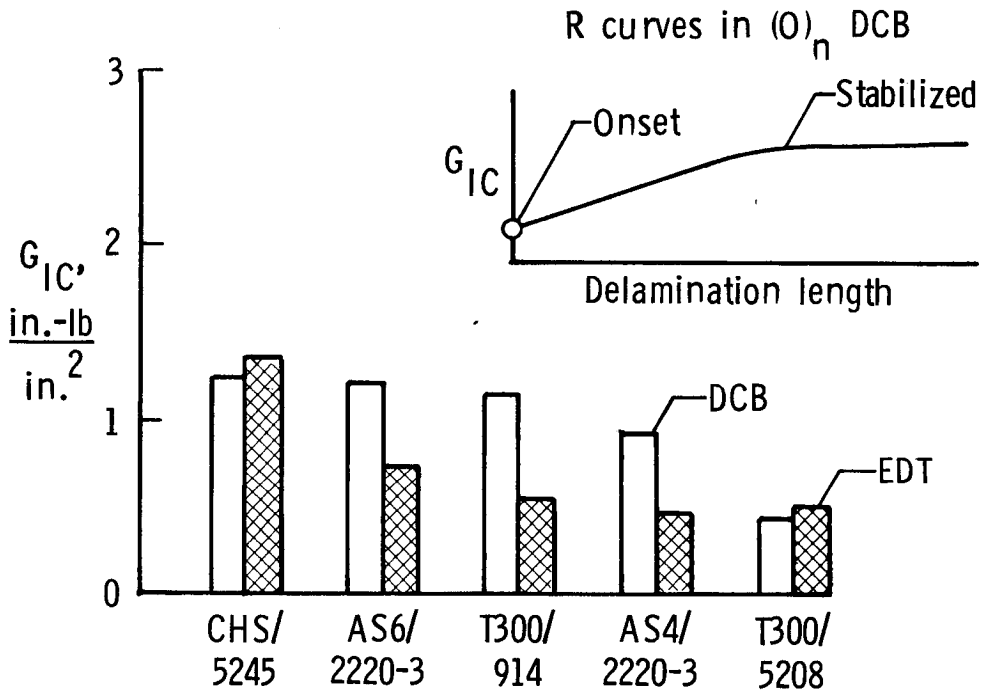

Figure 8

INTERLAMINAR FRACTURE TOUGHNESS OF TOUGHENED MATRIX COMPOSITES

Figure 9 compares G_{Ic} values for several materials including (1) brittle epoxies: T300/5208 and AS4/3502, (2) five materials analyzed in the ACEE key technologies programs, (3) three "model" tough composites: T300/BP907, CHS H205, and CHS F185, and (4) a semi-crystalline thermoplastic Courtaulds/PEEK. Except for Courtaulds/PEEK, all the data represent the average G_I component of G_c measured for the two EDT layups. The Courtaulds/PEEK data were measured with a double cantilever beam (DCB) test as reported in reference 5. Figure 9 indicates that all five of the key technologies contract materials have low G_{Ic} values and, at best, they represent only minor improvements over the baseline brittle epoxy composites.

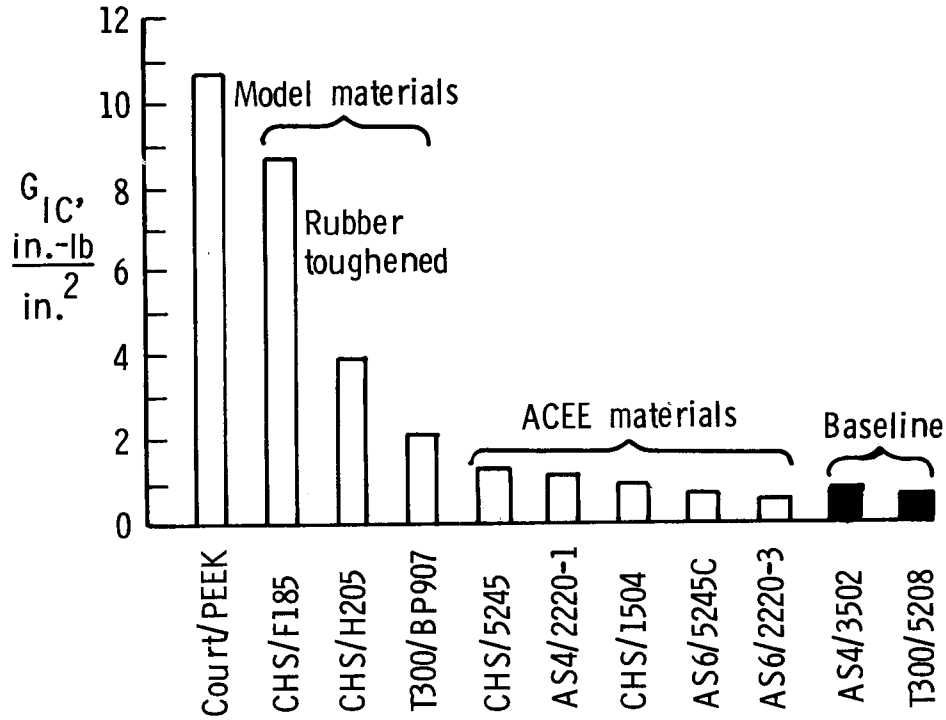

Figure 9

OPEN HOLE TENSION FAILURE STRESS (ST-3)

Tension failure stresses of specimens having a 0.25-inch diameter hole are shown in figure 10. The tests were performed according to standard test method ST-3 described in reference 1. Laminate failure stress is shown as a function of the representative ultimate tensile strain of the graphite fiber used in each material. Although failure stress generally increases with higher fiber ultimate strain, there is as much as twenty percent variation in the failure stresses of different materials systems containing the same fiber, depending on which resin system is used. Material containing the 5245C resin matrix system exhibited the highest strength with both intermediate and high strain fibers.

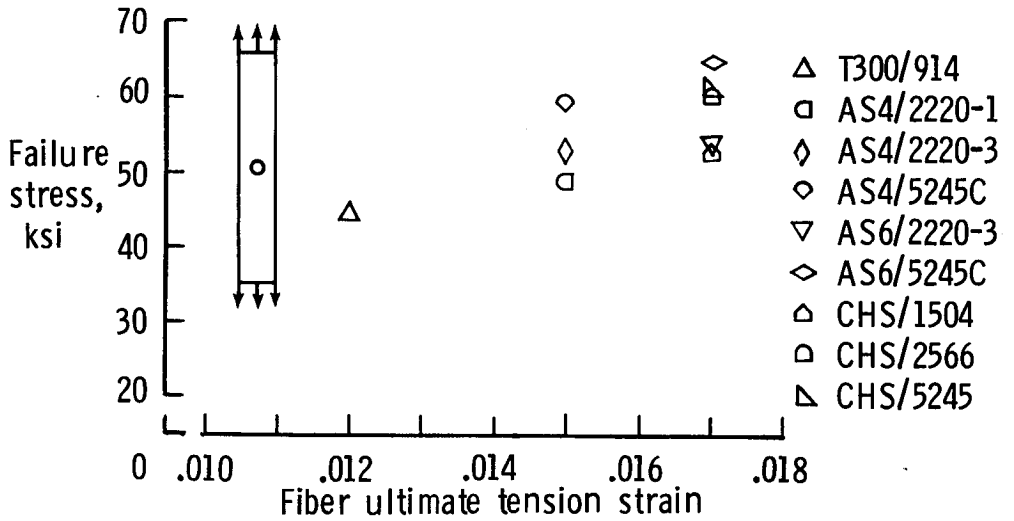

Figure 10

OPEN-HOLE COMPRESSION FAILURE STRAIN (ST-4)

A comparison of failure strain data for specimens containing a 1-inch diameter hole tested according to the standard test method ST-4 is presented in figure 11. Most of the materials have a failure strain of 0.005 to 0.006 with little improvement relative to the baseline materials. One exception is AS4/5245C, which has a failure strain of 0.007. The failure mode for 0^{o}-dominated laminates with local discontinuities loaded in compression is dominated by the stability of the fiber (ref. 13) which depends heavily on the shear modulus of the matrix and on the bending stiffness of the fiber. Examination of data for specimens with the same matrix but different fibers shows the failure strain for laminates with higher strain T700 and AS6 fibers to be lower than corresponding data for T300 and AS4 fibers. Celion High Strain specimens, however, have a higher failure strain than laminates with regular Celion fibers. The explanation for this difference may relate to the fiber diameter which is smaller for T700 and AS6 than T300 and AS4 but approximately the same for Celion and Celion High Strain fibers. Comparison of data generated by Industry and NASA shows good agreement with the exception of data for materials AS4/2220-1 and CHS/1504 in which a variation on the standard test method was used to generate the industry data.

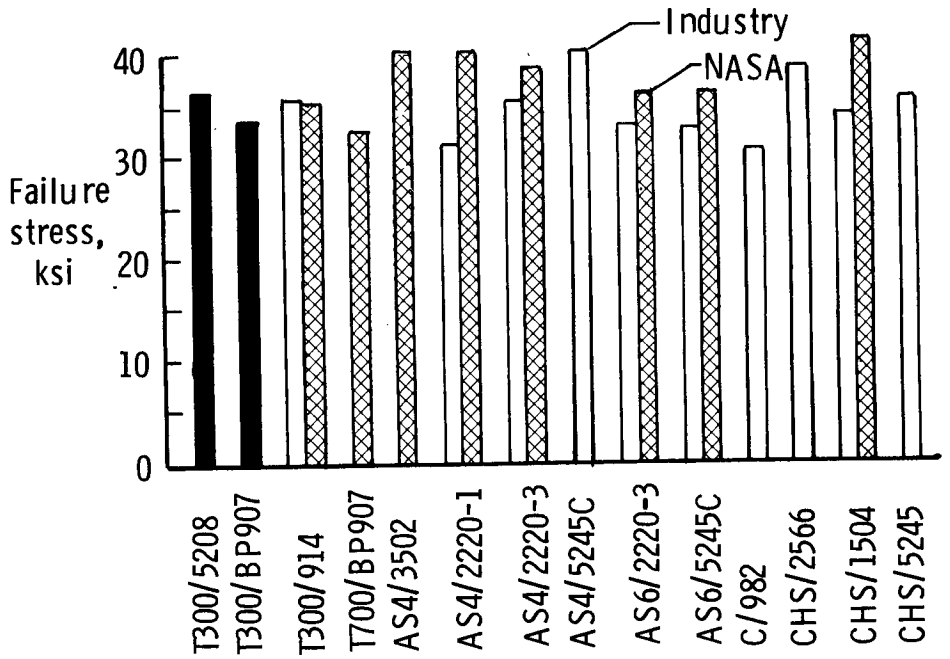

Figure 11

OPEN-HOLE COMPRESSION FAILURE STRESS (ST-4)

Data for the failure stress for the same open-hole compression specimens for which failure strain data were presented in figure 11 are presented in figure 12. Most of the materials systems have a failure stress between 35 and 40 ksi.

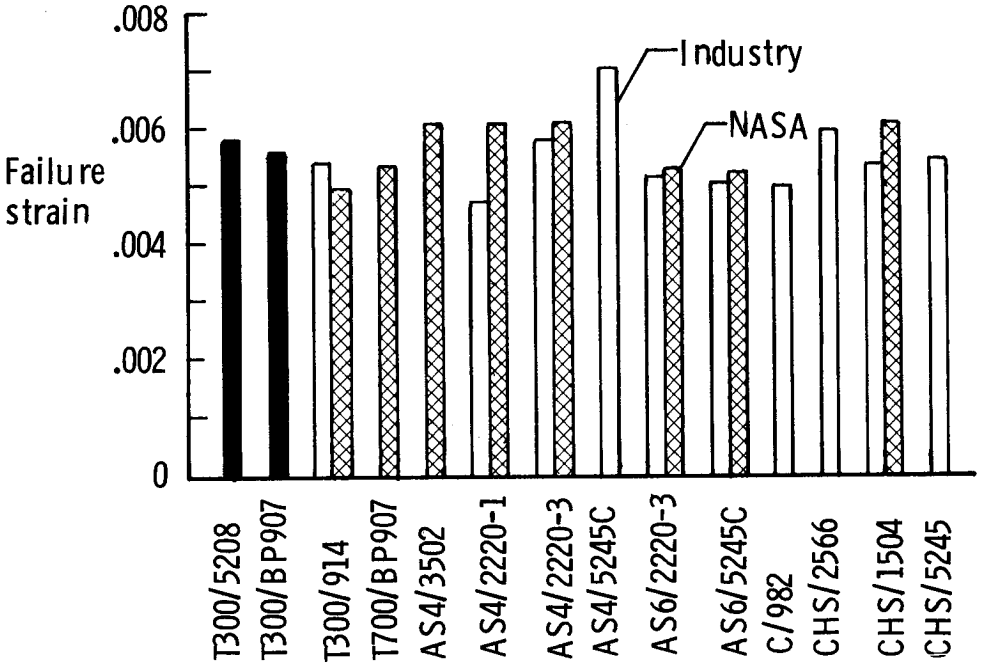

Figure 12

IMPACT DAMAGE TEST METHODS

The ST-1 test method for damaging a laminate is specified in reference 1 to be conducted in the following manner. The impactor shall weigh 10 pounds, be less than 10 in. in length, and have a 0.5-in. diameter hemispherical steel tip which strikes the specimen normal to its plane. The 7-in. by 12.5-in. specimen is mounted in an impact test fixture in which a picture frame with a 5-in. by 5-in. window is clamped over the specimen. The 10 pound weight is dropped from a height of 2 feet to provide the 20 ft-lb test condition. The specimen is then trimmed to a 5-in. by 10-in. size and placed in a compression fixture which imposes approximately fixed end boundary conditions on the loaded ends and simple support conditions on the lateral edges. With minor variations, this method is the test technique used by industry to damage specimens.

The technique used to impose impact damage on specimens tested by NASA involves propelling a small mass (0.5-in. diameter aluminum sphere) at approximately 443 ft/sec to achieve the 20 ft-lb impact condition. This damage test was conducted in the same fixture used to conduct the residual strength test. In both test methods, the specimen was removed from the fixture following the impact test to measure the damage size using ultrasonic equipment. The two test methods imposed identical impact energies; however, results presented in the following figures will show that the two tests are not necessarily equivalent. Photographs of the two test set-ups are presented in figure 13.

Industry

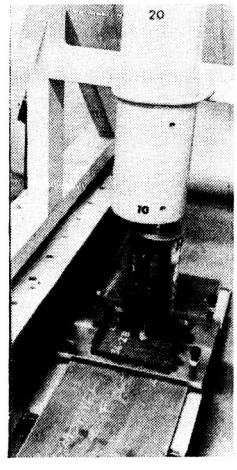

- ½-inch hemispherical steel tip
- 10 pound
- 11 ft/sec

20 ft-lb impact

NASA

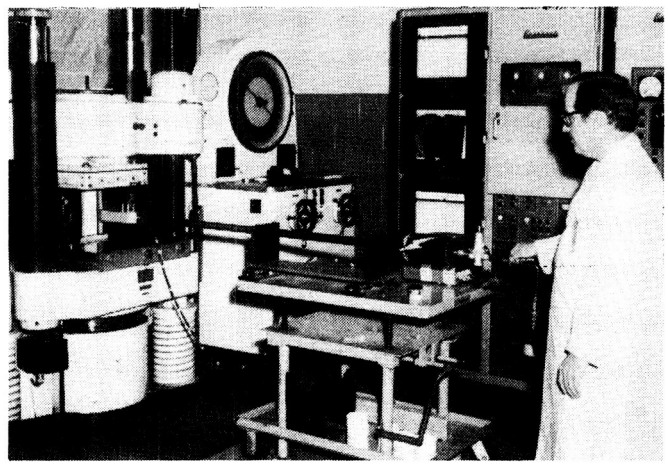

- ½-inch aluminum ball
- 0.0065-pound
- 443 ft/sec

Figure 13

IMPACT DAMAGE SIZE

In addition to the 20 ft-lb standard test impact condition, data were obtained for a range of impact energies. The damage size plotted as a function of impact energy is presented in figure 14 for the standard, approximately 0.25-in thick, quasi-isotropic laminate. The damage area was determined using ultrasonic C-scan equipment. The data indicate the damage size depends on the properties of both the resin and fiber with some materials showing considerably less damage for a specific impact energy than others. Industry data are indicated by solid lines and NASA data by dashed lines. For materials systems tested by both industry and NASA, results show considerably greater damage for the NASA low-mass/high-velocity impact test than for the industry dropped-weight test method. For the materials systems studied using the NASA test technique, none of the toughened epoxy systems has resistance to impact damage as high as the laminate with the baseline BP907 resin. The data for the Courtaulds/PEEK material taken from reference 5 is for a 0.2-inch thick 0-degree dominated orthotropic laminate. The Courtalds/PEEK material shows large damage for energies up to 20 ft-lb; however, the slope of the curve is reduced for higher energies.

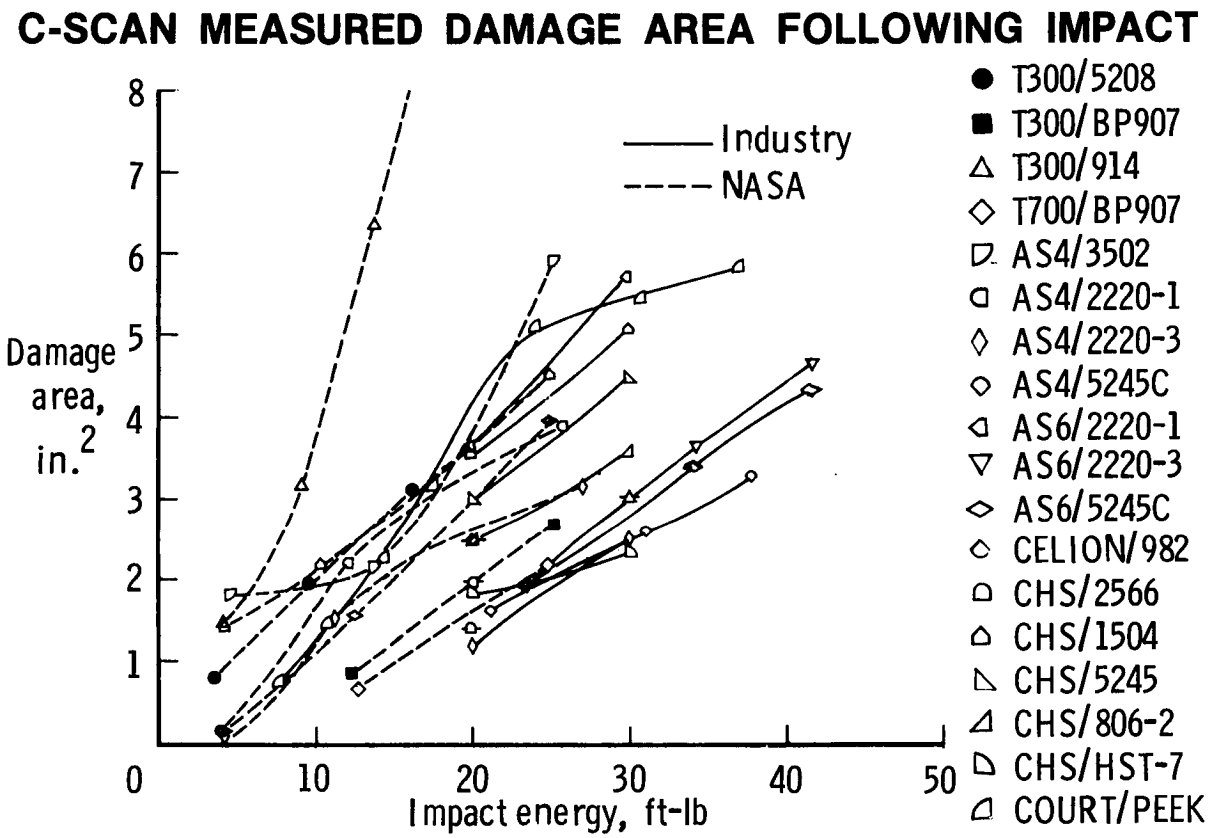

Figure 14

COMPRESSION AFTER IMPACT FAILURE STRAIN (ST-1)

The failure strain for specimens loaded in compression following impact damage at selected impact energies is presented in figure 15. Industry data are represented by solid lines and NASA data by dashed lines. In general, the NASA low-mass/high-velocity impact condition caused a greater reduction in failure strain than did the industry dropped-weight test. None of the materials tested by NASA has a higher failure strain at 25 ft-lb impact energy than the baseline T300/5208 material and all are substantially lower than the baseline T300/BP907 material. Laminates constructed using BP907 resin and the higher strain T700 fiber recorded a higher failure strain than did BP907 laminates with T300 fiber. For the materials tested by industry, Courtalds/PEEK and CHS/HST-7 had the highest failure strains.

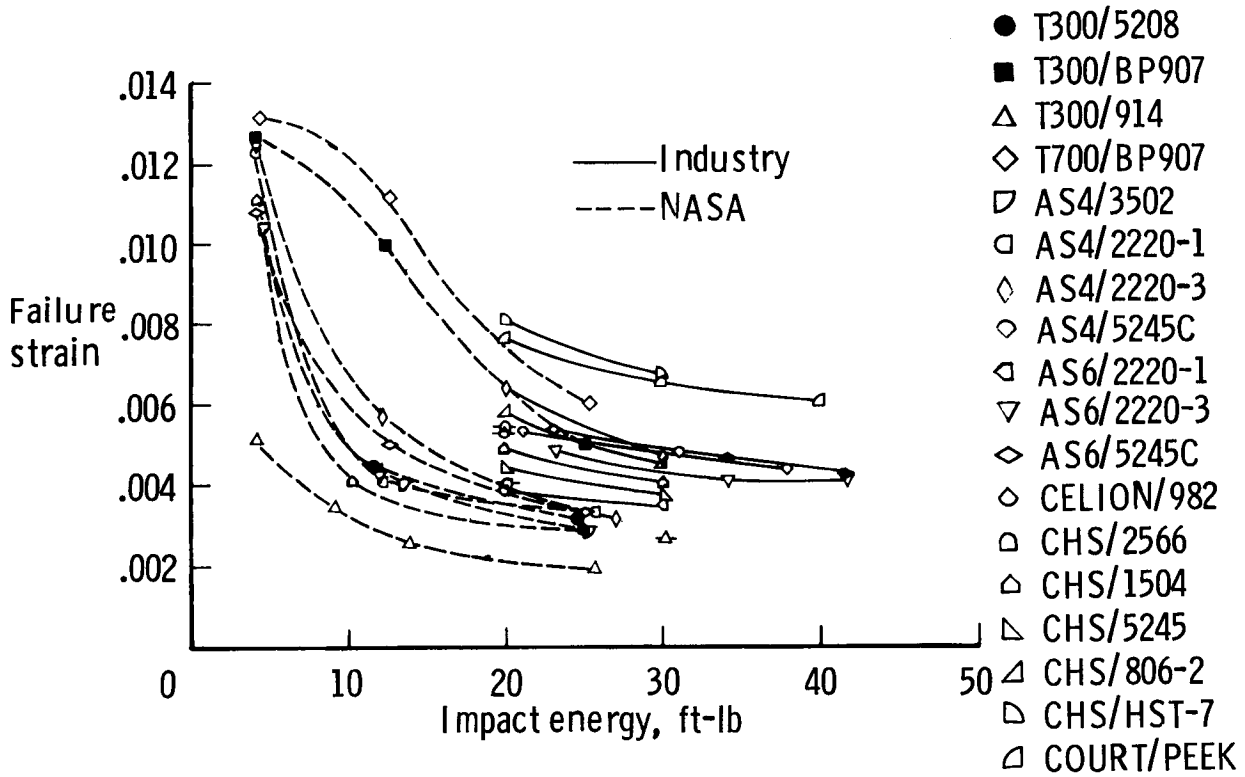

Figure 15

COMPRESSION AFTER IMPACT FAILURE STRESS (ST-1)

The stress at failure following impact damage for most of the data presented in igure 15 is presented in figure 16. Failure stress is a useful parameter for making aterials comparisons for quasi-isotropic laminates because it predicts the relative oad carrying capability and introduces the effect of variations in resin content and hickness. High resin content, for example, is the reason CHS/HST-7 shows less dvantage on the basis of stress than strain. The T300/914 specimens were con-tructed using prepreg material with approximately twice the thickness of the other aterials systems. The effect that ply thickness has on the compression strength of amaged laminates is not established. On the basis of failure stress, some improve-ent in performance can be credited to higher strain fibers. As was the case for the ailure strain comparison, the NASA low-mass/high-velocity impact caused greater eductions in the failure stress than did the industry dropped-weight test.

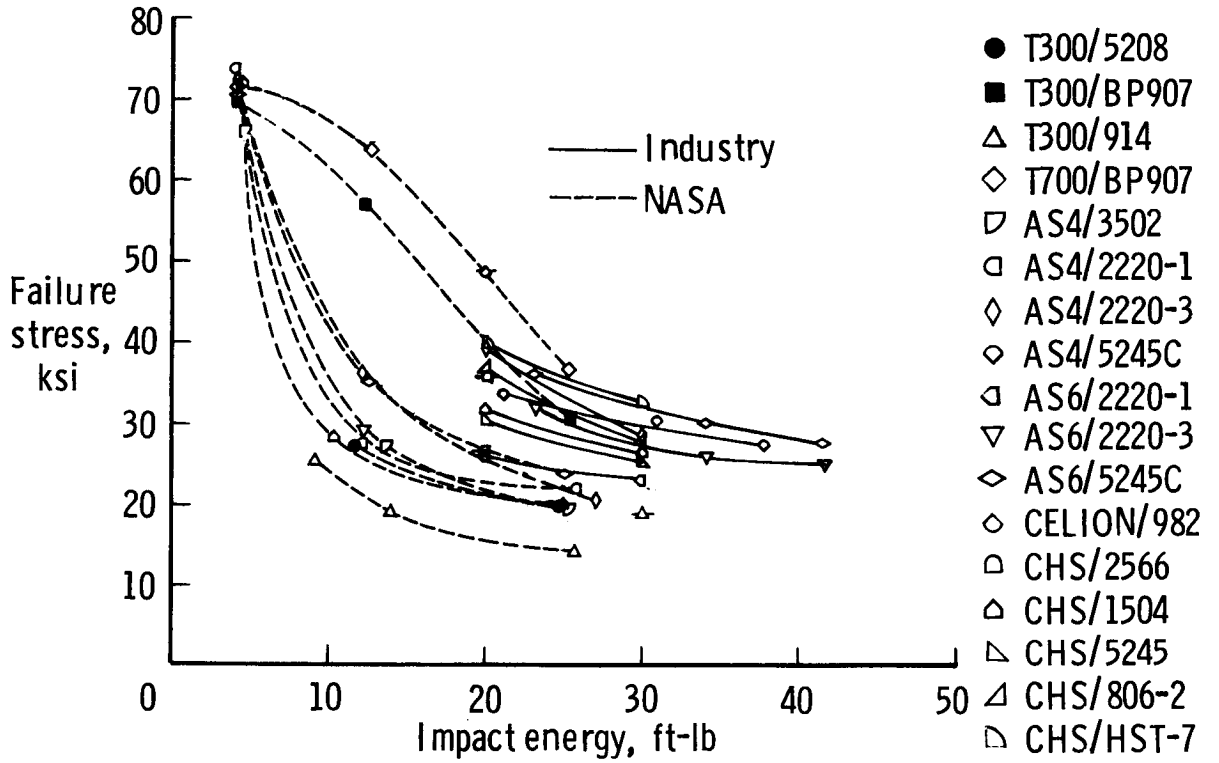

Figure 16

The deformation response of the laminate during and following impact is illustrated in figure 17. Impact by the low mass 0.5-in.-diameter aluminum sphere at velocities from 300 to 500 ft/sec creates a compression stress wave which causes the material directly under the projectile to translate laterally in a time frame much less than that required for the overall response of the plate structure. This highly localized deformation gradient causes large transverse shear and normal stresses which can cause failure within the laminate. The compression wave reflects from the back surface as a tension wave and may cause further damage propagation. The local transient bending deflections of a 0.25-in.-thick laminate following a 300 ft/sec impact has been measured to have a maximum out-of-plane deflection of approximately .04 in. and affect a region approximately 1.5 in. in diameter (ref. 14). Impact by a high mass at low velocity with the same energy causes a smaller transient deformation gradient response. It is this difference which is believed responsible for the larger damage size and greater reduction in strength for the NASA low-mass/high-velocity impact test condition compared to that for the industry dropped-weight test.

IMPACT DEFORMATION RESPONSE MECHANISMS

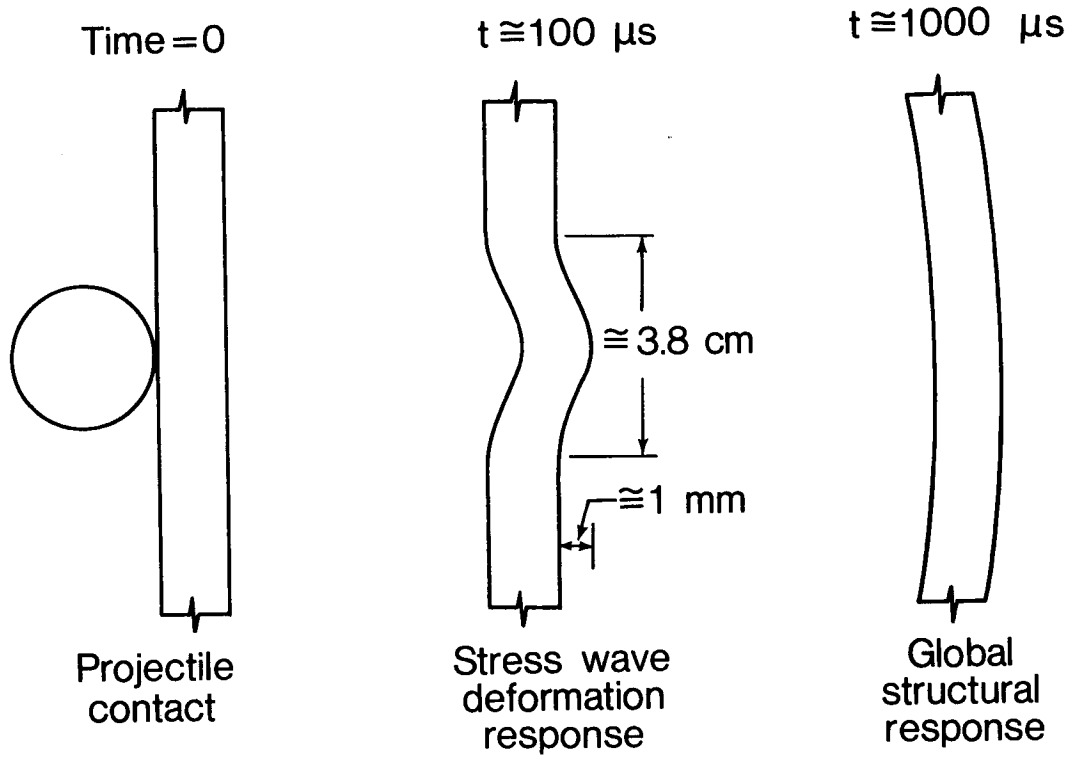

Figure 17

COMPARISON OF IMPACT DAMAGE TEST TECHNIQUES

The impact damage threat to aircraft structure includes dropped tools, runway debris and hailstones. A 2-in.-diameter hailstone, for example, would strike the upper (compression) surface of a stationary aircraft wing with a terminal velocity of approximately 176 ft/sec and 30 ft-lb of energy. The standard damage tolerance tests are not intended to generate aircraft design allowables, but were developed to assess the relative damage tolerance merit of new material systems and to provide indications of the bounds on the effect damage may have on structural performance. The data presented in preceding figures for the damage size and for the residual compression strength following impact indicate that the low-mass/high-velocity impact test is more severe than the dropped-weight test. In the context of establishing a lower bound, the low-mass/high-velocity test method would seem preferred to the low-velocity/dropped-mass technique (figure 18). The low-mass/high-velocity test may have the further advantage of being less influenced by the edge support boundary condition since much of the damage is believed to occur due to local deformation gradients in a time frame which precedes the overall structural response of the plate.

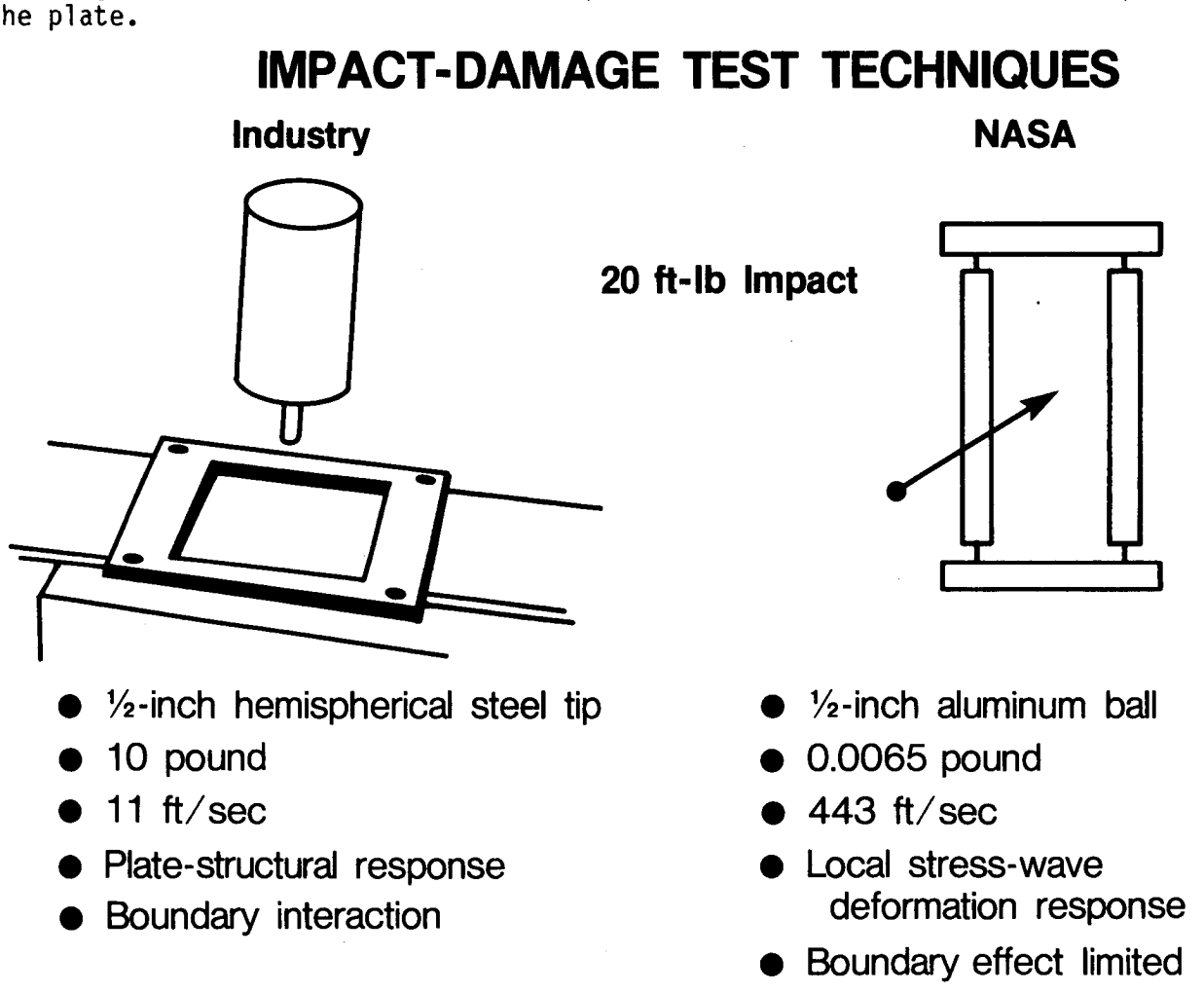

Figure 18

COMPRESSION AFTER IMPACT FAILURE STRAIN VERSUS INTERLAMINAR FRACTURE TOUGHNESS

Figure 19 shows a plot of compression failure strain for laminates subjected to impacts of 1000 in.-lb/in. versus the mode I interlaminar fracture toughness G_{Ic}. The solid symbols represent tests using the low-mass/high-velocity aluminum projectile as the impactor, whereas the open symbols represent tests using the high-mass/low-velocity dropped weight. Most of the baseline and ACEE materials have G_{Ic} values less than 1 in.-lb/in.^{2} Data for T300/BP907 and Courtaulds/PEEK (ref. 5) suggest that if G_{Ic} is increased, a corresponding increase in compression failure strain after impact will be observed. More data are needed to further substantiate this observation and to define better the correlation curve suggested in figure 19.

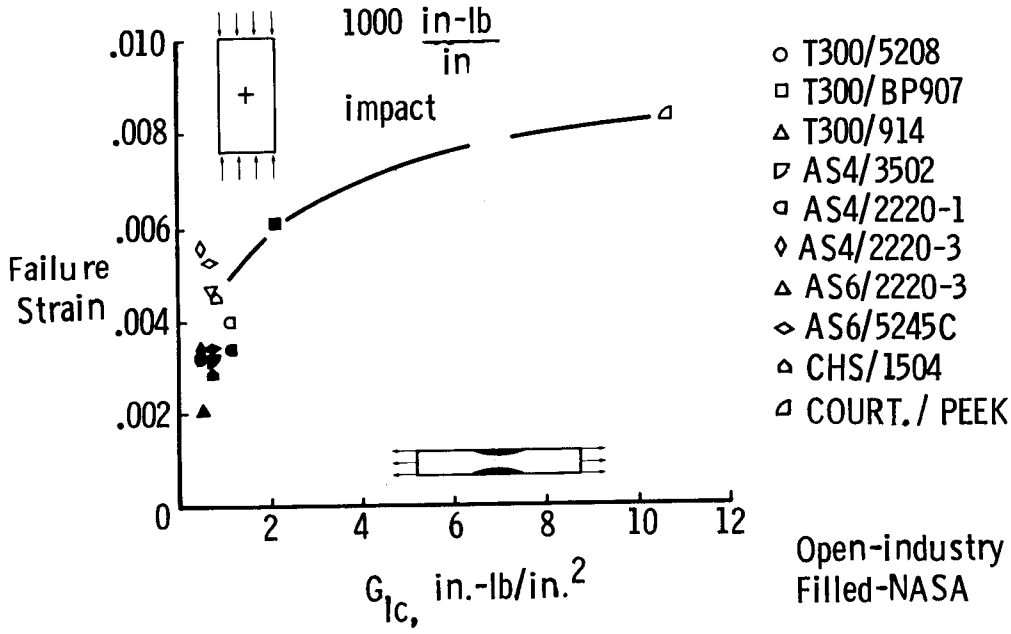

Figure 19

CONCLUDING REMARKS

Numerous candidate "tough" composite materials are available from the resin and fiber suppliers for evaluation as candidate materials for improved tolerance to impact damage and higher residual strength (see fig. 20). This proliferation of new materials makes difficult and expensive the determination of characteristic material properties and emphasizes the need for standardized test methods and the generation of a transportatable data base. The development of NASA/Industry Standard Test Methods (ref. 1) for evaluating damage tolerance is an initial attempt to serve this need.

The edge delamination and double cantilever beam interlaminar fracture toughness test methods provide results which are in reasonable agreement for the relatively brittle systems evaluated. If a simple ranking of a material's relative toughness is all that is needed, than perhaps one of the test methods could be dropped from the Standard Tests set. Open-hole compression tests conducted by industry and NASA are in close agreement. Results for impact damage size and compression strength following impact appear to be affected by the velocity of the projectile at imapct with the low-mass/high-velocity test method causing the most reduction in strength. The low-mass/high-velocity test method may have the further advantage of yielding results which are almost independent of the support boundary conditions.

The higher strength provided by high strain fibers seems to translate directly into improved laminate tension performance. For compression, however, where failure is usually controlled by the stability of the fiber, a smaller fiber diameter seems to offset the potential improvement available from a higher failure strain.

In summary, the most serious damage tolerance technology deficiency is still associated with the compression strength following impact. Most new materials systems have provided only marginal improvement in this property. The problem is complex and the fundamental mechanics of the problem are only now beginning to be understood. It would appear that the resin should exhibit high initial shear modulus and have a nonlinear stress-strain behavior initiating at high strains near ultimate. In addition, it should have a high interlaminar fracture toughness to resist delamination propagation. The highest potential for improved performance currently seems to favor the semi-crystalline thermoplastic resin systems such as PEEK.

- NUMEROUS NEW FIBER AND RESIN MATERIALS AVAILABLE FROM INDUSTRY
- STANDARD TEST METHODS AND COMMON DATA BASE DESIRABLE
- INTERLAMINAR FRACTURE TOUGHNESS AND OPEN-HOLE COMPRESSION TEST RESULTS REPEATABLE
- LOW-MASS/HIGH-VELOCITY IMPACT TEST PROVIDES LOWER BOUND TO STRENGTH REDUCTION AND MAY BE LESS SENSITIVE TO BOUNDARY CONDITIONS
- HIGH STRAIN FIBER TRANSLATES INTO IMPROVED LAMINATE TENSION PERFORMANCE
- MATERIALS TESTED UNDER ACEE CONTRACTS HAVE LOW INTERLAMINAR FRACTURE TOUGHNESS AND EXHIBIT LIMITED IMPROVEMENT IN COMPRESSION STRENGTH FOLLOWING IMPACT

Figure 20

1. Standard Tests for Toughening Resin Composites. NASA RP-1092, July 1983.

2. Rhodes, Marvin D.; Williams, Jerry G.; and Starnes, James H., Jr.: Low Velocity Impact Damage in Graphite-Fiber Reinforced Epoxy Laminates. Proceedings of 34th Annual Conference Reinforced Plastic/Composite Institute, The Society of the Plastics Industry, Inc., Jan. 29-Feb. 2, 1979.

3. Starnes, James H., Jr.; and Williams, Jerry G.: Failure Characteristics of Graphite-Epoxy Structural Components Loaded in Compression. Mechanics of Composite Materials - Recent Advances. Hashin and Herakovich, Editors, Pergamon Press, 1983.

4. Williams, Jerry G.; and Rhodes, Marvin D.: Effect of Resin on the Impact-Damage Tolerance of Graphite-Epoxy Laminates. ASTM STP 787, pp. 450-480, 1983.

5. Carlile, D. R.; and Leach, D. C.: Damage and Notch Sensitivity of Graphite/PEEK Composite. Proceedings of the 15th National SAMPE Technical Conference, October 1983, pp. 82-93.

6. O'Brien, T. K.: Characterization of Delamination Onset and Growth in a Composite Laminate. Damage in Composite Materials, ASTM STP 775, June 1982, p. 140.

7. O'Brien, T. K.; Johnston, N. J.; Morris, D. H., and Simonds, R. A.: A Simple Test for the Interlaminar Fracture Toughness of Composites. SAMPE Journal, Vol. 18, No. 4, July/August 1982, p. 8.

8. Johnston, N. J.; O'Brien, T. K.; Morris, D. H.; and Simonds, R. A.: Interlaminar Fracture Toughness of Composites II - Refinement of the Edge Delamination Test and Application of Thermoplastics. Proceedings of the 28th National SAMPE Symposium and Exhibition, Anaheim, California, April 1983, p. 502.

9. O'Brien, T. K.: Mixed-Mode Strain-Energy-Release-Rate Effects on Edge Delamination of Composites in the Effect of Defects in Composite Materials. ASTM STP 836, 1984. Also NASA TM-84592, January 1983.

10. O'Brien, T. K.; Johnston, N. J.; Morris, D. H.; and Simonds, R. A.: Determination of Interlaminar Fracture Toughness and Fracture Mode Dependence of Composites Using the Edge Delamination Test. Proceedings of the International Conference on Testing, Evaluation, and Quality Control of Composites, University of Surrey, Guildford, England, September 1983, pp. 223-232.

11. Russell, A. J.: Factors Affecting the Interlaminar Frature Energy of Graphite/Epoxy Laminates. Progress in Science and Engineering of Composites, Proceedings of ICCM - IV, Tokyo, 1982, pp. 279-286.

12. deCharentenay, F. X., et. al.: Characterizing the Effect of Delamination Defect by Mode I Delamination Test. ASTM STP 836, Effect of Defects in Composites, 1984.

3. Hahn, H. Thomas; and Williams, Jerry G.: Compression Failure Mechanisms in Unidirectional Composites. NASA TM-85834, July 1984.

4. Williams, Jerry G.; Anderson, Melvin S.; Rhodes, Marvin D.; Starnes, James H., Jr.; and Stroud, W. Jefferson: Recent Developments in the Design, Testing, and Impact-Damage Tolerance of Stiffened Composite Panels. Proceedings of Fourth Conference on Fibrous Composites in Structural Design, San Diego, California, November 14-17, 1978.

Page intentionally left blank

SYNTHESIS AND TOUGHNESS PROPERTIES OF RESINS AND COMPOSITES

Norman J. Johnston
NASA Langley Research Center
Hampton, Virginia 23665

ACEE Composite Structures Technology Conference
Seattle, Washington
August 13-16, 1984

TOUGHENED COMPOSITE MATERIALS PROGRAM

The multidisciplinary nature of the Langley Research Center toughened composite materials program is illustrated in figure 1, with each discipline shown in a different shaded section of the chart, from resin synthesis (upper left) clockwise to applications (lower left). Generally, materials technology, designed to develop new tougher matrices and to enhance our fundamental understanding of material behavior, is shown in the top half of the chart. Structures technology, aimed at the development and verification of new structural concepts for improved damage tolerance, is shown in the bottom half of the chart.

One of the basic objectives of the program is to establish key relationships between the various disciplines. Correlations between matrix chemistry, matrix-fiber micromechanics, fracture mechanics, and structural mechanics are sorely needed to expand both intra- and interdisciplinary capabilities and to establish trends. The main purpose of this paper is to propose relationships between matrix resin properties and selected composite properties. Such correlations will enable prediction of composite performance on the basis of resin evaluation and will be especially welcome to chemists and formulators for screening new polymer compositions without having to fabricate and test laminates.

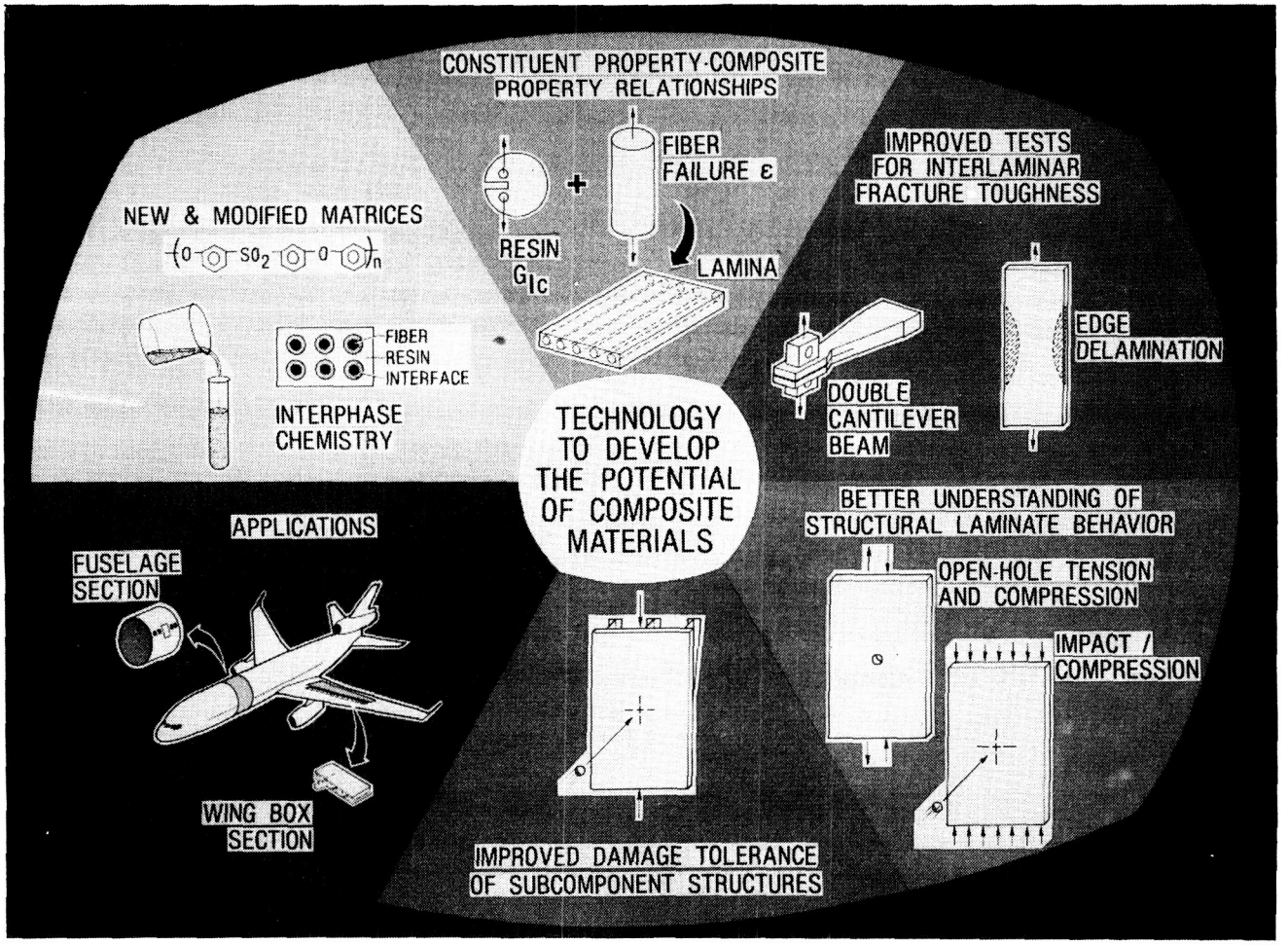

Figure 1

OUTLINE

Three important composite properties are being investigated for their relationship to resin performance: stiffness, 0° compression strength, and interlaminar fracture toughness. Only two resin properties were used in these correlations: stiffness and fracture toughness. A list of desirable properties for neat resins used as matrices in composites for structural applications on commercial aircraft and some selected approaches to the synthesis of tough matrix resins will also be presented. An outline of the information to be discussed is shown in figure 2.

- ACEE resins and composites: 3502, 914, 2220-1, 2220-3
  - Tensile and shear moduli of resins
  - Composite modulus predictions from micromechanics
- Fracture toughness properties of resins and composites
- Relationship between neat resin properties and composite properties
  - Resin modulus/0° composite compression strength
  - Resin fracture toughness/composite interlaminar fracture toughness
  - Resin modulus/composite interlaminar fracture toughness
- Resin criteria and some synthetic approaches

Figure 2

MATERIALS LIST

THERMOSETS

First Generation Brittle Materials

3502	Hercules, Inc.
3501-6	Hercules, Inc.
5208	Narmco Materials, Inc.
V378A	U.S. Polymeric
934	Fiberite Corporation

First Generation Tough Materials

914	Ciba-Geigy Corporation
BP907	American Cyanamid Company
F185	Hexcel Corporation
HX205	Hexcel Corporation
HX206	Hexcel Corporation

Second Generation Tough Materials

2220-1	Hercules, Inc.
2220-3	Hercules, Inc.
R6376	Ciba-Geigy Corporation
5245	Narmco Materials, Inc.
1806	American Cyanamid Company
985	American Cyanamid Company
HST-7	American Cyanamid Company
1504	Hexcel Corporation

THERMOPLASTICS

P1700	Polysulfone (Udel)	Union Carbide Corporation
PEEK	Polyetheretherketone (Victrex APC-1)	Imperial Chemical Industries
PEI	Polyetherimide (Ultem)	General Electric Company
PC	Polycarbonate (Lexan)	General Electric Company
PAI	Polyamideimide (Torlon)	Amoco Chemicals Corporation
PPS	Polyphenylenesulfide (Ryton)	Phillips Chemical Company

TENSILE MODULI OF NEAT RESINS

The University of Wyoming, under grant to NASA Langley, has a continuing program to fully characterize the mechanical and fracture properties of selected commercial and experimental resin matrix materials. In Phase I, four matrix resins used in composites being investigated by the ACEE contractors were chosen for study (refs. 1,2). Uncured neat resins were carefully deairated, poured into molds shaped to yield dogbone tensile and torsion specimens, and cured at temperatures similar to those used in composite fabrication. The cured specimens were tested both dry and moisture-saturated at three temperatures: room temperature (RT), 54°C (130°F), and 82°C (180°F). The specimens were instrumented, complete tensile and shear stress-strain curves to failure were obtained, and Poisson's ratio at each of the six exposure conditions was calculated. Coefficients of thermal and moisture expansion were determined from dilatometric measurements.

Dry and wet tensile moduli for the four resins at the three test temperatures are shown in figure 3. The largest drop in modulus from RT/dry to 180°F/wet was exhibited by 914, whereas 3502 retained the highest moduli under moisture saturation at all temperatures. Moduli at moisture saturation were almost identical for 914, 2220-1, and 2220-3.

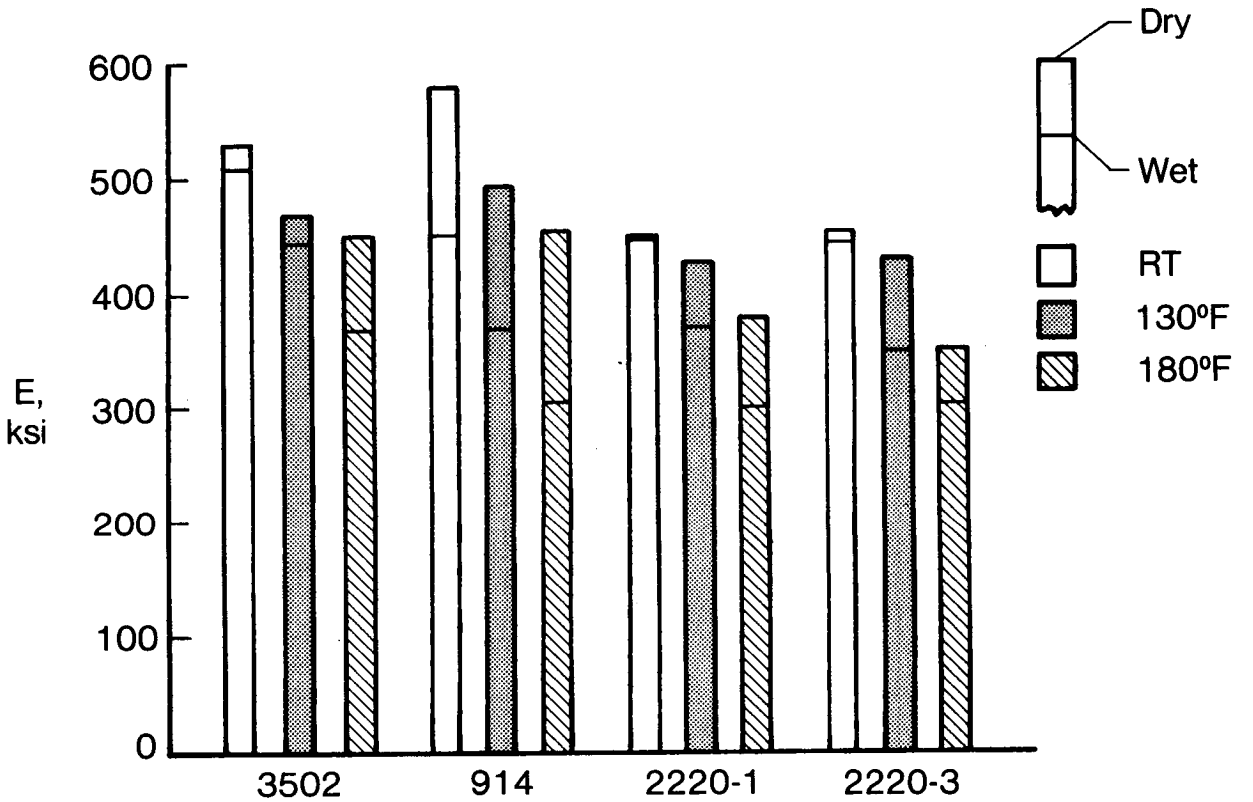

Figure 3

SHEAR MODULI OF NEAT RESINS

Dry and wet shear moduli for the four matrix resins, 3502, 914, 2220-1, and 2220-3 (refs. 1,2), are shown in figure 4. Interestingly, 3502 had the largest drop in shear modulus from RT/dry to 180°F/wet. Shear moduli of 914, 2220-1, and 2220-3 were almost identical at all conditions except 130°F/dry.

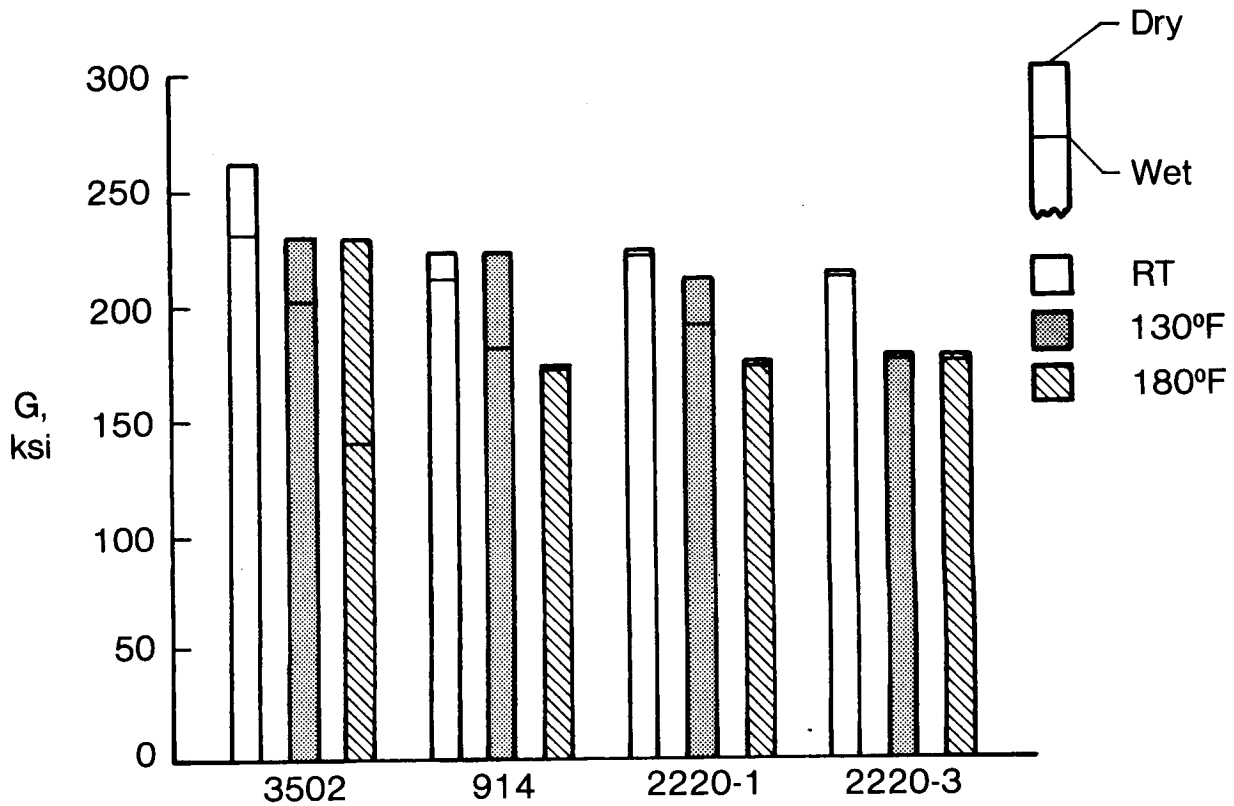

Figure 4

PREDICTIONS OF COMPOSITE PROPERTIES USING MICROMECHANICS

Using the neat resin data shown in figures 3 and 4 (refs. 1,2) and standard high tensile strength carbon fiber properties, predictions of composite longitudinal and transverse tensile moduli (E_{11}, E_{22}) and shear moduli (G_{12}) were calculated using micromechanics relationships developed at the University of Wyoming (refs. 3-5). Predicted numbers for both dry and moisture-saturated conditions at two temperatures, RT and 212°F (100°C), are shown in figure 5. The E_{11}, E_{22}, and G_{12} values for the four composite systems under any one set of conditions were very close. This would be expected for E_{11}, a fiber-dominated property. But most of the E_{22} and G_{12} values were also strikingly close, reflecting the similarities in resin moduli. Inexplicably low calculated values were observed for the 914 dry/100°C E_{22} and the 2220-3 dry and wet 100°C G_{12}.

Experimental lamina moduli under RT/dry conditions for composites made from the four resins were obtained as part of the edge delamination test program and are also listed in figure 5. These values correlated well with the predicted moduli in all cases except for the unusually high experimental RT/dry values for 3502 E_{22} and 2220-3 G_{12}. Notably, all experimental lamina moduli were higher than predicted.

	E_{11}, msi		E_{22}, msi		G_{12}, msi ★	
	Calc.	Exp.	Calc.	Exp.	Calc.	Exp.
3502						
Dry RT	20	21.4	1.40	1.64	0.69	0.77
Dry 100°C	20	—	1.29	—	0.69	—
Wet RT	20	—	1.43	—	0.60	—
Wet 100°C	20	—	1.28	—	0.54	—
914						
Dry RT	20	20.3	1.30	1.36	0.70	0.80
Dry 100°C	20	—	0.88	—	0.60	—
Wet RT	20	—	1.33	—	0.62	—
Wet 100°C	20	—	1.18	—	0.54	—
2220-1						
Dry RT	20	20.2	1.36	1.49	0.65	0.70
Dry 100°C	20	—	1.28	—	0.58	—
Wet RT	20	—	1.39	—	0.62	—
Wet 100°C	20	—	1.22	—	0.60	—
2220-3						
Dry RT	20	18.0	1.30	1.35	0.60	0.95
Dry 100°C	20	—	1.20	—	0.48	—
Wet RT	20	—	1.40	—	0.60	—
Wet 100°C	20	—	1.18	—	0.40	—

★ Secant modulus at 1% strain

Figure 5

RELATIONSHIP BETWEEN NEAT RESIN MODULUS AND 0° COMPOSITE COMPRESSION STRENGTH

The second important composite property to be related to resin properties is 0° compression strength. A parametric exercise involving four hypothetical resins is shown in figure 6. Values of RT/dry tensile moduli (E_R) from 300 to 600 ksi were selected and then were decreased by about 25 percent to obtain 180°F/wet moduli. Shear moduli (G_R) for both conditions were calculated from E_R using the standard equation shown and assuming a Poisson's ratio of 0.4. From either E_R or G_R, the 0° composite compression strengths at both conditions were calculated using an equation developed by Hahn and Williams (ref. 6) where K includes the volume fraction of the fiber, nonlinear material properties, and effects of local imperfections.

It is easily seen that if one desired a RT/dry 0° composite compression strength above 200 ksi, the RT/dry tensile modulus of the resin matrix should be above 500 ksi. Also, a 180°F/wet strength above 150 ksi would require a 180°F/wet resin tensile modulus above 350 ksi. It should be kept in mind that the 0° compressive strengths in undamaged composites should be as high as possible because of the severe strength reduction due to cross-plied construction and hole or impact damage. Thus, when developing tougher resin matrices, these strengths and their related resin moduli, especially under hot/wet conditions, should not be severely compromised.

$$G_R = \frac{E_R}{2(1+\nu)}$$

Assume $\nu = 0.4$

$$\sigma_c = KG_R \quad \bigstar$$

Hypothetical resin	E_{resin} (ksi)		G_{resin} (ksi)		σ composite (ksi)	
	RT/dry	180°F/wet	RT/dry	180°F/wet	RT/dry	180°F/wet
1	600	450	214	161	232	182
2	500	370	179	132	203	160
3	400	300	143	107	167	138
4	300	200	107	71	138	94

★ From reference 6

Figure 6

PREDICTIVE CAPABILITY IMPROVED FOR UNIDIRECTIONAL COMPOSITE COMPRESSION STRENGTHS

The capability of the Hahn-Williams equation (ref. 6) to accurately predict 0° composite compression strengths from neat resin tensile moduli is shown in figure 7. Measured values of RT/dry and 180°F/wet tensile moduli for the four matrix resins, 3502, 914, 2220-1, and 2220-3 (refs. 1,2; cf. fig. 3), are given in the two columns on the left. For composites made with the four resins, predicted strengths at both conditions are listed along with measured values. The latter were obtained mostly from ACEE contractors and were usually measured on composites made with AS4 and T300 fibers. Where either experimental 0° compression data were unavailable or only one value could be found, strains from quasi-isotropic compression failures were used to calculate strengths. Overall, the agreement between prediction and experiment is very good and illustrates not only the efficacy of this predictive procedure but also the relatively high modulus values that candidate tough resins must have to afford good 0° compression strengths.

	E_{resin} (ksi)		$\sigma_{composite}$ (ksi)			
	RT dry	180°F/Wet	RT/dry		180°F/wet	
Resin	Measured		Predicted[a]	Measured	Predicted[a]	Measured
3502 (Hercules)	530	370	210	178[b], 236, 270[b]	160	151[b]
914 (Ciba Geigy)	580	310	225	160[b], 203	139	158[c]
2220-1 (Hercules)	430	300	181	174[b], 181, 220[b]	138	140[b], 148[c]
2220-3 (Hercules)	460	310	189	183-240, 240[b]	139	118-148[d], 161-168[c]

[a] From reference 6

[b] Calculated from $\varepsilon_{quasi} \times E_O$

[c] 200°F/dry

[d] 200°F/wet

Figure 7

RESIN MODULUS VERSUS COMPOSITE 0° COMPRESSIVE STRENGTH

In figure 8, resin experimental E and G values for RT/dry and 180°F/wet conditions are plotted against respective experimental RT/dry and 180°F/wet 0° composite compressive strengths. The four materials discussed previously (3502, 914, 2220-1, and 2220-3) are included as well as an additional six (PEEK, 985, 1805, 5245, 5208, and P1700). The data for the latter materials were obtained from the open literature and product data sheets. Roughly, a linear relationship with a slope of 2.5 seems to exist between resin E and compression strengths in the E range from 300 to 600 ksi. Based on data available from product literature, PEEK appears to be an exception, possibly because its neat resin modulus does not coincide with the resin modulus in the composite. The relationship between resin G and composite compression strength is also linear for the range shown with a slope of about 1.

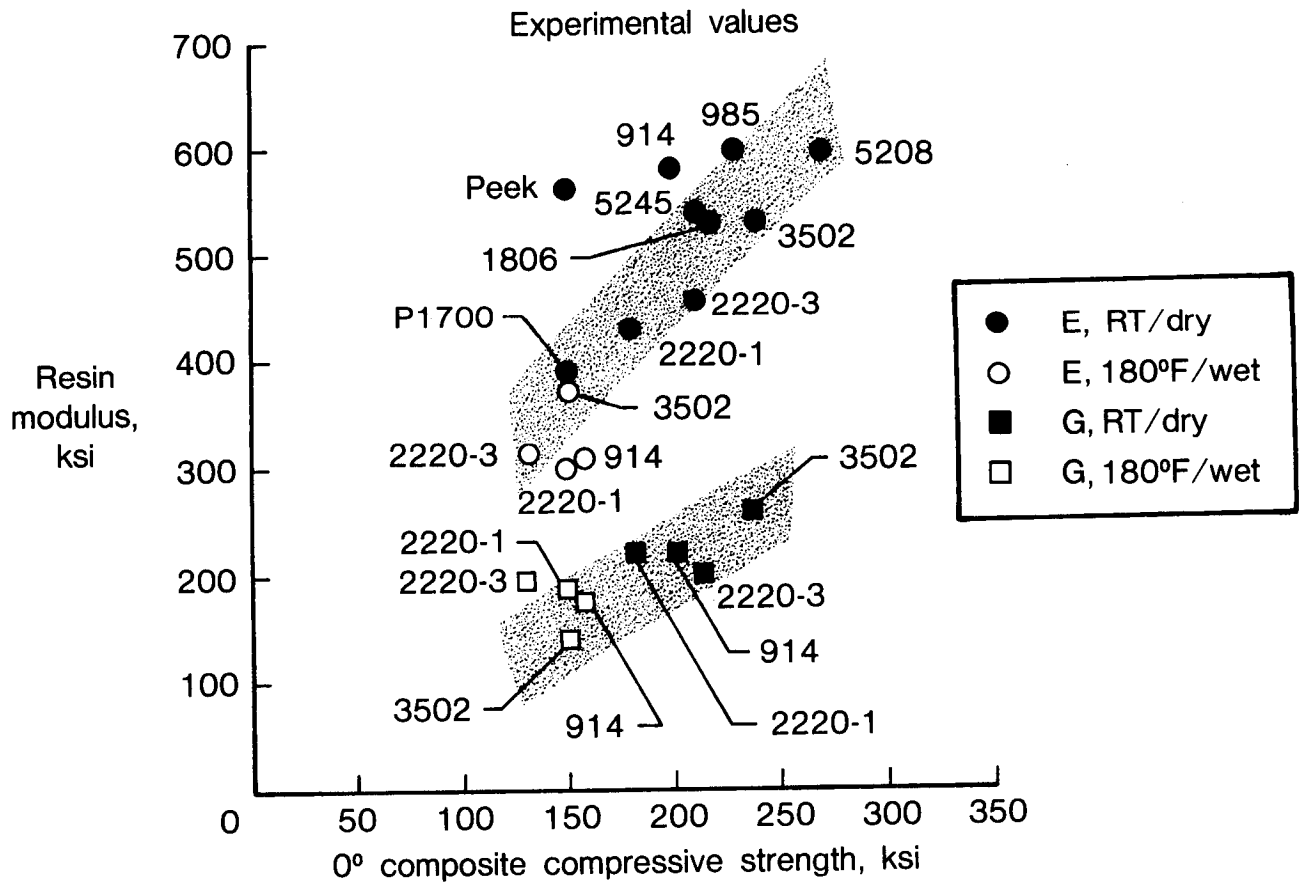

Figure 8

INTERLAMINAR FRACTURE TOUGHNESS OF COMMERCIAL GRAPHITE COMPOSITES

The third composite property that can be related to resin performance is interlaminar fracture toughness. A long list of G_{Ic} values (measured using double cantilever beam and edge delamination tests) from in-house research, open literature, and product brochures was compiled and the data summarized on the bar charts in figure 9. Although the data are not exhaustive, they are sufficient to illustrate the following general trends.

1. Second generation 350°F cure (toughened) thermosets have, on the average, about double the G_{Ic} fracture toughness values exhibited by the first generation 350°F thermosets. Since the latter were so low, it is doubtful if this increase is significant, although the desired G_{Ic} value for optimum retention of properties in damaged panels has yet to be defined.

2. Thermoplastic materials yield significantly higher interlaminar G_{Ic} values than thermosets, even those from second generation materials. The price to be paid for this gain is an increase in fabricating temperatures and, in some cases, solvent and creep sensitivity.

3. The large gap between G_{Ic} values of 350°F thermosets and thermoplastics needs to be closed by further innovative research without compromising resin modulus and composite compression properties. This "third generation" of thermosets would fill a current need until an adequate data base and improved fabrication technology could be generated for thermoplastics.

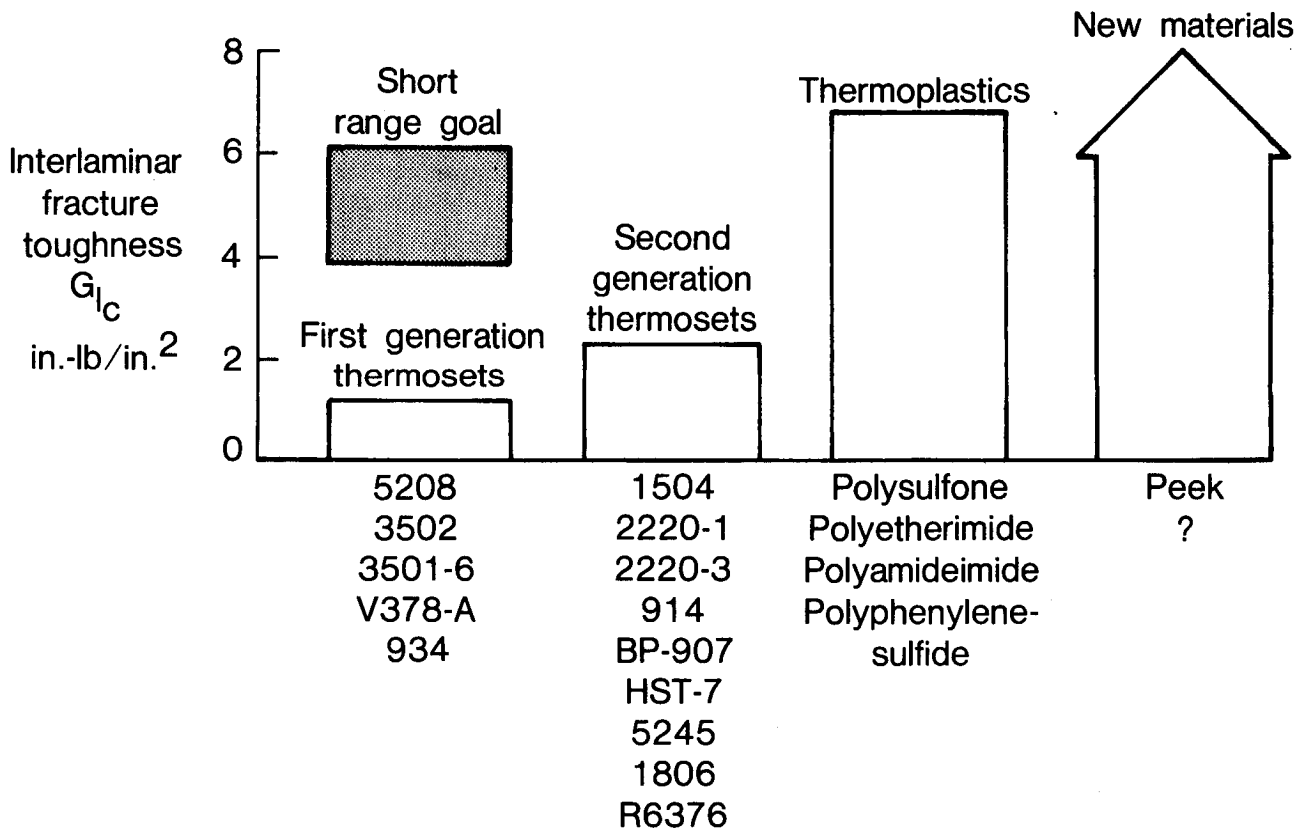

Figure 9

EMPIRICAL RELATIONSHIP BETWEEN RESIN G_{Ic} AND COMPOSITE INTERLAMINAR G_{Ic}

Figure 10 illustrates an initial attempt to establish a relationship, albeit empirical, between composite interlaminar fracture toughness and neat resin fracture toughness. The correlation can be divided into two ranges. At low G_{Ic} values, the points for brittle materials such as 5208, 3502, and 3501-6 fall roughly above a line of slope 1, indicating the resin behavior is generally transferred fully to the composite. Because of the relatively low G_{Ic} values of second generation materials, we may speculate that the points for these materials will also fall close to this line. For the tougher materials, such as rubber-toughened epoxies (F155, HX206, F185) and the thermoplastics (P1700, PAI, PEI, PC), this relationship does not hold. The neat resin fracture behavior is not fully transferred into the composite; the relationship is roughly 3:1 to 4:1, as shown by the dotted line. One simple explanation for this is that the fibers restrict the size of the crack tip deformation zone in the composite compared to the size of the large plastic zone normally obtained with tough materials in the bulk, thereby limiting interlaminar G_{Ic}. The fact that three of the four thermoplastics fall below the dotted line can be attributed to resin-fiber interfacial failures which tend to decrease interlaminar G_{Ic} values. More data will be required, especially at the higher G_{Ic} levels, before the two relationships depicted in figure 10 can be more firmly established. Also, micromechanics analysis will be needed to understand and predict this behavior.

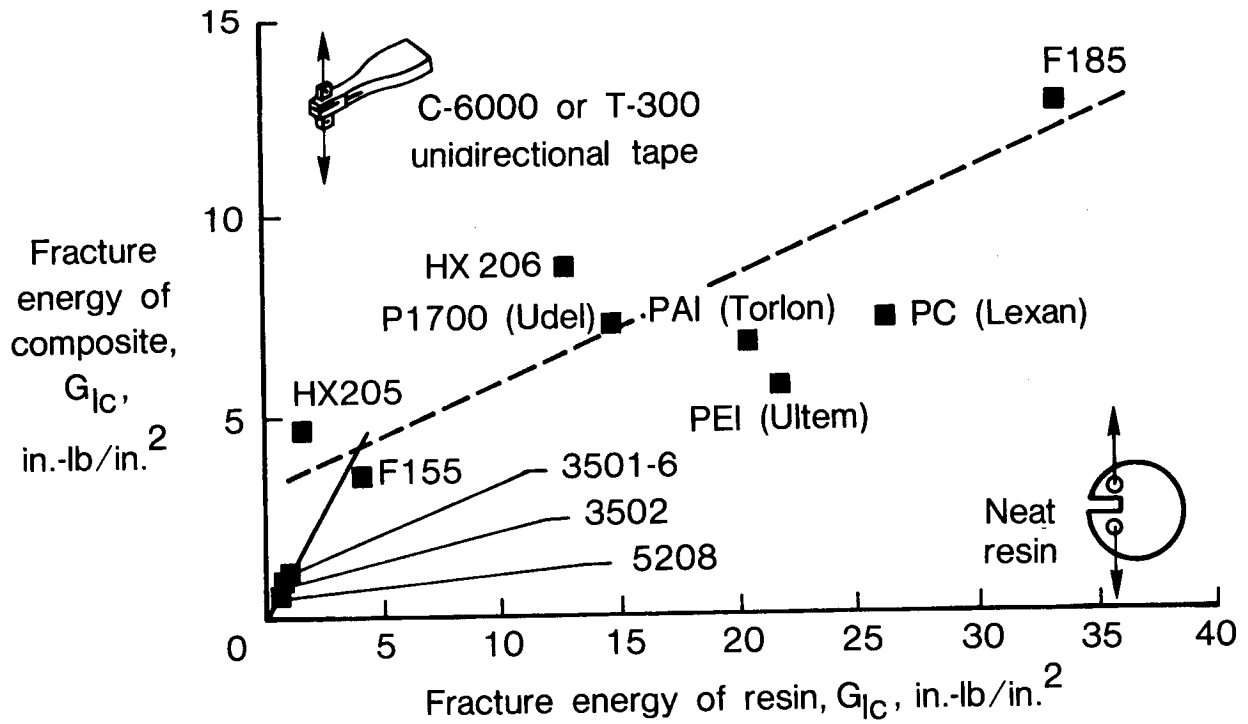

Figure 10

RESIN MODULUS VERSUS COMPOSITE INTERLAMINAR FRACTURE TOUGHNESS

Resin tensile and shear moduli, RT/dry and 180°F/wet, were also correlated with composite interlaminar fracture toughness. Figure 11 shows the relationship for tensile modulus only, using data from the University of Wyoming studies (refs. 1,2) and commercial product literature. As expected, the trend is toward lower resin moduli as G_{Ic} values increase. However, several notable exceptions exist, namely, the values for Torlon (polyamideimide or PAI) and PEEK (polyetheretherketone). The challenge for the chemist is to develop materials such as these that do not severely compromise resin modulus (and, therefore, composite compression strength) in order to increase G_{Ic}.

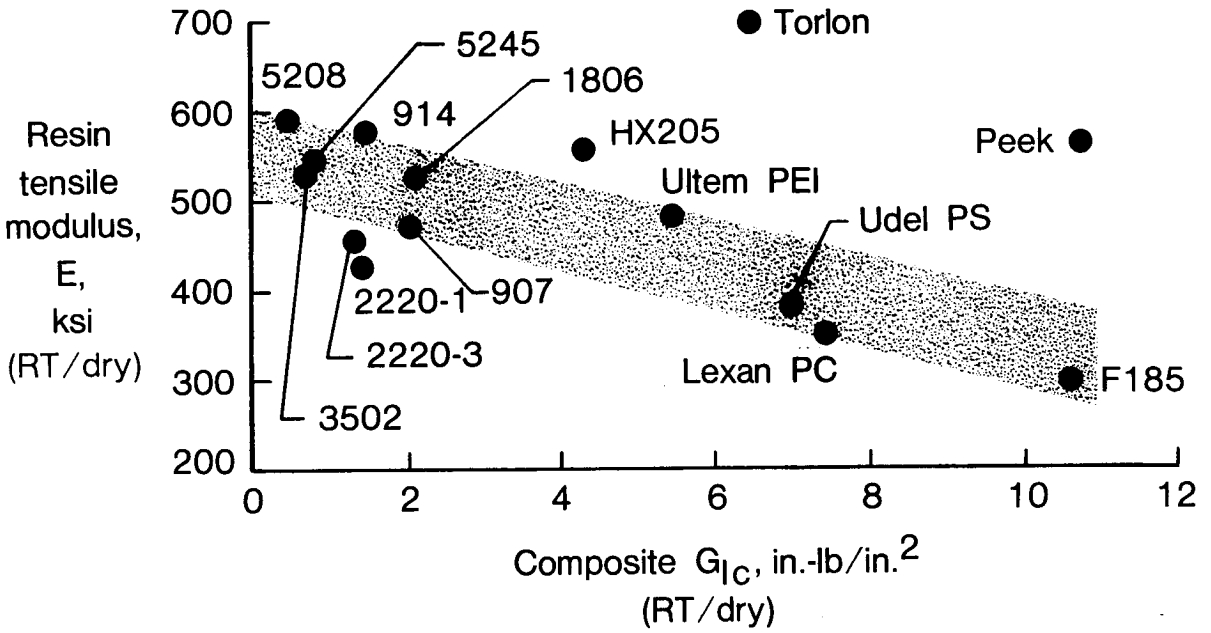

Figure 11

DESIRABLE PROPERTIES OF NEAT RESINS FOR USE AS COMPOSITE MATRICES ON COMMERCIAL AIRCRAFT

A list of desirable properties that a "third generation" of resins might possess in order to qualify as matrices for graphite composites to be used in structural applications on future commercial transports is proposed in figure 12. Until such time as an adequate data base and required fabrication technology can be built for thermoplastics, it is suggested that a maximum 350°F/200 psi processability be required. Resin G_{Ic} values of 11 to 17 in-lb/in^2 (1900 to 3000 J/m^2) should be sufficiently high to afford (after a 3- to 4-fold decrease) composite interlaminar G_{Ic} values of 4 to 6 in-lb/in^2 (700 to 1050 J/m^2). Resin tensile moduli should be well above 400 ksi, RT/dry, and above 350 ksi, 180°F/wet, to achieve acceptable composite compression strengths. For the same reason, resin shear moduli should be above 200 ksi, RT/dry, and 150 ksi, 180°F/wet.

- Thermal performance range: -65° to +200°F
- Solvents: Resistance to dissolution and swelling in organic solvents in stressed state
- Moisture: Tg values sufficiently high to allow satisfactory hot/wet strengths at 200°F
- Autoclave processability: Max 350°F/200 psi
- Fracture toughness: 11 - 17 in.-lb/in.^{2} (1900-3000 J/m^2)
- Impact resistance: No requirment established for neat resin
- Stiffness: Young's modulus >400,000 psi
  Shear modulus >200,000 psi

Figure 12

SYNTHETIC APPROACHES

Four general approaches to the synthesis of tough resins are shown in figure 13. Examples will be presented for three of these approaches: toughened thermosets (specifically, elastomer-toughened epoxies), lighty crosslinked thermoplastics (specifically, ethynyl-terminated polysulfones), and linear thermoplastics (specifically, flexible polyimides). Some basic research into toughening mechanisms for thermosets will be presented first.

Methods for toughening thermoset matrices include adding thermoplastics, interleafing "soft" and "hard" layers, increasing the length between crosslinks, creating interpenetrating networks, using novel curing agents, and adding a second phase. Second phases may consist of a reactive rubber, an unreactive rubber, chopped fiber, fibrils, a thermoplastic, or a crystalline segment. The approach described herein is that of adding to an epoxy a reactive rubber which precipitates as a second phase when cured.

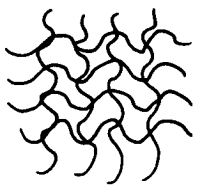

- TOUGHENED THERMOSETS
  EPOXIES, BISMALEIMIDES + THERMOPLASTIC ADDITIVES

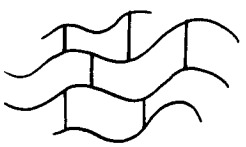

- LIGHTLY CROSSLINKED THERMOPLASTICS
  POLYSULFONES, POLYIMIDES + CROSSLINKERS

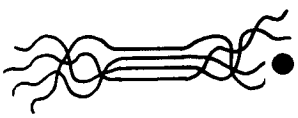

- CRYSTALLINE THERMOPLASTICS
  POLYESTERS, POLYARYLETHERS (PEEK, ETC.,)

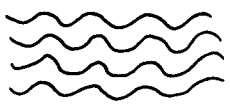

- LINEAR THERMOPLASTICS
  POLYIMIDESULFONE, TPI

Figure 13

FRACTURE TOUGHNESS IN EPOXIES CONTAINING SYSTEMATIC CHANGES IN CROSSLINK DENSITY

It is well known that brittle epoxies can be toughened by addition of a second phase, although the nature of the toughening mechanism has remained unclear. Contractual research by the General Electric Research and Development Laboratory (refs. 7,8) has elucidated this mechanism. The fracture toughness and volumetric tensile behavior of three DGEBA-DDS epoxies of varying epoxy equivalent weight were studied with and without CTBN reactive elastomer additives. Some of the data are presented in figure 14. Very little toughness enhancement occurred in the unmodified resins in spite of the reduction in crosslink density. However, for the elastomer-modified epoxies, which displayed much voiding and shearing along the fracture surface, a pronounced toughening effect of almost two orders of magnitude was observed. These results indicate that the main source of the toughness is the intrinsic ductility (as measured by crosslink density) of the host resin, in combination with enhanced shear band formation promoted by the presence of a second phase elastomer. Such information should prompt innovators to search for (1) appropriate second phases which do not compromise hot/wet properties and (2) host polymers which possess the intrinsic ductility required to unleash the toughening mechanism without severely compromising modulus.

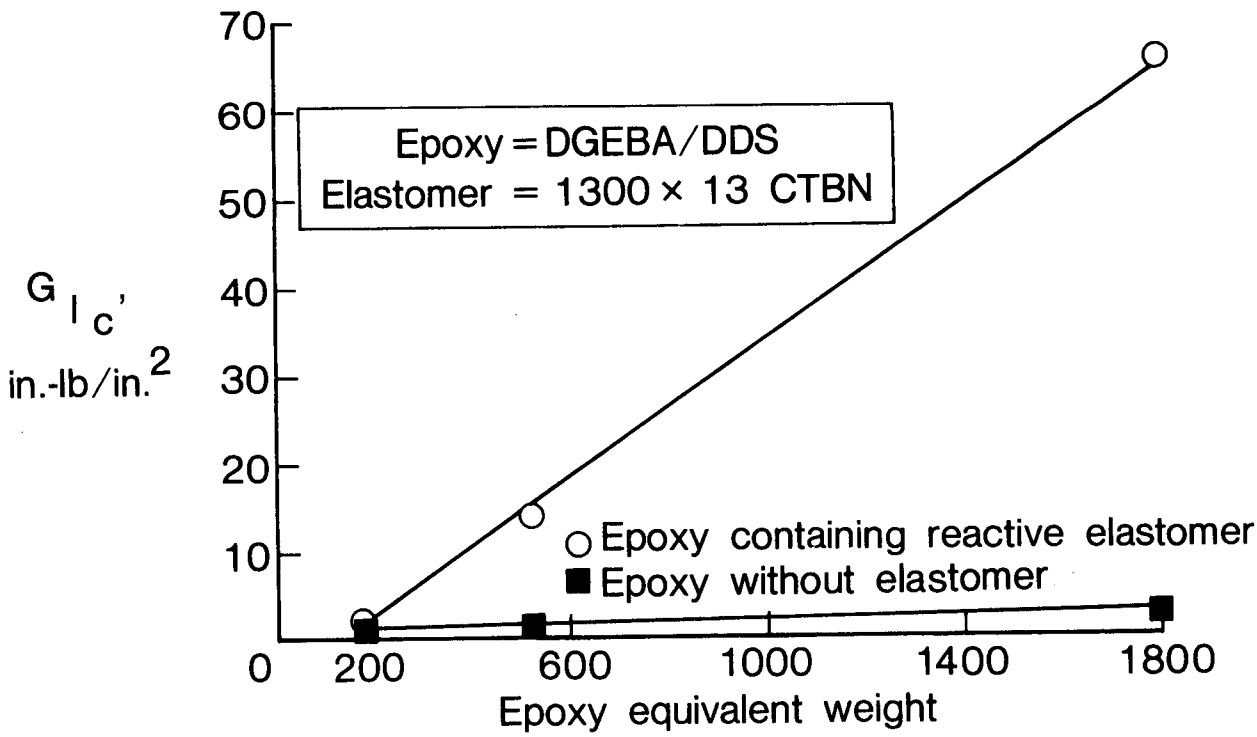

Figure 14

CROSSLINKED THERMOPLASTICS: CHEMISTRY OF CURED ETHYNYL-TERMINATED POLYSULFONES

Hergenrother and coworkers (ref. 9-11) have recently synthesized and characterized thermoplastic precursor polymers which contain thermally crosslinkable ethynyl groups either pendant or terminal to the main chain. The main chain repeat units included sulfone, ester, phenoxy, and phenylquinoxaline. Main chain lengths were systematically varied to determine the effect on various cured resin properties.

Figure 15 outlines the chemistry of the ethynyl-terminated polysulfone system. The repeat unit, n, was varied from approximately 7 to 59, thereby affording number average molecular weights ranging from approximately 3000 to 26000 g/mole. On thermal treatment at temperatures up to 250°C (488°F), the terminal ethynyl groups react to yield a mixture of products involving chain extension, branching, and crosslinking.

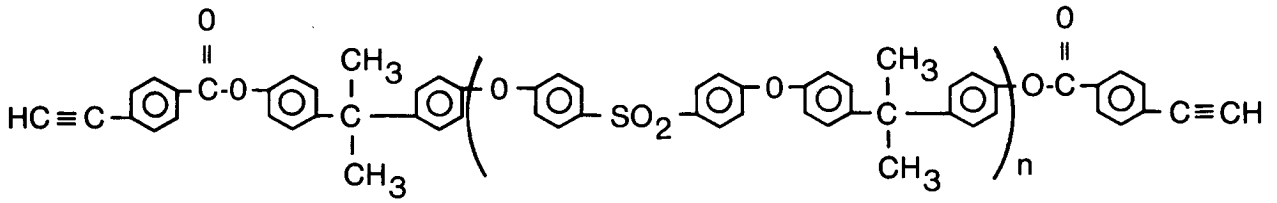

Thermoplastic precursor

$\downarrow \Delta$

Cured resin

Chain extension, branching, crosslinking

n = ~7 to ~59 ($\bar{M}_n$ ~3,000 to ~26,000 g/mole)

Figure 15

PROPERTIES OF CURED ETHYNYL-TERMINATED POLYSULFONES

Figure 16 presents some key properties of the cured ethynyl-terminated polysulfones (refs. 9-11). Molded specimens made from three molecular weight species, 4000, 8000, and 12000 g/mole, displayed increased resistance to swelling in chloroform as the molecular weight between crosslinks decreased. The property tradeoff to achieve this was fracture toughness (G_{Ic}), which decreased perceptively from 12 to 4.5 in-lb/in^2 (2100 to 790 J/m^2) as molecular weight decreased.

The properties of cured thin film having a molecular weight between crosslinks of 12000 g/mole are also shown in figure 16. The percentage elongation indicates strains to failure that are desirable in toughened materials, but the tensile modulus does not appear to be sufficiently high to produce good composite compressive strengths. The overall desirable balance of properties (modulus, solvent resistance, and fracture toughness) required in a matrix material has not yet been achieved with this class of polymers, but further property enhancements seem possible.

Molded resin

	Molecular weight, $\bar{M}_n$ (g/mole)		
	4000	8000	12,000
T_g, °C (250°C cure)	202	200	196
Swelling in chloroform, %	< 10	~ 20	~ 55
G_{Ic}, in.-lb/in.^{2} (J/m^2)	4.5 (790)	7.4 (1300)	12 (2100)

Thin film ($\bar{M}_n$ ~ 12,000 g/mole)

	Test temperature	
	26°C	93°C
Tensile strength (ksi)	12.1	9.6
Tensile modulus (ksi)	355.0	336.0
Elongation, %	4.6	8.2

Figure 16

HOT MELT PROCESSABLE POLYIMIDE

Figure 17 presents the chemistry and characterization data for a new breed of hot melt processable linear polyimides (refs. 12,13). Their main chemical structural feature is the large number of flexibilizing atoms located between the aromatic rings. These atoms serve to reduce the rigidity of the polymer backbone and, combined with the phenyl groups, tend to dilute the effect of the intractable imide moieties. The overall result is a large decrease in melt viscosity vis-a-vis ABS rubber and Torlon polyamideimide. The excellent fracture toughness combined with the high flexural modulus value and solvent resistance make these materials attractive candidates for scale-up and further evaluation as composite matrices for a variety of structural applications.

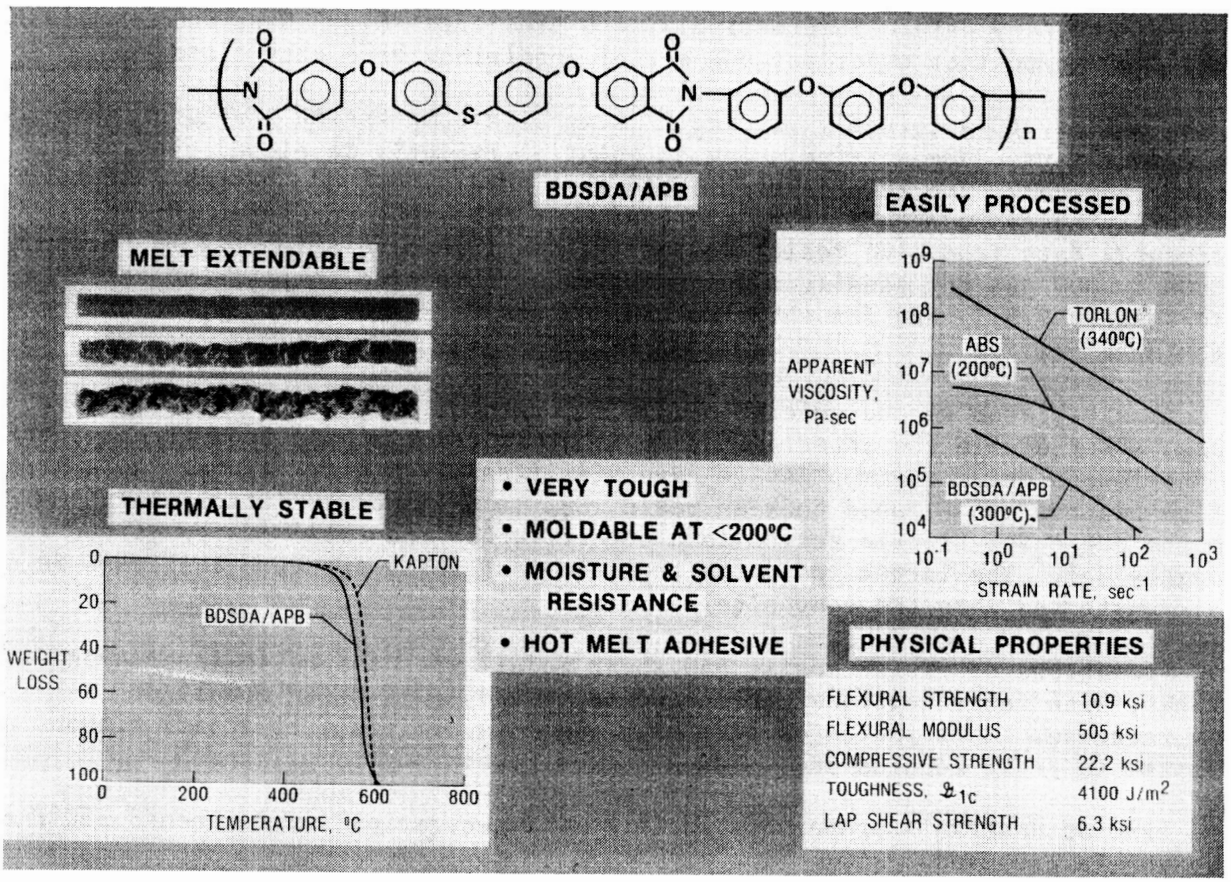

Figure 17

CONCLUDING REMARKS

Measurements of the stiffness properties of 3502, 914, 2220-1, and 2220-3 neat resins at RT, 130°F, and 180°F under dry and moisture-saturated conditions showed that 3502 had the best retention of tensile moduli at all temperatures after moisture exposure but the poorest retention of shear modulus under 180°F/wet conditions. The largest drop in tensile modulus from RT/dry to 180°F/wet was observed for 914. The moisture-saturated tensile and shear moduli for 914, 2220-1, and 2220-3 were almost identical.

Using micromechanical relationships, stiffness properties of carbon fiber reinforced composites made from these four resins were predicted for RT and 212°F exposures under both dry and wet conditions. The RT/dry values correlated well with experimental RT/dry data. Interestingly, the predicted E_{11}, E_{22}, and G_{12} values for the four composites under any one set of conditions were very close.

The ability to accurately predict 0° composite compression strengths from resin tensile moduli was demonstrated using an equation recently developed by Hahn and Williams (ref. 6). The relationship shows that candidate tough resins must have relatively high resin moduli to afford good 0° composite compression strengths. Experimental data from nine resins demonstrated a linear relationship in the range from 300 to 600 psi for tensile modulus versus 0° composite compression strength (approximately 2.5:1) and for shear modulus versus 0° composite compression strength (approximately 1:1).

Composites from second generation 350°F toughened thermosets have, on the average, about double the interlaminar G_{Ic} exhibited by those from first generation thermosets while thermoplastics have significantly higher values. An empirical relationship was established between resin G_{Ic} and composite interlaminar G_{Ic} in which the ratio for brittle resins is about 1:1 while the ratio for toughened resins is roughly 3:1. The latter indicates that the neat resin fracture toughness is not fully transferred into the composite.

Correlations of resin tensile and shear moduli with composite interlaminar G_{Ic} show that, with few exceptions, the trend is toward lower resin moduli as G_{Ic} values increase. This indicates that high G_{Ic} is difficult to attain without a compromise in resin modulus and related composite compression strength.

A list of desirable properties for a "third generation" of toughened 350°F cure thermosets is proposed.

For two-phase toughened thermosets, the main source of toughness was shown to be the intrinsic ductility of the host resin.

Synthetic studies show that while lightly crosslinked polysulfones do not yet exhibit the desirable balance of properties required in a matrix material, linear "flexibilized" polyimides remain attractive candidates for further evaluation.

REFERENCES

1. Zimmerman, R. S.; Walrath, D. E.; and Odom, E. A.: Investigation of Toughened Neat Resins and Their Relations to Advanced Composite Mechanical Properties. Presented at the Tough Composite Materials Workshop, NASA Langley Research Center, Hampton, VA, May 24-26, 1983.

2. Zimmerman, R. S.; Adams, D. F.; and Walrath, D. E.: Investigation of the Relations Between Neat Resin and Advanced Composite Mechanical Properties. NASA CR-172303, 1984.

3. Crane, D. A.; and Adams, D. F.: Finite Element Micromechanical Analysis of a Unidirectional Composite Including Longitudinal Shear Loading. AMMRC TR-81-7, Feb. 1981. (Also Report UWME-DR-101-101-1, University of Wyoming, Department of Mechanical Engineering, Feb. 1981.)

4. Miller, A. K.; and Adams, D. F.: Micromechanical Aspects of the Environmental Behavior of Composite Materials. Report UWME-DR-701-111-1, University of Wyoming, Department of Mechanical Engineering, Jan. 1977.

5. Miller, A. K.; and Adams, D. F.: Inelastic Finite Element Analysis of a Heterogeneous Medium Exhibiting Temperature and Moisture Dependent Material Properties. Fibre Science and Technology, vol. 13, no. 2, 1980, pp. 135-153.

6. Hahn, H. T.; and Williams, J. G.: Compression Failure Mechanisms in Unidirectional Composites. NASA TM-85834, 1984.

7. Yee, A. F.; and Pearson, R. A.: Toughening Mechanism in Elastomer-Modified Epoxy Resins - Part 1. NASA CR-3718, Aug. 1983.

8. Pearson, R. A.; and Yee, A. F.: The Effect of Crosslink Density on the Toughening Mechanism of Elastomer Modified Epoxies. Polymer Materials Science and Engineering, vol. 49, 1983, p. 316.

9. Hergenrother, P. M.: Ethynyl-Terminated Polysulfones: Synthesis and Characterization. Journal of Polymer Science, Polymer Chemistry Ed., vol. 20, 1982, p. 3131.

10. Hergenrother, P. M.; and Jensen, B. J.: Ethynyl-Terminated Polysulfone: Preliminary Mechanical Properties. Organic Coatings and Applied Polymer Science, vol. 48, 1983, p. 914.

11. Hergenrother, P. M.; Jensen, B. J.; and Havens, S. J.: Thermoplastic Composite Matrices with Improved Solvent Resistance. 29th National SAMPE Symposium/ Exhibition, vol. 29, 1984, p. 1060.

12. Burks, H. D.; and St. Clair, T. L.: Synthesis and Characterization of a Melt Processable Polyimide. NASA TM-84494, 1982.

13. Burks, H. D.; and St. Clair, T. L.: The Effect of Molecular Weight on the Melt Viscosity and Fracture Energy of BDSDA/APB. Journal of Applied Polymer Science, vol. 29, 1984, p. 1027.

Page intentionally left blank

Page intentionally left blank

Page intentionally left blank

CONFIGURATION OF STIFFENED PANELS

The configuration of the panels is shown in figure 1. They were 12 inches wide and 24 inches long between the grips of the testing machine. The sheet and stringers were made with graphite/epoxy prepreg tape. The graphite fibers were T300 made by Union Carbide and the epoxy was 5208 made by Narmco Materials Inc. The sheet and stringers were cocured with film adhesive added to the stringer-sheet interface. The sheets were 16 plies thick and made with $(45/0/-45/90)_{2S}$ and $(45/0/-45/0)_{2S}$ layups. The stringers were unidirectional and had various widths and thicknesses. The values of stringer area were chosen such that the ratios of stringer stiffness to panel stiffness μ were 0.3, 0.5, and 0.7. Consequently, for a given stiffness ratio, the stringers were thicker for the stiffer $(45/0/-45/0)_{2S}$ sheets than for the $(45/0/-45/90)_{2S}$ sheets.

Three or six panels were made of each type. The panels were loaded in tension at the ends to produce uniform axial strain parallel to the stringers. Load and not displacement was controlled. Crack-like slots of various lengths were machined into the sheets at the middle of the panels to represent damage.

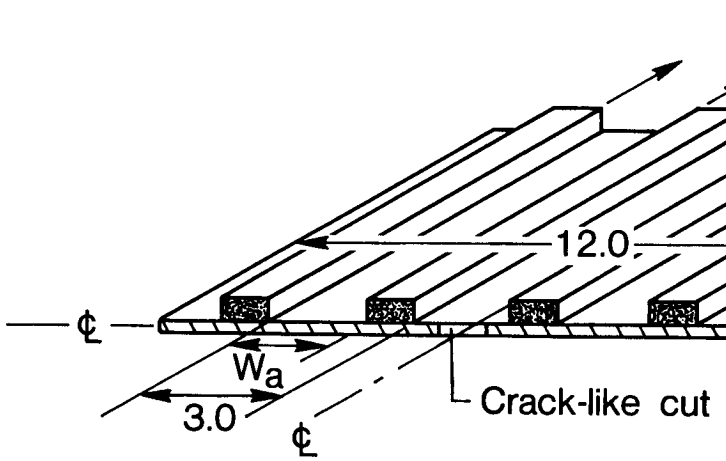

W_a, in.	$\mu = \frac{\text{Stringer stiffness}}{\text{Panel stiffness}}$
2.0	0.3
.5 2.0 2.5	.5
2.0	.7

Figure 1

TEST RESULTS FOR $(45/0/-45/90)_{2S}$ PANELS WITH $\mu = 0.7$

First, some typical test results are presented to show how the cracks initiated and were arrested. Strain versus crack tip position is shown in figure 2 for the three $(45/0/-45/90)_{2S}$ with $\mu = 0.7$. As the panels were loaded, cracks initiated and ran from the slot ends at strains that correspond to the the failing strains of unstiffened sheets. (The failing-strain curve without stringers is associated with initial crack length or slot length, not final length. Thus, the strains at instability actually agree better with the curve than indicated.) For the shortest slot, the crack was not arrested. But for the longest slots, the stringers arrested the cracks and loading was continued. Eventually, the sheet and stringers appeared to fail simultaneously at a strain considerably larger than that for a sheet without stringers. This behavior is typical of all the panels. Usually, when cracks were not arrested, failing strains were greater than or equal to those when cracks were arrested.

During each test, crack-opening displacements were measured continuously, and loading was halted numerous times to make radiographs of the crack tips. An opaque dye (zinc iodide) was used to enhance the visibility of matrix damage. The radiographs and crack-opening displacements were used to estimate the crack tip positions plotted in figure 2. The last radiograph of panel C, which was made at a strain corresponding to 97 percent of the failing strain, is also shown in figure 2. (The last radiograph of panel B has the same appearance as that of panel C.) The two dark rectangular regions are the stringers. (Strain gages and wires can also be seen.) The even darker regions at the ends of the crack are disbonds between the sheet and stringers. Probably large shear stresses were the principal cause of the disbonds. The radiograph indicates that the arrested crack ran under the stringers about 1/3 inch. Usually the cracks extended to the disbond fronts.

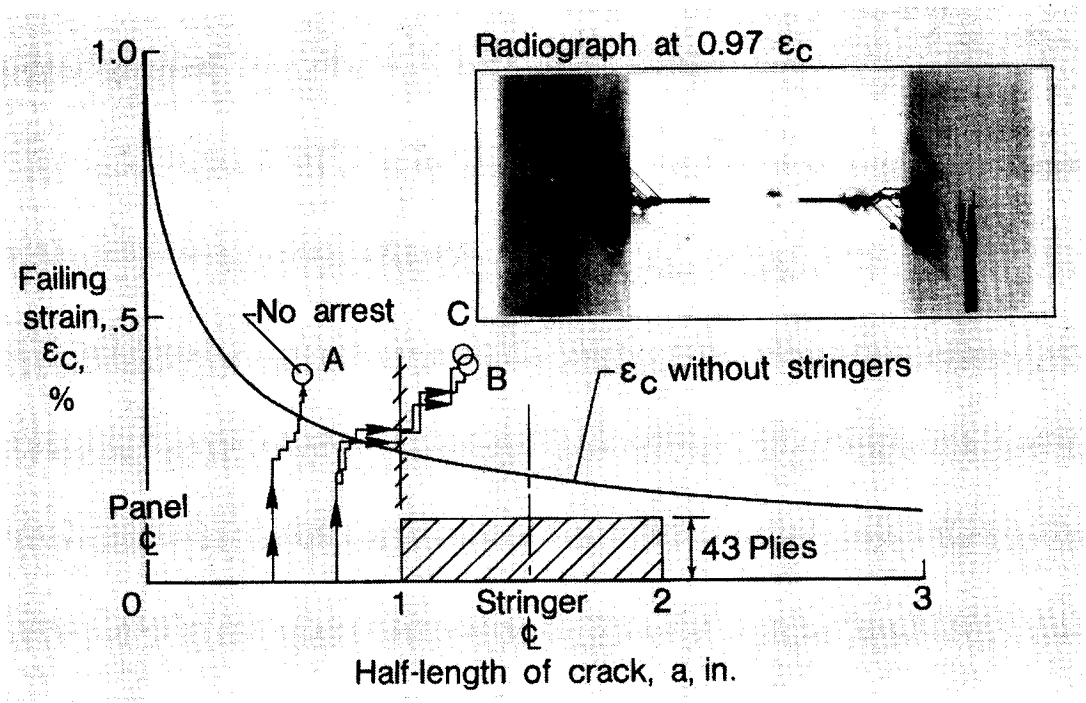

Figure 2

TEST RESULTS FOR $(45/0/-45/90)_{2S}$ PANELS WITH $\mu = 0.5$

Strain versus crack-tip position is shown in figure 3 for three of the panels with $\mu = 0.5$ and stringers of different thicknesses and widths. The initiation and arrest of cracks are similar to those in figure 2. The last radiographs are also shown in figure 3. They were made within 5 to 10 percent of the failing load. For lack of space, only one crack tip is shown. (Both crack tips had virtually the same position and appearance.) For the thinnest stringers, panel A, the crack arrested at the inside edge of the stringer. However, for the thicker stringers, panels B and C, the stringers disbonded locally, and the cracks ran beneath the stringers. For the thickest stringers, panel C, the crack ran slightly beyond the outside edge of the stringer. The shear stresses that caused the disbonds are larger for thicker stringers. Thus, although the size of disbonds varied quite a bit, they tended to be larger for thicker stringers. The variations seemed somewhat random, as though they were caused by variations in interface strength.

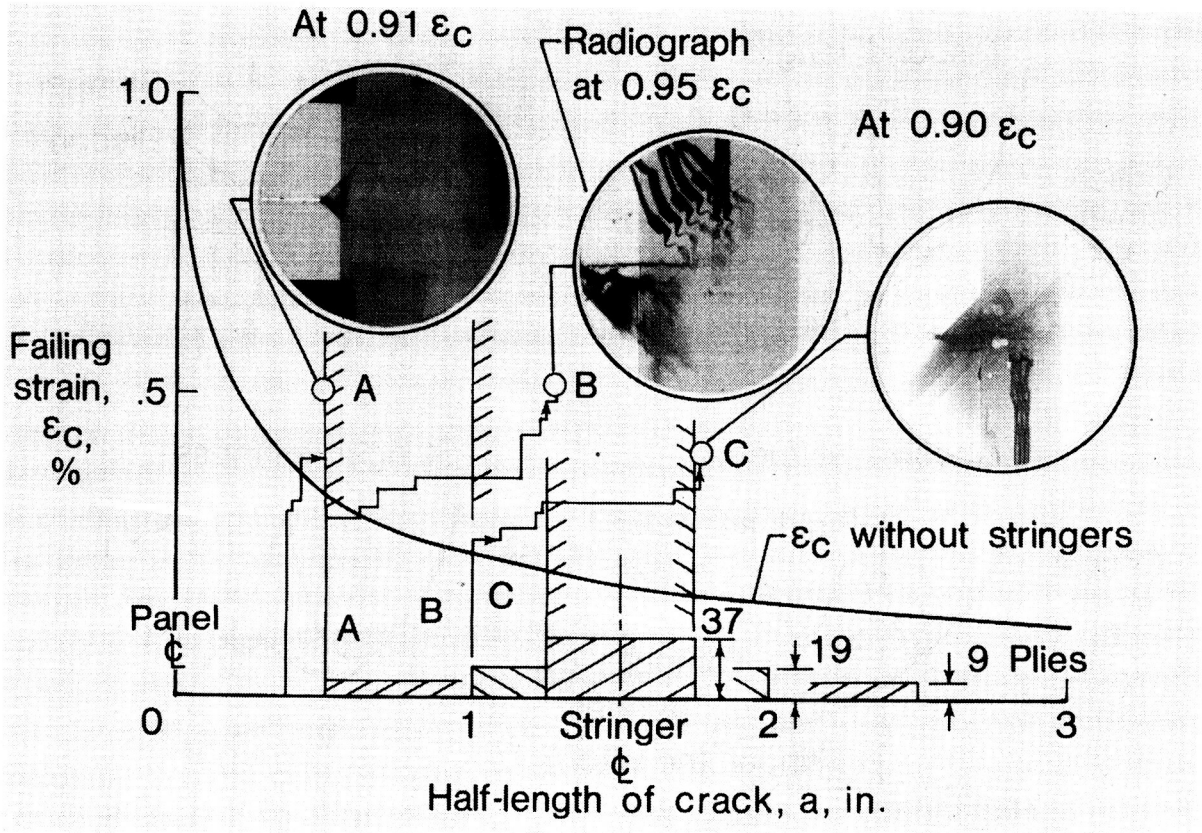

Figure 3

ANALYSIS FOR BONDED STRINGERS

The stress intensity factor has been determined for a cracked sheet with bonded and partially disbonded stringers (ref. 1). The stiffnesses of the stringers and adhesive were taken into account. The stringer was assumed to act along its centerline, that is, to have no width. For a critical value of the stress-intensity factor, the corresponding strain was calculated and plotted against half-length of crack in figure 4. Results are shown with and without stringers for different values of stringer and adhesive stiffness and disbond length. Because the stringers reduce the stress intensity factor, the critical-strain curves with stringers are above that without stringers. They have high peaks when the crack tip is just beyond the stringer. The curve is lower with a disbond ($\ell > 0$). If the stringers were completely disbonded, the curves with and without stringers would be the same. The curve is higher for a stiffer adhesive and stiffer stringers. For a rigid adhesive and $\ell = 0$, the critical strain would go to infinity for the crack tip at the stringer centerline, regardless of the stringer stiffness.

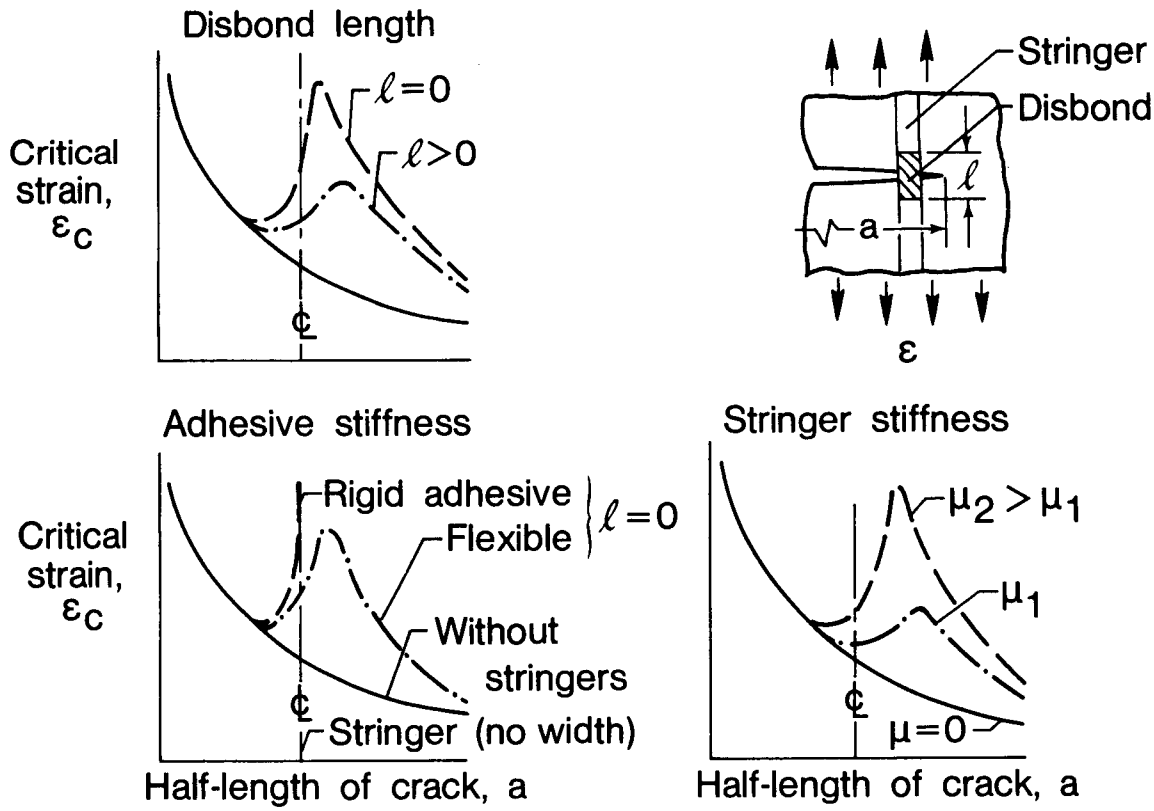

Figure 4

PREDICTING FAILING STRAINS

The critical strain is replotted against half-length of crack for different disbond lengths in figure 5. For an initial crack length of $2a_o$, the results indicate that the crack would run at a far-field strain of ε_{ci} and be arrested at the stringer if $\varepsilon_{ci} < \varepsilon_{cu}$. (Dynamic effects may require ε_{ci} to be even less for arrest.) Upon increasing the load further, the arrested crack would run at ε_{cu}. Short cracks, where $\varepsilon_{ci} > \varepsilon_{cu}$, would not be arrested, and failing strains would be greater than ε_{cu}. Thus, for arrested cracks, the failing strain ε_{cu} would be given by the peak value of ε_c, which decreases with disbond length and increases with adhesive and stringer stiffness. Also, for a given adhesive and stringer stiffness and disbond length, ε_{cu} is independent of a_o. For short cracks that are not arrested, $\varepsilon_{cu} = \varepsilon_{ci}$. Typically, the data followed this trend.

Note that thin well-bonded stringers would also have large local stresses when the crack tip approached. Thus, they could fail and reduce the failing strain below that given by the curves in figure 5.

Although this analysis gives insight into how the failing strains of stiffened panels are affected by configuration and material, it could give very inaccurate predictions. Failing strains would be greatly overestimated for wide stringers when there is little or no disbonding because the stringers are assumed to act (or to be concentrated) at their centerlines. Predictions would be more accurate if the disbond was long compared to stringer width. However, only a few panels with very thick, narrow stringers had long disbonds.

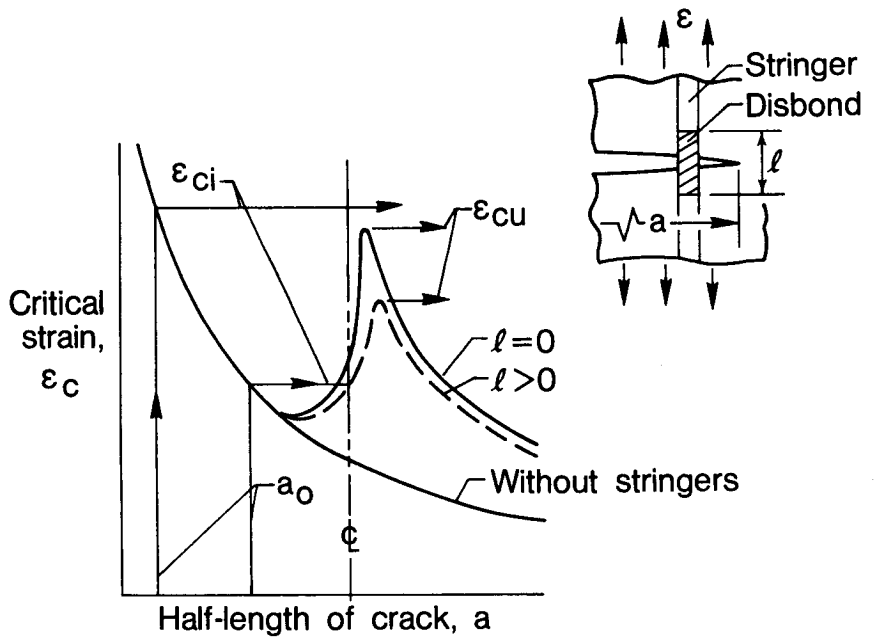

Figure 5

SHEAR LAG ANALYSIS

A shear lag analysis was made of a stiffened panel, treating the stringers and sheet as monolithic regions in the sheet. The sheet and stringers have Young's moduli E_{sh} and E_{st} in the loading direction and thicknesses t_{sh} and t_{st}, respectively. (See figure 6.) Within the region of the stringers, the stringers and sheet are assumed to act in parallel, and the stiffness is given by $(Et)_1 = (Et)_{sh} + (Et)_{st}$. The crack was assumed to extend completely across the sheet between stringers as though it were arrested.

Typical results are shown in figure 6. The logarithm of the strain concentration factor (SCF) is plotted against the logarithm of an effective crack length $W_a(Et)_{sh}/(Et)_1$ or $W_a/(1 + \alpha)$, where $\alpha = (Et)_{st}/(Et)_{sh}$. The SCF is the ratio of the strain at the crack tip to the far-field strain. (The crack tip strain is finite in the shear lag analysis.) Also, the analysis indicates that stringer width W_{st} has little effect on the SCF as long as W_{st} is large compared to a characteristic dimension of the order of fiber spacing. For $W_a = 0$, SCF = 1 as required. For a large effective crack length, SCF $\propto \sqrt{[W_a/(1 + \alpha)]}$, much as the stress intensity factor is proportional to $\sqrt{W_a}$ for an unstiffened sheet. Thus, the shear lag and stress intensity factor analyses give similar results for an unstiffened sheet $\alpha = 0$. This similarity suggests that a stress intensity factor can be synthesized using the shear lag results.

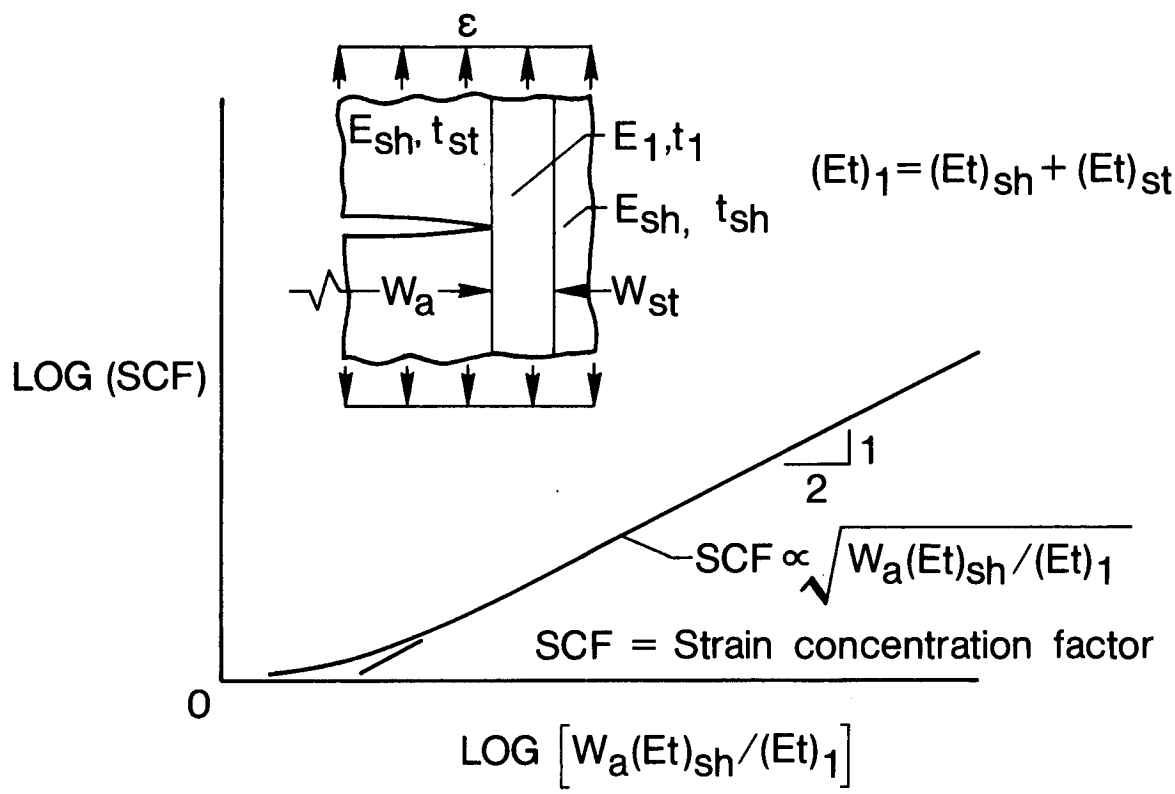

Figure 6

SYNTHESIZED STRESS INTENSITY FACTOR

Without stringers, the stress intensity factor K_Q is given by equation (1) in figure 7, where S_{sh} is the stress applied to the sheet and F_{tu} is the uncracked strength of the sheet. (Note that the stress applied to the stringer region in figure 6 is $S_{sh}E_1/E_{sh}$.) The term $(K_Q/F_{tu})^2$ was included in equation (1) to give $S_{sh} = F_{tu}$ when $a = 0$ as required. For a state of uniaxial stress, $S_{sh} = E_{sh}\varepsilon_c$ and $F_{tu} = E_{sh}\varepsilon_{tu}$. Substituting these expressions into equation (1) for stresses and solving for $\varepsilon_{tu}/\varepsilon_c$ gives equation (2) in figure 7. The left-hand side of equation (2) is equivalent to the SCF in figure 6. Replacing a in equation (2) by $\frac{1}{2} W_a/(1 + \alpha)$, the effective crack length from the shear lag results, gives equation (3) in figure 7. For small and large effective crack lengths, equation (3) models the essential features of the shear lag results in figure 6; that is, for $W_a = 0$, SCF = 1, and for large W_a, SCF $\propto \sqrt{(W_a/(1 + \alpha))}$.

Failing strains were predicted with equation (3) and compared with the test data. The values of K_Q, the elastic constants, and ε_{tu} used to make the calculations are given in reference 2 as "Manufacturer A" material.

Without stringers,

$$K_Q = S_{sh}\sqrt{\pi a + K_Q^2/F_{tu}^2} \qquad (1)$$

For uniaxial stress ($S_{sh} = E_{sh}\,\varepsilon_c$ and $F_{tu} = E_{sh}\,\varepsilon_{tu}$),

$$\frac{\varepsilon_{tu}}{\varepsilon_c} = \sqrt{1 + \frac{\pi a\,\varepsilon_{tu}^2 E_{sh}^2}{K_Q^2}} \qquad (2)$$

Where

$$SCF = \varepsilon_{tu}/\varepsilon_c$$

With stringers, replace a by $1/2\ W_a\ (Et)_{sh}/(Et)_1$

$$\frac{\varepsilon_{tu}}{\varepsilon_c} \sqrt{1 + \frac{\pi\, W_a\,(Et)_{sh}\,\varepsilon_{tu}^2 E_{sh}^2}{2\,(Et)_1\,K_Q^2}} \qquad (3)$$

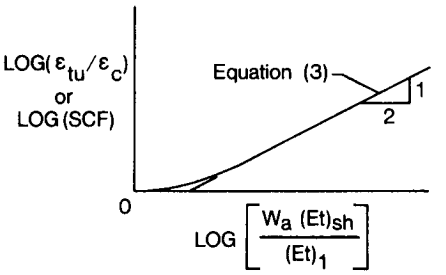

Figure 7

FAILING STRAIN VERSUS STRINGER THICKNESS

Failing strains are plotted against stringer thickness in figure 8 for panels in which cracks were arrested. Failing strains of panels without arrested cracks are not plotted. (As noted previously, they are usually larger than those of like panels with arrested cracks.) The panels had 1-inch-wide stringers and both $(45/0/-45/90)_{2s}$ and $(45/0/-45/0)_{2s}$ sheets. Predicted curves are plotted for comparison. For stringer thicknesses less than 20 or 30 plies, depending on sheet layup, the differences between measured and predicted failing strains are within the scatter among like specimens. For thicker stringers, equation (3) overestimates the failing strain. This discrepancy is probably due to out-of-plane effects, which give rise to strain gradients through the thickness. These strain gradients are not modeled in the plane analysis. They increase the membrane components of the crack tip strains by reducing the effective stiffness of the stringers, and they give rise to bending components. Both would reduce the failing strain of the panels.

Initially, three panels were made of each type. Some months later, an additional three panels of some types were made with stronger ends to avoid the possibility of failure in the grips. In some cases, both groups of the same type of panels failed in the test section, and the failing strains were noticeably different. (Data for panels that failed in the grips are not shown.) These discrepancies are usually apparent when there are more than three symbols, as for the 19-ply stringers in figure 8. Strain measurements indicate that the stiffnesses of the two groups of like panels are equal. Thus, the discrepancies are probably not due to an error in layup but may be due to differences in interface strength.

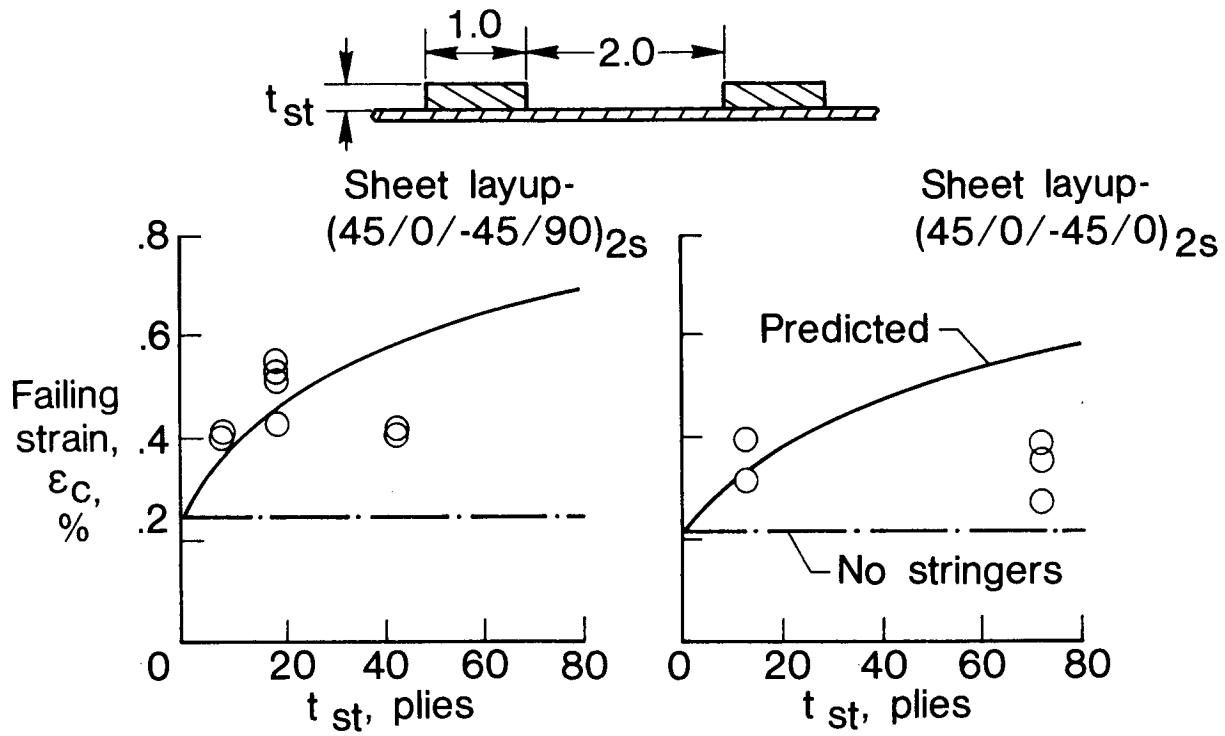

Figure 8

MODIFICATIONS TO ACCOUNT FOR OUT-OF-PLANE EFFECTS

To account for out-of-plane effects, $(Et)_1 = (Et)_{sh} + (Et)_{st}$ in equation (3) was replaced by $(Et)_1 = (Et)_{sh} + (Et)_{st}e^{-\gamma\alpha}$, where γ was determined to be 0.194 by fitting equation (3) to the data in figure 7 for panels with the thickest figure stringers of each sheet layup. The exponential factor was chosen because it is unity for small α and zero for large α. Predictions with the modified equation (3) are shown in figure 9 along with the results in figure 8. The original and the modified equation (3) give about the same results for the thinnest stringers. But, for thicker stringers, the modified equation agrees with the data and gives much lower failing strains.

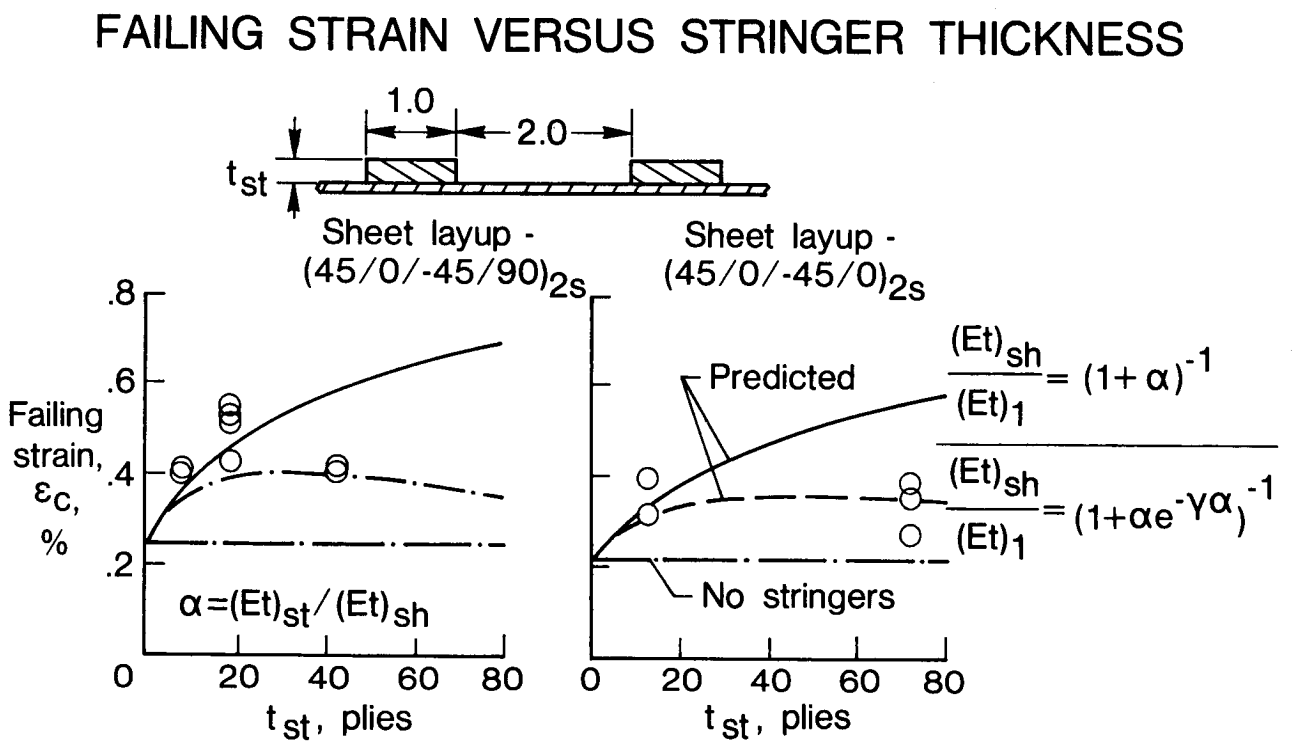

Figure 9

FAILING STRAIN VERSUS STRINGER SPACING

The failing strains are plotted against W_a in figure 10 for all the panels with a stringer stiffness ratio $\mu = 0.5$ and with arrested cracks. Values predicted with the modified equation (3) are also plotted for comparison. The measured and predicted failing strains agree. The differences are within the scatter among like specimens.

The results in figures 8 - 10 indicate that, due to the out-of-plane effects, an increase in stringer thickness above the 9 or 15 plies does not result in much further increase in failing strain.

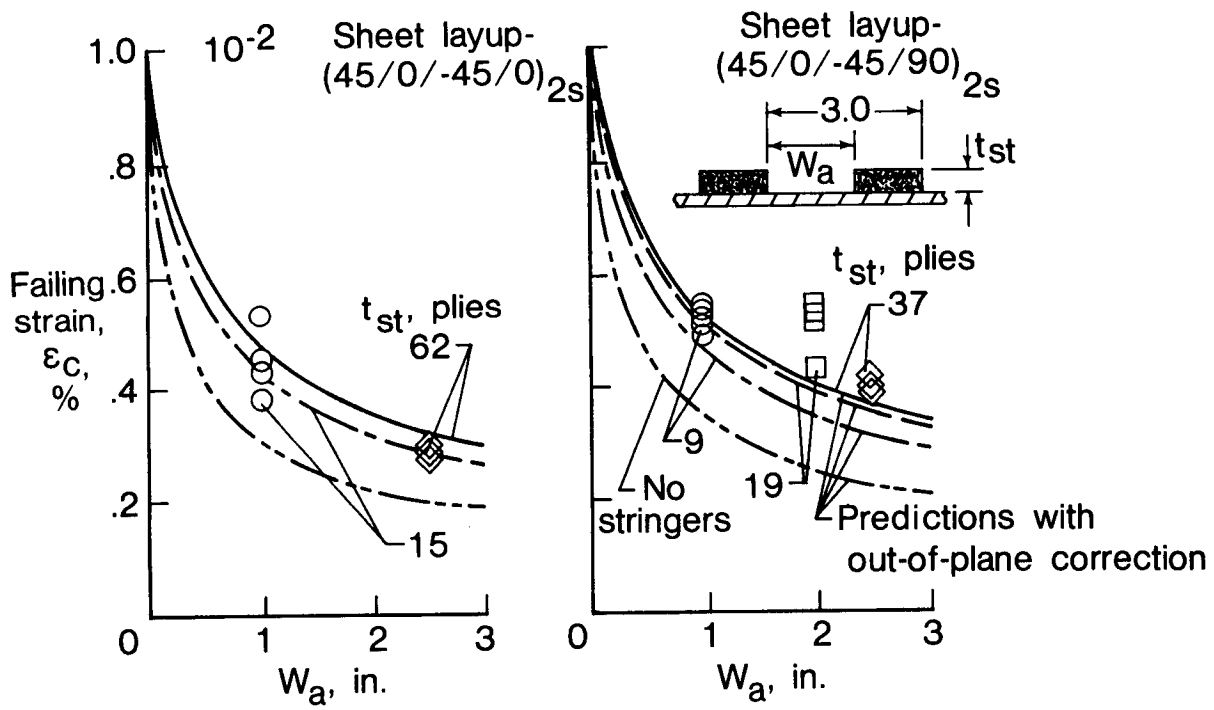

Figure 10

DESIGN CURVE FOR STIFFENED PANELS

It was shown in reference 3 that when crack tip damage is small, fracture toughness K_Q can be predicted with $K_Q = Q_c E_x/\xi$. The general fracture toughness parameter Q_c, in contrast to the fracture toughness K_Q, is independent of layup and varies only with ε_{tuf}, the fiber failing strain. For laminates with little or no crack tip damage, $Q_c = 0.30\ \varepsilon_{tuf}\sqrt{in.}$ The term $\xi = 1-\nu_{xy}\sqrt{(E_y/E_x)}$ accounts for the effect of sheet layup. The ν_{xy}, E_x, and E_y are the elastic constants of the sheet, where x denotes the loading direction.

Substituting the above equation for K_Q into equation (3) (modified to account for out-of-plane effects) and assuming that $\varepsilon_{tu} = \varepsilon_{tuf}$, a single design equation is produced for stiffened panels with any sheet layup and made of any material.

The resulting equation is shown as a single design curve in figure 11 by plotting the ratio of failing strains with and without cracks against $\xi^2 W_a/(1 + \alpha e^{-0.194\alpha})$. The $(45/0/-45/0)_{2S}$ data tend to be below the $(45/0/-45/90)_{2S}$ data because K_Q tends to be overpredicted for thin $(45/0/-45/0)_{2S}$ laminates and underpredicted for thin $(45/0/-45/90)_{2S}$ laminates (refs. 3 and 4). In comparison to scatter among like specimens, the agreement between the data and the design curve is good. A lower bound curve could be calculated using a value of $Q_c/\varepsilon_{tuf} < 0.30\ \sqrt{in.}$

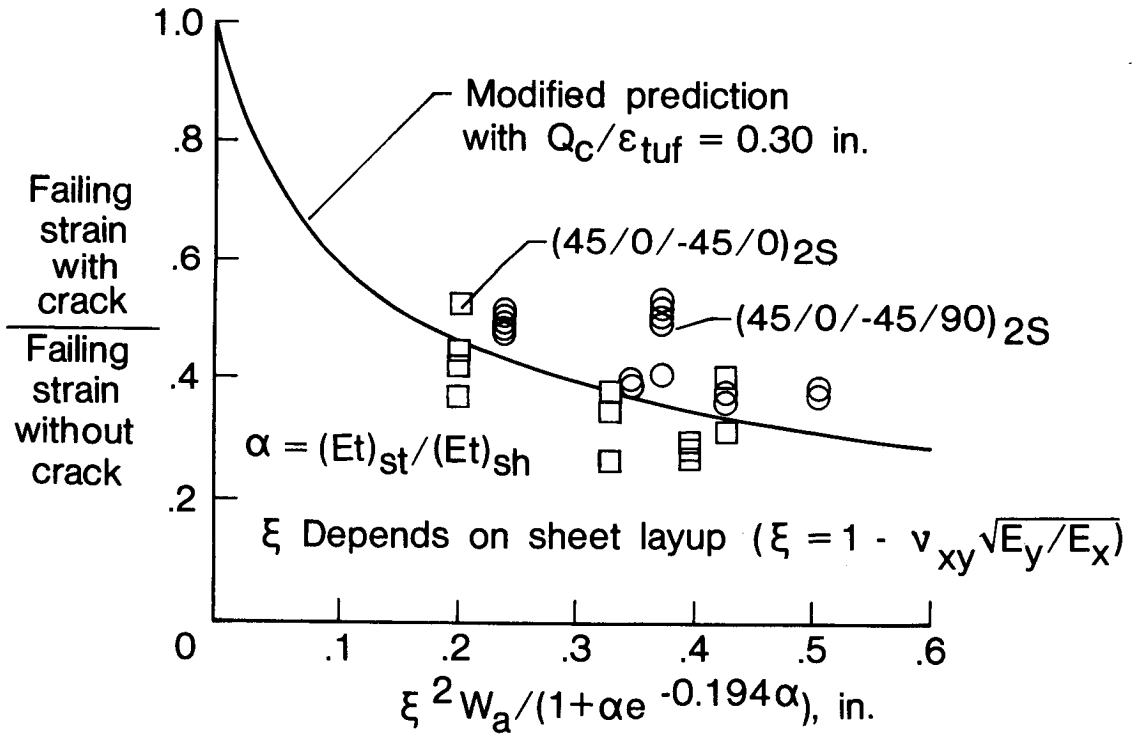

Figure 11

MAXIMUM PREDICTED IMPROVEMENT WITH STRINGERS

Equation (3) with $(Et)_{sh}/(Et)_1 = 1/(1 + \alpha e^{-0.194\alpha})$ predicts a maximum increase in failing strain of stiffened panels over unstiffened panels. Calculations of the ratio of failing strain with stringers to that without stringers is plotted against α in figure 12 for various values of W_a. The failing strain ratio has a maximum value at $\alpha = \alpha^*$, where $\alpha^* = 1/0.194$. The maximum value increases with W_a and asymptotically approaches 1.7. However, it is not very sensitive to W_a for $W_a > 1$ inch nor to α for $2 < \alpha < \alpha^*$. For the sheet layups here, $t_{st}/t_{sh} = 2.1$ and 2.9 for $\alpha = \alpha^*$. Note that the curve in figure 13 without the out-of-plane correction indicates no limit in improvement.

$$(Et)_{sh}/(Et)_1 = (1 + \alpha e^{-0.194\alpha})^{-1}$$

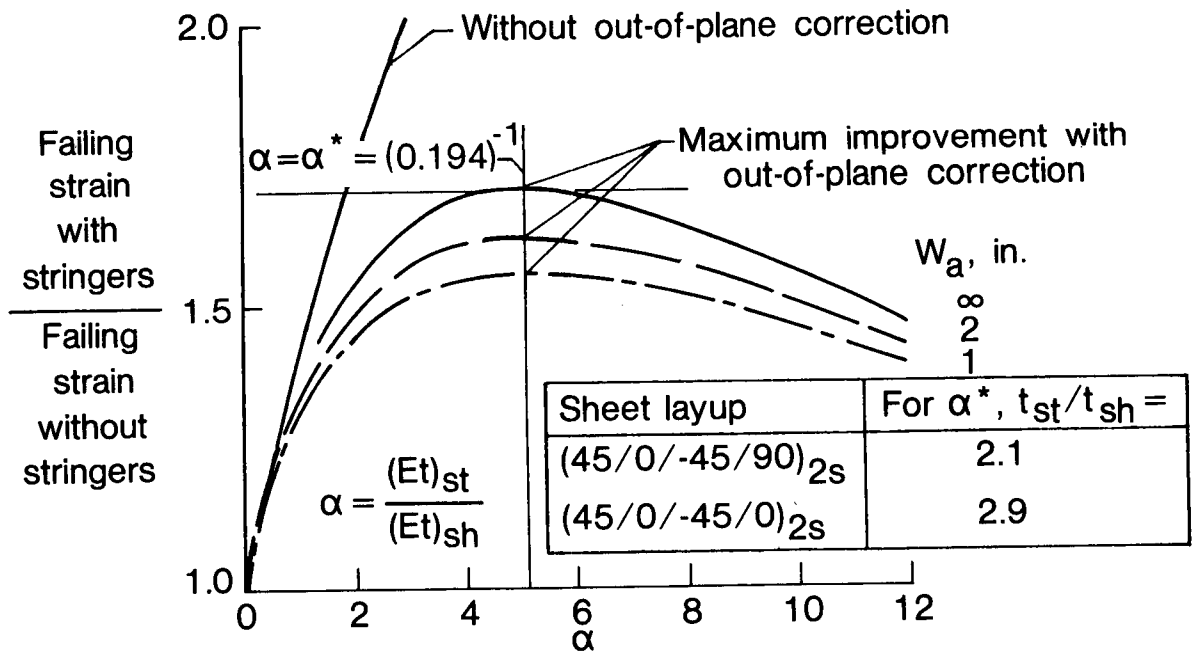

Sheet layup	For α^*, t_{st}/t_{sh} =
$(45/0/-45/90)_{2s}$	2.1
$(45/0/-45/0)_{2s}$	2.9

Figure 12

CONCLUSIONS

1. Bonded stringers can arrest cracks.

2. Stringers can increase failing strains as much as 80%.

3. Failing strains are larger for thicker and more closely spaced stringers.

4. Stringer width seems relatively unimportant.

5. Failing strains are a maximum when the thickness of unidirectional stringers is 2 to 3 times that of the sheet.

6. Very strong and stiff bonds or very weak bonds may weaken a sheet with bonded stringers.

7. A fracture mechanics analysis predicts the failing strains well.

8. A single design curve was developed using the analysis and the fracture toughness parameter Q_c.

REFERENCES

1. Arin, K.: "A Plate With a Crack, Stiffened By A Partially Debonded Stringer." Engineering Fracture Mechanics, 1974, Vol. 6, pp. 133-140.

2. Kennedy, J. M.: "Fracture Behavior of Hybrid Composite Laminates." AIAA/ASME/ASCE/AHS 24th Structures, Structural Dynamics and Materials Conference. Lake Tahoe, NV, May 2-4, 1983.

3. Poe, Jr., C. C.: "A Unifying Strain Criterion for Fracture of Fibrous Composite Laminates." Engineering Fracture Mechanics, Vol. 17, No. 2, pp. 153-171, 1983.

4. Harris, C. E.; and Morris, D. H.: "Fracture Behavior of Thick, Laminated Graphite/Epoxy Composites." NASA CR-3784, 1984.

Page intentionally left blank

IMPACT DYNAMICS RESEARCH ON COMPOSITE TRANSPORT STRUCTURES

Huey D. Carden
NASA Langley Research Center
Hampton, VA

ACEE Composite Structures Technology Conference
August 13-16, 1984
Seattle, WA

INTRODUCTION

Composite materials have in the past few years gained increased use in the aircraft industry because of their excellent mechanical properties, tailorability, and light weight. Much research has been concentrated on composite structures to determine their strength capabilities and to characterize failure mechanisms, damage tolerance, and fatigue behavior under in-flight conditions. Any potential problems with failure, damage, or fatigue (see reference 1) must be resolved before sufficient confidence is established to fully commit to composite materials. Additionally, under realistic and survivable crash conditions, the design of a composite fuselage must assure that occupants have every reasonable chance of escaping serious injury. In areas where failure could create a hazard to occupants, the impact dynamics capabilities (crashworthiness) and global response of composite structures need to be well understood. To achieve this understanding for a composite fuselage shell design, an extensive data base supported by appropriate analyses will be required. Investigations of structural response and integrity of composite fuselage structural components subjected to typical crash loading conditions are therefore required.

This paper reviews some of the experimental and analytical efforts being undertaken to investigate the response of composite and aluminum structures with the goal of gaining an understanding of the behavior of generic composite structural components under simulated crash loading conditions.

IMPACT DYNAMICS RESEARCH

NASA Langley Research Center has been involved in crash dynamics research (crashworthiness) of general aviation aircraft for over 10 years (see figure 1). In this program 32 crash tests were performed under controlled free-flight impact conditions to determine the dynamic response of airplane structures, seats, and occupants during a crash (refs. 2 to 4) and to determine the effects of flight parameters at impact on the load and structural damage experienced by the airplane and occupants (refs. 5 and 6).

Recently, research emphasis has shifted to impact dynamics of transport-category aircraft. The FAA and NASA have obtained a Boeing 720 airplane to be used in a remotely piloted air-to-ground controlled-impact demonstration (CID) test. Data from this fully instrumented airplane demonstration test will contribute to a metal airplane benchmark data base for comparison with future tests of composite structures.

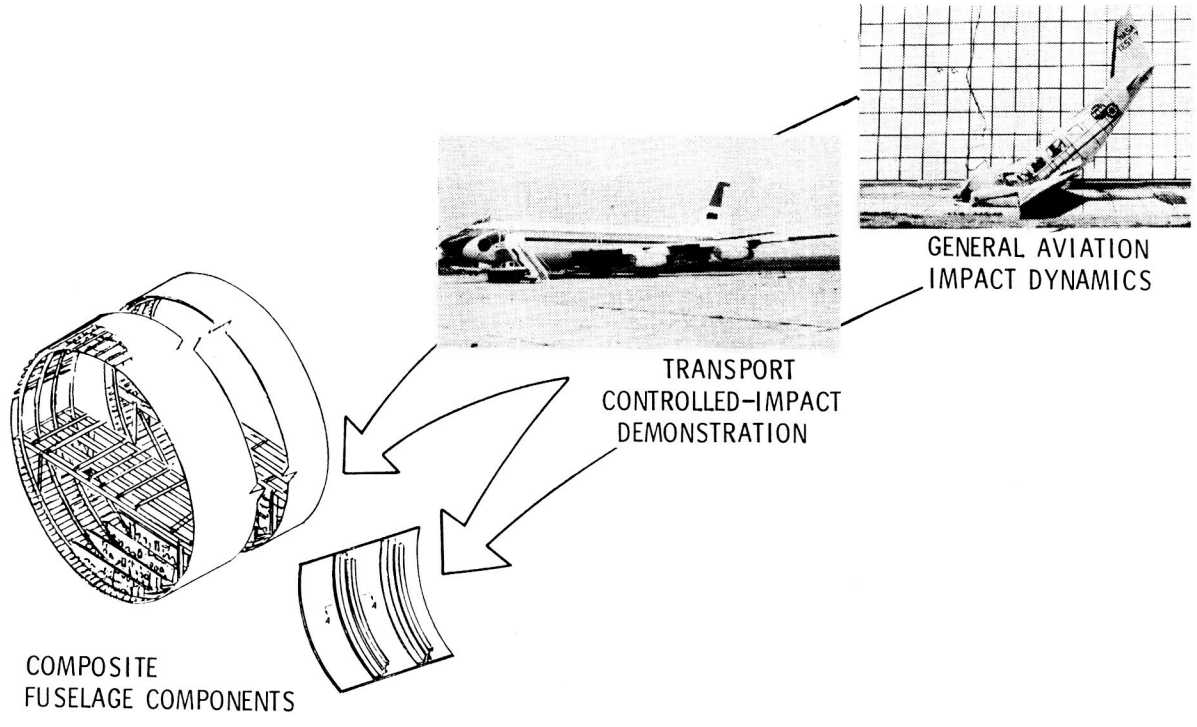

Figure 1

TYPICAL TRANSPORT FUSELAGE STRUCTURE

It is apparent from figure 2 that a typical transport fuselage, whether metal or composite, is composed of many different elements. For example, in figure 2, structures such as curved and flat panels, curved and straight beams (frames, stringers, and floor beams) as well as cylindrical sections (on a larger scale) are apparent as elements and substructures of the aircraft. In a crash situation these structures may experience loading conditions which could cause failure and thereby create hazards to occupants of the aircraft. Thus any investigation concerned with impact dynamics should address the global response and integrity of generic composite fuselage structural components subjected to typical expected crash loading conditions to provide an understanding of their behavior under such loadings.

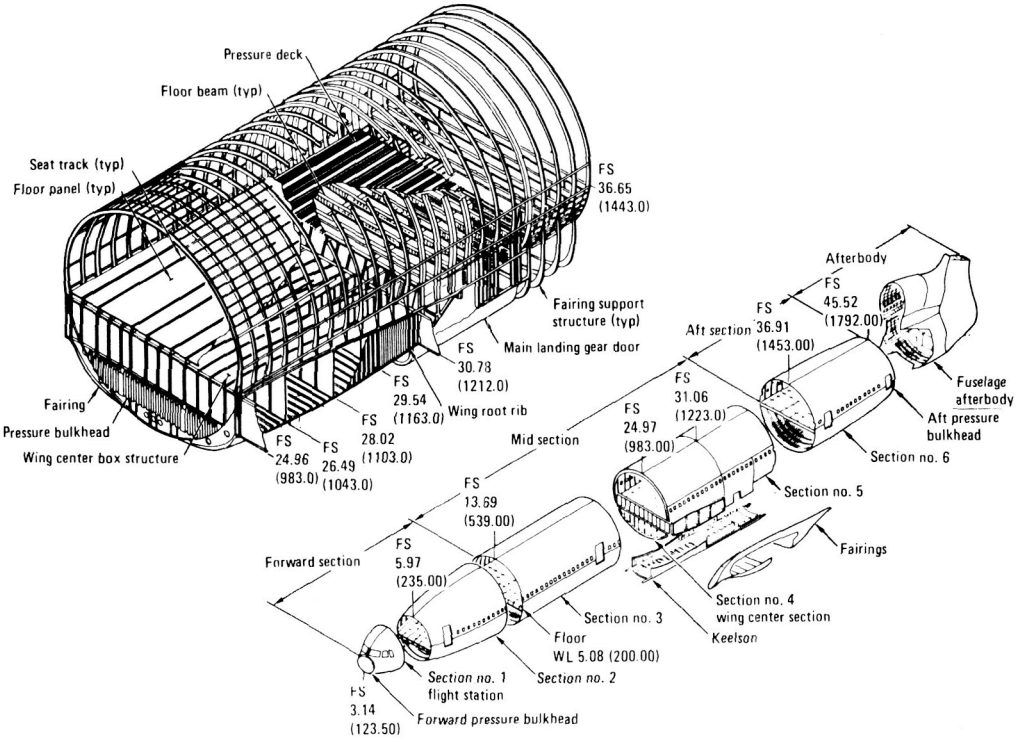

Figure 2

RESPONSE CHARACTERISTICS OF GENERIC COMPOSITE COMPONENTS TO SIMULATED CRASH LOADINGS

A research program has been formulated to investigate the response characteristics of generic composite components to simulated crash loadings. As shown in figure 3, this new program has been arranged to focus on three levels: the laminate level for material properties such as energy-absorbing qualities and the behavior of skin materials; the element level focusing on more complex geometry and behavior of beams, frames (rings), arches, and panels; and the substructure level dealing with cylindrical shells, floors, and large-scale components. The metal baseline is represented by the Boeing 720 controlled-impact demonstration test as well as some metal comparison in the laminate, element, and substructure levels themselves.

The goal of research on the generic components is to provide a data base and understanding of generic composite component behavior subjected to crash loading conditions supported by validated analytical methods. To help achieve this goal, in-house research, contractural efforts, and university grants are included in the program.

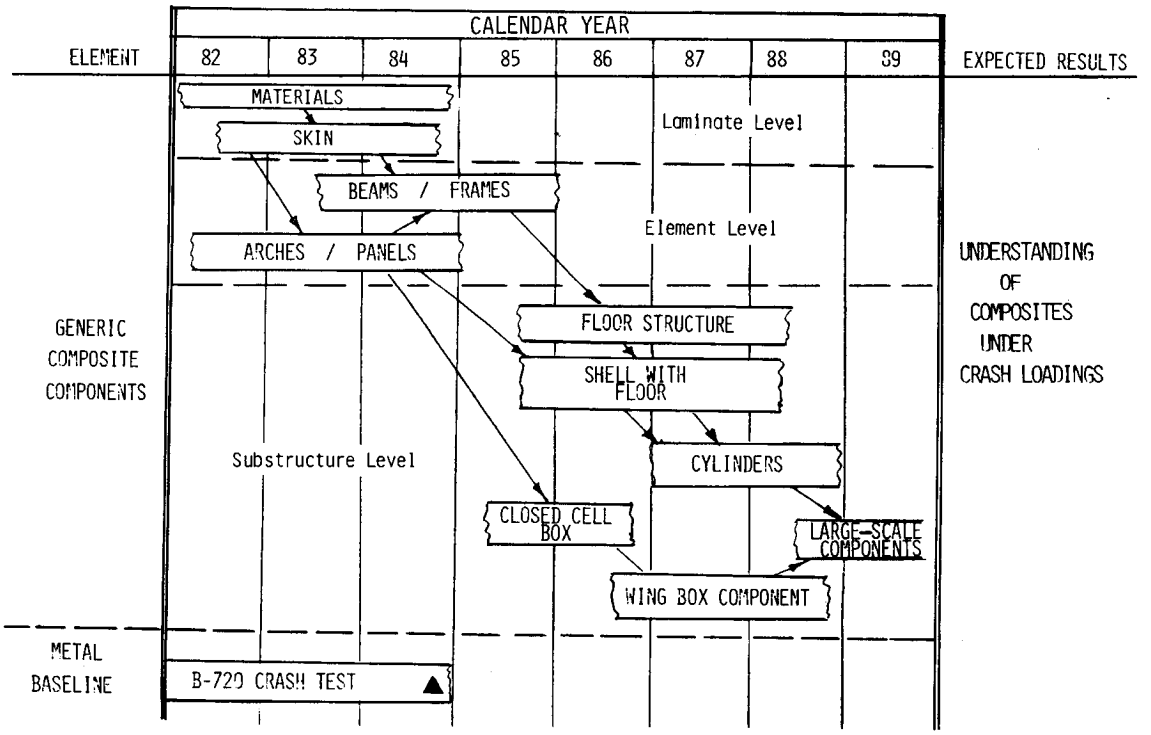

Figure 3

COMPOSITE LAMINATE LEVEL STUDIES

On the laminate level of the program, the thrust of the investigations of composite materials (see figure 4) involves:

- study of energy absorption characteristics of laminate materials
- characterization of behavior of metal and composite laminates under abrasion (sliding) forces associated with gears up, belly landings, or collapsed-gear situations
- assessment of response of laminates (skins), both all graphite/epoxy and hybrid designs, to representative crash loads which simulate inplane and out-of-plane tearing forces which can be experienced during a crash event

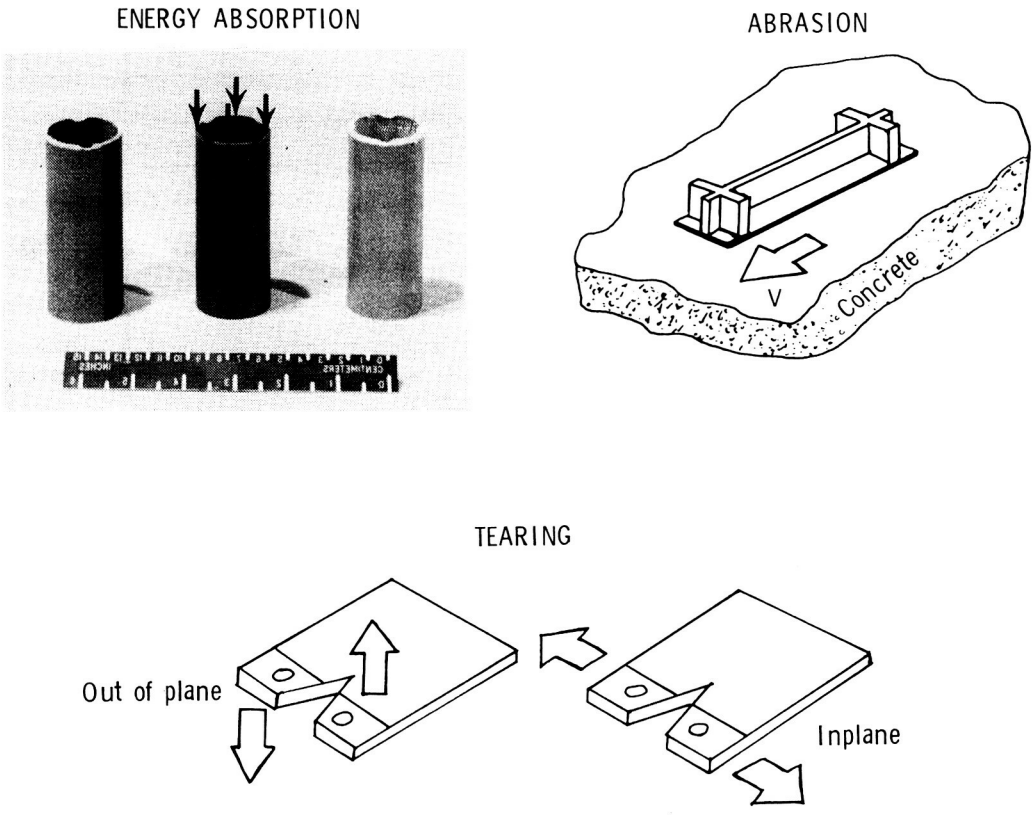

Figure 4

ENERGY ABSORPTION OF COMPOSITE MATERIALS

A joint US Army/NASA program is underway to study energy absorption characteristics of selected composite material systems (ref. 7). As depicted in figure 5, composite compression tube specimens (chosen for stability and ease of manufacturing) were fabricated with both tape and woven fabric prepreg using graphite/epoxy (Gr/Ep), Kevlar[1] epoxy (K/Ep), and glass/epoxy (Gl/Ep). Typical test results of static and dynamic specific sustained crushing stress (σ/ρ) versus ply orientation are presented. For the Gr/Ep the results varied significantly with ply orientation. In general the Gr/Ep tubes absorbed more energy than the Gl/Ep or K/Ep tubes for the same ply orientation. The [0/ $\pm$ 15] Gr/Ep tubes absorbed more energy than the aluminum tubes. Failure mechanisms for the Gr/Ep involve interlaminar cracks at the crushing front which produce beam-like elements that carry load until they buckle and subsequently fracture. The interlaminar cracks propagate and the crushing continues. K/Ep exhibits a ductile folding mode of energy absorption where extensive interlaminar cracks occur, but fiber fracture is not prevalent. Based upon the knowledge of the different failure mechanisms, follow-on efforts are underway to exploit the failure patterns to advantage in impact situations. High-strain-to-failure graphite hybridized with Kevlar is being tested, and initial results are promising in that energy absorption higher than aluminum is achieved together with desirable post-crush integrity. Material data such as discussed will be useful in designing efficient energy-absorbing structures that have good post-failure structural integrity.

[1]Kevlar is a registered trademark of Du Pont.

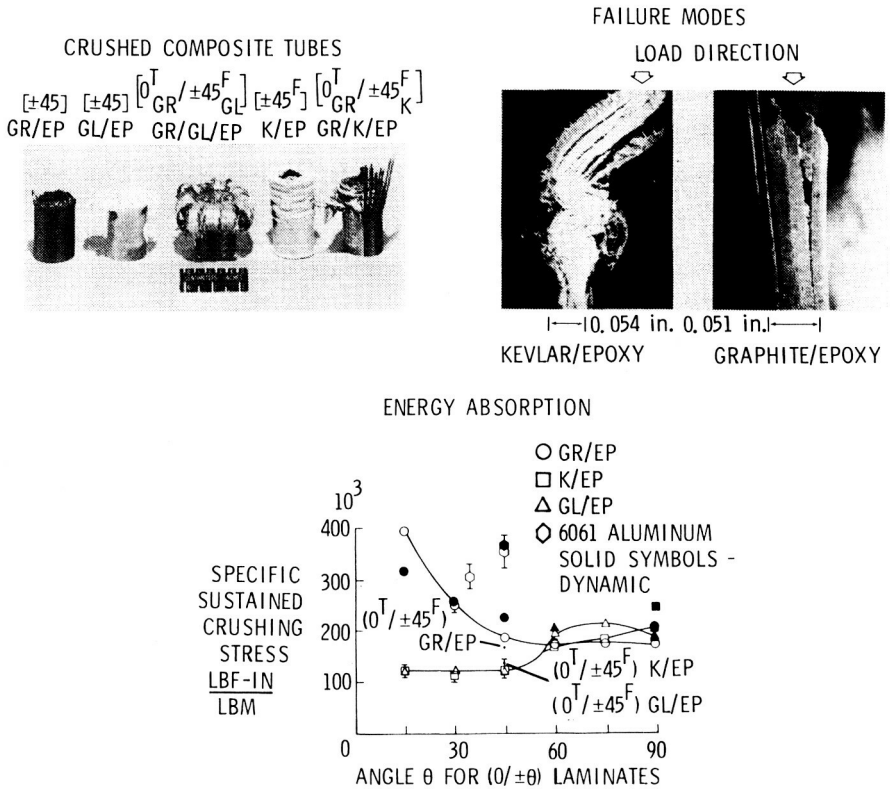

Figure 5

TEARING OF FUSELAGE SKIN PANELS
Inplane Loads

A potential crash loading condition that airplane skin panels could experience includes tearing forces during slide-out. A series of 24 tearing tests were therefore performed (on contract NAS1-15949 to Lockheed-California) on aluminum, graphite/epoxy, and two hybrid graphite/epoxy/glass laminates to experimentally assess the response of composite laminates to simulated tearing forces that might be experienced by lower fuselage skin panels during a crash event. The typical specimen configuration, inplane energy absorption, and load deflections are shown in figure 6. Load deflection data for the 5 different specimens under inplane (mode 1) tearing loads indicate that the hybrid 1 sustained the highest load and exhibited a more plastic regime from yield to ultimate and post-failure. The Gr/Ep and hybrid 2 sustained essentially the same peak load; however, the Gr/Ep shows an almost total loss of load-carrying capability after peak load, whereas the hybrid 2 had a plastic behavior similar to the hybrid 1 but at lower loads. The aluminum specimens show gradual loss of load-carrying capability after failure with the 2024-T3 aluminum exhibiting a peak load approximately the same as the Gr/Ep and hybrid 2.

The energy absorption (area under load deflection) for the inplane tearing loads indicates that 2024-T3 and the hybrid 1 specimen had the highest absorption. The 7075-T76 aluminum and hybrid 2 specimens exhibited comparable energy absorption, but were somewhat lower than 2024-T3 and hybrid 1. The Gr/Ep specimen showed substantially the lowest energy absorption capability. When efficiency (specific energy) is considered, the trends are unaltered except the hybrid 2 material clearly performed better than the 7075-T76 material, and Gr/Ep on a relative basis was below 7075-T76.

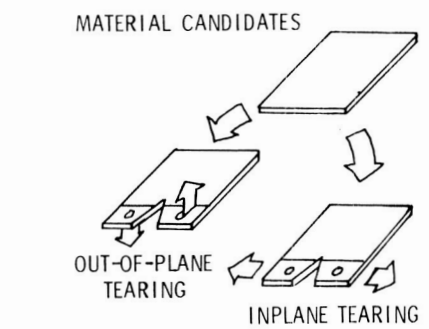

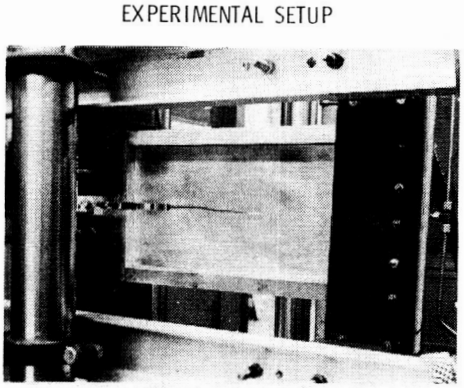

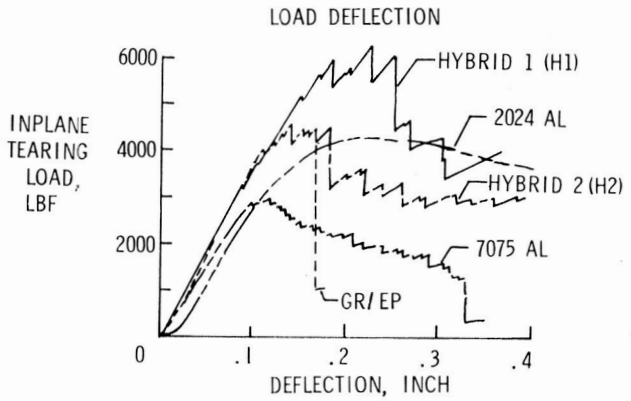

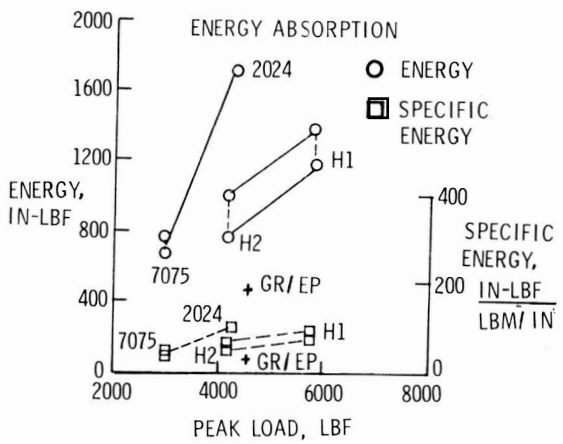

Figure 6

TEARING OF FUSELAGE SKIN PANELS
Out-of-Plane Loads

Tearing tests were also performed for out-of-plane forces (mode III) on the various metal and composite skin panels. A typical failed specimen, load deflections, and energy absorption are shown in figure 7. As may be noted, the peak loads sustained by each material specimen varied from 766 lbf for the 7075-T76 aluminum to 1800 lbf for the hybrid 1 panel. The deflections at peak load however are reasonably close, 1.6 to 1.8 inches for most all materials. The exception was the deflection of the Gr/Ep at 1.4 inches. The load deflection data indicate that both the Gr/Ep and the hybrid 1 specimens had a drastic loss of load-carrying capability following initial failure compared to the metal behavior. The hybrid 2 exhibits a more plastic-like deformation after initial failure and prior to peak load thus achieving higher energy absorption. Indeed, the results show that hybrid 2, hybrid 1, and 2024-T3 materials exhibit more energy absorption capability than the Gr/Ep or the 7075-T76 specimens. However, the specific energy (a measure of the design efficiency) shows Gr/Ep to be better than the 2024-T3. The trend indicates increased energy absorption for metallic materials going from 7075-T76 to more ductile 2024-T3 and for the composites going from Gr/Ep to hybrid 1 to hybrid 2. Since there was judged to be significant fixture interference for the hybrid 1 tests, it is not possible to predict exactly where this material should fit. From the test results and known material properties, it appears that ductility and relatively low shear stiffness are desirable characteristics to enhance crash performance of the composite materials subjected to both inplane and normal tearing forces during slide-out.

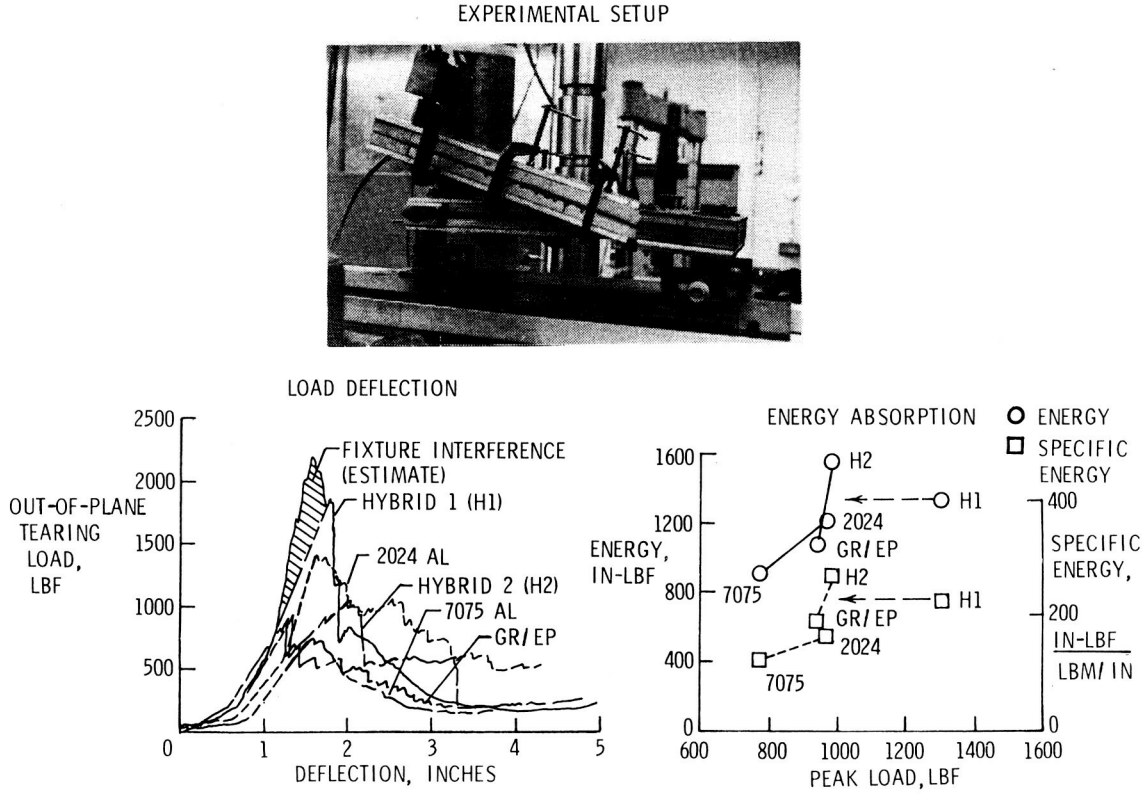

Figure 7

FRICTION AND ABRASION BEHAVIOR OF COMPOSITE SKINS

One consideration which can be important in the design of crashworthy airplanes is the abrasion and wear behavior of the skin material. In the last 5 years, at least a dozen transport airplanes have experienced collapse of the landing gear leading to sliding landings on runway surfaces (ref. 8). Typically, these transport airplanes slide 4000 to 5000 ft with touchdown velocities of approximately 140 mph. In some sections of the airplane, wear damage to the aluminum skin is considerable, although usually repairable. The anticipated use of composite materials in transport airplane/skins raises the question of how composite skins would behave under these circumstances as compared with current aluminum construction. Experiments were performed (ref. 9) to compare the friction and wear behavior of aluminum and composite materials when subjected to sliding or abrasion loading conditions. Four types of materials (aluminum, standard graphite/epoxy, aramid/epoxy, and toughened-resin composites) were used to fabricate small skin test specimens. The specimens were abraded (see figure 8) under conditions of varying pressures, abrasive surface textures, and surface velocities.

Comparisons of the materials were made based on coefficient-of-friction data and the wear rate (defined as the loss of thickness per unit of run time) as a function of the test variables. The composite materials exhibited wear rates 5 to 8 times higher than the aluminum, with the toughened-resin composites having the highest wear rates under identical test conditions. The wear behavior was a linear function of pressure, surface texture, and velocity. The coefficient of friction of each material was independent of the test variables. The standard graphite/epoxy composite had a coefficient of friction (0.10 to 0.12) approximately half that of aluminum (0.20), whereas the aramid/epoxy and toughened-resin composites had coefficients of friction about the same as aluminum. The increased wear rate of the composites will influence the question of repairability and strength degradation of understructure on the aircraft.

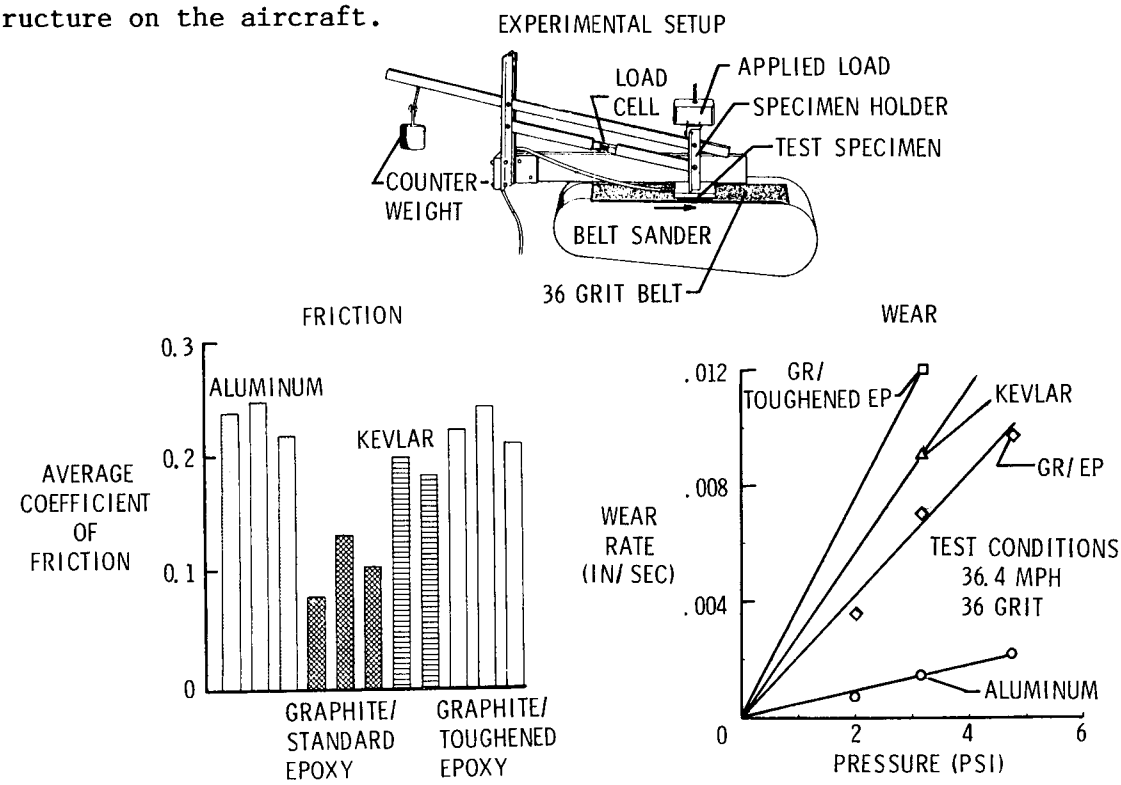

Figure 8

RUNWAY ABRASION STUDY

To extend the data base from laboratory studies on friction and wear behavior of composite and metal skin materials, abrasion tests will be conducted on actual runway surfaces. These results will provide data for a comparison with laboratory results. As shown in figure 9, a runway abrasion test apparatus will be used to obtain friction and wear characteristics of metal and composite I-beam/skin specimens, and curved and flat panels. The test matrix, which encompasses the pressure and velocity range used in the laboratory abrasion studies, will provide wear and friction data versus pressure for a constant velocity, wear and friction versus velocity for constant pressure, and other pertinent measurements on the behavior of the specimens on actual runway roughnesses in the same texture range as the laboratory experiments. It is hoped that correlations will permit the use of the laboratory tests for determining wear and friction behavior of skin panels.

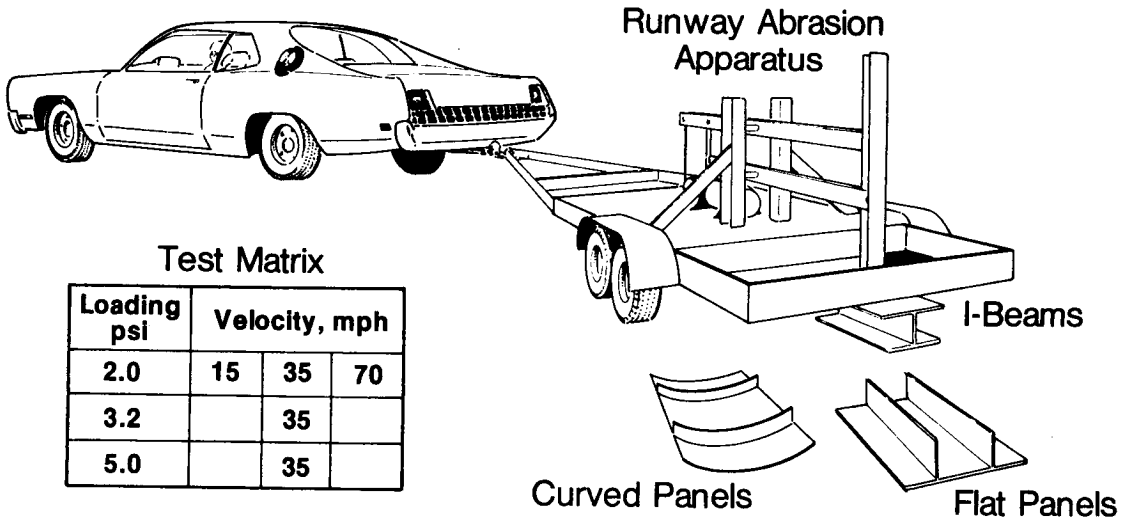

Test Matrix

Loading psi	Velocity, mph		
2.0	15	35	70
3.2		35	
5.0		35	

Figure 9

COMPOSITE ELEMENT LEVEL STUDIES

As the research effort moves from the laminates to the elements of the composite dynamics program of figure 3, the geometry of the composite components becomes somewhat more complex. For example, figure 10 illustrates several typical structural components being used in the element level studies. Tests and related analyses or analytical simulation studies are being undertaken on: shallow circular cylindrical panels subjected to lateral loads (line load); the impact of similar shallow panels on a contact plane, I-beams typical of keelsons found in the lower crown of a transport fuselage subjected to crushing loads; and the dynamics of composite frames (rings) under impact conditions. The study of the impact dynamics of such structural elements represents what are considered to be prudent first studies of the response of subassemblies or individual components of the fuselage under dynamic crash-related loadings prior to the study of the response of a complete fuselage under such loadings.

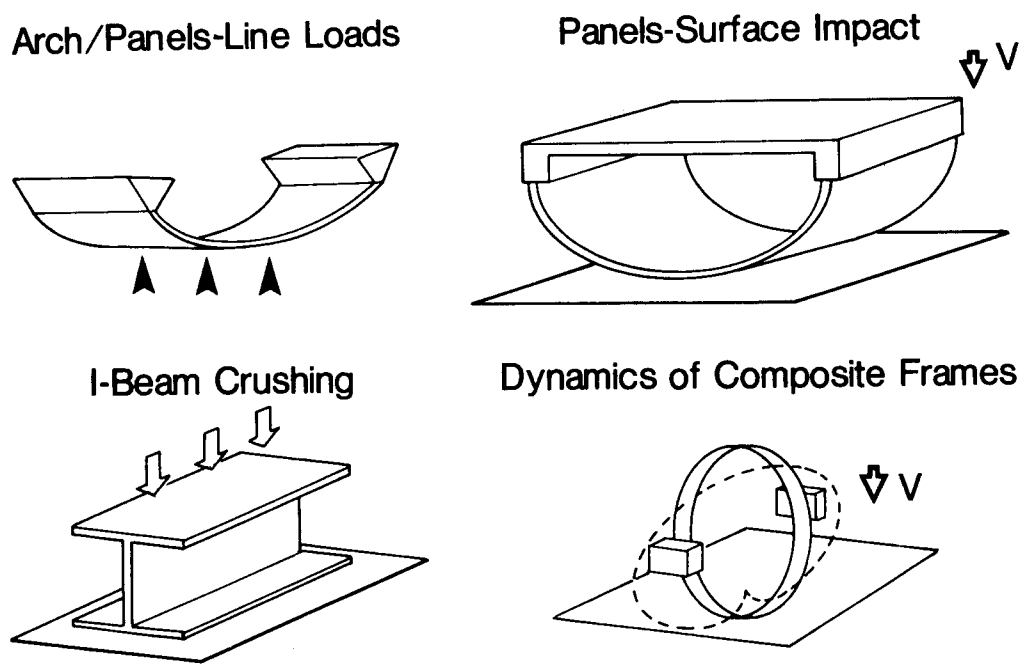

Figure 10

RESPONSE OF SHALLOW CYLINDRICAL COMPOSITE PANELS

An important aspect of crash dynamics is the study of large displacement response of structural components under impact loads. For example, in a gears-up landing of an aircraft not only are the structural components on the underside of the fuselage subjected to the abrasive and tearing loads previously discussed but they are also subjected to lateral impact loads. Initial studies on circular composite panels have been undertaken that include both closed-form analytical solutions extended to handle orthotrophic materials (see refs 10 and 11) and finite-element analysis (DYCAST, ref. 12) as well as experimental investigations. Large displacement response (both static and dynamic) of composite panels (with radii, thicknesses, and arc lengths), which are representative of fuselage panels on transport aircraft, has been determined. Figure 11 presents a photograph of the displacement-controlled loading apparatus (refs. 10 and 11) along with representative theoretical and experimental results on a $[(90/0)_3]_s$ lay-up composite panel (radius, R = 55.42 in.). Although the simple support boundaries do not match those that exist for transport fuselage panels, the behavior of panels in this study does provide information for long panels (width >> than thickness). Closed-form analytical predictions are solid lines with symbols representing experimental data. Non-dimensional load displacements and load thrust are presented, and correlation between theory and experiment is quite good. Results from this study demonstrated that panel shallowness, material orthotrophy, and stacking sequence influence the non-linear static response of graphite/epoxy curved panels. The response of the panels may exhibit no instability, snap-through instability at a limit point, or snap-through at a bifurcation point, depending upon the values of circumferential extensional stiffness, bending stiffness, radius, and semi-opening angle of the panel. DYCAST analysis results are to be determined for comparison with the closed-form solutions. It is anticipated that good correlations will be found, thus providing further validations of the DYCAST capabilities but also indicating the greater efficiency and ease of use of the closed-form solutions to understanding the behavior of shallow cylindrical composite panels. Furthermore, the work may be extended to other boundary conditions and to a possible dynamic analysis.

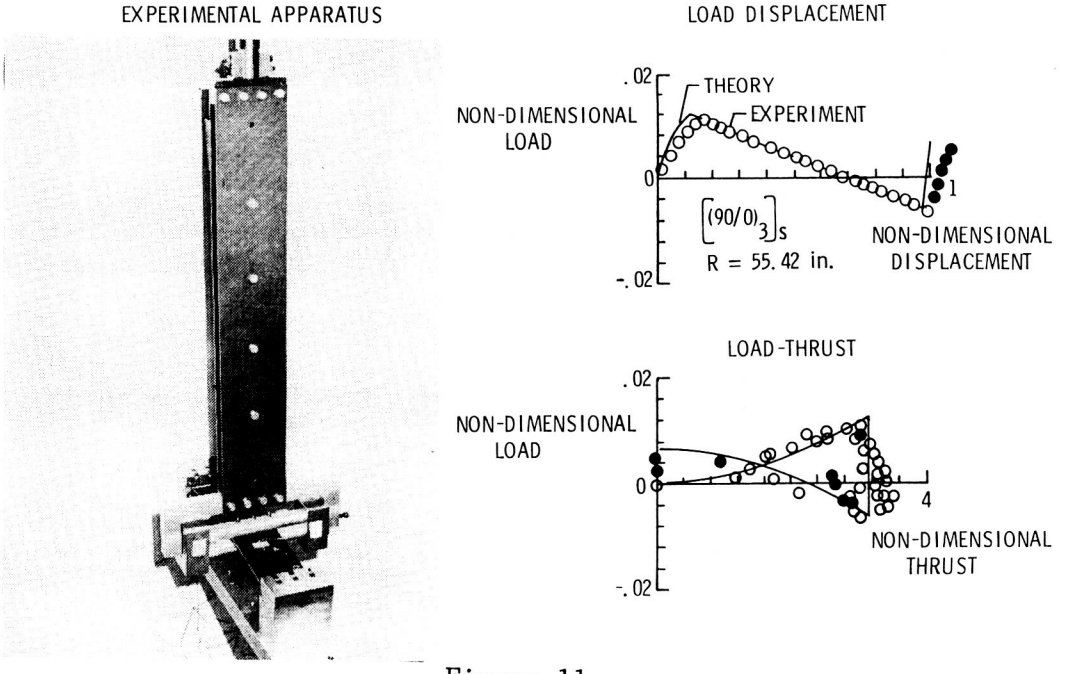

Figure 11

CRUSHING BEHAVIOR OF COMPOSITE KEELSON-LIKE BEAMS

Static loading tests simulating the normal crushing force associated with a crash landing were performed on I-beam configurations selected as representative of fuselage structural components, such as a single-member frame or keelson design. These tests were also performed by Lockheed-California Company on contract NAS1-15949 for NASA LaRC to investigate the effects that variations in materials and ply lay-up have on the structural response and failure modes of these components. Five configurations, one aluminum, two graphite/epoxy, and two hybrid I-beams, were designed to have the same bending stiffness, web column strength, and at least the same web shear stiffness.

A typical setup for the crush testing and the failed I-beam crush elements are shown in figure 12. The load deflection data indicate that all the specimens exhibited a sharp buildup of load at a deflection (crush) of less than 0.2 inches. A major loss of load-carrying capability in the graphite/epoxy specimens as a result of buckling/delamination occurred after crushing less than 0.8 inches. The 7178 aluminum specimen ruptured, thus losing all load-carrying capability. The Gr/Ep specimens retained some residual load capability out to about 4 inches of crush; however, the sustained load was only about 10% of the peak failure load. Specific Peak Force (SPF) and Specific Energy Absorption (SEA) values were determined by dividing the peak force and energy absorption by the section weight-per-unit length for comparing the efficiency of the designs. From the results summarized in the table of figure 12, it can be seen that the hybridization of the graphite/epoxy I-beams with Owens-Corning S-2 glass strips (hybrid 2) influenced peak load but had negligible influence on total specific energy absorbed.

The crushing-test results indicate that designs of keelson-type I-beams using advanced composite materials have the potential of achieving both higher SPF and SEA values than 7178 aluminum. Areas of further evaluation should focus on boundary conditions, combined loads, and the effects of Kevlar; toughened resin systems, and high-strain graphite fibers, being developed under the Army/NASA energy absorption studies (figure 5), should be examined.

EXPERIMENTAL SETUP

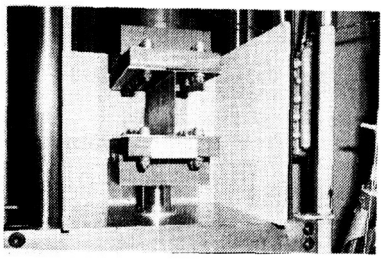

TYPICAL LOAD-DEFLECTION

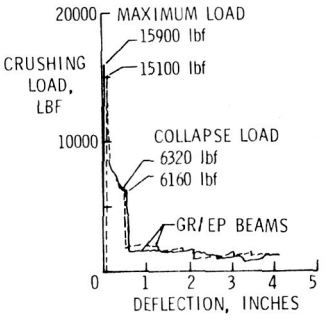

TYPICAL FAILED SPECIMENS

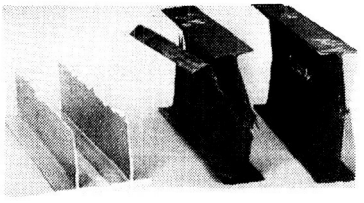

SUMMARY OF CRUSH TEST RESULTS

SPECIMEN MATERIAL	PEAK LOAD LBF	ENERGY ABSORBED		
		TOTAL IN-LBF	SPF LBF / (LBM/IN)	SEA IN-LBF / (LBM/IN)
7178 AL	20000	6217	14620	45445
GR/EP	13000	4987	16414	62967
HYBRID 1	12000	7193	11952	71643
HYBRID 2	13000	5451	16414	68825
MODIFIED GR/EP	15500	8900	16298	93585

Figure 12

DYNAMIC RESPONSE OF COMPOSITE BEAMS

As previously indicated, the goal of the relatively new NASA composite impact dynamics program is to obtain an understanding of the structural response and integrity of generic advanced composite structural components appropriate to transport fuselage construction subjected to crash-related loadings. One effort on the element level of this program is an experimental and analytical study initiated under the NASA/Virginia Polytechnic Institute and State University Composites Program to determine the large deformation response and failure of composite structural beam elements subjected to transient dynamic loadings. The objectives of this study are: (1) to predict global failure; (2) to determine the strain rate effects, and (3) to quantify non-catastrophic damage of composite beams. Relative to the global failure, an analytical model will be developed to predict large deformation response and failure (with an appropriate failure criteria) for comparison with experimental results. Composite beams fabricated from different materials systems, with various stacking arrangements and geometry, will be dynamically tested in the apparatus shown in figure 13. The dynamic load will be applied to the end of the composite beam specimens in an eccentric manner to cause buckling of the beam due to bending. Load history, displacements, and strains will be determined under various impact conditions. Additionally, energy damage correlations will be investigated. It is anticipated that parameters which control the response and failure of the composite elements under impact loads will be determined during the study.

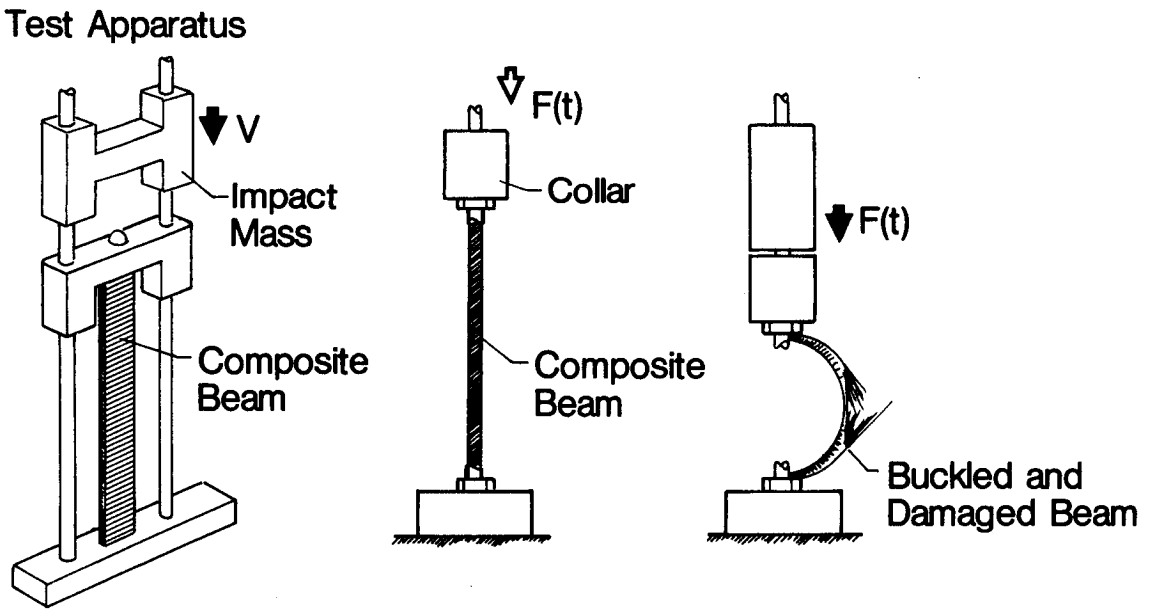

Figure 13

DYNAMICS OF CURVED COMPOSITE FRAMES

As shown in the typical airframe structure in figure 2, one very common structural element is the curved beams or frames of the fuselage. Consequently, another element being studied under dynamic loadings is the curved composite frame. The study will be concerned with the dynamic response and failure modes and loads which occur under impact. Curved composite frame specimens with an inner radius of 36 inches and a Z cross section typical of many such elements in transport fuselage construction are being fabricated for experimental evaluation. During the tests, bending-moment distribution, inplane tensile loads, and failure loads/modes will be determined for verification of and correlation with analytical data. In addition to the studies on the complete frames, various segments (quarter or half segments) will be available from damaged frames or untested specimens for experimental loading and study. As part of the study, a DYCAST model has been formulated and preliminary analytical static and dynamic predictions for a curved composite Z-section frame are presented in figure 14. DYCAST-predicted static-moment (M) distribution and circumferential zero-moment locations are compared to results for a uniform ring loaded by its own weight (from ref. 13). Excellent comparison is noted for both the distribution of moment and null points computed by DYCAST. Additionally, the DYCAST model was used to predict dynamic responses wherein mass was added to the outer horizontal radius. The altered (from static results) moments are shown along with predicted failure locations of the frame during the impact loading. It is anticipated that predicted global failure locations and loads such as these will be verified experimentally, and detailed analysis of critical areas can be conducted using laminate analysis with loading conditions to evaluate whether failure is actually predicted. Verified analytical frame models should be useful in constructing analytical models of complete composite fuselage structures and provide accurate stiffness data and expected failure locations and behavior of more complex fuselage structure under impact loads.

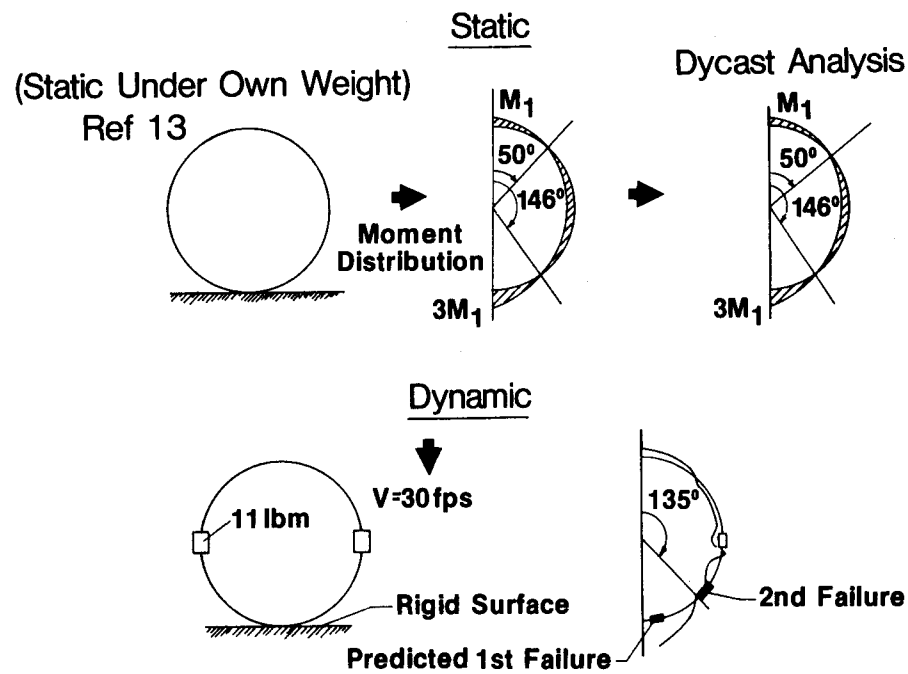

Figure 14

SUBSTRUCTURE LEVEL STUDIES

The third level (large-scale substructures) in the NASA composite impact dynamics program is the most ambitious of the efforts to help achieve the overall goal of providing the necessary data base needed to support the introduction of advanced composite materials into fuselage structure of future transport airplanes. Although the full-scale substructures that are illustrated in figure 15 are expensive, these substructures would provide the confidence level required before proceeding to production by exercising the design and analysis methods and the manufacturing and inspection procedures that are critical requirements. Data from the full-scale substructure level should allow evaluation of the effects of design restraints, multi-element interactions, and combined loading on crash behavior. Furthermore, substructure load deflection data along with the element level data are highly desirable to permit validation of analysis methods, which can in turn be used to predict the sensitivity of response to a wide range of variations in design or load. It is also important that the crash behavior of the substructure be known since this is critical to the understanding of the response of the floor structure and subsequently of the occupants.

Efforts at this level of the generic composites program in all likelihood will rely on contractural efforts such as continuations of the ACEE program or follow-on programs. Indeed, one such contractural effort is discussed in a subsequent section.

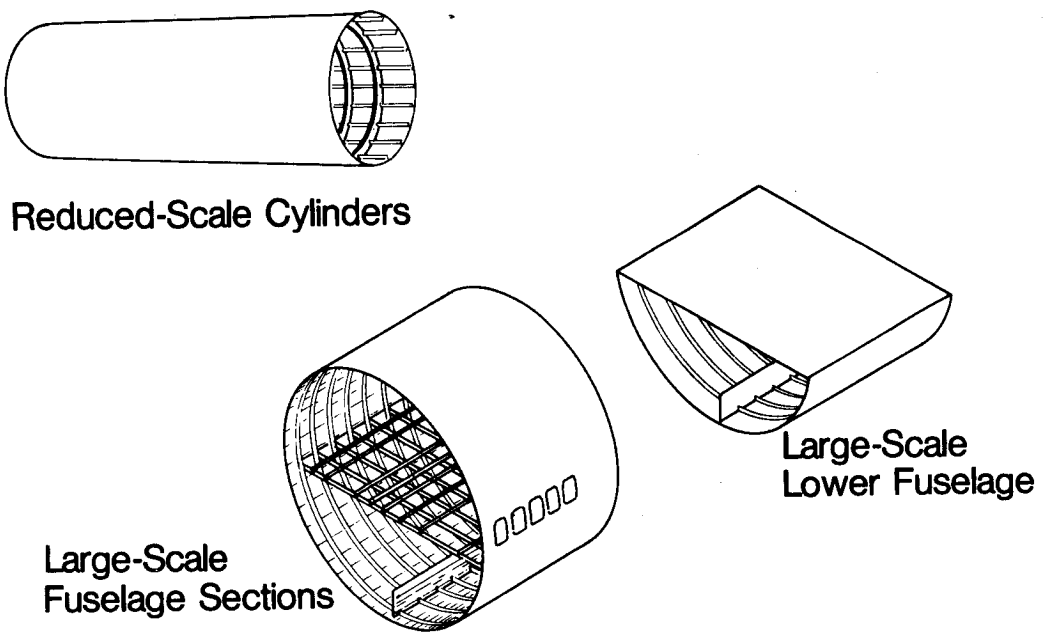

Figure 15

METAL TRANSPORT SUBSTRUCTURE DATA BASE STUDIES

As part of the NASA Langley Research Center's transport crash test program (ref. 14), various fuselage sections from transport aircraft (Boeing 707) have been acquired for dynamic drop testing. The purpose of these tests (see refs. 15 and 16) is to determine structural, seat, and occupant response to vertical loads. This effort is part of the support of the full-scale controlled-impact demonstration (CID) test of a remotely piloted Boeing 720 airplane to be conducted at NASA/Dryden as part of a joint NASA/FAA program. Additionally, the structural response data will permit correlation of the capabilities of the DYCAST computer program (ref. 12) being developed for crash analysis of aircraft structures, and will provide a metal transport substructure data base for comparison with tests of any future composite fuselage structure. Figure 16 presents typical experimental and analytical results for a transport section located forward of the wings of the airplane. During the impact, the lower fuselage section collapsed upward approximately 24 inches as a result of tensile failures which occurred along holes beneath the baggage compartment floor due to bending and shearing out of bolt holes along the edge of the floor covering. DYCAST predictions (Hayduk, R. J.: NASA LaRC) using a two-frame model for this section are in excellent agreement with the experiment. For example, the predicted deflection of the underside of the fuselage of 22 to 23 inches compares well with the measured deflection of about 24 inches. The physical behavior also matches the observed behavior of the test section. Additionally, the magnitude and basic lower frequency content of the accelerations at the intersection of the passenger floor and the outer cylindrical fuselage structure are in good agreement. Structural stiffnesses have been developed from the simpler analytical models of the fuselage for formulating an analytical model of the complete Boeing 720 airplane. This larger model is being used to study dynamic behavior and failure of the aircraft under various impact scenarios. The data from both the sections and the full-scale airplanes will serve as part of the data base relative to composite impact dynamic studies which are discussed in the next section.

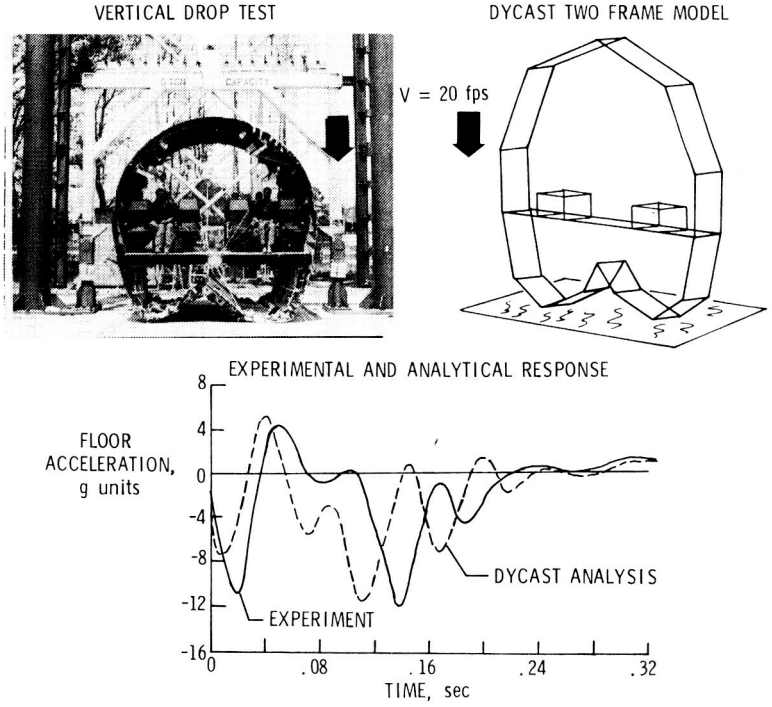

Figure 16

COMPOSITE FUSELAGE SUBSTRUCTURE STUDIES

One highly desirable phase of research on composite impact dynamics is the composite fuselage substructures studies. This part of future efforts on impact dynamics should parallel the past and on-going studies on metal fuselage components. It is apparent that difficult manufacturing requirements and high costs would at present accompany the fabrication of large-scale composite fuselage components such as illustrated in figure 17. Consequently, it is probable that projects such as the continuation of the Aircraft Energy Efficiency Program or similar follow-on programs in composites would be by necessity the vehicle for obtaining and/or conducting such substructure studies. As a matter of fact, proposed contractural efforts addressing major technology issues including impact dynamics are being considered by the ACEE Project Office. As illustrated in figure 17, various subelement studies would support the initial study of large-scale subcomponents of the fuselage. Indeed, as shown in the figure, the initial structure of the proposed effort is not a full section or floor and lower fuselage shell but addresses only the lower crown region of the fuselage. Full-scale sections, because of their cost, would necessarily incorporate not only impact dynamics (crashworthiness) considerations but also include other technology issue areas such as fatigue, damage tolerance, and acoustic transmission design concepts.

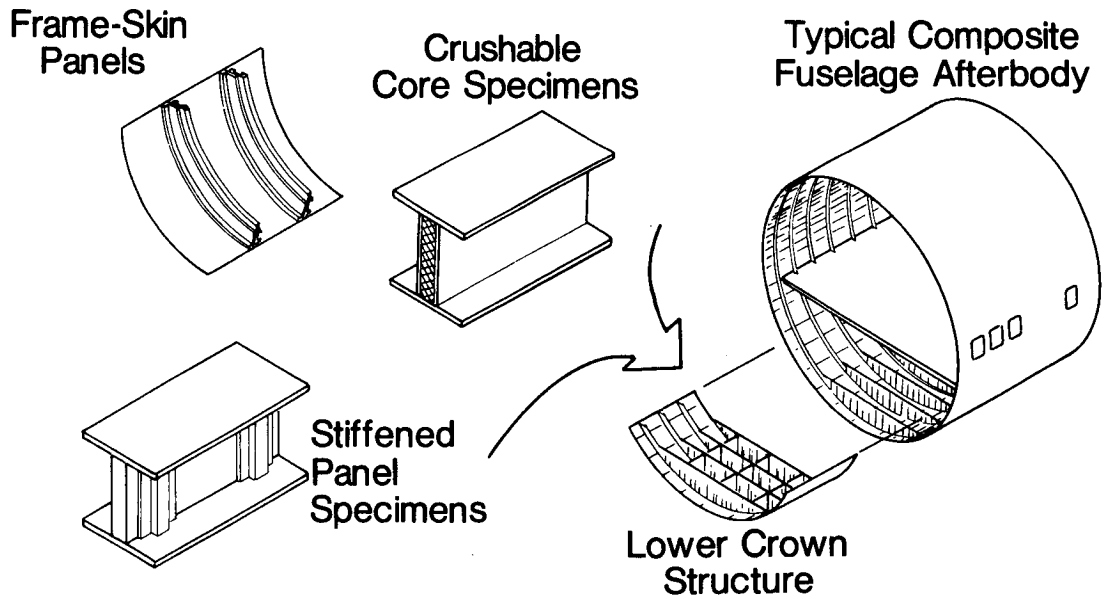

Figure 17

CONCLUDING REMARKS

The Langley Research Center's Crash Dynamics Group is in transition from a general aviation crash test program to transport-related research. A composites impact dynamics program (still in its infancy) has been formulated to focus on composite laminates, composite structural elements, and composite substructures. Studies are being conducted to investigate the impact dynamics behavior (crashworthiness) of generic composite components subjected to crash-related loadings. Supporting analytical efforts are also a part of the research efforts.

Results of studies on energy absorption on the composite laminate level indicate that composite materials (Gr/Ep) can absorb more energy than aluminum but may have poor post-crush structural integrity. Making use of knowledge of the different failure mechanisms of various composite materials is leading to hybrids of high-strain-to-failure graphite woven with Kevlar, which appears to provide higher energy absorption but has post-crush integrity.

Tests of composite skin materials subjected to inplane and out-of-plane (mode I and III, respectively) tearing loads indicate that Gr/Ep panels generally compare to 7075-T76 aluminum in energy-absorbed and resisting tears whereas hybrids (using glass) generally compare to the more ductile 2024-T3 aluminum.

Abrasive loads on composite fuselage skin materials may have a major influence on the potential repairability of composite fuselage underbelly panels that experience abrasive loads during gears up or collapsed-gear emergency landings. Laboratory tests indicate that the composite materials, both standard Gr/Ep and Gr/toughened epoxy, exhibit wear rates 5 to 8 times higher than aluminum under identical test conditions. Friction coefficients for Gr/Ep were 50% that of aluminum (0.2), whereas aramid and toughened composites were about the same as aluminum. Runway tests will be correlated to the laboratory tests to verify and extend this data base.

Curved panel elements on the underside of composite fuselage structure would also be subjected to radial impact loads; therefore, experimental and analytical studies on circular composite panels were undertaken. Results from the studies have indicated panel shallowness, material orthotrophy, and stacking sequence influenced the nonlinear response of the panels.

Crushing behavior of composite and aluminum keelson-like beams indicated that all materials (Gr/Ep and hybrids) were very similar in energy absorbed; however, the failure mode for the aluminum (fracture) was different from the delamination/buckling failure of the composites. Improved hybrid composites developed under the Army/NASA energy absorption study should be evaluated for potentially achieving higher specific energy absorption.

Both experimental and analytical studies have been initiated to not only determine the large deformation response and failure of composite beams subjected to impact buckling loadings but also to investigate the dynamic response and failure loads/modes of curved composite frames (Z cross section).

On the substructures level, metal transport sections have been dynamically tested and are being analyzed using the DYCAST nonlinear finite-element computer codes. Good correlation was indicated between large deflection/failure of the fuselage understructure and floor accelerations and DYCAST predictions. These tests along with a full-scale controlled-impact demonstration (CID) test of a Boeing 720 airplane will serve as the metal data base for possible future composite substructure tests and provide validation of the DYCAST computer program for crash analysis of aircraft structures.

Future composite substructure studies are highly desirable and should parallel past and on-going metal structure research. A proposed initial composite fuselage study will focus only on the lower crown with subelement support tests. Because of

the cost, the full-scale composite fuselage structure will by necessity involve other technology issues such as damage tolerance and acoustic transmission along with the impact dynamics (crashworthiness) behavior.

REFERENCES

1. Davis, G. W.; and Sakata, I. F.: Design Considerations for Composite Fuselage Structure of Commercial Transport Aircraft. Lockheed-California Company, Burbank, California, NAS1-15949, NASA CR-159296, March 1981.

2. Alfaro-Bou, Emilio; Williams, M. Susan; and Fasanella, Edwin L.: Determination of Crash Test Pulses and Their Application To Aircraft Seat Analysis. SAE Tech. Paper 810611, April, 1981.

3. Carden, Huey D.; and Hayduk, Robert J.: Aircraft Subfloor Response to Crash Loadings. Paper 810614 presented at SAE Business Aircraft Meeting and Exposition, Wichita, KS, April, 1981.

4. Thomson, Robert G.; Carden, Huey D.; and Hayduk, Robert J.: Survey of NASA Research on Crash Dynamics. NASA TP-2298, April 1984.

5. Carden, Huey D.: Correlation and Assessment of Structural Airplane Crash Data With Flight Parameters at Impact. NASA TP-2083, Nov. 1982.

6. Carden, Huey D.: Impulse Analysis of Airplane Crash Data With Consideration Given to Human Tolerance. Paper 830748 presented at SAE Business Aircraft Meeting and Exposition, Wichita, KS, April 1983.

7. Farley, Gary L.: Energy Absorption of Composite Materials. NASA TM-84638, AVRADCOM Technical Report TR-83-B-2, March 1983.

8. Passengers Praise Pilot for Actions in Accident. Times-Herald (Newport News, VA), 83rd year, no. 71, March 24, 1983, p. 13.

9. Jackson, Karen, E.: Friction and Wear Behavior of Aluminum and Composite Airplane Skins. NASA TP-2262, AVARDCOM TR-83-B-7, February 1984.

10. Carper, Douglas M.; Hyer, Michael W.; and Johnson, Eric R.: Large Deformation Behavior of Long Shallow Cylindrical Composite Panels. M.A. Thesis, Virginia Polytechnic Institute and State University, Blacksburg, VA, VPI-E-83-37, September, 1983.

11. Johnson, Eric R.; Hyer, Michael W.; and Carper, Douglas M.: Response of Long Shallow Cylindrical Panels To Radial Line Loads. Presented at AIAA/ASME/ASCE/AHS, 25th Structures, Structural Dynamics and Materials Conference, Palm Springs, California, AIAA-84-0954-CP, May 14-16, 1984.

12. Pifko, A. B.; and Winter, R.: Theory and Application of Finite Element Analysis to Structural Crash Simulation. Computers and Structures, Vol. 13, pp 227-285, 1981.

13. Van Den Broek, J. A.: Elastic Energy Theory. John Wiley and Sons, Inc., New York, Second Edition, August 1946. pp. 108-117.

14. Thomson, R. G.; and Caiafa, C.: Designing for Aircraft Structural Crashworthiness. Journal of Aircraft, Vol 19 No. 10, AIAA 81-0803R, Oct. 1982.

15. Williams, M. Susan; and Hayduk, Robert J.: Vertical Drop Test of a Transport Fuselage Section Located Forward of the Wing. NASA TM-85679, August 1983.

16. Williams, M. Susan; and Hayduk, Robert J.: Vertical Drop Test of a Transport Fuselage Center Section Including the Wheel Wells. NASA TM-85706, October 1983.

Page intentionally left blank

Page intentionally left blank

Page intentionally left blank

POSTBUCKLING RESPONSE OF GRAPHITE-EPOXY PLATES LOADED IN COMPRESSION

Flat unstiffened rectangular plates were loaded to failure in compression to study their postbuckling behavior (ref. 1). Unidirectional tapes of Thornel 300 graphite fibers preimpregnated with Narmco 5208 epoxy resin (T300/5208) were used to make 16- and 24-ply quasi-isotropic and 24-ply $[\pm 45/0_2/\pm 45/0_2/\pm 45/0/90]_s$ orthotropic plates. The plates were 20 inches long and from 3.5 to 9.0 inches wide. The loaded ends of the plates were clamped and the sides were simply supported.

Load-shortening results from the tests are summarized below in Figure 1. The applied load P is normalized by the buckling load P_{cr} and the measured end shortening u is normalized by the end shortening at buckling u_{cr}. Buckling is indicated by the filled circle and failure is indicated by the open symbols. All specimens had some postbuckling response. Specimens with lower values of width-to-thickness ratio (e.g, b/t = 24) failed at applied loads that are slightly higher than the buckling load. Specimens with higher values of width-to-thickness ratio (e.g., b/t = 115) failed at applied loads that are several times larger than the buckling load.

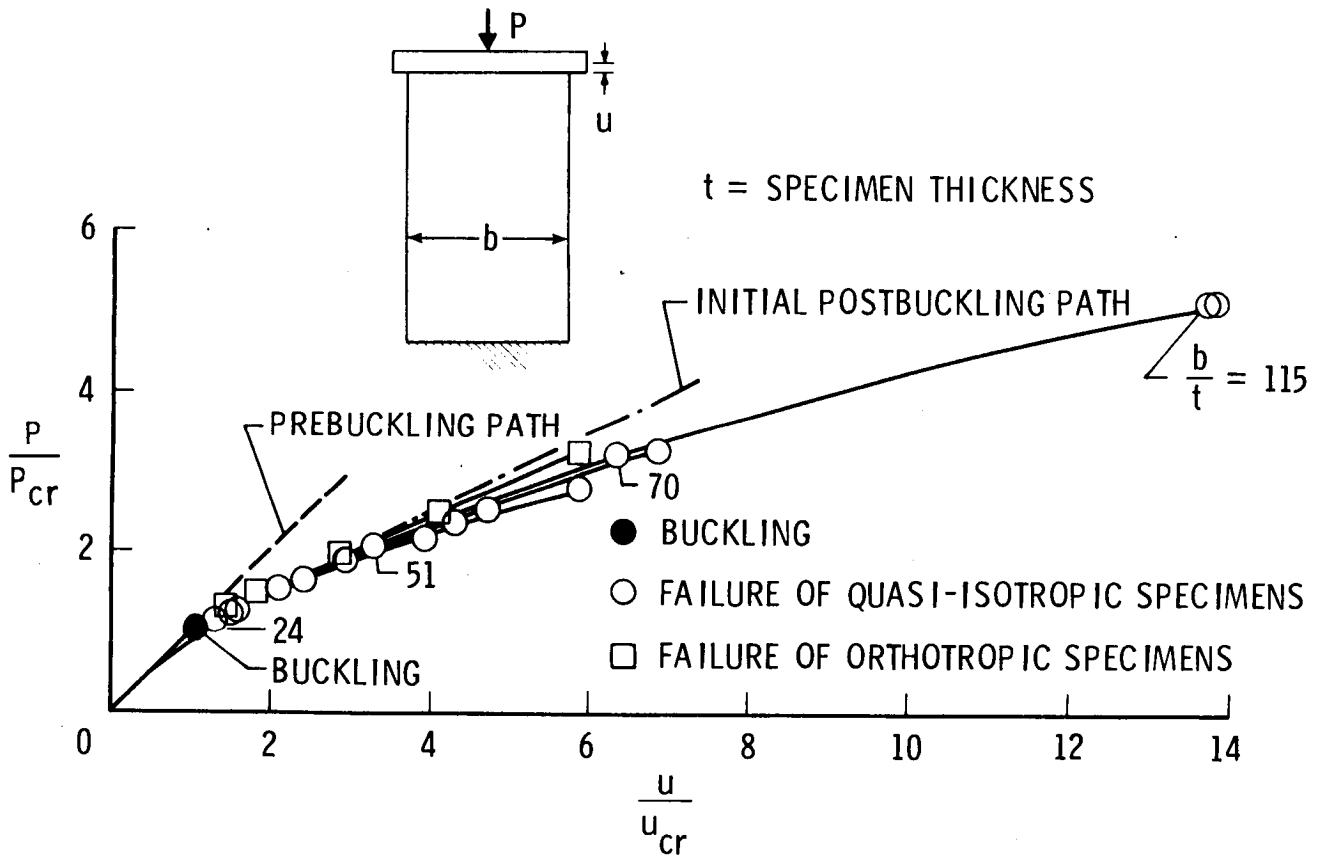

Figure 1

STRAIN DISTRIBUTION AND FAILURE MODE OF A GRAPHITE-EPOXY PLATE

Longitudinal strain distributions across the width of a typical buckled specimen in Figure 1 are shown below in Figure 2 for an applied compressive load of about three times the buckling load. The figures on the left of Figure 2 show typical measured surface strain data from back-to-back strain gages and the resulting computed membrane strains across a nodal line of the buckling mode and across the plate at a point of maximum buckling mode amplitude. These data show that the membrane strains are low in the interior of the buckled plate and high at the edges of the plate.

The buckling mode shape of the typical specimen is represented by the moire-fringe pattern shown in the left photograph. The panel failed along a nodal line of the buckling mode as indicated by the moire-fringe pattern shown in the center photograph. Apparently, the higher membrane strains near the specimen edges couple with the out-of-plane deflection gradients at the nodal line to cause the shear failure shown in the right photograph.

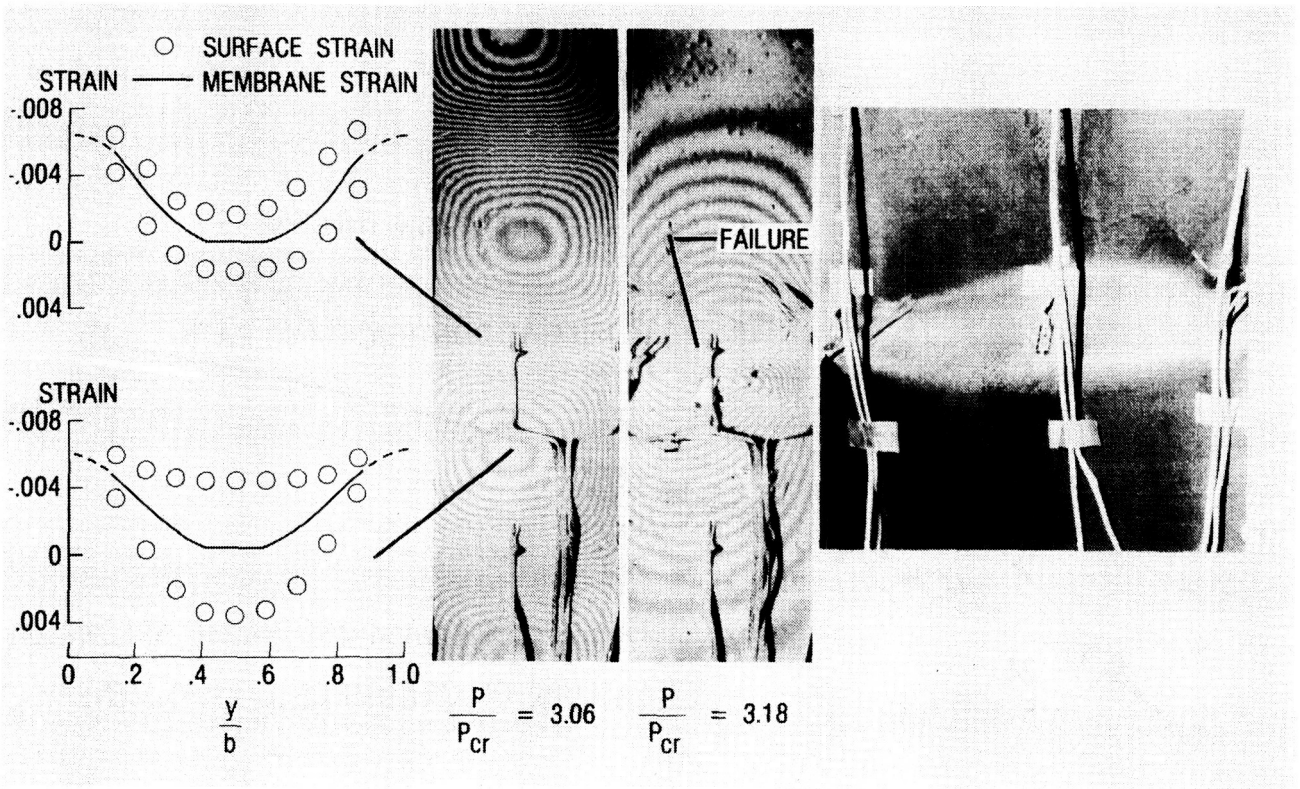

Figure 2

POSTBUCKLING RESPONSE OF FLAT GRAPHITE-EPOXY PLATES WITH HOLES

The effects of circular holes on the postbuckling behavior of flat T300/5208 graphite-epoxy plates similar to those described in Figure 1 were studied in reference 1 and some typical results are shown in Figure 3. Back-to-back strain gages were distributed across the specimen along a lateral line (labeled Y on the lower right figure) that passes through the center of the hole. For applied loads P less than the buckling load P_{cr} these strain gages indicate that a membrane strain gradient exists near the hole as shown in the upper left figure. The left photograph shows a moire-fringe pattern of the specimen before buckling and indicates that no out-of-plane deformations have occurred. The right photograph shows a moire-fringe pattern of the buckling mode shape with four longitudinal waves. For applied loads greater than the buckling load, the back-to-back strain gages indicate that the buckling mode shape has caused a severe local bending strain gradient to occur near the hole as shown in the upper right figure.

Measured end shortening results U for typical specimens with various hole diameters D and plates aspect ratios L/b equal to 2.2 and 5.0 are shown in the lower left figure as a function of the applied load P. End shortening is normalized by the plate length L and the applied load is normalized by the plate longitudinal modulus E and cross-sectional area A. The filled circles represent failure of specimens without holes and the open circles represent failure of specimens with holes. The results indicate that a hole had little effect on the postbuckling strength of the low-aspect-ratio specimens but the postbuckling strength of the high-aspect-ratio specimens decreased as the hole diameter increased.

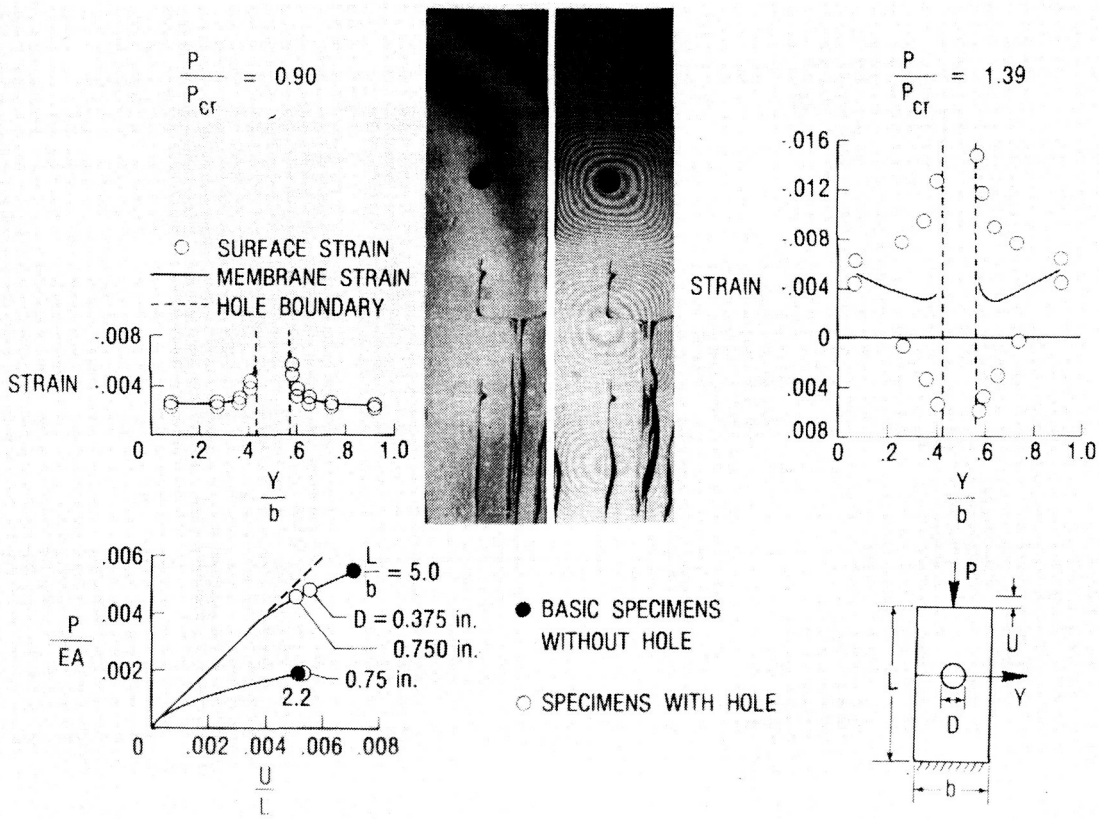

Figure 3

POSTBUCKLING RESPONSE OF FLAT GRAPHITE-EPOXY PLATES WITH LOW-SPEED IMPACT DAMAGE

The effects of low-speed impact damage on the postbuckling behavior of flat T300/5208 graphite-epoxy plates similar to those described in Figure 1 were studied in reference 1 and some typical results are shown below in Figure 4. Specimens were impacted with 0.5-inch-diameter aluminum balls at various impact speeds V and then tested to failure. Measured end shortening results U for typical 16- and 24-ply quasi-isotropic specimens are shown in the lower left figure as a function of the applied load P. End shortening is normalized by the plate length L and the applied load is normalized by the plate longitudinal modulus E and cross-sectional area A. The filled circles represent failure of specimens without impact damage and the open symbols represent failure of specimens with impact damage. The open circles represent failure of specimens impacted in the center and the open squares represent failure of 16-ply specimens impacted near a specimen side. The results indicate that impact damage in the center of the 16-ply specimens had little effect on postbuckling strength regardless of the impact speed. The left photograph shows the moire-fringe pattern corresponding to the out-of-plane deformations of a 16-ply specimen loaded to approximately three times the buckling load and the right photograph shows the moire-fringe pattern corresponding to the failed specimen. Failure occurred along a buckling-mode nodal line away from the impact site. The membrane strain distribution across the specimen just before failure is indicated in the upper left figure. Apparently, the strain in the center of a 16-ply specimen is not high enough to cause the impact damage to propagate to fail the specimen. The results also indicate that impact damage in the center of the 24-ply specimens and at the sides of the 16-ply specimens decreases postbuckling strength as impact speed increases. Apparently, the strains at these impact sites are high enough to cause the impact damage to propagate to fail the specimens.

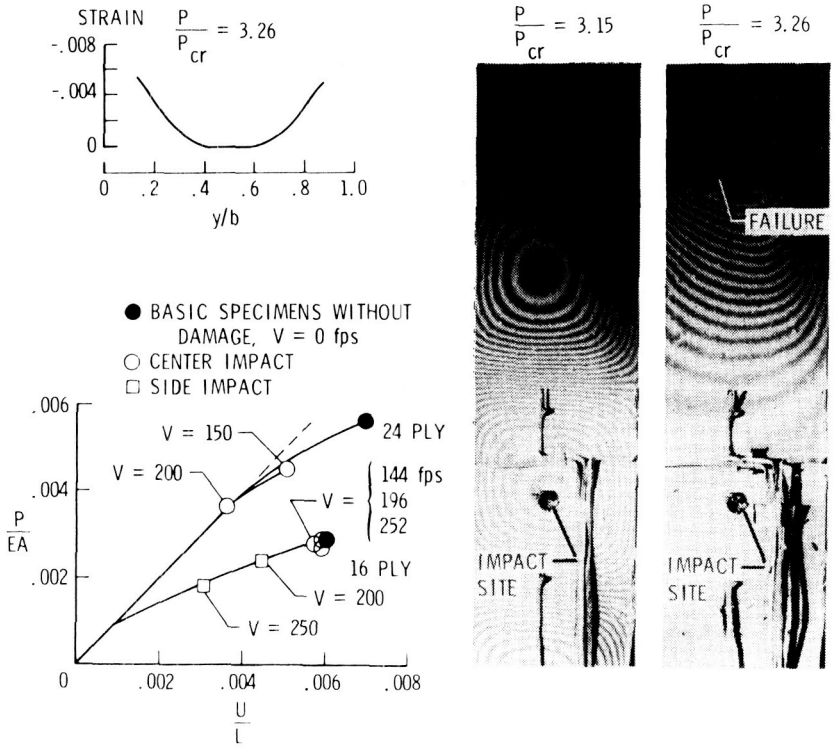

Figure 4

POSTBUCKLING RESPONSE OF FLAT GRAPHITE-EPOXY STIFFENED COMPRESSION PANELS

Flat graphite-epoxy stiffened panels were loaded to failure in compression to study their postbuckling behavior (ref. 2). The specimens were made from T300/5208 graphite-epoxy unidirectional tape and had four stiffeners of a common stiffener design. Specimens with 16- and 24-ply skins and 4.0-, 5.5- and 7.0-inch stiffener spacing were tested. A typical specimen is shown in the upper left photograph of Figure 5. Some typical results are also shown in Figure 5. Measured end shortening results u for specimens with various stiffener spacing b and skin thicknesses are shown in the upper figures as a function of the applied load P. End shortening is normalized by the panel length L and the applied load is normalized by the panel longitudinal modulus E and cross-sectional area A. All specimens exhibited some postbuckling capability. The open circles represent buckling and the crossed circles represent failure. The end loadings N_x at failure for the specimens ranged from 1400 lb/in to 4920 lb/in which is representative of transport fuselage loads. Back-to-back strain gages were distributed across the skin of the panels between the two interior stiffeners and some typical membrane strain results e are shown in the lower left figure for several values of applied load. The membrane strain is normalized by the strain at buckling e_{cr} and the applied load is normalized by the buckling load P_{cr}. The results indicate that the strains near the stiffeners are significantly higher than the strains in the center of the skin between stiffeners. All panels failed when the stiffeners separated from the skin as shown in the photograph and sketch at the lower right. Apparently, the high longitudinal strains at the stiffeners (shown in the lower left figure) interact with the out-of-plane deflection gradients at the stiffeners (shown in the lower center photograph of the moire-fringe pattern of out-of-plane displacements) to fail the panels.

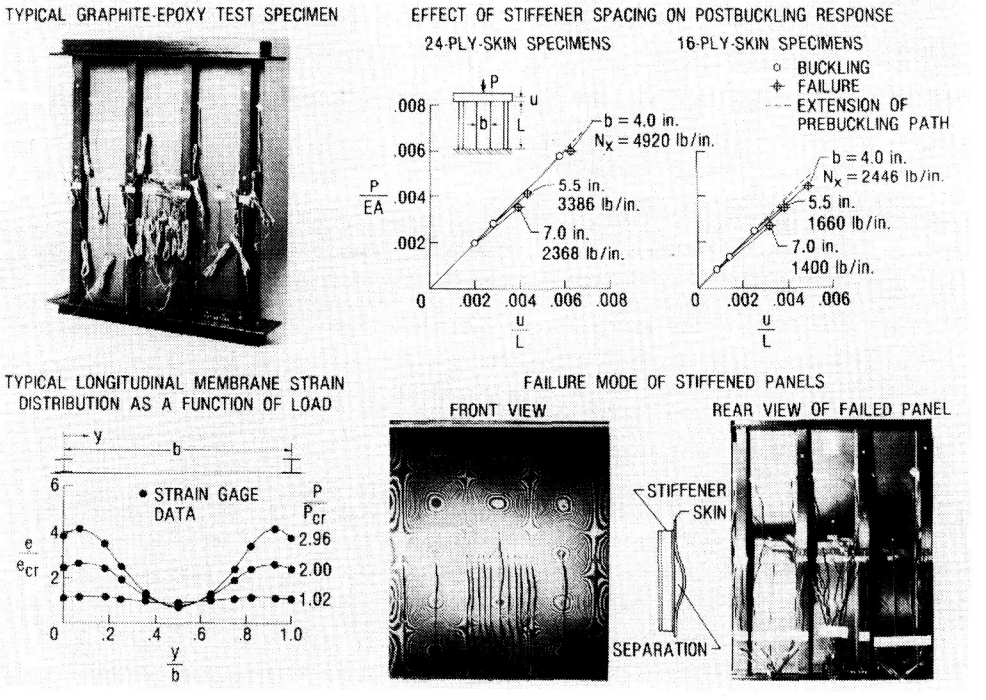

Figure 5

POSTBUCKLING ANALYSIS OF FLAT GRAPHITE-EPOXY
STIFFENED COMPRESSION PANEL

The STAGSC-1 nonlinear structural analysis code (ref. 3) was used in reference 2 to predict the response of a typical panel described in Figure 5 and the results are shown below in Figure 6. The results shown are for a panel with a 16-ply skin and 7.0-inch stiffener spacing. It was necessary to model the stiffener attachment flanges and webs with flexible plate elements in the finite element model used for the analysis in order to obtain the close agreement between test and analysis shown below. The contour plot at the upper left of the figure compares well with the photograph of the moire-fringe pattern of the out-of-plane deflections. The open circles in the figures below are test data and the solid lines are analytical data. The crossed circles represent failure of the specimens. The upper right figure compares results for end shortening u (normalized by end shortening at buckling u_{cr}) as a function of applied load P (normalized by the buckling load P_{cr}). The lower left figure compares results for measured out-of-plane deflection w at a point on the skin (normalized by the skin thickness t) as a function of applied load. The lower center figure compares strain results e from back-to-back strain gages on the skin (normalized by the strain at buckling e_{cr}) as a function of applied load. The lower right figure compares membrane strain distribution results across the panel skin between two stiffeners for several values of applied load. The results indicate that test and analysis compare well up to failure.

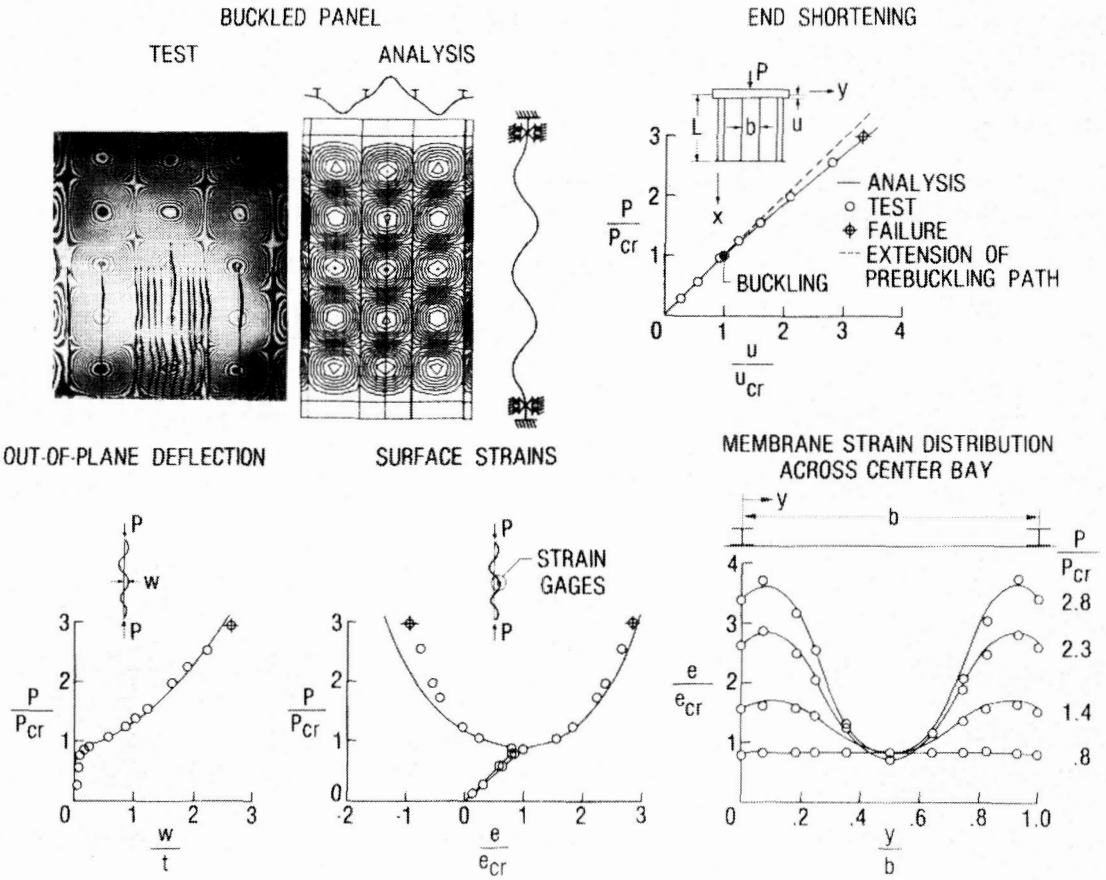

Figure 6

EFFECT OF CUT STIFFENERS ON POSTBUCKLING STRENGTH OF FLAT GRAPHITE-EPOXY COMPRESSION PANELS

Several T300/5208 graphite-epoxy stiffened panels, similar to those described in Figure 5, were subjected to low-speed impact damage and the results of residual strength tests on these damaged panels are presented in reference 2. It was found in reference 2 that low-speed impact damage could degrade the postbuckling strength of a panel if a region near a stiffener attachment flange were damaged. Several other stiffened panels, similar to those described in Figure 5, were damaged by cutting a 2.0-inch-long slot completely through the skin and one stiffener as indicated by the upper left figure in Figure 7. A slot was cut into panels with 16- and 24-ply skins and 4.0- and 7.0-inch stiffener spacing and then tested to failure to determine their residual strength. The results of these residual strength tests are shown below in Figure 7. End shortening results u (normalized by panel length L) are shown as a function of applied load P (normalized by panel longitudinal modulus E and cross-sectional area A). The results for undamaged specimens from Figure 5 are shown for comparison. The open circles represent panel buckling and the filled circles represent failure of the undamaged panels. The filled squares represent failure of the panels with slots. The results indicate that the slots degraded the postbuckling strength of the panels. The reduction in postbuckling strength observed for the slotted panels was greater than the reduction in postbuckling strength observed for the low-speed impact damaged panels reported in reference 2.

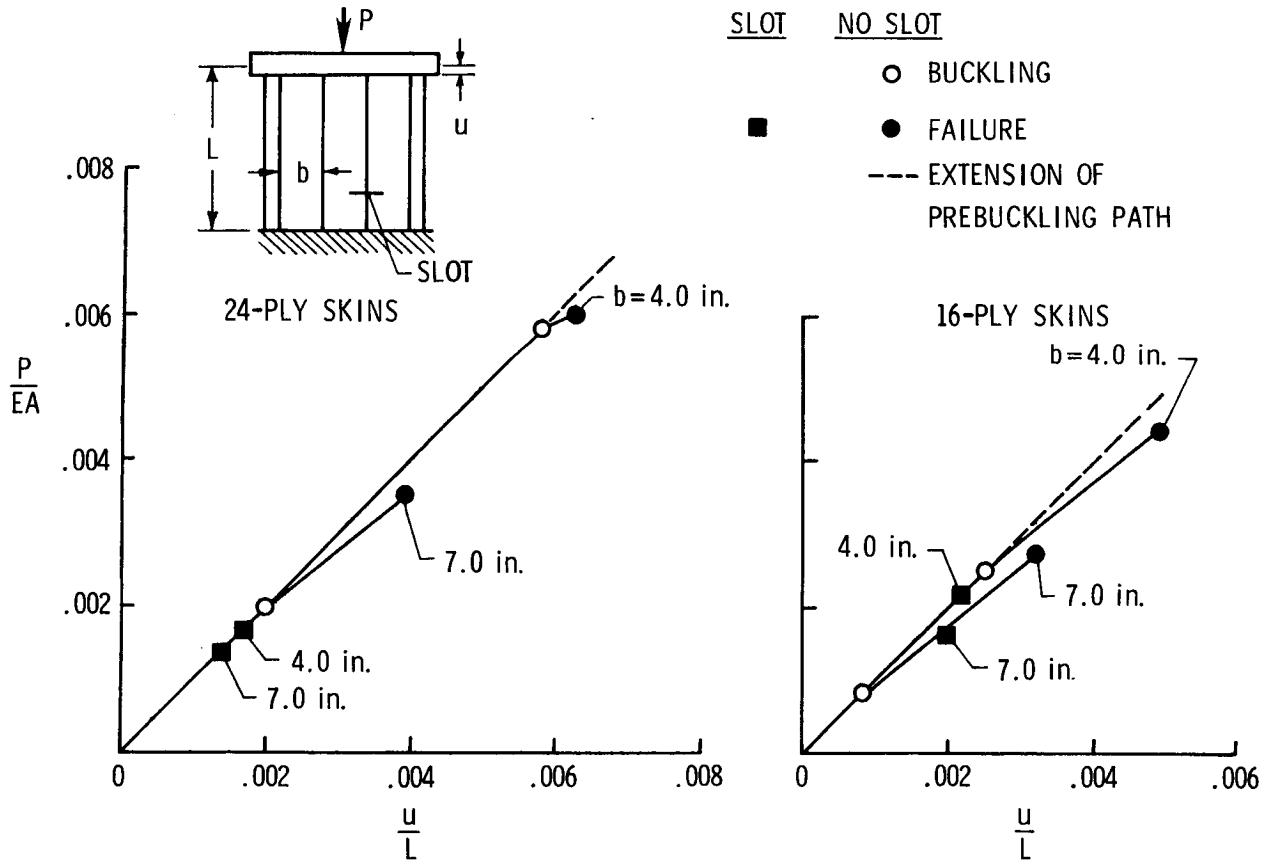

Figure 7

STIFFENER ATTACHMENT CONCEPTS FOR PANELS DESIGNED TO BUCKLE

Failure of the stiffened panels described in Figure 5 was caused by separation of the stiffener from the panel skin. Three stiffener attachment concepts that were intended to suppress the skin-stiffener separation failure mode have been evaluated to determine their effectiveness. Four Hercules AS4/3502 graphite-epoxy panels with 16-ply skins were made with a single stiffener attached to a skin with one of four stiffener attachment concepts. A typical specimen is shown in the upper left photograph in Figure 8. One specimen had the stiffener bonded to the skin with a secondary bonding operation to represent the stiffener attachment concept used for the panels described in Figure 5. The second specimen had a bonded stiffener reinforced with mechanical fasteners through the skin and stiffener attachment flanges. The attachment flanges of the third specimen were stitched to the skin and the skin and stiffener were cocured. The fourth specimen was based on the padded skin concept described in reference 4 and includes an additional twelve plies of AS4/3502 tape in the skin under the stiffener as shown in the lower left figure. The four panels were tested to failure and the results of the tests are shown in the lower right figure. The failure loads of the panels with mechanical fasteners and stitching were both higher than the failure load for the panel with the constant-thickness 16-ply skin and bonded stiffener. However, the failure load of the panel with the padded skin was higher than the failure loads of the other three panels. While the panel with the padded skin was approximately nine percent heavier than the panel with the bonded stiffener, its failure load was 30 percent higher. The panel with the padded skin failed by stiffener crippling as shown in the upper right photograph rather than by skin-stiffener separation.

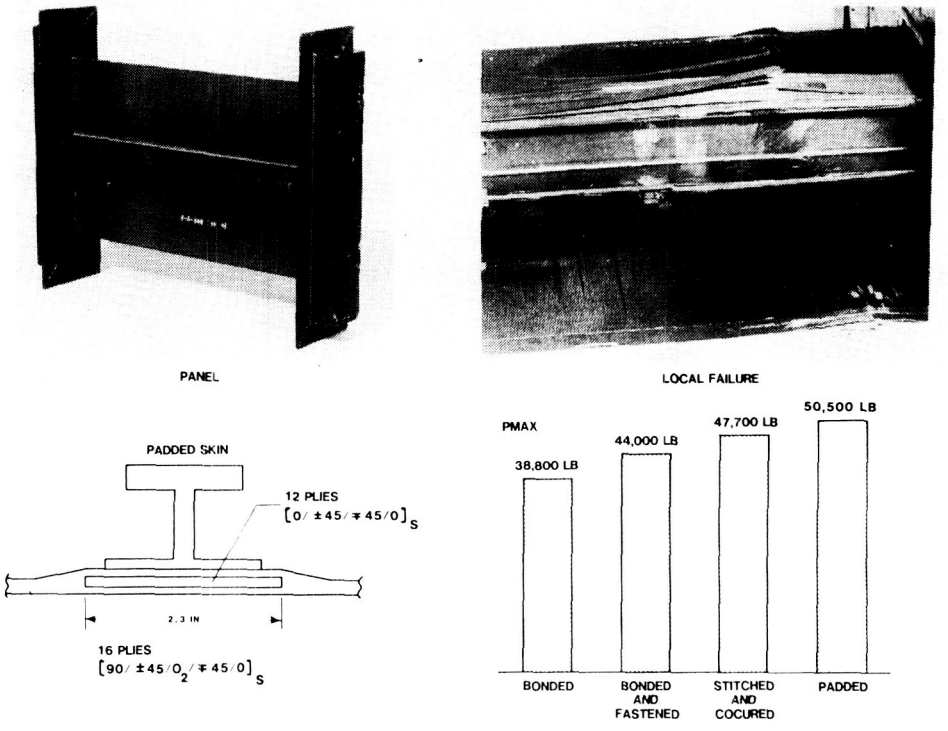

Figure 8

The effect of circular holes on the postbuckling response of curved T300/5208 graphite-epoxy panels is shown below in Figure 9. The results are for 16-ply quasi-isotropic panels with a 15 inch radius. The panels are 14 inches long and have a 14 inch arc length. Panels with no hole and with 0.5-, 1.0- and 2.0-inch-diameter holes were tested to failure. The panels were tested in a manner similar to that described for the panels in Figure 1. All panels exhibited some postbuckling capability. As shown in the figure, the panel with no hole (a = 0) and the panel with the 0.5-inch-diameter hole supported higher postbuckling loads than the panels with 1.0- and 2.0-inch-diameter holes. Severe local bending occurs near the hole after buckling as indicated in the photograph of the moire-fringe pattern of the buckling mode of the panel with the 1.0-inch-diameter hole. This severe local bending caused delamination to occur at the hole edge as shown in the photograph of the 2.0-inch-diameter hole edge shown in Figure 10. Apparently, the delamination at the hole edge reduced the local stiffness of the panel enough to reduce the postbuckling strength of the panels with the larger holes.

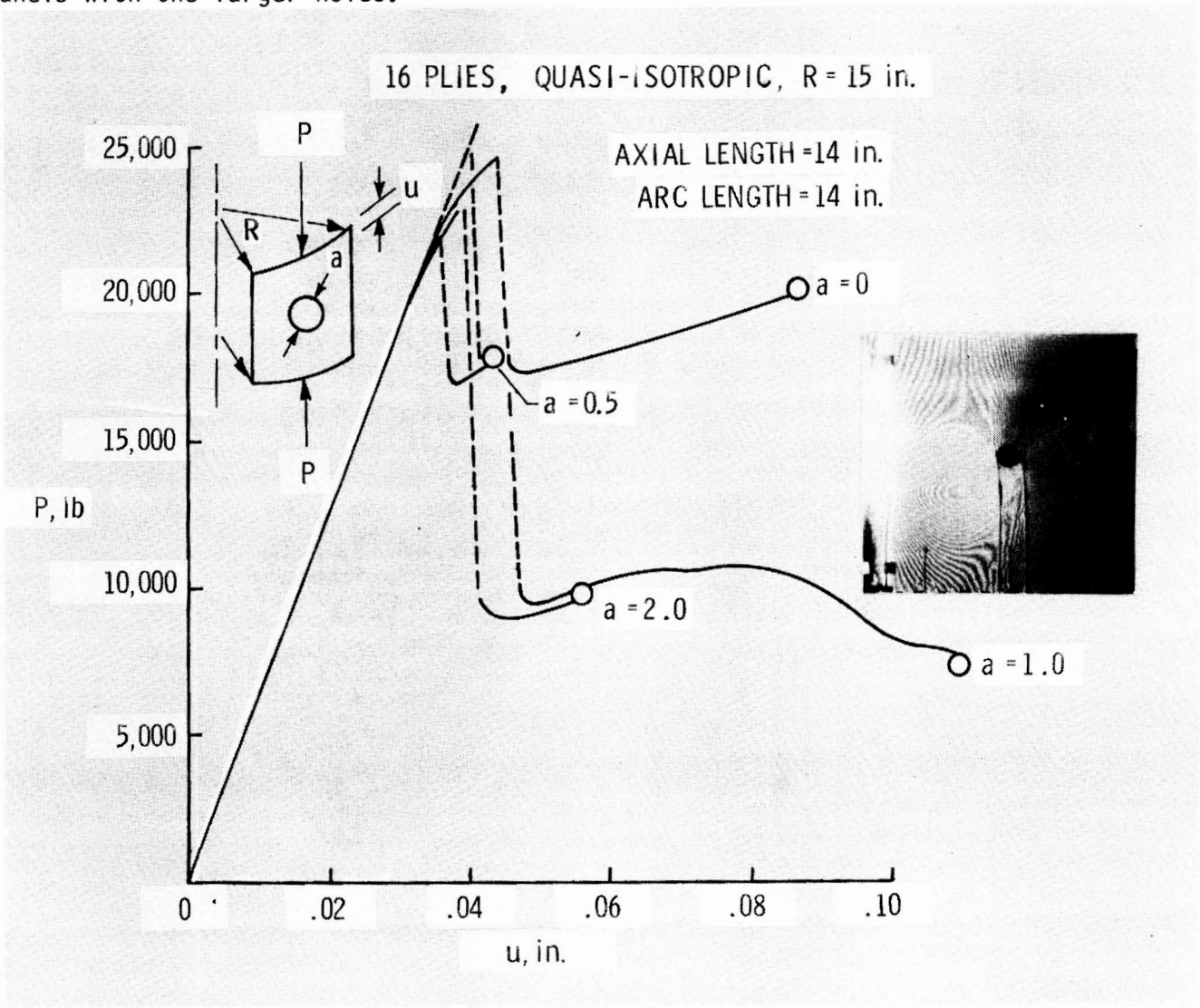

Figure 9

DELAMINATED HOLE EDGE OF CURVED GRAPHITE-EPOXY PANEL

The delaminated hole edge of the panel with the 2.0-inch-diameter hole described in Figure 9 is shown in Figure 10.

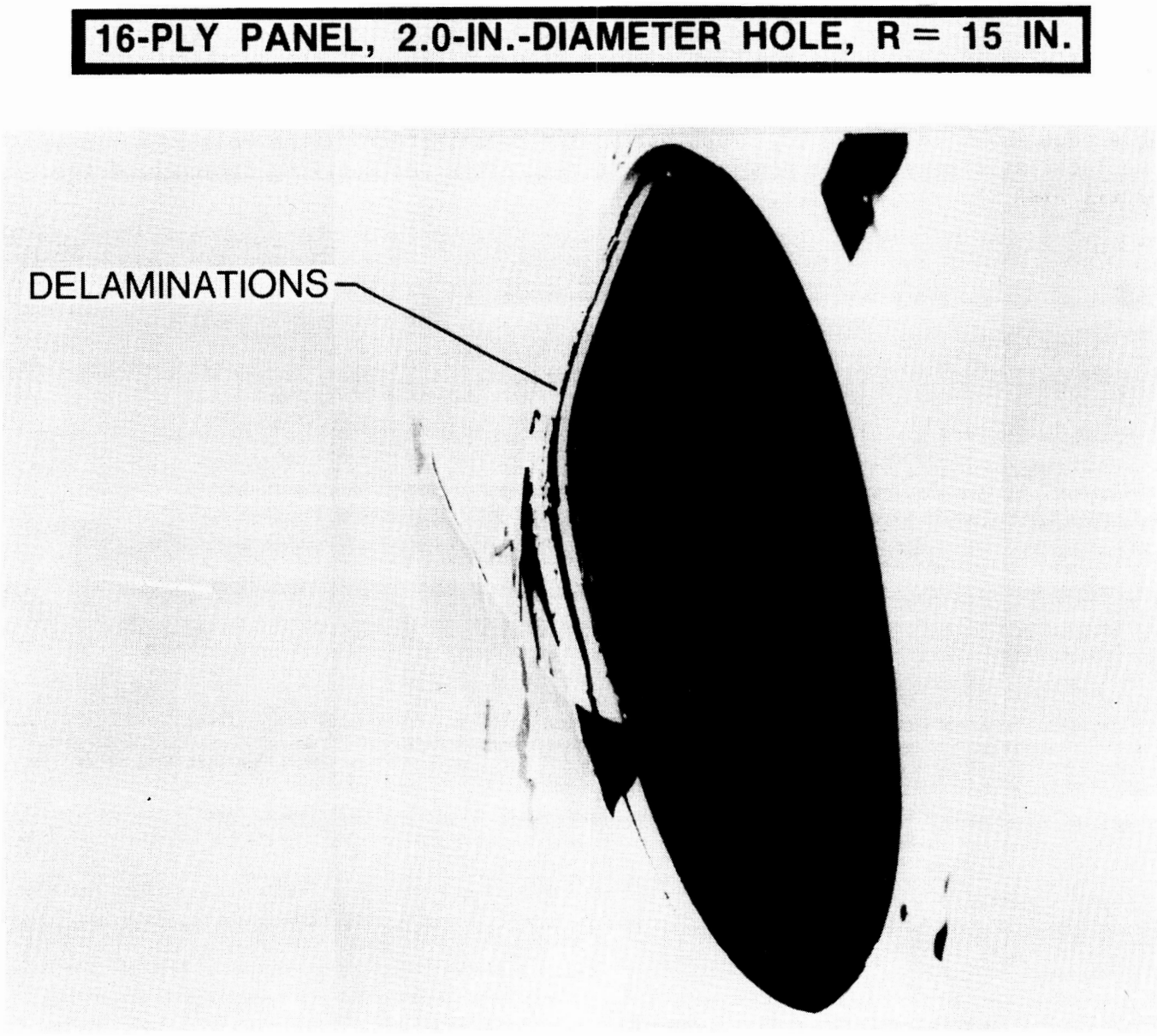

Figure 10

POSTBUCKLING ANALYSIS OF A CURVED GRAPHITE-EPOXY COMPRESSION PANEL WITH A HOLE

The STAGSC-1 nonlinear structural analysis code (ref. 3) was used in reference 5 to analyze the postbuckling response of the curved T300/5208 panel with a 2.0-inch-diameter hole described in Figure 9. The analytical results are compared with the test results in the upper left figure in Figure 11. The end shortening u (normalized by the panel length L) is shown as a function of the applied load P (normalized by the panel longitudinal modulus E and cross-sectional area A). Test and analysis compare reasonably well until the buckling load is approached. Near buckling the analysis predicts large symmetric local radial deflections w near the hole as indicated by the lower left contour and deformed shape plots for the load corresponding to point A on the upper left figure. An arc-length projection method (ref. 6) was used to continue the analysis past the limit point and onto the unstable postbuckling equilibrium path. After buckling the analysis predicts severe local bending and large nonsymmetric radial deflections near the hole as indicated by the lower center contour and deformed shape plots for the load corresponding to point B on the upper left figure. On the stable postbuckling equilibrium path, the analysis again predicts severe local bending and large nonsymmetric radial deflections as indicated by the lower right contour and deformed shape plots for the load corresponding to point C on the upper left figure. Apparently, the severe local bending near the hole causes sufficiently large surface rotations to exceed the capability of the moderate rotation formulation used in STAGSC-1. Also, this severe local bending apparently causes enough local transverse shearing deformations to delaminate the panel at the edge of the hole as shown in Figure 10. Once delamination occurs, the finite element model does not accurately represent the panel near the hole.

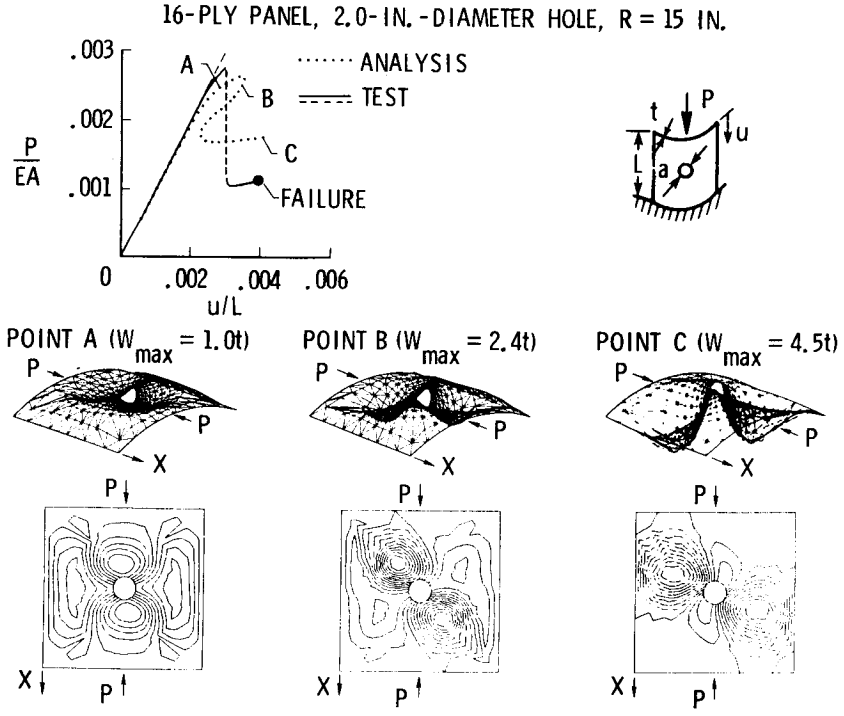

Figure 11

POSTBUCKLING RESPONSE OF CURVED GRAPHITE-EPOXY STIFFENED COMPRESSION PANELS

Curved graphite-epoxy stiffened panels were loaded to failure in compression to study their postbuckling behavior. The panels were made from T300/5208 graphite-epoxy tape and had an 85 inch radius. The panels had the same 16-ply-skin and stiffener designs as the flat panels described in Figure 5 and had a 4.0- or 7.0-inch stiffener spacing. The results of the tests of these panels are shown in Figure 12. End shortening results u (normalized by panel length L) are shown as a function of the applied load P (normalized by the panel longitudinal modulus E and cross-sectional area A). The results for the corresponding flat specimens from Figure 5 are shown for comparison. The square symbols represent the curved panel results and the circles represent the flat panels. The open symbols represent buckling and the filled symbols represent failure. As expected, buckling loads for both curved panels are higher than for the corresponding flat panels. However, the flat panel with 4.0-inch stiffener spacing failed at a higher load than the corresponding curved panel, and the curved panel with the 7.0-inch stiffener spacing failed at a higher load than the corresponding flat panel. Additional testing and analyses are currently being conducted to resolve this apparent anomaly.

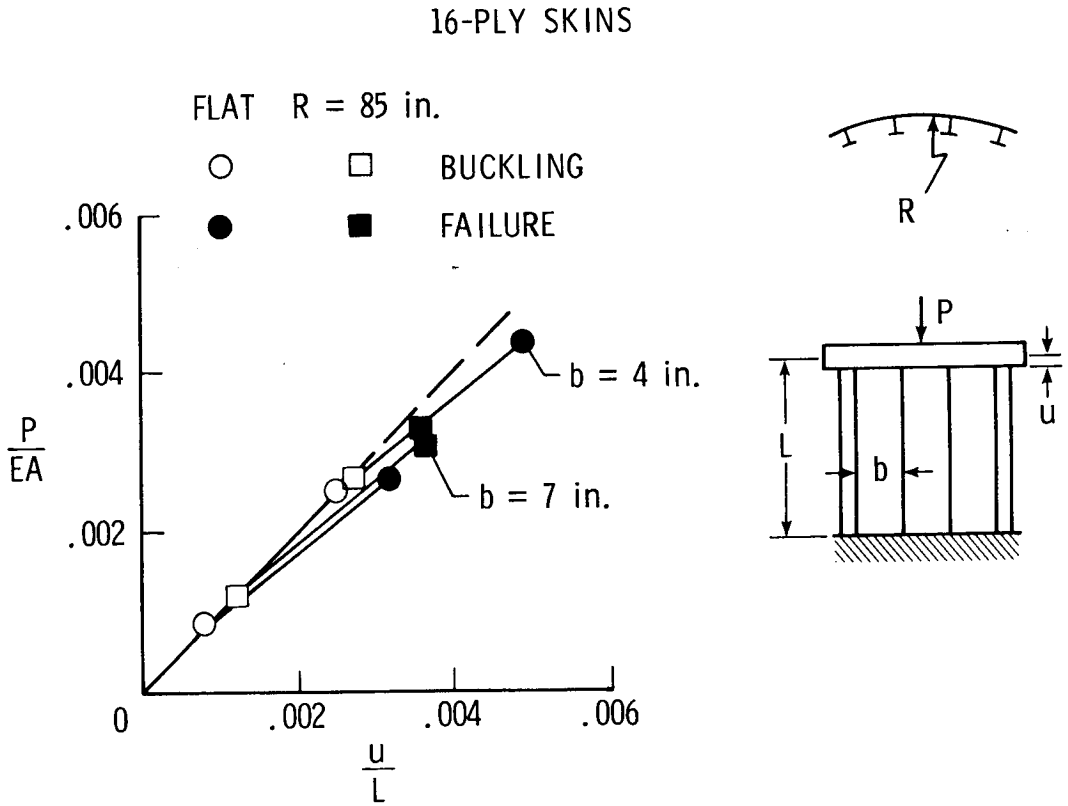

Figure 12

POSTBUCKLING RESPONSE OF UNSTIFFENED GRAPHITE-EPOXY SHEAR WEBS

Flat unstiffened shear webs were loaded to failure in shear to study their postbuckling behavior and failure characteristics. The results of this study of unstiffened shear webs are part of the research being conducted by the third author to fulfil the requirements for the degree of Master of Science from the School of Engineering and Applied Science of George Washington University. Unidirectional tapes of Hercules AS4 graphite fibers and 3502 epoxy resin (AS4/3502) were used to make 8-, 16-, and 24-ply webs with quasi-isotropic, orthotropic, and all-±45 stacking sequences. All of the webs had 12.0-inch by 12.0-inch test sections and were tested in a picture-frame shear fixture.

Membrane shear strain results are shown in figure 13. The applied load T is normalized by the applied load at buckling T_{cr} and the membrane shear strain γ is normalized by the membrane shear strain at buckling γ_{cr}. The open symbols indicate failure of the webs. The failure loads of the 8- and 16-ply webs were approximately 50 and 8 times the buckling load, respectively. The failure loads of the 24- and 32-ply webs were approximately 4.5 and 2.5 times the buckling load, respectively. There was a significant reduction in postbuckling stiffness as indicated by the change in slope of the postbuckling curves when the stacking sequence of the 8-ply webs was changed from a quasi-isotropic to an all-±45 laminate. The 16-ply quasi-isotropic and orthotropic webs had essentially the same postbuckling stiffness, but the all-±45 webs had a slightly lower postbuckling stiffness. The 24-ply webs had essentially the same postbuckling stiffness. Test results indicate that laminate stacking sequence and thickness can influence the postbuckling stiffness and strength of graphite-epoxy shear webs.

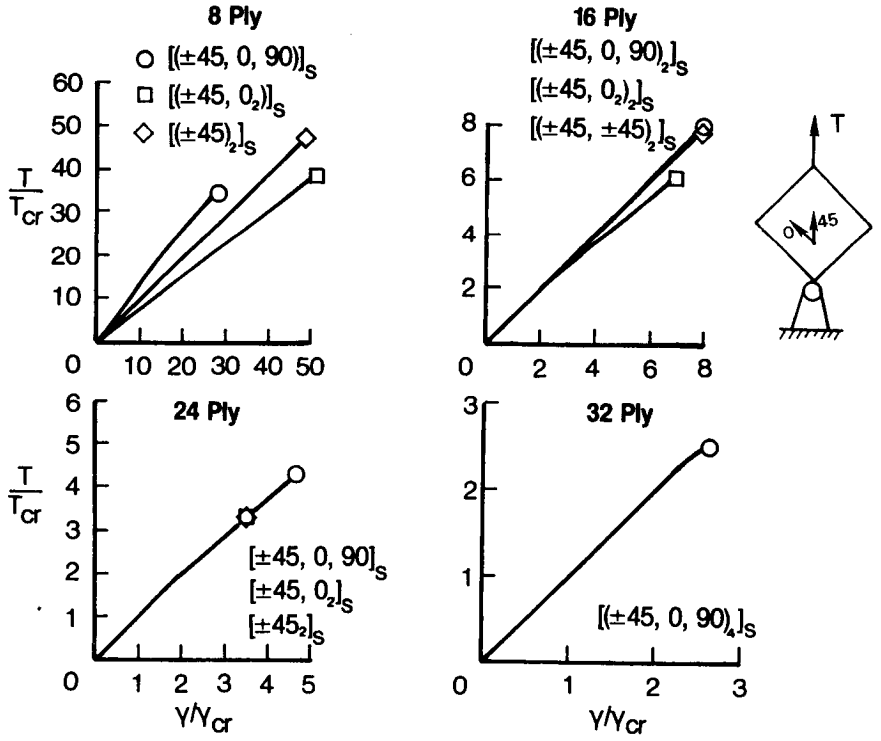

Figure 13

OUT-OF-PLANE DEFLECTIONS OF UNSTIFFENED SHEAR WEB

Out-of-plane deflections measured near a point of maximum buckling-mode amplitude are shown in Figure 14 for the 8-, 16-, and 24-ply webs described in Figure 13. The applied shear flow ($T/\sqrt{2}b$) is plotted on the vertical axis and the out-of-plane deflection w normalized by the web thickness is plotted on the horizontal axis. The symbols represent test data for the various laminates defined in the figure. The filled symbols indicate failure. The 8-ply webs had maximum out-of-plane deflections at failure of over five times the thickness. There was significant reduction in the maximum deflection when the thickness of the specimen was increased from 8 plies to 16 plies and a further reduction when the thickness was increased to 24 plies. The results shown in the figure indicate that a significant amount of bending can occur when a graphite-epoxy shear web is loaded into the postbuckling range and the bending stiffness is influenced by the thickness.

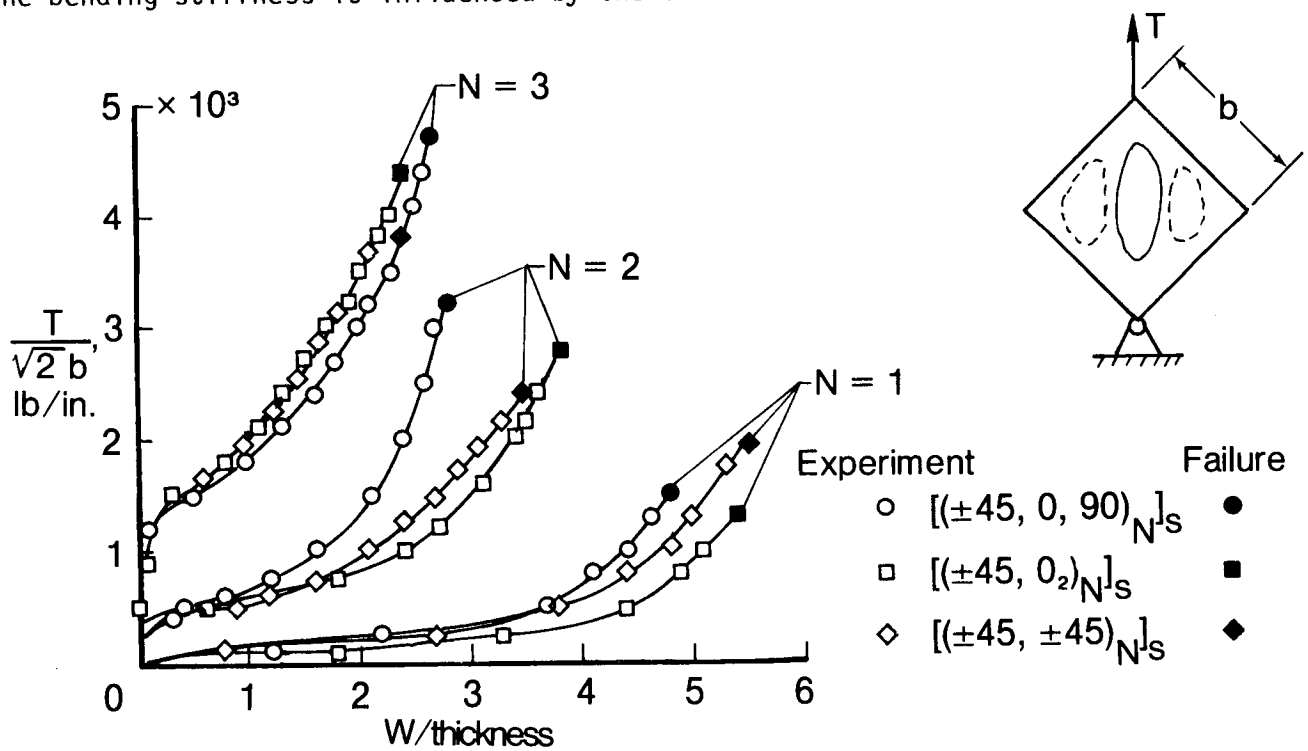

Figure 14

FAILURE CHARACTERISTICS OF AN 8-PLY SHEAR WEB

Some failure characteristics of an 8-ply shear web that was loaded into the postbuckling range are shown in Figure 15. The specimen was loaded well into the postbuckling range and then unloaded for inspection. The photograph on the left shows the moire-fringe pattern of the buckled web at its maximum load. The panel was cross sectioned so the interior could be examined. The center photographs show a cross section of the web. The photograph on the right shows the results of an ultrasonic C-scan inspection of the web.

The photograph of the moire-fringe pattern indicates that a high displacement gradient occurred near the center of the web prior to failure. The photograph of the ultrasonic C-scan indicates that a delamination had occurred in the web. The center photographs show a transverse crack in the laminate and a delamination between plies. Results for 8-ply shear webs indicate that delamination may be a failure mode limiting the postbuckling strength of a graphite-epoxy shear web.

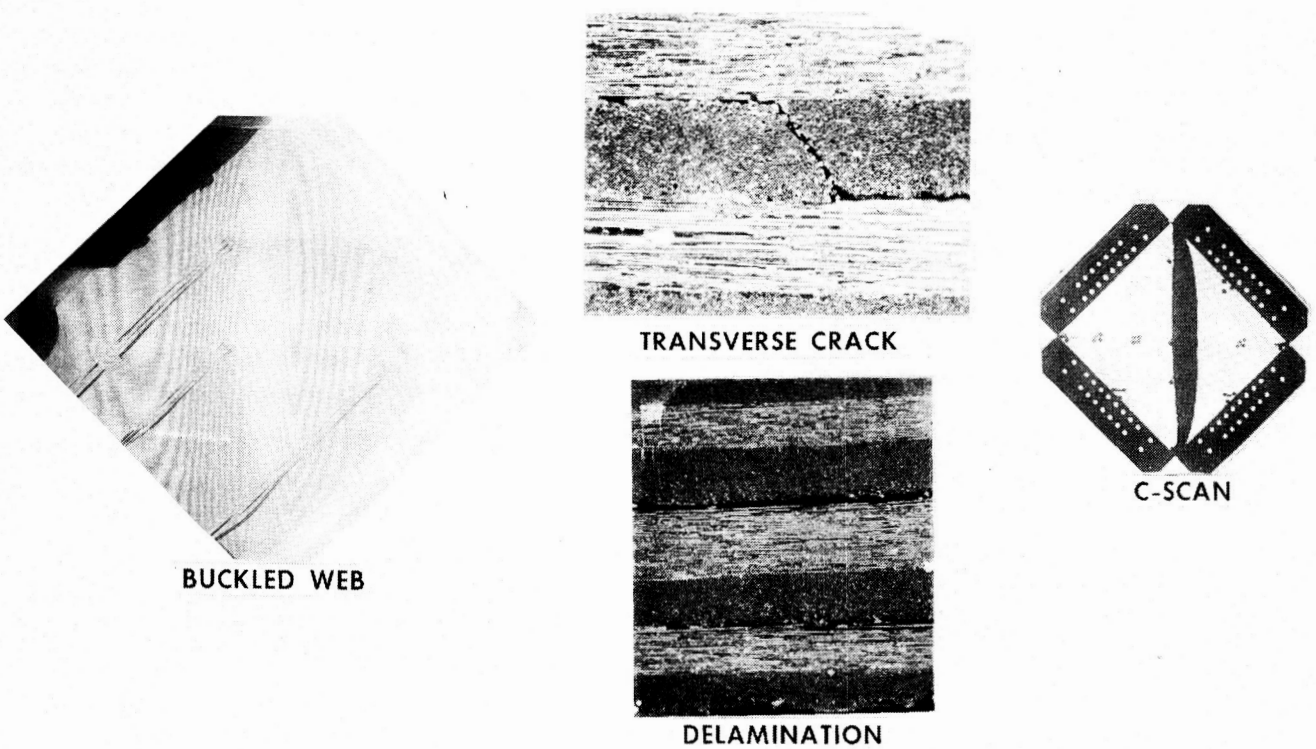

Figure 15

POSTBUCKLING BEHAVIOR OF STIFFENED GRAPHITE-EPOXY SHEAR WEBS

Flat stiffened graphite-epoxy shear webs were loaded to failure in shear to study their postbuckling behavior. Unidirectional tapes of Hercules AS4/3502 graphite-epoxy were used to make 19-, 25-, and 33-ply shear webs. All of the shear webs had 22.5-inch by 22.5-inch test sections. The 19-ply shear webs had a 4.5-inch stiffener spacing and the 25- and 33-ply webs had a 7.5-inch stiffener spacing. There was a common stiffener design for all of the webs that were tested. The stiffeners were attached to the skins with mechanical fasteners and/or bonding. A photograph of a 19-ply shear web is shown in the upper left of Figure 16.

Membrane shear strain results from the tests are summarized below in the lower left of Figure 16. The applied shear flow q is plotted as a function of membrane shear strain. Buckling is indicated by the open symbols and the filled symbols indicate failure. All of the shear webs exhibited some postbuckling capability. The 33-ply shear webs failed soon after buckling. The 19- and 25-ply shear webs had more postbuckling response after buckling. Test results for 25-ply shear webs indicate that specimens with mechanically fastened stiffeners did not exhibit significant improvements in postbuckling performance compared to the specimen with adhesively bonded stiffeners. An improved fastener concept did improve the postbuckling performance of 19-ply shear webs with mechanically fastened and adhesively bonded stiffeners. The photograph in the upper right of Figure 16 shows the typical failure mode for all of the shear webs. These specimens failed when the stiffeners separated from the skin along the skin-stiffener interface.

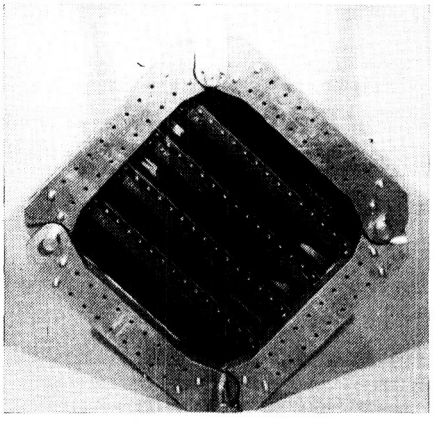

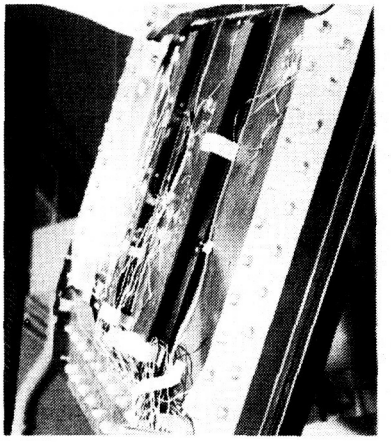

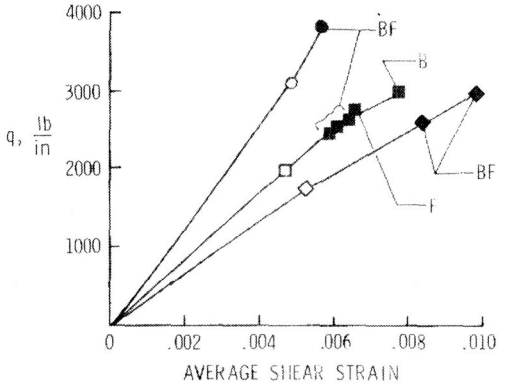

B - BONDED ONLY
F - MECHANICAL FASTENERS ONLY
BF - BONDED AND MECHANICAL FASTENERS

BUCKLING		FAILURE
○	$[(\pm 45, \mp 45)_2, 90_2, \bar{0}_S]_S$	●
□	$[(\pm 45, \mp 45)_2, 0_2, \overline{90}_S]_S$	■
◇	$[\pm 45, \mp 45, \pm 45, 90_2, \bar{0}_3]_S$	◆

Figure 16

POSTBUCKLING RESPONSE OF CURVED GRAPHITE-EPOXY STIFFENED PANELS LOADED IN SHEAR AND COMPRESSION

Curved AS4/3502 graphite-epoxy stiffened panels were loaded to failure in shear and combined shear and compression to study their postbuckling behavior. The panel designs were based on a minimum-weight buckled-skin design obtained from the POSTOP structural optimization code (ref. 7) and had both stiffeners and frames as indicated in Figure 17 below. The padded-skin stiffener attachment concept described in Figure 8 was used at each stiffener location and a failsafe strap was included under each frame and midway between each frame. The panels were 60 inches long, 42 inches wide and had a 143 inch radius. The panels were mounted in a D-box type fixture to provide a closed torque box suitable for shear loading and tested in the Lockheed-Georgia Company's multi-axis combined load test machine.

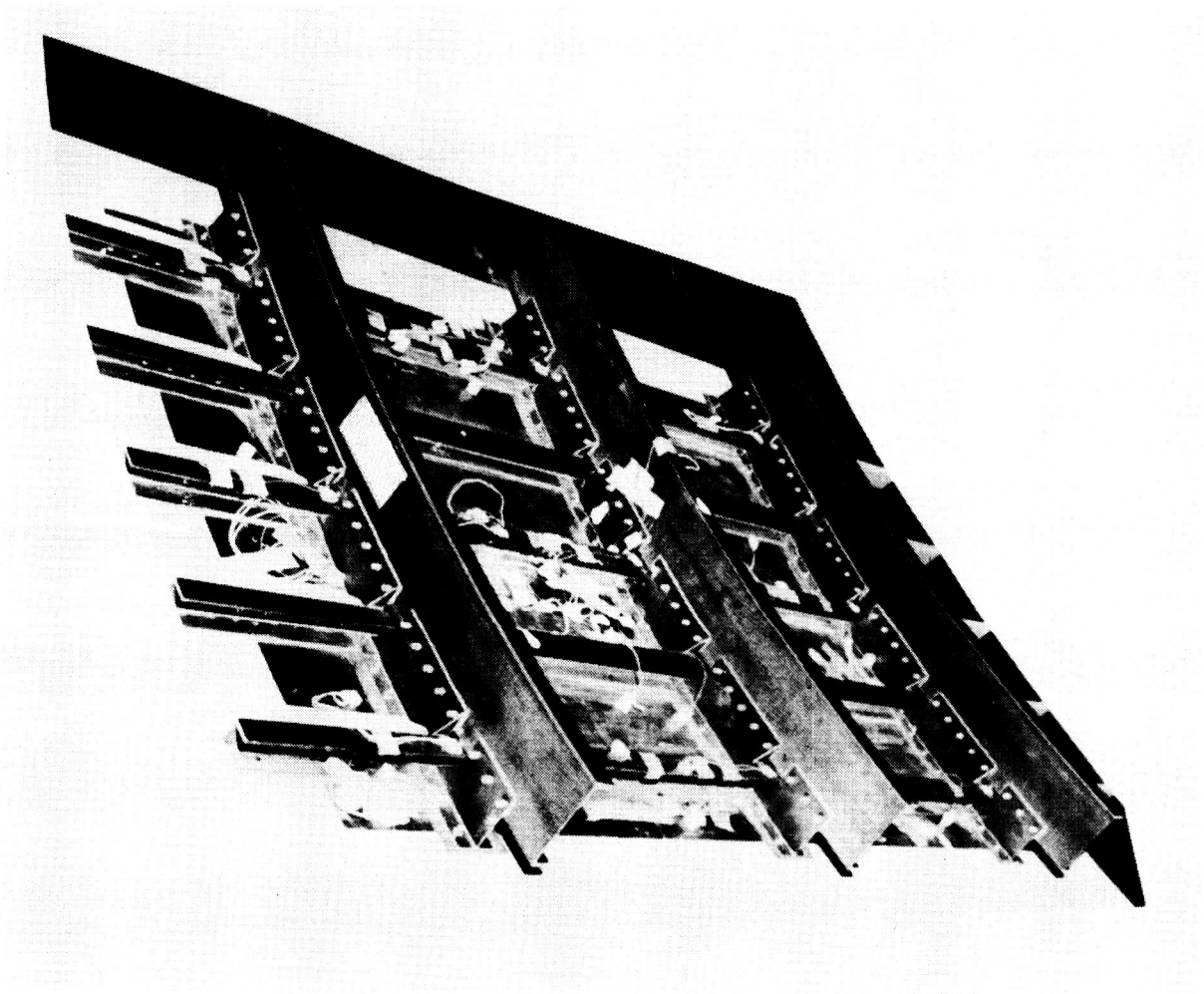

Figure 17

POSTBUCKLING RESPONSE OF CURVED GRAPHITE-EPOXY PANELS
LOADED IN SHEAR AND COMPRESSION

The results of the shear and combined shear and compression tests of the panels described in Figure 17 are shown in Figure 18. Three panels were tested to failure. The first panel was loaded in shear only, the second panel was loaded with approximately equal magnitudes of shear and compression stress resultants and the third panel was loaded with approximately three times as much compression as shear. The predicted buckling and failure interaction curves for shear N_{xy} and compression N_x loading are shown on the figure. The open circles on the figure represent the buckling data from the tests and the filled circles represent failure of the specimens.

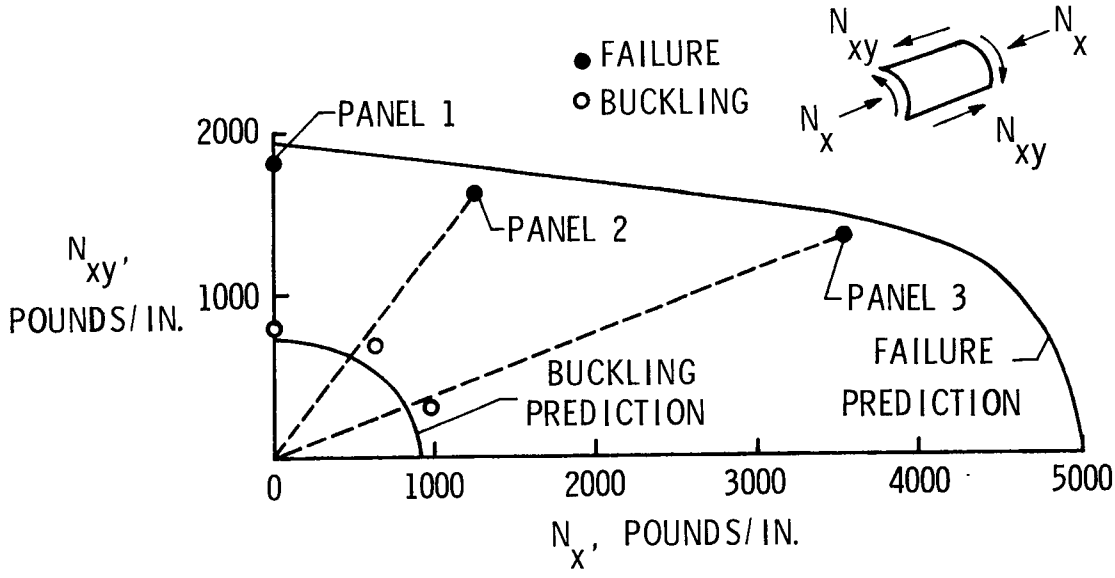

Figure 18

FAILURE MODES OF CURVED GRAPHITE-EPOXY PANELS
LOADED IN SHEAR AND COMPRESSION

A typical failed specimen that had been loaded in combined shear and compression is shown in Figure 19. The panel failed along a diagonal from frame to frame as shown in the left photograph. The stiffeners appear to have crippled where the diagonal failure intersected the stiffeners as shown in the magnified photograph of the stiffener on the right. No stiffener crippling was observed in the panel that was tested in shear only since no compression load was applied to the stiffeners of this panel. Some frame damage was observed after failure of the panel loaded in shear only; however the frame damage may have been caused by the test fixture.

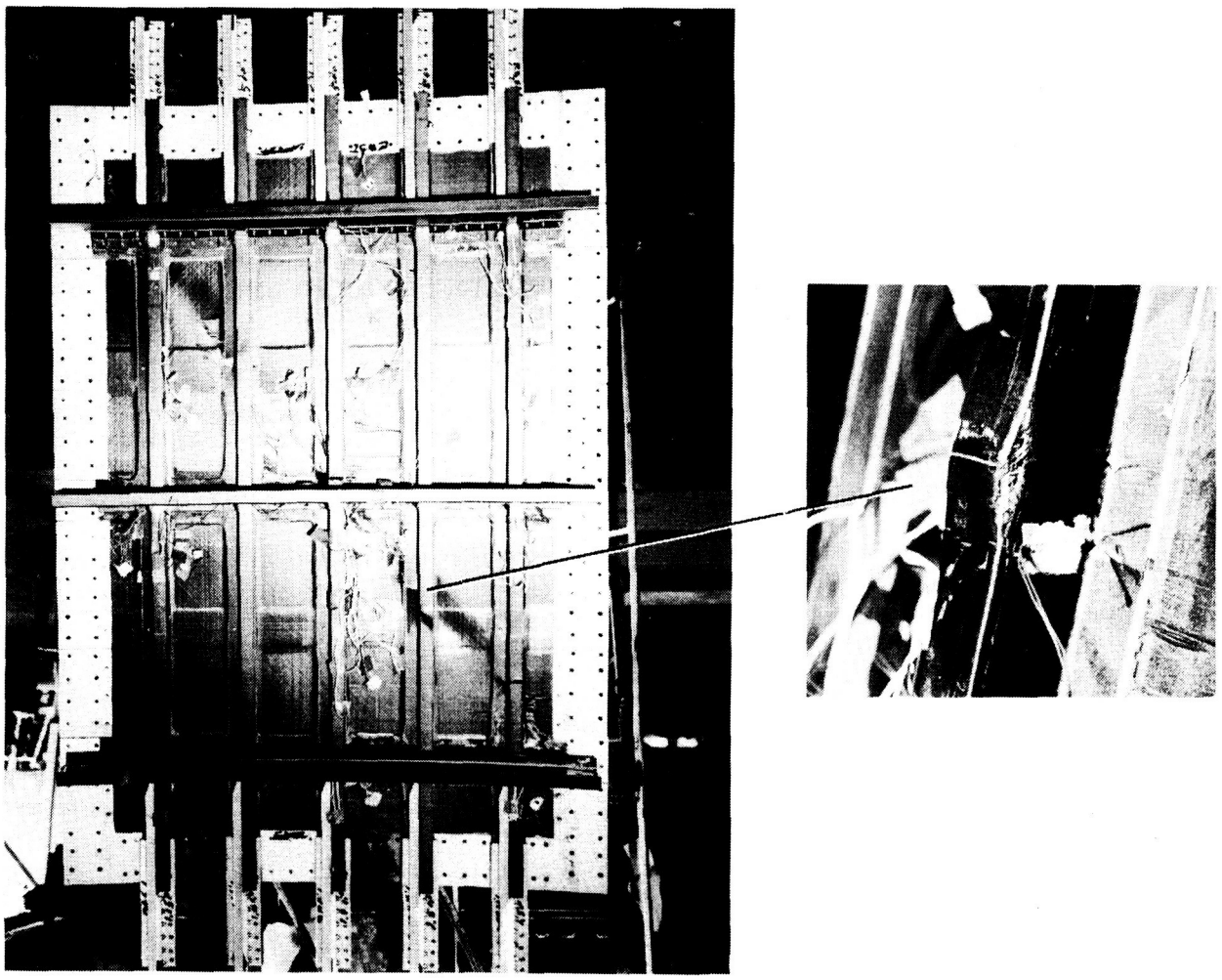

Figure 19

CONCLUDING REMARKS

- Graphite-epoxy structural components loaded in compression, shear and combined shear and compression can exhibit substantial postbuckling strength.
- Unstiffened laminates fail along buckling-mode nodal lines where interlaminar shear stresses are large.
- Holes and low-speed impact damage can degrade postbuckling strength if local strains are high enough to initiate and propagate damage.
- Postbuckling strength of stiffened panels can be limited by skin-stiffener separation.
- Increasing the skin thickness under a stiffener suppresses skin-stiffener separation.
- Stiffened panels can fail by stiffener crippling if skin-stiffener separation is suppressed.
- Damaged stiffeners can degrade postbuckling strength.
- Local delamination degrades postbuckling strength of curved panels with holes.
- Postbuckling response can be predicted analytically if local bending flexibility is adequately modeled.
- Large rotation and transverse shear deformation theories may be needed to accurately predict postbuckling behavior of components with severe local bending gradients.

REFERENCES

1. Starnes, James H., Jr.; and Rouse, Marshall: Postbuckling and Failure Characteristics of Selected Flat Rectangular Graphite-Epoxy Plates Loaded in Compression. Proceedings of the AIAA/ASME/ASCE/AHS 22nd Structures, Structural Dynamics and Materials Conference, Atlanta, GA, April 6-8, 1981. AIAA Paper No. 81-0543.

2. Starnes, James H., Jr.; Knight, Norman F., Jr.; and Rouse, Marshall: Postbuckling Behavior of Selected Flat Stiffened Graphite-Epoxy Panels Loaded in Compression. Proceedings of the AIAA/ASME/ASCE/AHS 23rd Structures, Structural Dynamics and Materials Conference, New Orleans, LA, May 10-12, 1982. AIAA Paper No. 82-0777.

3. Almroth, B. O.; Brogan, F. A.; and Stanley, G. M.: Structural Analysis of General Shells, Vol. II, User Instructions for STAGSC-1. Report No. LMSC-D633873, Lockheed Palo Alto Research Laboratory, Palo Alto, CA, December 1982.

4. Wang, J. T. S.; and Biggers, S. B.: Skin/Stiffener Interface Stresses in Composite Stiffened Panels. NASA CR-172261, January 1984.

5. Knight, Norman F., Jr.; and Starnes, James H., Jr.: Postbuckling Behavior of Axially Compressed Graphite-Epoxy Cylindrical Panels with Circular Holes. Collapse Analysis of Structures, Sobel, L. H. and Thomas, K., Eds., PVP Vol. 84, ASME, June 1984, pp. 153-167.

6. Riks, E.: The Application of Newton's Method to Problems of Elastic Stability. Journal of Applied Mechanics, Vol. 39, December 1972, pp. 1060-1066.

7. Dickson, J. N.; and Biggers, S. B.: POSTOP: Postbuckling Open-Stiffener Optimum Panels - Theory and Capability. NASA CR-172259, January 1984.

Page intentionally left blank

STUDIES OF NOISE TRANSMISSION IN ADVANCED COMPOSITE MATERIAL STRUCTURES

Louis A. Roussos, Michael C. McGary, and
Clemans A. Powell
NASA Langley Research Center
Hampton, Virginia 23665

1984 ACEE Composite Structures Conference
Seattle, Washington

August 13, 1984

CONCERNS AND POTENTIAL PROBLEMS RELATED TO NOISE TRANSMISSION IN COMPOSITE FUSELAGES

The noise transmission characteristics of advanced composite material structures must be taken into account early in the design phases of composite fuselages so that the weight-saving advantage of composite construction will not be compromised by high noise transmission and heavy add-on acoustic treatments. Some of the noise transmission concerns and potential problems related to advanced composite material fuselages are indicated in figure 1. Noise from a variety of noise sources can enter an aircraft fuselage through a number of paths or mechanisms. Noise from these sources is frequently classified as being either airborne or structureborne. In many instances the airborne and structureborne noises are highly correlated and indistinguishable once inside the aircraft. The airborne noise transmission characteristics of a fuselage can be either favorably or adversely affected by the use of advanced composites materials depending on the frequency of the incident noise. At low frequencies, a composite fuselage may transmit less noise because of increased stiffness. In the region where structural resonances and damping control noise transmission, a composite fuselage may transmit either more or less noise depending on the damping characteristics of the materials. At mid frequencies a composite fuselage should transmit more noise for an equivalent stiffness design. Noise frequencies for which the lengths of acoustic and structural waves coincide should be lower for composite constructions and therefore could allow more overall noise transmission for most aircraft noise sources (upper mid frequency range). The effects of composite construction on structureborne noise in the low and mid frequencies are hard to generalize although noise problems may be found in the upper mid frequency range because radiation efficiency is very high in the coincidence region.

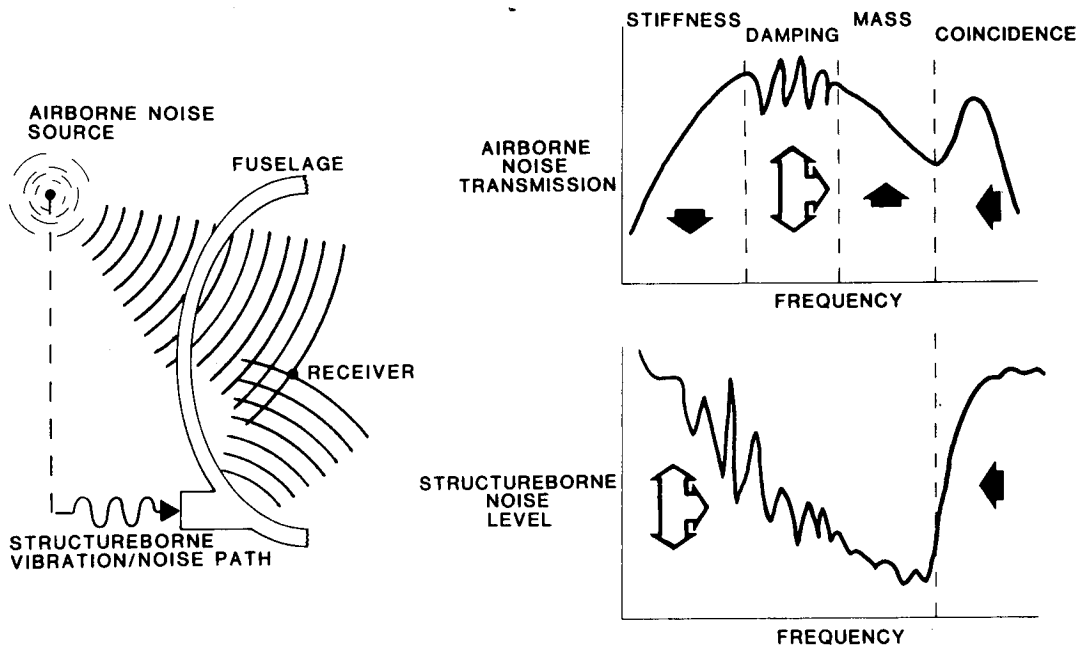

Figure 1

RESEARCH PROGRAM

The Structural Acoustics Branch at the NASA Langley Research Center has begun a research program in noise transmission of advanced composite material structures with the ultimate goal of providing optimum design from the standpoint of aircraft interior noise. Figure 2 outlines the elements and overall strategy for the research program and the topics which are addressed in this report. The initial emphasis is to develop models for the noise characteristics of simple structural panels of composite materials. Elements included in the model are: 1) transmission loss in infinite anisotropic panels, 2) transmission loss in finite panels with consideration of their modal behavior, 3) effects of different advanced composite materials, and 4) radiation characteristics of both airborne and structureborne noise of composite panels. The future emphasis of the program will be to develop models for the more complicated structures representative of aircraft fuselages. The research elements in these models include (1) a finite element representation of the structure and acoustical processes, (2) effects of stiffeners and other non-panel elements, (3) effects of add-on acoustical treatments, (4) consideration of cylindrical and other curved structural configurations, and (5) use of optimized structural configurations to enhance noise transmission characteristics. In addition to the model development, the research program includes noise transmission testing and verification of the various elements in the models. This report will concentrate on the progress and plans of the elements of the simple panel models and finite element representations and on noise transmission loss tests which have been conducted or are in progress.

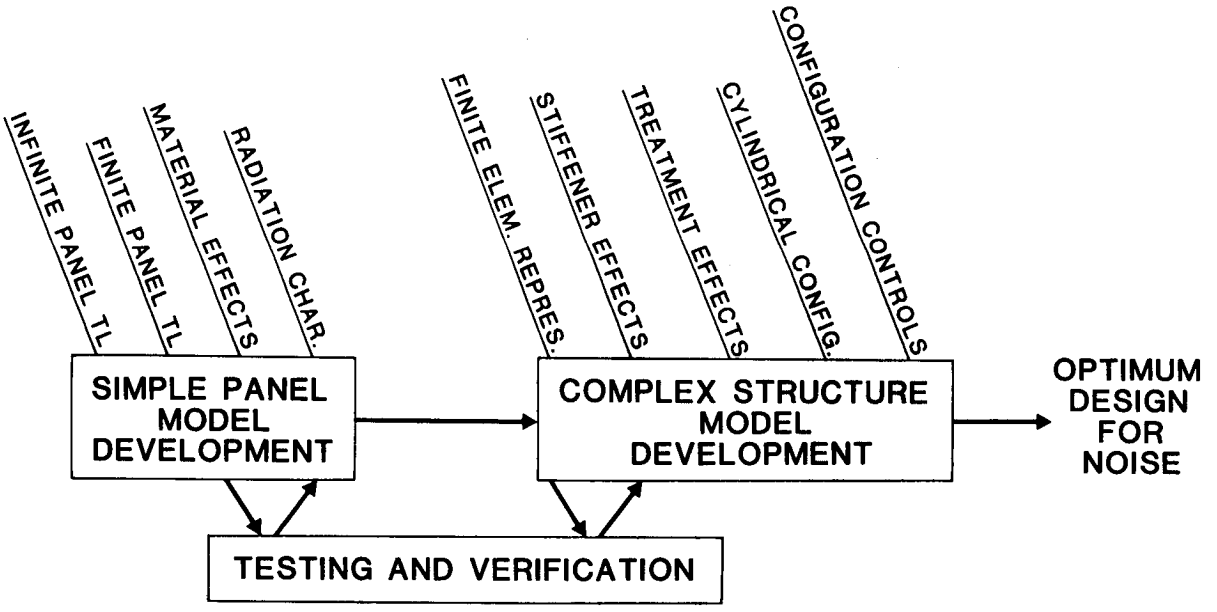

Figure 2

INFINITE PANEL THEORY TRANSMISSION LOSS MODEL

In infinite panel theory the panel is modelled as a thin plate with infinite area. For oblique incidence transmission loss, the incident sound is modelled as a single plane wave that impinges on the panel at an arbitrary angle. Because the panel is infinite, the reflected and transmitted pressures are also plane waves. The geometry of the transmission is shown in figure 3. Since the intensity of a plane wave is linearly proportional to the mean square pressure, the oblique incidence transmission loss, which is calculated from the ratio of incident to transmitted intensities, reduces to the simple relationship between incident and transmitted pressures shown in the figure. The ratio of incident to transmitted pressure is calculated from the differential equation of motion of the plate: the general form of the equation is given in the figure. The frequency at which the term in brackets is a minimum is called the coincidence frequency and corresponds to a wavelength resonance condition at which the trace wavelength of the incident noise is equal to the free bending wavelength in the infinite plate. At frequencies below the coincidence frequency, the first term within the brackets, the so-called "mass law" term, governs the transmission. Above coincidence the curve rises sharply and is a function mainly of the damping, which is represented by the loss factor in the equation in the figure. In summary, the infinite panel theory transmission loss model is applicable only in the mass controlled and coincidence frequency regions of transmission loss.

$$T.L. = 10 \log \left| \frac{p_i}{p_t} \right|^2$$

$$\frac{p_i}{p_t} = 1 + j \left[\frac{\bar{m} \pi f \cos \theta_i}{\rho c} - g \left(D_{ij}, f, \eta, \theta_i, \Phi_i \right) \right]$$

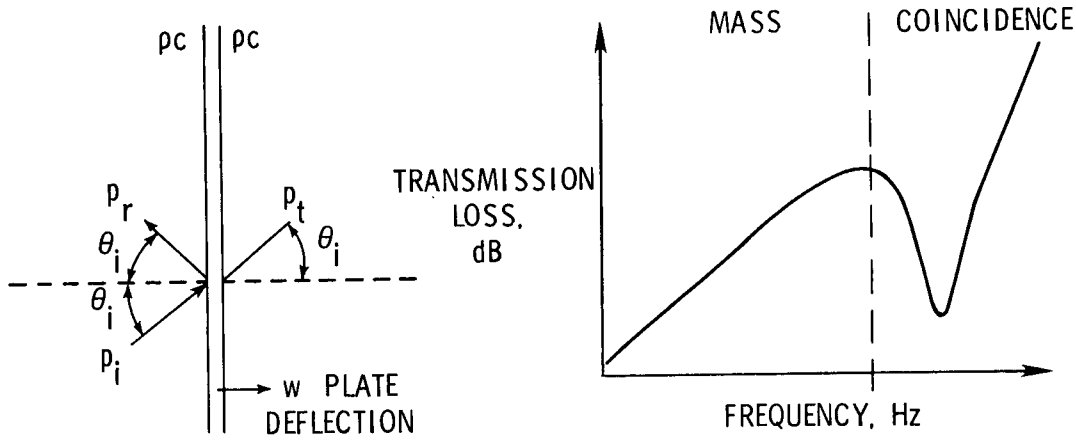

Figure 3

TRANSMISSION LOSS TESTS OF LARGE PANELS

Facility and Method

To validate the infinite panel theory and experimentally establish the noise transmission loss characteristics of large composite test panels, the panels were mounted in the ANRD Transmission Loss Apparatus as partitions between two adjacent rooms which are designated the source room and the receiving room. Top and side views of the apparatus are shown in figure 4. In the source room a diffuse field is established by two reference sound power sources. Sound is transmitted from the source room into the receiving room only by way of the test panel, which has a sound exposed vibrating area of 0.85 m by 1.46 m (2.8 ft by 4.8 ft). The test specimen is mounted in a steel frame which is designed for minimum structural flanking. The receiving room is acoustically and structurally isolated from the rest of the building. A space and time average of the sound pressure levels is taken in each of the rooms by a microphone mounted at the end of a rotating boom. The microphones measure the panel's noise reduction, which is defined as the difference between the measured average sound pressure levels in the source and receiving rooms. Noise reduction includes characteristics of the test specimen as well as room characteristics. Transmission loss, which is a function of the properties of the test specimen only, is calculated from noise reduction by correcting for the absorption in the receiving room as well as for the non-diffusivity of both rooms.

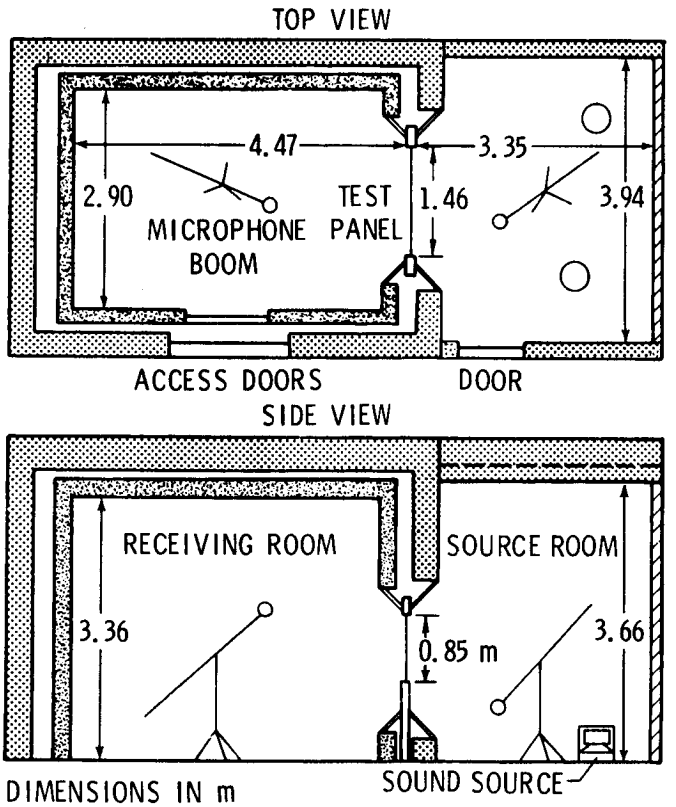

Figure 4

TRANSMISSION LOSS TESTS OF LARGE PANELS

Panel Configurations

A total of 28 fiber-reinforced composite panels were tested. Twelve of these panels were of tape construction, fourteen were of fabric construction, and two were of sandwich construction with fabric composite skins and syntactic (microballoon-filled epoxy) cores. The tape panels were made by bonding together several plies of unidirectional fibers. Each ply has a "ply angle" which refers to the angle at which the fibers are laid up in relation to the longer boundary of the panel. Thus, a 0° or 90° ply has its fibers parallel to one of the boundaries. The panels with fabric construction were similarly made by bonding several plies together. Since a fabric ply consists of two sets of fibers woven perpendicular to each other, two ply angles are associated with each ply. Also, in one fiber direction called the fill direction, the fibers are straight, while in the opposite warp direction, the fibers bend up and down as they weave around the straight fibers. For a 0°/90° ply, the warp of the fabric was oriented in the direction of the longer boundary of the panels, i.e., in the 0° direction. Descriptions of ply material, ply angle lay-up, thickness, and number and type of plies for each panel are given in figure 5. As can be seen in the figure, three ply materials were tested (graphite-epoxy, Kevlar*-epoxy, and fiberglass-epoxy) for both tape and fabric construction, for two thicknesses, and for various ply angle lay-ups.

*Kevlar aramid fibers, manufactured by E. I. du Pont de Nemours & Co., Inc.

TAPE PLY ANGLE CONFIGURATIONS

G/E, K/E, AND F/E

8 PLIES (0.10 CM) ... ±45, 0/90

16 PLIES (0.20 CM) ... ±45, 0/90

FABRIC PLY ANGLE CONFIGURATIONS

G/E, K/E, AND F/E

4 PLIES (0.10 CM) ... ±45, 0/90

8 PLIES (0.20 CM) ... ±45, 0/90/±45

OTHER G/E (0/90) FABRIC CONFIGURATIONS

3 PLIES (0.10 CM)

6 PLIES (0.20 CM)

6 PLIES w/0.10 CM SYNTACTIC CORE

6 PLIES w/0.20 CM SYNTACTIC CORE

Figure 5

TRANSMISSION LOSS TESTS OF LARGE PANELS

Typical Results

In figure 6 the measured field incidence transmission loss of two graphite-epoxy panels is compared with infinite panel theory. Infinite panel theory is seen to be in good agreement (within 1 dB) with the data over the entire mass controlled frequency region. In the coincidence frequency region, the agreement is again quite good. The theory follows the slope of the coincidence dip for both panels and is within 1 to 3 dB of the measured levels. The agreement between theory and measured data in this figure is typical of the agreement that occurred for all 28 panels.

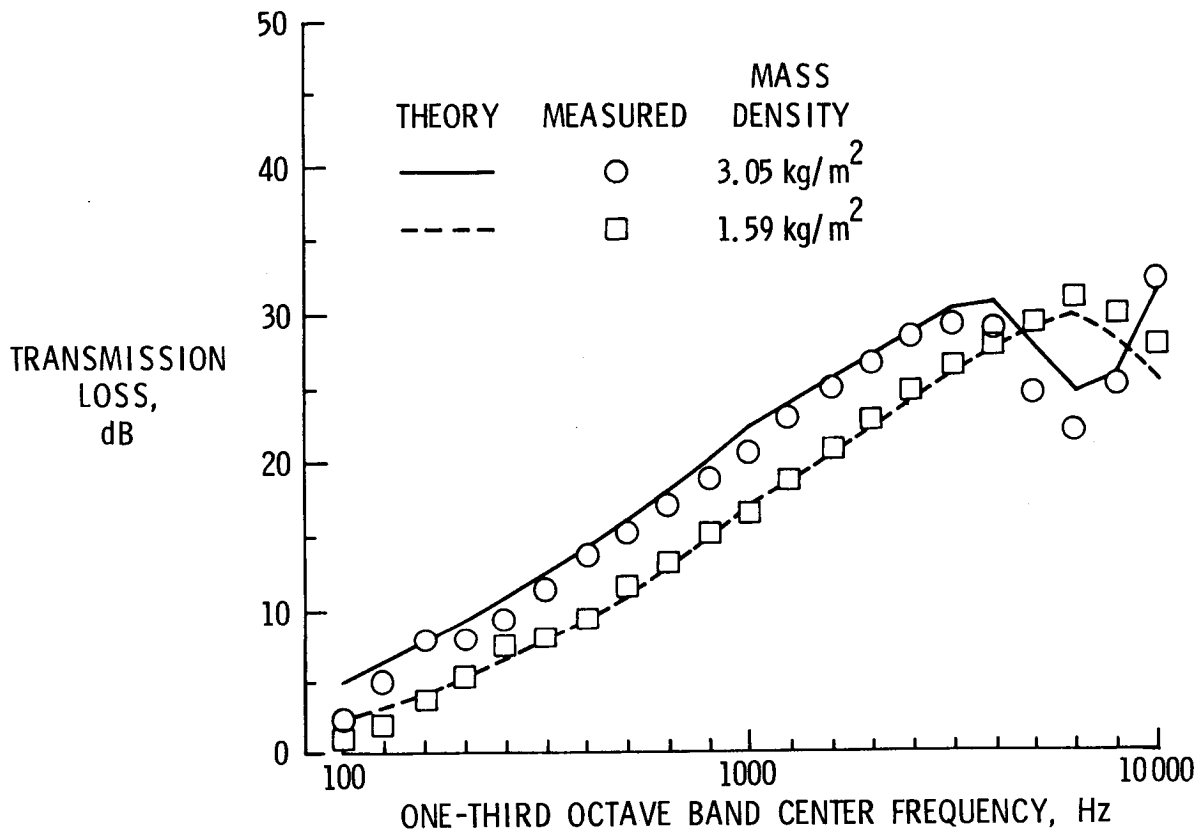

Figure 6

TRANSMISSION LOSS TESTS OF LARGE PANELS

Overall Prediction Ability

The noise transmission loss prediction ability of infinite panel theory for the large composite panels is indicated in figure 7. The prediction error, the difference between predicted and measured transmission loss, is plotted for 14 of the 28 composite panels. The frequency scale on the abscissa has been normalized by dividing by the critical frequency, the lowest frequency for which coincidence occurs. The prediction error in the mass controlled region (f/f-critical < 1) is seen to be generally less than ±3 dB. In the coincidence region, the error is somewhat greater (generally within ±6 dB). This is because the stiffness and damping properties used in the infinite panel theory model were only rough estimates and these properties govern the transmission loss in the coincidence region.

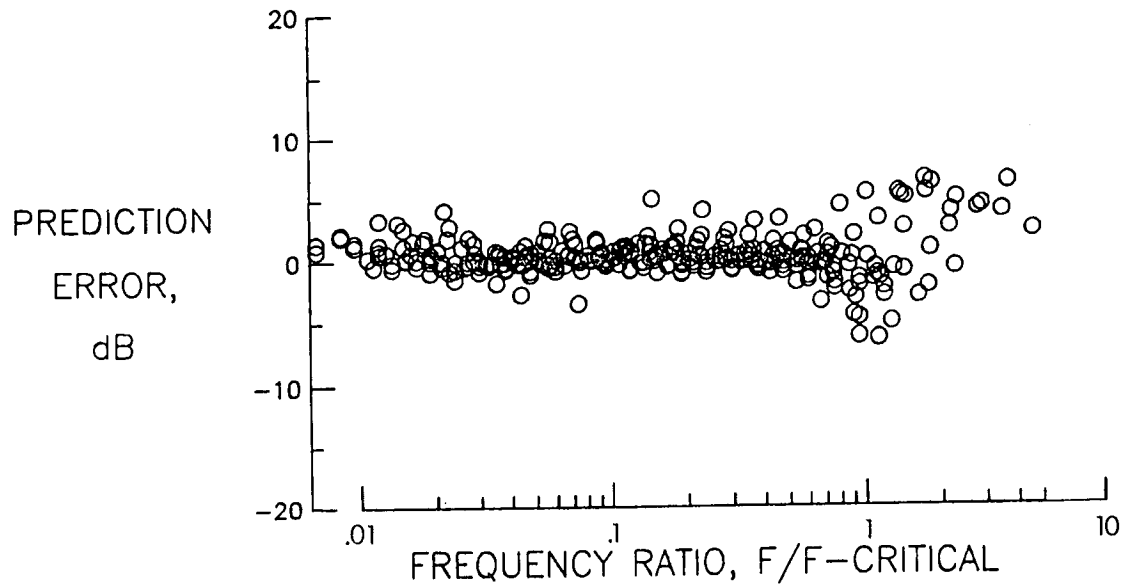

Figure 7

FINITE PANEL THEORY DEVELOPMENT

For low frequency noise, the dimensions of the transmitting panel are comparable to or smaller than the sound wavelengths so that boundary effects are important. Therefore, for this case, a new finite panel noise transmission theory, as indicated in figure 8, has been developed. In this theory the panel is modelled as a rectangular plate simply supported in an infinite rigid baffle. The incident acoustic pressure is modelled as a plane wave impinging on the plate at an arbitrary angle of incidence. The incident, reflected, and transmitted pressures are approximated by the blocked pressure which is assumed to be much greater than the reradiated pressure. This assumption allows the plate vibrations to be calculated by a normal-mode approach. The Rayleigh Integral is used to link the plate vibrations to the transmitted acoustic pressure. The incident and transmitted acoustic powers are calculated by integrating the incident and transmitted intensities over their appropriate areas, and transmission loss is calculated from the ratio of incident to transmitted acoustic power.

- RECTANGULAR PLATE SIMPLY SUPPORTED IN INFINITE BAFFLE
- BLOCKED PRESSURE ASSUMPTION
  $$p_i + p_r - p_t \approx 2p_i$$
- MODAL SOLUTION FOR PANEL VIBRATIONS
- RAYLEIGH INTEGRAL WITH FAR-FIELD APPROXIMATIONS
- INTEGRATION OF INTENSITIES FOR INCIDENT AND TRANSMITTED ACOUSTIC POWERS
- $$\text{T. L.} = 10 \log \left(\frac{\text{INCIDENT ACOUSTIC POWER}}{\text{TRANSMITTED ACOUSTIC POWER}} \right)$$

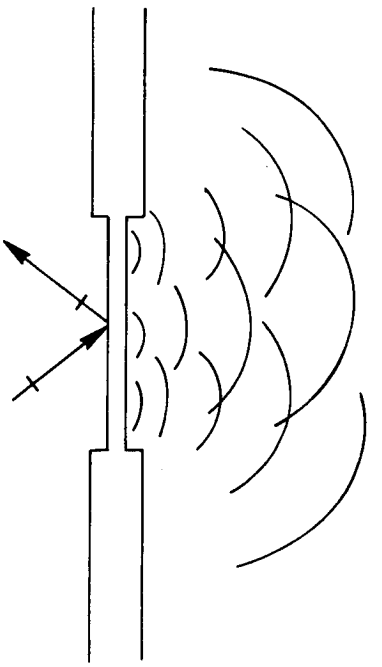

Figure 8

FINITE PANEL THEORY DEVELOPMENT

Radiation Directivity Results

An example of the use of the model for calculating radiation directivity is shown in figure 9. Plotted here is the variation of transmitted intensity in the far field of a 36-cm by 20-cm by 0.01-cm graphite-epoxy panel for a plane wave incident on it at a polar angle of 45° and an azimuthal angle of 0° (parallel to the 36-cm side of the plate). The ply angle lay-up of the panel consisted of 8 alternating +45° and -45° plies laid up symmetrically about the midplane. Transmitted intensity was calculated for two frequencies, 500 Hz and 3000 Hz. The sample results show that as frequency increases, more of the transmitted sound becomes concentrated at a transmitted angle equal to the incident angle. The results showing the variation of transmitted intensity with azimuthal angle display an example of symmetry which helps reduce integration time. With an incident azimuthal angle of $\phi_i = 0°$, symmetry occurs about $\phi = 0°$. Though not shown, for an incident azimuthal angle of $\phi_i = 90°$, symmetry occurs about $\phi = 90°$. And, for an incident polar angle of $\theta_i = 0°$, symmetry occurs about both $\phi = 0°$ and $\phi = 90°$. Studying these transmitted intensity radiation patterns is thus seen to aid in both the understanding of the physics of the problem and the understanding of the numerics involved in calculating transmission loss.

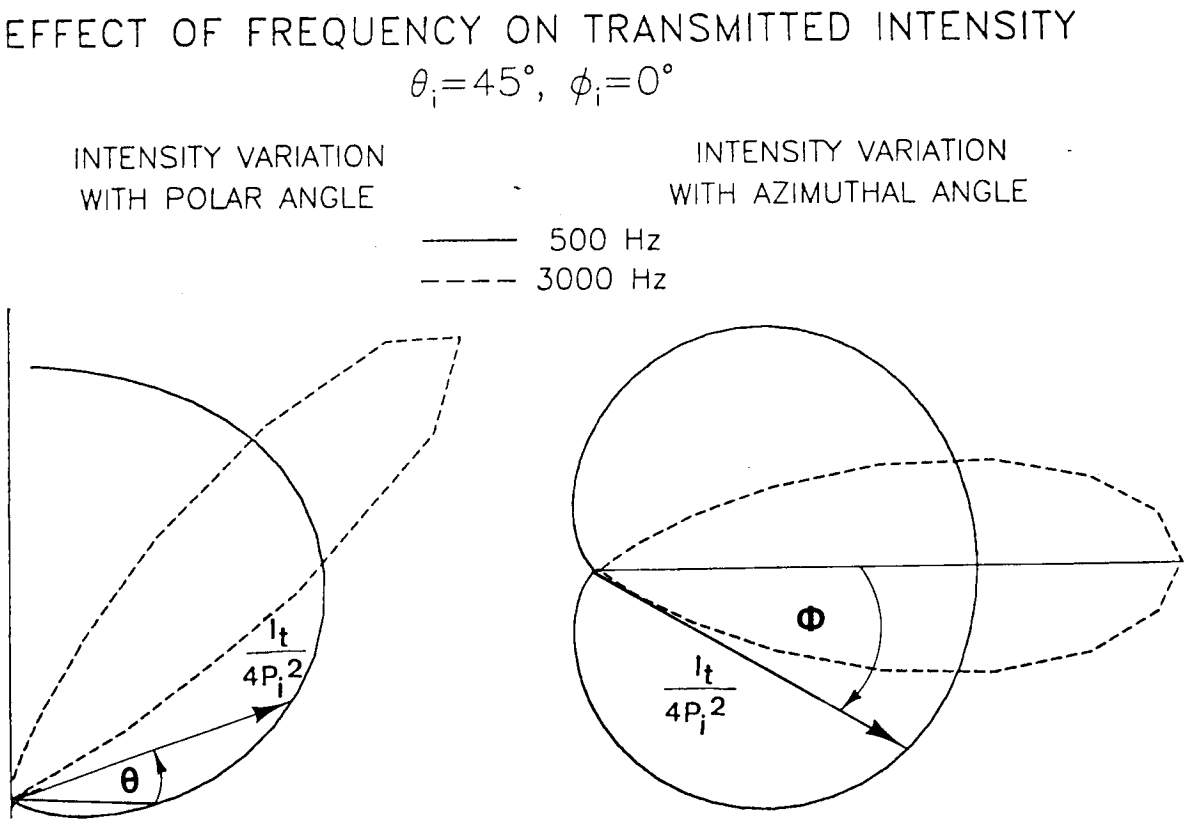

Figure 9

FINITE PANEL THEORY DEVELOPMENT

Prediction of Effect of Ply Angle and Incidence Angle on Transmission Loss

In a composite panel the flexural rigidity moduli will be different in different directions depending on ply angle lay-up. Therefore, panels with different ply angle lay-ups or with different orientations with respect to the incident noise could have markedly different low frequency noise transmission characteristics. The effects of ply angle and incidence angle on transmission loss have been calculated for a 36-cm by 20-cm by 0.10-cm graphite-epoxy panel and the results are shown in figure 10. The curves showing ply angle effect, which were calculated for the case of normal incidence, indicate that a panel made of +45°/-45° plies has significantly higher (6 to 14 dB) transmission loss in the stiffness controlled low frequency region than a panel made of 0°/90° plies. In the frequency range immediately following the fundamental resonance of the +45°/-45° panel, the 0°/90° panel has 2 to 9 dB more transmission loss. Since the panels weigh the same, the transmission loss curves merge together in the high frequency mass controlled region. In comparing the transmission loss for the +45°/-45° panel for two different angles of incidence, very little difference (less than 2 dB) is found in the stiffness and resonance controlled regions, while in the mass controlled region the normal incidence curve rises up to a maximum of 3 dB above the 45° incidence case. These predictions indicate that the ability to tailor the ply angle lay-up of a composite panel can significantly affect the low frequency noise transmission characteristics, and the effect of varying the angle of incidence is not as important an effect at low frequency. Further study is needed to fully understand the ply angle effect and to determine the effect of varying the azimuthal incident angle.

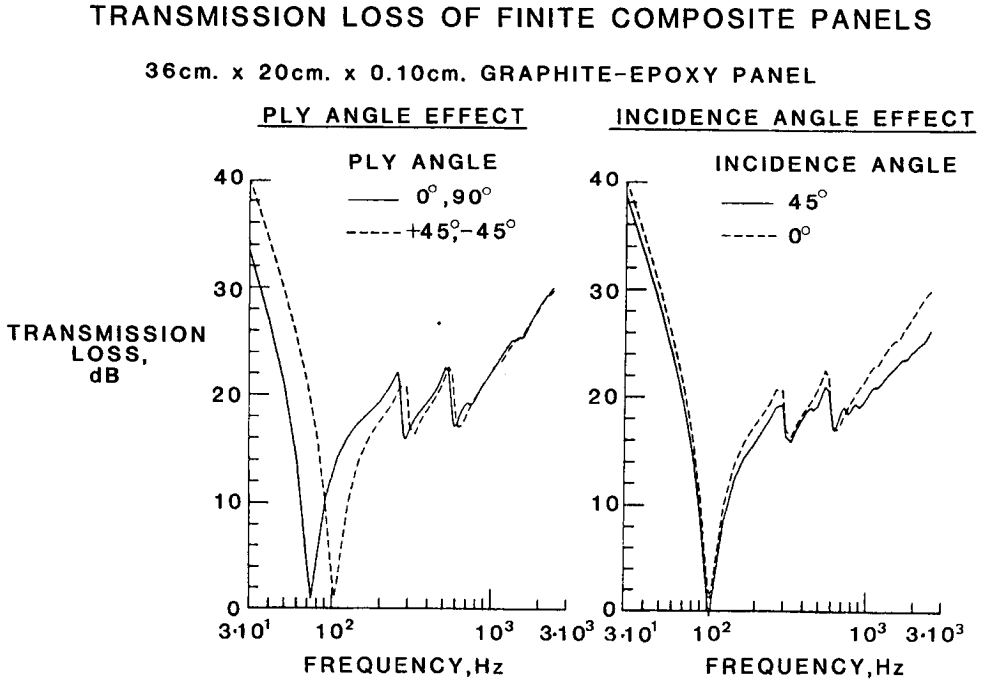

Figure 10

FINITE PANEL THEORY DEVELOPMENT

Design Comparison

The analytical model has been used to investigate the effect on noise transmission of replacing a typical general-aviation type aluminum skin with either graphite-epoxy or Kevlar-epoxy skins. The design comparison presented here is based on equal critical shear load for the composite and aluminum panels. The panels were assumed to be approximately 36 cm by 20 cm with simply supported boundary conditions. The composite panels were assumed to be of tape construction with each ply being 0.013 cm thick. The critical shear load was first calculated for the aluminum panel which was assumed to be 0.10 cm thick. Each composite panel was then designed for the minimum thickness necessary for its critical shear load to be greater than or equal to that of the aluminum panel. The incidence sound is assumed to impinge at an angle of 60°. In figure 11, it can be seen that because of their higher fundamental frequencies, the graphite-epoxy and Kevlar-epoxy panels have over 12 dB more transmission loss at the aluminum panel's resonance (79 Hz). The increase in transmission loss over the aluminum panel is about 4 dB at the lowest frequencies plotted. In the high frequency mass controlled region, the graphite-epoxy and Kevlar-epoxy panels have about 3 to 4 dB less transmission loss because they would be about 34 percent lighter than the aluminum panel. Such transmission loss characteristics indicate that composites may be beneficial for low frequency noise transmission problems at or below the resonance of conventional aluminum panels.

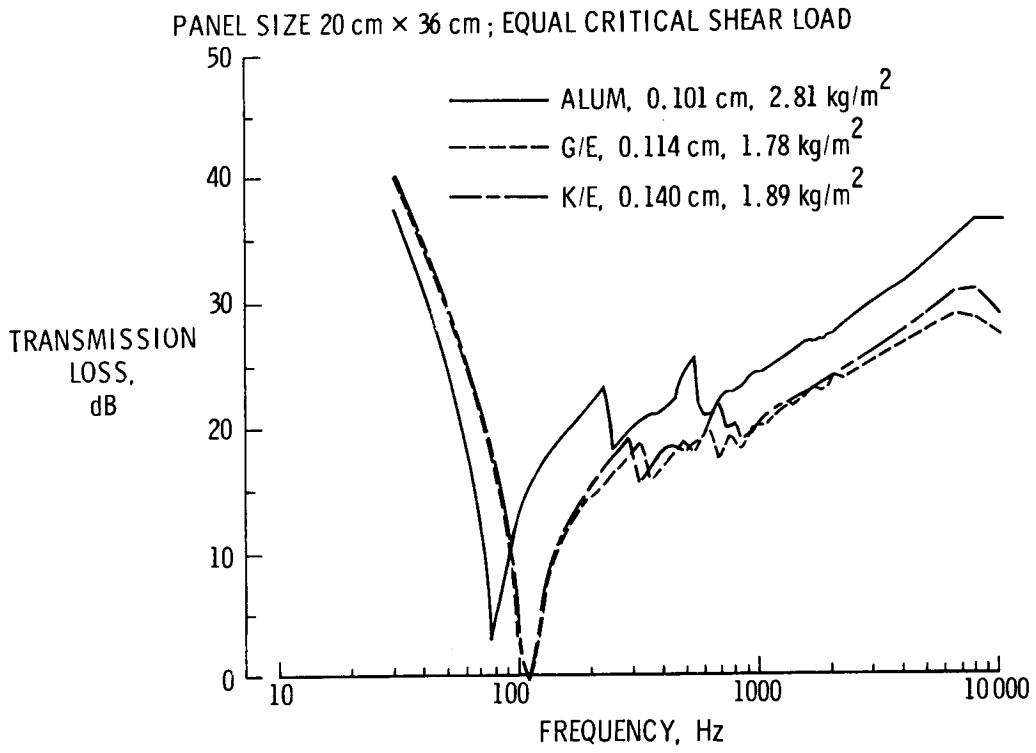

Figure 11

TEST PLAN FOR FINITE PANELS

To investigate the effects of high-strength/lightweight composites in the low frequency regions of transmission loss, experimental studies are planned for small panels (40 cm by 24 cm) whose fundamental frequencies will typically be 150 Hz or more. The small panels will be cut from 10 of the 28 large panels that had been tested earlier. The calculated simply supported and clamped fundamental frequencies for the panels to be tested are shown in figure 12. The actual fundamental frequencies will be measured and are expected to fall somewhere in between these extremes. The percent critical damping will also be measured. Ply angle lay-up and damping will be investigated especially for their effects on noise transmission in the stiffness and resonance controlled regions of transmission loss.

TRANSMISSION LOSS TESTS OF SMALL PANELS

PANEL CONFIGURATIONS

PLY MATERIAL	NUMBER OF PLIES	PLY ANGLES	TOTAL THICKNESS, CM	SURFACE DENSITY, KG/M^2	NATURAL FREQUENCY, Hz	
					SIMPLY SUPPORTED	CLAMPED
G/E TAPE	16	+45/-45/0/90	0.21	3.36	127	252
G/E TAPE	16	+45/-45	0.19	3.05	130	218
G/E FABRIC	8	(+45/-45)/(0/90)	0.23	3.58	168	324
G/E FABRIC	8	(+45/-45)	0.23	3.56	165	320
K/E TAPE	16	+45/-45/0/90	0.20	2.79	100	198
K/E TAPE	16	+45/-45	0.20	2.79	115	193
K/E FABRIC	8	(+45/-45)/(0/90)	0.15	2.10	80	155
K/E FABRIC	8	(+45/-45)	0.15	2.09	82	156
G/E FABRIC	6	(0/90)	0.21	3.31	154	299
G/E FABRIC W/SYNTACTIC CORE	6	(0/90)	0.32	4.16	251	458

Figure 12

FINITE ELEMENT MODEL DEVELOPMENT

In order to model more complicated structural configurations, a finite element model for the plate vibrations is being incorporated into the finite panel theory. Using finite elements, as indicated in figure 13, will allow more realistic modelling of the anisotropic behavior of composites, the modelling of stiffened plates and plates with windows, and the modelling of more realistic boundary conditions. Though the use of finite elements can become overly costly, it will be feasible in the current research because the concern here is at low frequency where only a few elements are needed to model the few modes that are being excited. Since the ultimate goal is to predict the interior noise levels in an aircraft cabin, the effect of cabin acoustics needs to be included in the model. As a step in this direction, finite elements are also being used to link the plate transmission problem with a receiving acoustic space. This problem is commonly referred to as noise transmission into an enclosure. These advancements in the structural and acoustical aspects of the problem are currently under development and the research is being conducted for NASA by Professor Leslie R. Koval of the University of Missouri at Rolla, Missouri.

OBJECTIVES: TO ACCOUNT FOR

- o COMPLEX STRUCTURAL CONFIGURATIONS
- o NON-IDEALISTIC BOUNDARY CONDITIONS
- o ANISOTROPIC STIFFNESS PROPERTIES
- o COUPLING TO CABIN ACOUSTICS

PRINCIPAL INVESTIGATOR:

- o DR. LESLIE R. KOVAL
  UNIVERSITY OF MISSOURI-ROLLA

Figure 13

STRUCTUREBORNE NOISE RADIATED BY COMPOSITE PANELS

Until recently, both the analytical and experimental research programs on the noise radiative properties of composite materials have been devoted almost exclusively to the study of airborne sound transmission through composite structures. Present and future research in this area includes a comprehensive study of the structureborne noise radiative properties of these materials. Evidence of the extreme differences in these two sound generating mechanisms (airborne vs. structureborne) can be predicted analytically and measured experimentally in terms of the acoustic source directivity, the acoustic radiation efficiency, and the complexity of the acoustic near field. Figure 14 shows the large difference in the acoustic radiation efficiency for the airborne and structureborne sound radiated by a rectangular sheet of plexiglass. Similar differences in the airborne and structureborne noise radiative properties of panels constructed with composite materials are expected.

CHARACTERISTICS OF STRUCTUREBORNE SOUND RADIATION IN TERMS OF THE ACOUSTIC RADIATION EFFICIENCY σ :

$$\sigma = \frac{\Pi}{\rho c \langle v^2 \rangle_{r,t} \bullet \text{Area}}$$

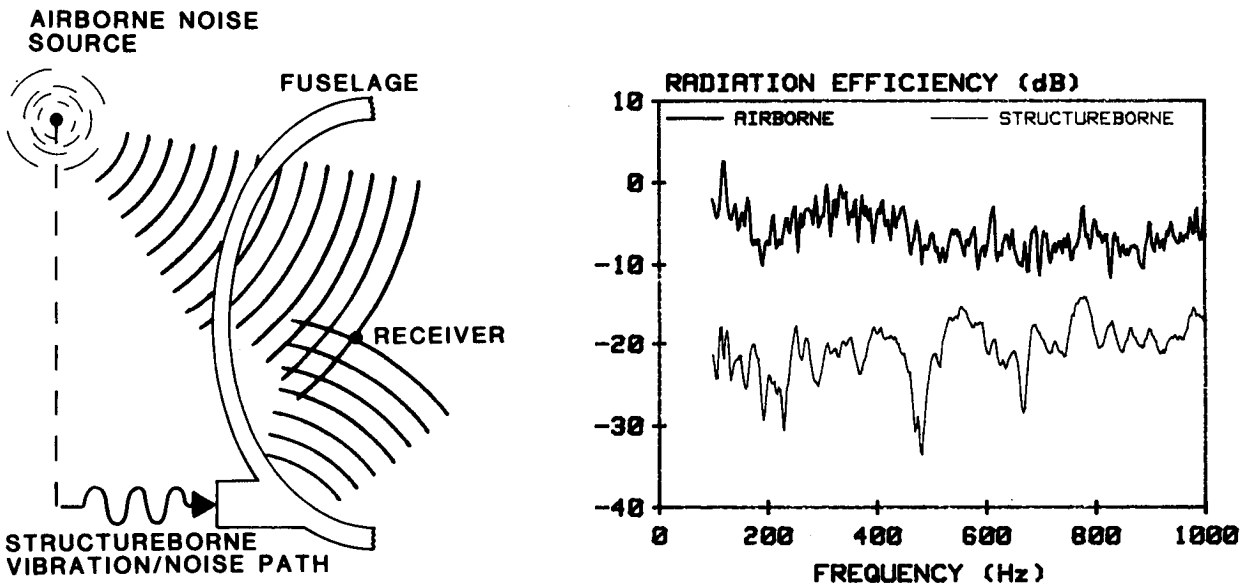

Figure 14

METHOD FOR SEPARATING AIRBORNE AND STRUCTUREBORNE NOISE IN COMPOSITE PANELS

Figure 15 illustrates a new measurement method for separating airborne and structureborne noise radiated by aircraft-type panels which is under development. The method is an extension of the two-microphone cross-spectral acoustic intensity measurement method combined with conventional methods for measuring the space-averaged mean square surface velocity of the structure. Both analytical and experimental studies are planned, with the aim of developing a comprehensive set of user guidelines for this method. The measurement method will be applied to panels constructed of both conventional aircraft materials and advanced composites. Parameters which will be studied include the frequency range of excitation, relative magnitude and phases of the combined airborne and structureborne inputs, and the effects of added structural damping.

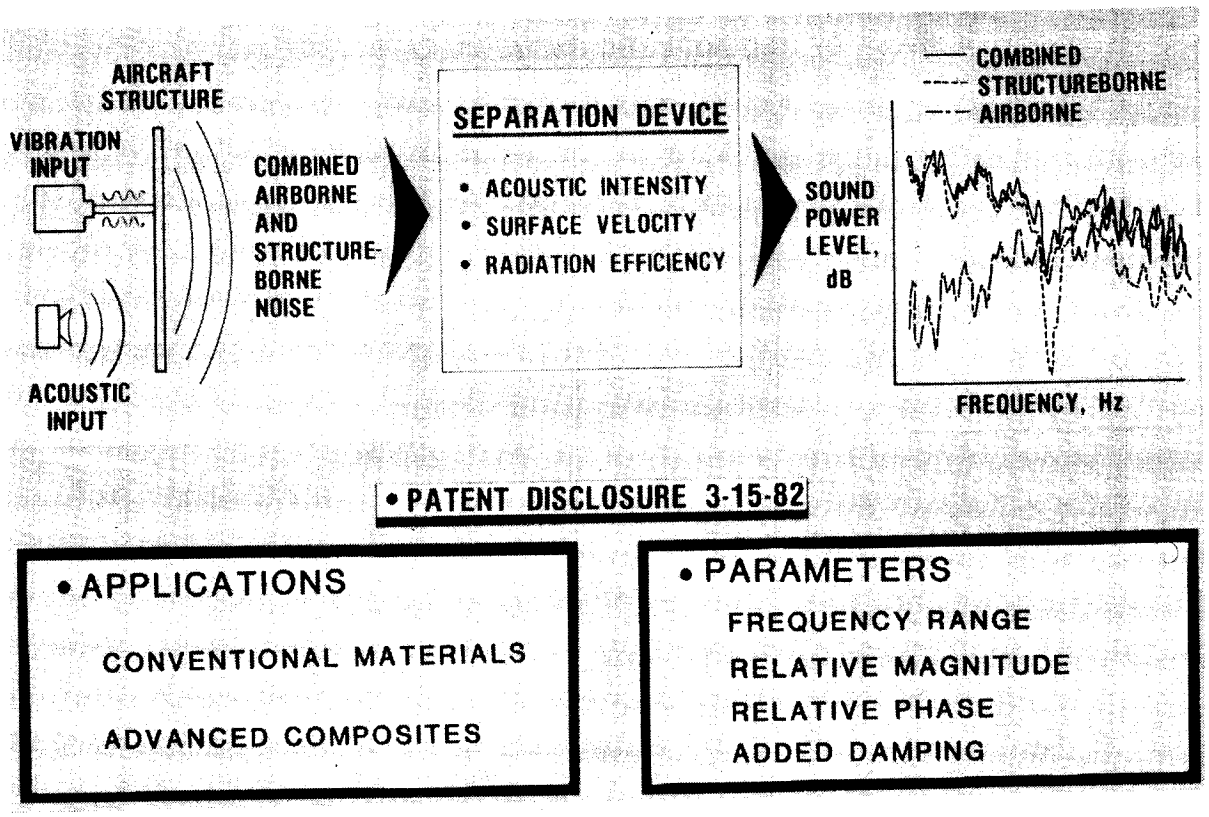

Figure 15

NOISE TRANSMISSION IN STIFFENED COMPOSITE STRUCTURES

Future research will also include studies of more complicated composite structures. It is expected that both analytical and experimental studies of the noise radiative properties of built-up composite panels, such as the panel shown in figure 16, will be undertaken. Presently, the analytical study of noise transmission through composite cylinders is being updated by Professor Koval to include the effects of frames and stringers. Parameters which will be studied include the geometry of the stiffeners (e.g. shape, size and spacing) and the methods of attaching the stiffeners to the panels (e.g. fabricated, adhesive bonded, riveted).

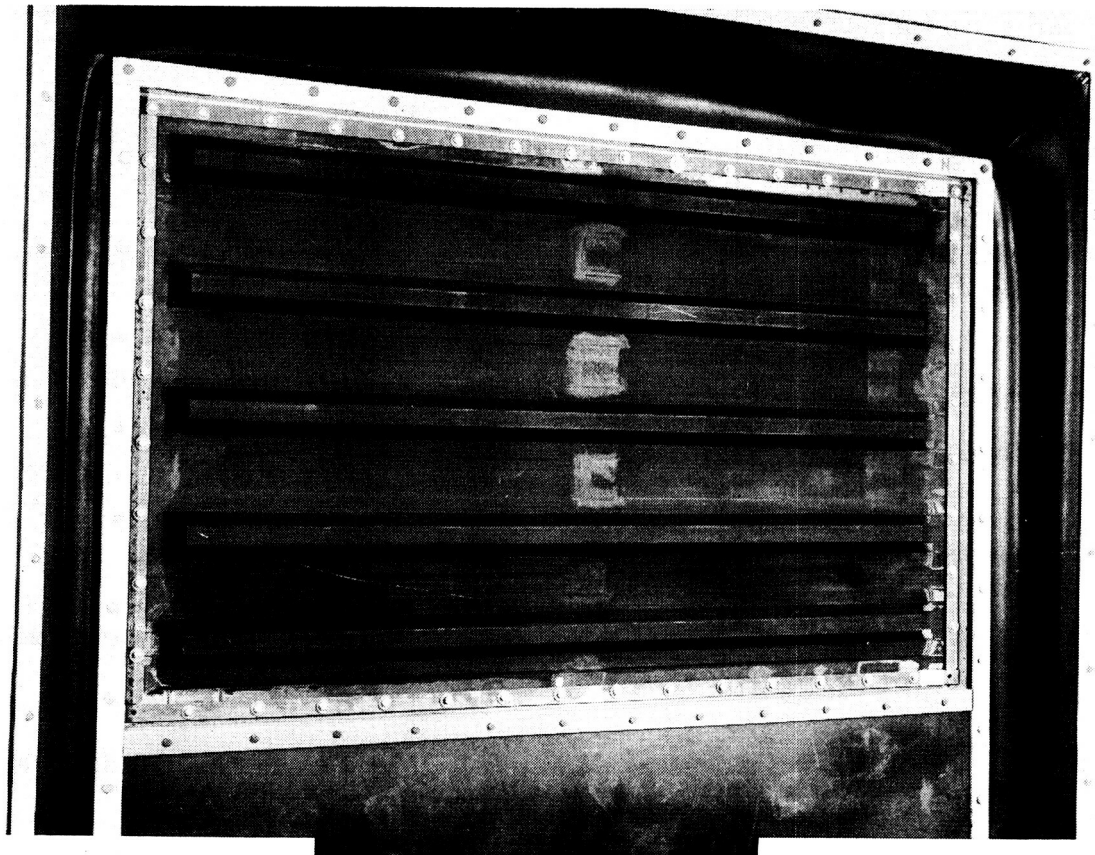

STIFFENER GEOMETRY
- SIZE
- SHAPE
- SPACING

STIFFENER ATTACHMENT
- FABRICATED WITH PANEL
- ADHESIVE BONDING
- RIVETED

Figure 16

SUMMARY/PROGRAM STATUS

Significant progress has been made in the program to determine noise characteristics of advanced composite material structures. Theory has been developed and verified for noise transmission loss of infinite panels which can have anisotropic stiffness characteristics. Similarly, theory has been developed and is being experimentally verified for orthotropic finite panels. An oblique incidence model of that theory is currently operational and a random incidence model is being programmed. Progress is also being made under a grant with Prof. Koval at the University of Missouri-Rolla to develop finite element models to account for added stiffness and coupling to acoustic volumes. A study is under way to determine radiation characteristics for airborne and structureborne noise and to separate those components in mixed situations. Finally, test plans to determine transmission loss characteristics of stiffened composite panels are being made with the cooperation of the Army Structures Laboratory at Langley Research Center. The successful completion of this program should make it possible to design composite structures with noise attenuation characteristics as good as current aluminum structures and which still provide the weight savings anticipated for equal stiffness designs. (See fig. 17.)

- ANISOTROPIC INFINITE PANEL THEORY DEVELOPED AND VERIFIED.
- ORTHOTHROPIC FINITE PANEL THEORY DEVELOPED, OBLIQUE INCIDENCE MODEL OPERATIONAL, RANDOM INCIDENCE MODEL BEING PROGRAMMED, VERIFICATION IN PROGRESS.
- FINITE ELEMENT MODEL DEVELOPED FOR SIMPLE PANELS, STIFFENED PANEL MODEL BEING DEVELOPED AT U. MISSOURI-ROLLA.
- PROGRAM TO DETERMINE RADIATION CHARACTERISTICS FOR AIRBORNE AND STRUCTUREBORNE NOISE INITIATED.
- TRANSMISSION LOSS OF STIFFENED PANELS TO BE INVESTIGATED.

Figure 17

1. Report No.	2. Government Accession No.	3. Recipient's Catalog No.
NASA CP-2321		

4. Title and Subtitle	5. Report Date
ACEE COMPOSITE STRUCTURES TECHNOLOGY - REVIEW OF SELECTED NASA RESEARCH ON COMPOSITE MATERIALS AND STRUCTURES	August 1984
	6. Performing Organization Code 534-06-13
7. Author(s)	8. Performing Organization Report No. L-15834
	10. Work Unit No.
9. Performing Organization Name and Address NASA Langley Research Center Hampton, Virginia 23665	11. Contract or Grant No.
	13. Type of Report and Period Covered Conference Publication
12. Sponsoring Agency Name and Address National Aeronautics and Space Administration Washington, DC 20546	14. Sponsoring Agency Code

15. Supplementary Notes

16. Abstract

The NASA Aircraft Energy Efficiency (ACEE) Composite Primary Aircraft Structures Program has made significant progress in the development of technology for advanced composites in commercial aircraft. Under NASA sponsorship, commercial airframe manufacturers have demonstrated technology readiness and cost effectiveness of advanced composites for secondary and medium primary components and have initiated a concerted program to develop the data base required for efficient application of safety-of-flight wing and fuselage structure. The third special oral review of the ACEE Composites Programs was held in Seattle, Washington, on August 13-16, 1984. The conference included comprehensive reviews of all composites technology development programs by ACEE Composites contractors. In addition, special sessions included review of selected NASA-sponsored research and several important Department of Defense programs in composite materials and structures. The papers were compiled in five documents. Papers prepared by personnel from Boeing Commercial Airplane Company, Douglas Aircraft Company, and Lockheed-California Company are contained in NASA CR-172358, CR-172359, and CR-172360, respectively. Papers on selected NASA-sponsored research are contained in NASA CP-2321. Papers on selected Department of Defense programs in composites are contained in NASA CP-2322.

17. Key Words (Suggested by Author(s))	18. Distribution Statement
Composite materials Composite structures Composite aircraft structures	Subject Category 24

19. Security Classif. (of this report)	20. Security Classif. (of this page)	21. No. of Pages	22. Price
Unclassified	Unclassified	187	A09

For sale by the National Technical Information Service, Springfield, Virginia 22161 NASA-Langley, 19